OPTICAL PHASE-LOCK LOOPS USING SEMICONDUCTOR LASERS

by

ROGERIO TADEU RAMOS

Submitted to the University of London
in fulfilment of the requirements for
the degree of Doctor of Philosophy

Supervised by Dr. A. J. Seeds

Department of Electronic and Electrical Engineering
University College London
Torrington Place, London, WC1E 7JE

September 1992

ProQuest Number: 10017266

All rights reserved

INFORMATION TO ALL USERS
The quality of this reproduction is dependent upon the quality of the copy submitted.

In the unlikely event that the author did not send a complete manuscript
and there are missing pages, these will be noted. Also, if material had to be removed,
a note will indicate the deletion.

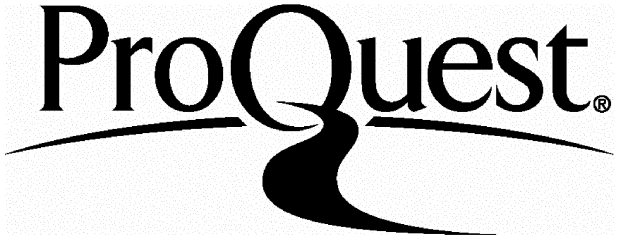

ProQuest 10017266

Published by ProQuest LLC(2016). Copyright of the Dissertation is held by the Author.

All rights reserved.
This work is protected against unauthorized copying under Title 17, United States Code.
Microform Edition © ProQuest LLC.

ProQuest LLC
789 East Eisenhower Parkway
P.O. Box 1346
Ann Arbor, MI 48106-1346

Abstract

Optical Phase-Lock Loops using Semiconductor Lasers

This thesis demonstrates theoretically and experimentally that it is possible to use semiconductor lasers without external cavities or other linewidth narrowing devices in Optical Phase-Lock Loops (OPLLs).

A comprehensive analysis of OPLL theory is presented including the effect of loop delay time. A performance comparison is made between modified first order loops and second order loops revealing that modified first order loops are less sensitive to loop delay time. Stability conditions are set and the main loop performance parameters of phase error spectrum and variance are calculated. A cycle-slip criterion is fixed and the relationship between laser linewidth, loop bandwidth and loop delay time is discussed to guide the loop design.

The optical and electrical design of an heterodyne OPLL is detailed. Experimental work is presented concerning temperature control, loop filter design, optical mixing and isolation. Double Quantum well lasers are described and characterised. Details of an heterodyne OPLL using laser diodes without external cavity or any other linewidth narrowing device are given. The loop has a measured phase error variance of $1.02 rad^2$.

To my Parents
José Ramos and Neide Ramos

Acknowledgements

My sincere thanks to Dr. A. J. Seeds for his expert supervision, for his support throughout the work and for his dedication and patience in reading and correcting the manuscript.

I would like to thank the many staff and students in this department who have helped during the course of this work, in particular the members of the antennas and radar group, the digital optics group and the workshop. I am also grateful to Northern Telecom (Europe) Opto-Electronic, Paignton, for supplying the lasers and to GEC-Marconi Ltd, Hirst Research Centre, for supplying the photodetector.

It is a pleasure to acknowledge my close association to all my fellow students, particularly B. Cai, I. Blanchflower, S. Hoskyns, P. N. Fernando and C. Zaglanikis. They have been a fertile source of ideas and comments.

I would like to acknowledge the support and encouragement from all my family and friends, mainly Suzanne, Renato and Regis. I also acknowledge the support form E. Conforti and all my former colleagues from Unicamp, Brazil.

This work was only possible thanks to the financial support from CNPq, Brazil, and the UK SERC.

CONTENTS:

List of symbols

A	amplitude of masteroscillator signal
A	illuminated photodetector active area
AM	amplitude modulation
AR	anti-reflection
a(t)	modulating signal
B	amplitude of slave oscillator signal
BER	bit error rate
BER_{cs}	cycle slip contribution to the bit error rate
B_n	loop noise bandwidth
C	amplitude of the reference offset generator frequency
Ct	thermal capacitance of the laser mounting
c	speed of light in vacuum
DQW	double quantum well
DQW-SCH	double quantum well separated confinement heterostructure
E	maximum amplitude of the electrical field
E^2	calibration constant
e	electronic charge
e_a, e_b	electrical fields
e_t	total electrical field
FDM	frequency division multiplex
FM	frequency modulation

FWHM	full width half maximum
f_c	loop filter cut-off frequency
f_m	modulating signal frequency
f_n	natural frequency
f_o	nominal laser frequency
f_{RF}	resonance frequency
$f(t)$	impulse response of the loop filter
$G(j\omega)$	open loop transfer function
HF	high frequency
Hi-Bi	High Birefringence
$H(s)$	loop transfer function
IM	intensity modulation
I	optical intensity
I_l	laser current
I_m	optical intensity of the master laser
I_s	optical intensity of the slave laser
I_{sig}	maximum amplitude of i_{sig}
i_{dc}	photocurrent dc component
in_a, in_b	intensity
i_p	photo current at the photodetector terminals
i_{p1}, i_{p2}	photo currents
i_{sig}	photocurrent signal component
$J_n(\beta)$	Bessel function of first kind and order n
K	constant which depends on the sensitivity of the temperature sensor
k	total gain
k_{cr}	critical gain for a stable system
k_d	phase detector gain
k_f	modulation constant
k_{fd}	frequency discriminator gain
k_m	maximum gain
k_g	loop filter gain
k_p	photodetector gain
k_s	slave oscillator gain
k_w	frequency modulation constant
k_ω	frequency response of the slave laser at the frequency ω_m
$k_\omega(\omega)$	frequency response of the slave laser
LAN	local area network
LF	low frequency
l	photodetector side
l_f	fibre length

l_b	Hi-Bi fibre beat length
M	amplitude of the modulating signal
MOCVD	metal organic chemical vapour deposition
MQW	Multiple Quantum Well
MZI	Mach-Zehnder interferometer
$m(t)$	modulating signal
N_m	master phase fluctuation
N_r	off-set reference oscillator phase fluctuation
N_s	slave laser phase fluctuation
N_{sn}	phase translated fluctuation due to the detector shot noise
n	an integer
n	fibre refractive index
n_f	refractive index of the film
n_m	refractive index of the material
n_o	refractive index of the air
OBFN	Optical Beam forming Network
OEIC	opto-electronic integrated circuit
OFLL	Optical Frequency-lock Loop
OPLL	Optical Phase-lock Loop
PI	proportional integral
PLL	Phase-lock Loop
PSK	phase shift keying
P_m	optical power from the master laser
P_o	optical power
P_s	optical power from the slave laser
Pu_1	power spectrum of the signal at the phase detector output
QW	quantum well
R	photodetector resposivity
R	reflectivity
R_c	reflectivity of the coated facet
R_u	reflectivity of the uncoated facet
R_{sp}	spontaneous rate
Rt	thermal resistance between the laser mounting and the ambient
r_l	photodetector load resistance
S_e	spectrum of the phase error signal
S_m	double sided spectra of the master laser phase noise
S_l	double sided spectra of the slave laser phase noise
S_{sn}	double sided spectra of the detector shot noise
S_{sna}	shot noise for heterodyne systems
S_{FM}	spectral densities of the FM noise

S_{PH}	spectral densities of the phase noise
s_c	coherence length
T_{av}	average time between cycle slips
T_d	loop propagation delay time
$u_1(t)$	signal after the phase detector
$u_2(t)$	convolution of $u_1(t)$ with $f(t)$
$u_3(t)$	photo detector signal
$u_4(t)$	continuous single frequency reference
$v_a(t)$	error signal for the temperature controller
$v_S(t)$	step function
WDM	wavelength division multiplex
$y_m(t)$	master signal
$y_s(t)$	slave oscillator signal
α	linewidth enhancement factor
β	FM modulation index
β_x	phase constant in the x direction
γ_e	damping constant of the laser
Δt	propagation time difference between the two optical path lengths
Δv_a	difference between the final and initial value of $v_a(t)$
$\delta(\,)$	dirac function
δf	summed linewidth
δf_m	maximum summed linewidth
δf_{mt}	FWHM linewidth of the master laser
δf_s	FWHM linewidth of the slave laser
δf_{ST}	linewidth of the laser due to spontaneous emission
ξ	magnitude of the flicker noise
η	characteristic impedance of the medium
η_c	photo-efficiency of the coated facet
η_u	photo-efficiency of the uncoated facet
θ	misalignment angle
λ	wavelength
ζ	damping factor
ζ_o	relative damping factor
σ^2	phase error variance
τt	rmal time constant of the system
Φ	s domain phase
$\Phi_e(s)$	phase error
ϕ	time domain phase
$\phi_m(t)$	phase of the master oscillator signal

$\phi_s(t)$	phase of the slave oscillator signal
ω	angular frequencie
ω_{cr}	critical angular frequency
ω_i	instantaneous frequency of the modulated signal
ω_d	frequency of the modulating signal
ω_m	angular frequency of the master oscillator
ω_n	loop natural frequency
ω_{no}	relative loop natural frequency
ω_o	centre optical frequency
ω_r	offset reference frequency
ω_s	angular frequency of the slave oscillator

List of Figures

Chapter 1

Introduction

This chapter introduces the optical phase-lock loop (OPLL) and its applications, considers alternative techniques, reviews previous work and describes the contents of the remainder of the thesis.

1.1- The Optical Phase Lock Loop

An optical phase-lock loop (OPLL) is a feedback system which controls an optical source in such a way that the phase of the light from this source follows the phase of an incoming optical signal. This is done by comparing the phase of the input signal to that of the internal source generating an error signal which is used to control the internal source. The internal source which will be controlled will be referred to as the slave laser, while the source of the incoming signal which provides the reference will be called the master laser.

Figure 1.1.1 gives the block diagram of a homodyne OPLL. This system is called homodyne because both master and slave lasers oscillate at the same frequency. Both signals are mixed at the surface of the photodetector, generating a photo-current proportional to the phase difference between the two signals. In the homodyne case the photodetector itself works as phase detector, producing the phase error signal necessary to close the loop. The phase error signal is then treated by the loop filter before being sent to the slave laser which is tuned by this signal in such a way that the phase of its emission is controlled to minimise the error.

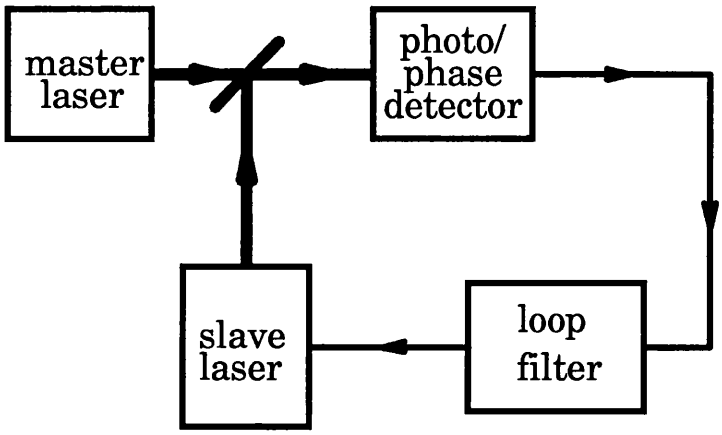

Figure 1.1.1: Block diagram of a homodyne Optical Phase-Lock Loop.

Figure 1.1.2 shows a block diagram of a heterodyne OPLL. In this case, master and slave lasers operate at two distinct optical frequencies. The signals from both lasers are mixed on the active area of the photodetector, producing a beat signal at a frequency corresponding to the frequency offset between the two lasers at the photodetector terminals. A phase detector compares the phase of the beat signal to that of an offset generator operating at the same frequency as the beat signal. A phase error signal is then produced at the output of the phase detector and treated by the loop filter. The slave laser is tuned by this signal in such a way that the phase of its emission is controlled to minimise the error.

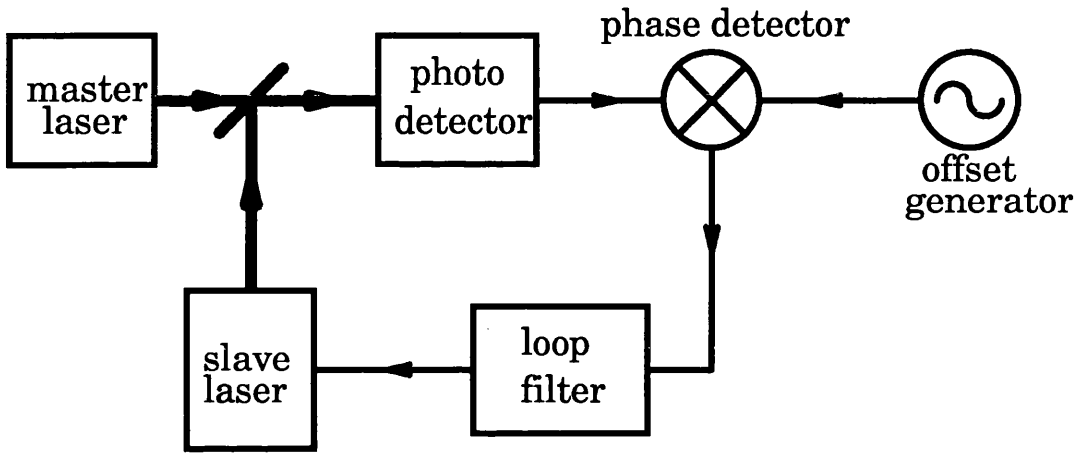

Figure 1.1.2: Block diagram of a heterodyne Optical Phase-Lock Loop.

In heterodyne OPLLs, the output of the slave laser tends to reproduce the whole spectrum of the master laser signal, translating its centre frequency to a new point different from the original one by the frequency of the offset generator. The linewidth of the slave laser is therefore altered by the action of the loop to be the same as the master laser, provided the performance of the loop is adequate. For this reason, heterodyne OPLLs are also known as translation loops [Gardner 79].

Heterodyne OPLLs present several advantages over the homodyne systems. The main advantages are:

-The slave laser frequency can be varied or even swept precisely by varying or sweeping the offset frequency generator.

-AC coupled filters and amplifiers can be used between the photodetector and the phase detector, rejecting DC drifts at the photodetector and improving the loop performance.

-Heterodyne OPLLs allow a very precise frequency tracking.

1.2- OPLL Applications

In this section, it is seen how the development of the OPLL technology is important for coherent optical communications, providing accurate channel selection, and how OPLLs can be used in these systems. Other more specific applications of OPLLs are also presented.

1.2.1- Coherent Communications

The most common transmission scheme used in optical fibre transmission systems is the intensity modulation (IM) of the optical source with respect to the input electrical signal. In this scheme no attention is paid to the frequency or the phase of the optical carrier, since a photodetector only responds to changes in the power level (the intensity) of an optical signal, and not to its frequency or phase content. Direct detection has been used at the receiving end to reconvert the optical signal into an electrical signal. In this respect a direct detection optical system is analogous to the way a primitive radio detects broadcast signals. This method offers system simplicity and relatively low cost, but suffers from limited sensitivity and does not take full advantage of the tremendous bandwidth capabilities of optical fibres.

Despite the theoretical possibilites, it was only at the end of the 70s that the spectral purity and frequency stability of semiconductor lasers had improved to the point where schemes using heterodyne or homodyne detection of the optical signal began to look feasible. In this technique the light is treated as a carrier medium which can be amplitude, frequency, or phase modulated similarly to the methods used in microwave radio systems.

The two main advantages of coherent optical communication schemes are a nearly ideal receiver sensitivity (up to 20dB improvement over direct detection) [Keiser 91] and a high degree of frequency selectivity. The selectivity of coherent systems is due to the fact that the selection of the channels is made by narrowband electronic filters rather than broad band optical filters.

Wavelength division multiplexing (WDM) can be used to increase the transmission throughput of the overall system, however, the number of optical channels that can be multiplexed is limited by the spectral bandwidth of the optical demultiplexer at the receiver. This results in a minimum channel spacing of, typically, 2nm and a transmission capacity of about 40 channels [Wagner 89]. The deployment of coherent receivers will enhance the capability of the network to transmit a greater number of

optical channels using frequency division multiplexing (FDM). This is a direct consequence of the higher selectivity achieved with the microwave filtering at the receiver. The optical channel spacing can now be reduced to frequencies of the order of a few GHz with a corresponding increase in the number of channels.

The advent of fibre amplifiers has diminished the importance of achieving high sensitivity, making the use of coherent techniques not as attractive as in the past for long distance communication links. However, the ability of providing effective demultiplexing for dense FDM systems is still very significant, making coherent systems a good option mainly for local area networks.

Figure 1.2.1 shows the diagram of the frequency response of a nominal 2nm wavelength optical filter, which is equivalent to a frequency bandwidth of 250GHz at the 1550nm region, compared with a 2GHz wide electrical filter. This illustrates that an electrical filter can provide several orders of magnitude more frequency selectivity than an optical one. Thus the channel density of a multichannel coherent system (that is, the number of channels per unit bandwidth) can be 100 times that for direct detection.

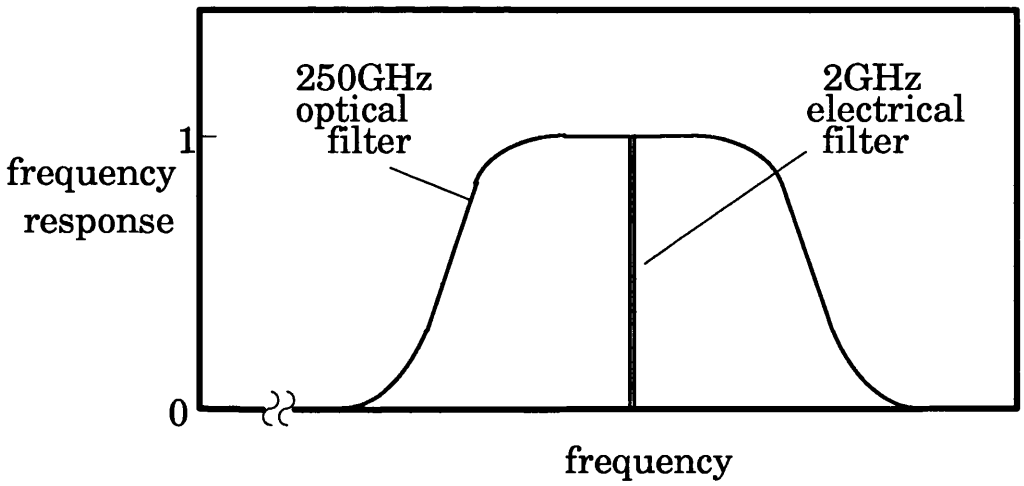

Figure 1.2.1: Diagram of the frequency response of a nominal 2nm bandwidth optical filter (equivalent to a frequency of 250GHz at the 1550nm region) compared with a 2GHz wide electrical filter.

The two transmission regions of an optical fibre which can be used for coherent systems are from 1270 to 1350 nm (1300nm window) and from 1480 to 1600 nm (1550nm window). For example, with a 10GHz channel spacing one could theoretically have at least 1000 channels in the 1300nm window, and 1500 channels in the 1550nm window.

The possibility of actually making such systems depends strongly on the ability to develop truly coherent semiconductor lasers that can be tuned over a significant portion of the 30,000 GHz bandwidth of a single mode optical fibre and the implementation of a proper coding method for inserting data on the optical carrier. Polarisation control of the local oscillator signal to match that of the received signal is also an obstacle to the use of coherent systems. However, several schemes have been proposed to overcome this problem.

Coherent optical detection is thus analogous to superheterodyne detection in modern radios, down converting the information from the optical carrier frequency to a much lower intermediate frequency, where it can be treated electrically. This down conversion is made by mixing the incoming signal with a local oscillator laser operating at a frequency equal to the received central frequency plus or minus the desired intermediate frequency. In the case of homodyne systems, the intermediate frequency is set to be 0Hz.

A key requirement for the realisation of a coherent lightwave system is the need for an electronically tunable optical source with a high degree of stability and temporal coherency. This is necessary since not only are the optical carriers spaced closely together in the frequency domain but also the modulation is typically encoded onto the frequency or phase of the carrier. The tunable capability of the laser allows the generation of both the optical transmitter channels and the local oscillators at the heterodyne receivers.

One technique to generate closely spaced optical channels is based on an optical frequency translation loop. This can take the form of either an optical phase-locked loop or an optical frequency-locked loop. The translation loop generates the channels by frequency off-setting the current controlled oscillator laser, within the loop, from a stable reference source, ideally to generate a large number of channels. This reference could be one frequency from an optical comb of frequencies.

1.2.2- Carrier generation in dense FDM systems

As was seen in section 1.2.1, dense frequency division multiplex FDM with channel spacing of a few GHz is possible using coherent techniques. OPLLs can be used not only at the receiver to allow the selection of an individual channel, but also at the transmitter to generate such a dense comb of carriers.

Figure 1.2.2 shows a block diagram of a carrier generator system using heterodyne OPLLs. A stable narrow linewidth master laser is used as reference for a chain of OPLL sub-systems. As the OPLL makes the slave laser reproduce the spectrum of the master laser at an offset frequency, the carriers are synthesised by using a sample of the slave laser signal from each OPLL block as master signal for the following one. The spacing between the carriers can be adjusted individually by tuning each offset generator, while the whole comb of carriers can be tuned by tuning the master laser optical frequency.

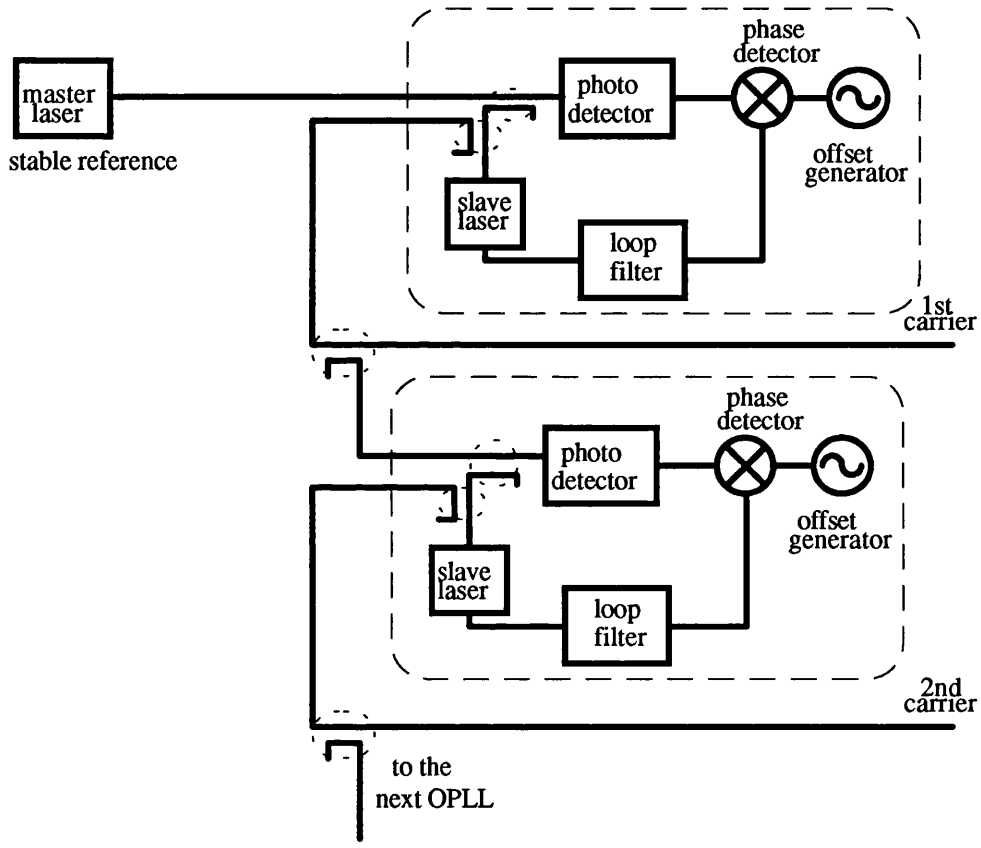

Figure 1.2.2: Block diagram of a carrier generator system using OPLLs.

1.2.3- Phase demodulator

If the phase of the master laser is modulated, the OPLL will see this modulation as phase error and it will try to modulate the slave laser equally in an attempt to cancel this "error". A signal proportional to the modulating signal becomes available at the phase detector output, as shown in Figure 1.2.3. Frequency demodulation can be achieved in the same way, as the frequency is given by the time derivative of the phase.

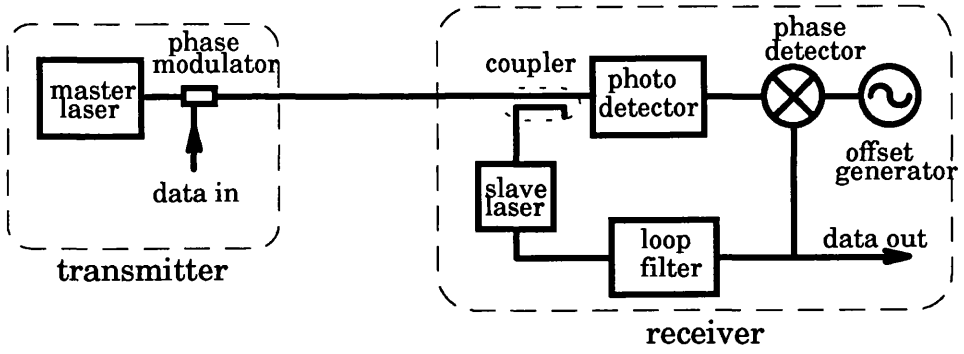

Figure 1.2.3: Block diagram of a optical phase modulation (PM) system using an OPLL as phase demodulator.

1.2.4- Local Area Networks (LANs)

A good example of the application of OPLLs was the European program ESPRIT 2054 Project UCOL (Ultra-wideband Coherent Optical LAN) [Fioretti 89] [Fernando 90]. Figure 1.2.4 shows a diagram of this system.

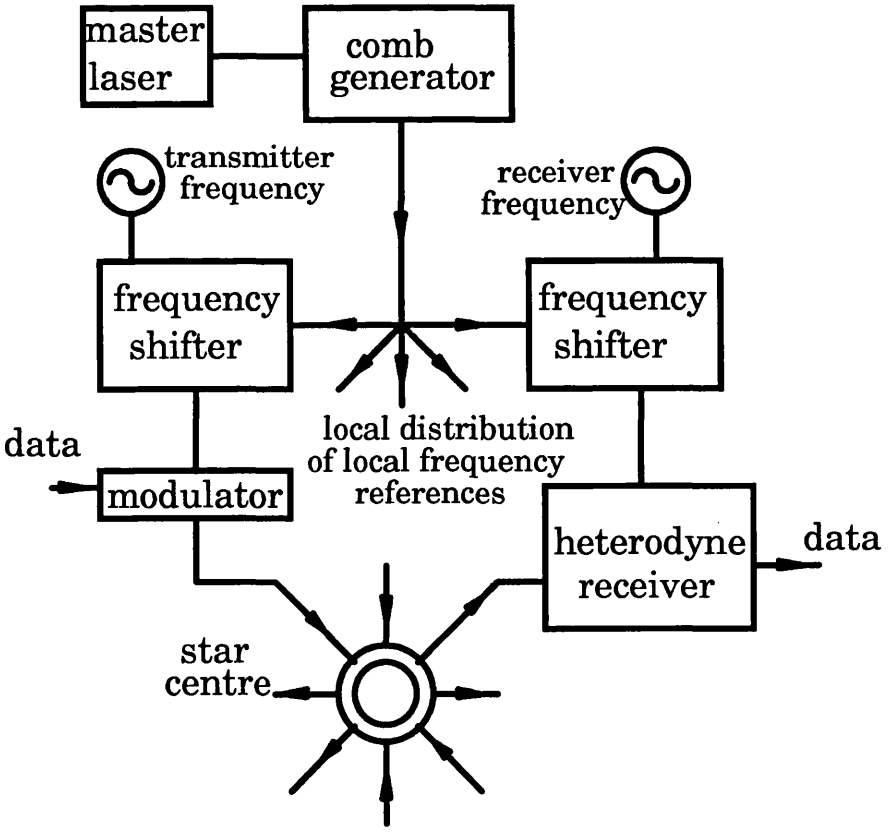

Figure 1.2.4: Block diagram of a LAN proposed by the European program ESPRIT 2054 Project UCOL.

A comb of optical signals is distributed to every station as frequency references to which frequency shifters would be locked, to provide both an optical carrier for transmitting and a local oscillator for the coherent reception. Again heterodyne OPLLs could be used as frequency shifters.

This kind of system could be used in a metropolitan area network (MAN) to integrate data voice and video transmission. However, such a system would only be feasible if stable and reliable OPLLs were available. Optoelectronic integrated circuit (OEIC) techniques may provide this in the future, also helping to bring the costs down.

1.2.5- Phased array antennas

The amplitude and the phase of the current at each element of the array determine the pattern of the radiated beam, while the number of elements sets the resolution of the antenna. A beam forming network is necessary to feed each element individually with the proper amplitude and phase to achieve the required pattern. However, when the number of elements is high, it becomes difficult to construct these networks using conventional waveguides or coaxial cables due to their size, weight, loss and narrow bandwidth. The use of optical fibres comes as a solution to these problems, being small, flexible, lightweight and practically immune to electromagnetic interference. Also, they have negligible losses, good phase accuracy and very large bandwidths. The optical fibre distribution network can not only provide the beam control, but also the distribution and transmission of the communication signal and the distribution of the phase and frequency reference.

Optical beam forming networks (OBFNs) can be produced by direct detection methods [Benjamin 90] or by coherent methods [Gliese 91]. When direct detection techniques are used, the lasers employed need to have a modulation bandwidth corresponding to the microwave frequency of the communication signal carrier, which is very difficult to obtain especially when high phase accuracy is required. However, it is possible to obtain a better carrier to noise performance with coherent schemes than with direct detection schemes, resulting in a better power budget which allows for more arrays or fewer laser transmitter modules. Furthermore, the generated microwave frequency at the antenna can easily be tuned by simply tuning one of the two lasers employed. Coherent techniques also give more possibilities for optical control and optical processing [Gliese 91].

Figure 1.2.5 shows the block diagram of an OBFN using coherent techniques. In this case a heterodyne OPLL is used to lock two lasers at an offset frequency equal to the

antenna transmitting frequency. The data to be transmitted modulates the master laser after a sample is taken for the phase locking of the salve laser. The beat signal is recreated at each element and amplified before being transmitted. A specific delay time is introduced using optical fibre delay lines for each element, providing the phase shift required for the individual element.

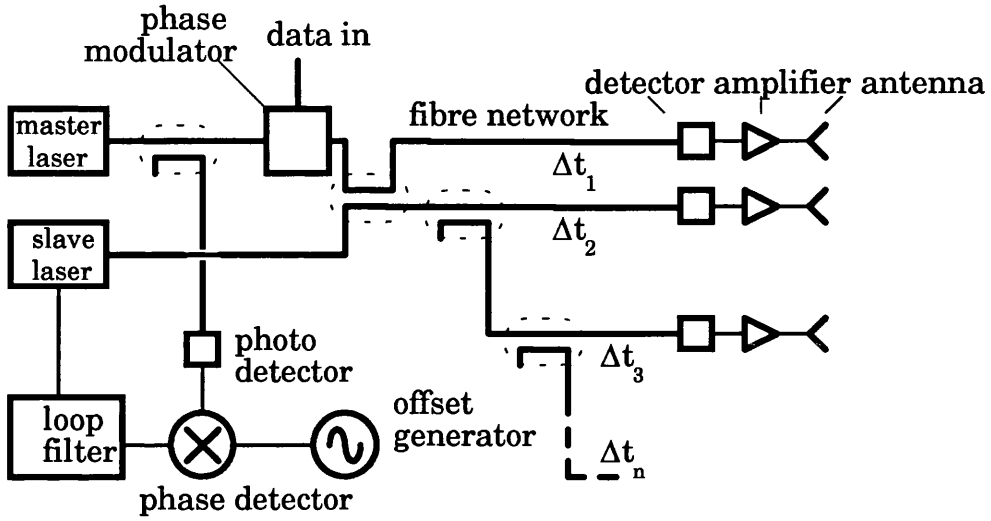

Figure 1.2.5: Block diagram of an OBFN using coherent techniques.

1.2.6- Optical sweep generator and optical measurements

It is possible to see from the block diagram of the heterodyne OPLL (Figure 1.1.2) that, if the offset generator is swept in frequency, this sweep will be transfered to the optical frequency of the slave laser in relation to the master laser. An optical sweep generator can then be built using an heterodyne OPLL, with applications in spectroscopy and optical measurements.

1.3- Comparison with other technologies

1.3.1- Optical Frequency Lock Loop

A block diagram of an optical frequency locked loop OFLL is shown in Figure 1.3.1. The signals from the master and slave laser are mixed on the active area of the photodetector producing a beat signal at a frequency corresponding to the frequency offset between the two lasers. The beat signal is then converted electrically to the operation frequency region of the frequency discriminator by a mixer and a generator operating at an offset frequency. The frequency discriminator translates the frequency variations into an electrical signal (voltage level) producing an error signal. The loop

filter arranges the error signal which tunes the slave laser in order to compensate for any fluctuation of the offset frequency.

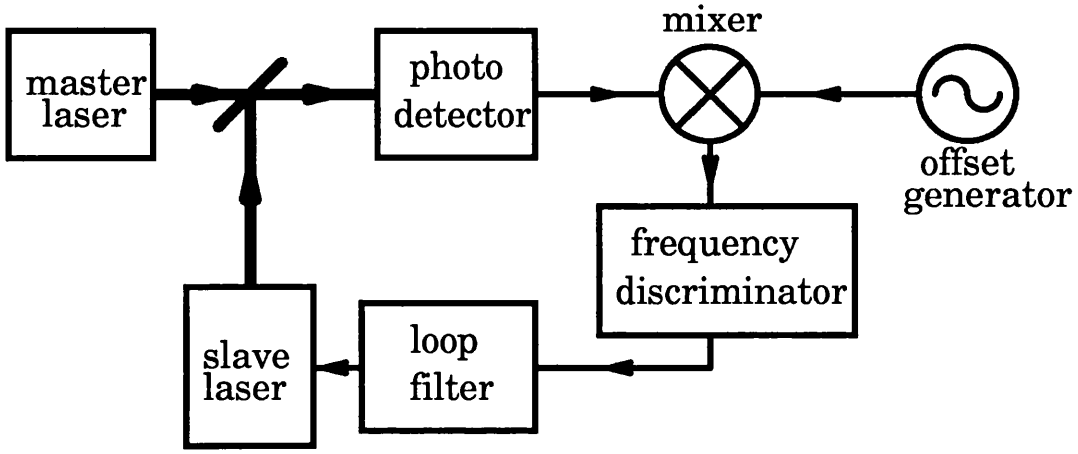

Figure 1.3.1: Block diagram of an optical frequency locked loop.

The frequency discriminator is basically a device whose frequency response presents a slope which can be approximated as linear. This can be achieved by a combination of a balanced mixer and a delay line in a kind of interferometer, as shown in Figure 1.3.2a. Alternatively, a low pass filter can be used, as in Figure 1.3.2b.

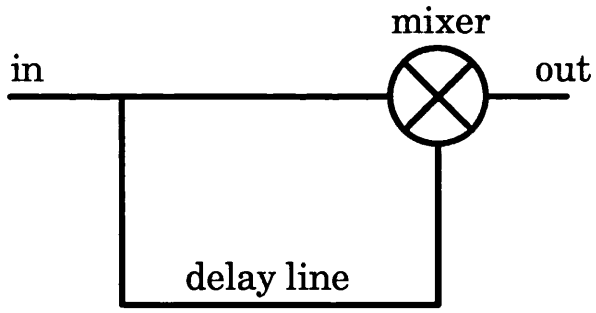

(a)

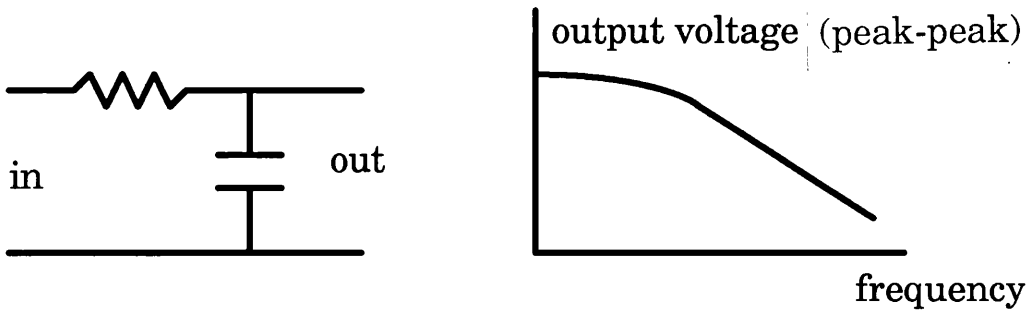

(b)

Figure 1.3.2: Examples of frequency discriminators: (a) using mixer and delay line; (b) using low pass filter.

In OFLLs, the centre frequency of the slave laser is controlled and kept stable in relation to the centre frequency of the master laser. Fluctuations of the central frequency of semiconductor lasers are usually slow (below 100kHz) due to the $1/f$ noise component of the FM noise spectrum [Fernando 91]. Therefore, narrow band loops can be used and the loop delay time is not an important factor.

The advantage of using a heterodyne OPLL instead of an OFLL is that not only the centre frequency of the beat signal is fedback by the loop, but also the instantaneous phase. The whole spectrum of the slave laser is altered by the action of the loop, making the slave laser reproduce the line shape of the master laser at a new centre frequency. This feature becomes particularly important when several narrow linewidths signals are required at different frequencies. In this case, only one narrow linewidth laser is required, while the others have their linewidths narrowed when locked to this reference.

1.3.2- Injection Locking

Phase lock is also possible though injecting the signal from the master laser into the active region of the slave laser waveguide [Kobayashi 80] [Lidoyne 91]. Figure 1.3.3 gives a diagram of an injection locking experiment.

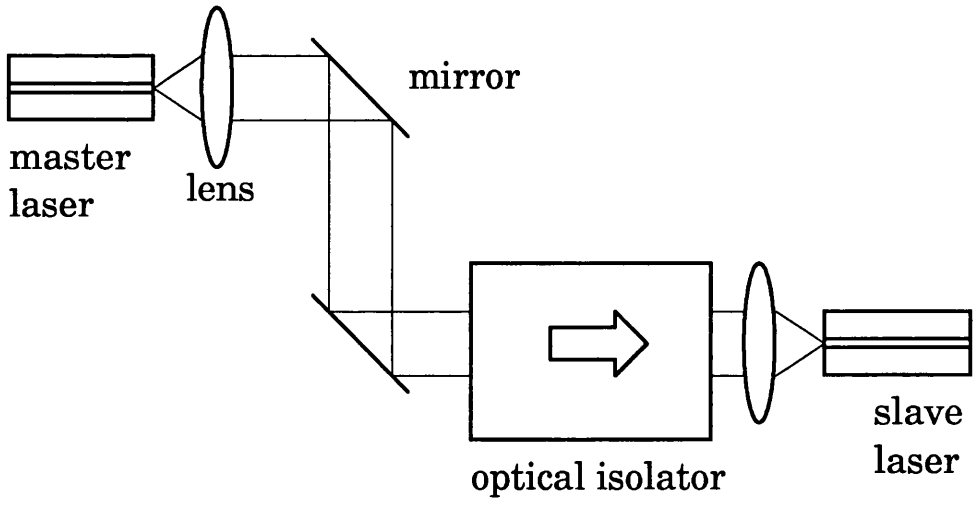

Figure 1.3.3: Diagram of an injection locking experiment.

In this case, locking is achieved directly by the optical signal from the master laser stimulating the emission in the slave laser waveguide to be in phase with the incoming master laser signal phase and, unlike the OPLL shown before, it does not use electrical feedback. It is basically a homodyne technique, but it is possible to lock the two lasers

at different frequencies by modulating the master laser and locking the slave laser to one of the sidebands generated by the modulation of the master laser signal. The main disadvantage of this method is that the frequency offset is limited by the frequency response of the laser, while for the OPLL it is limited by the response of the photodetector, the phase detector and the offset generator, which are already well developed components and available for high frequencies.

Figure 1.3.4 shows a diagram of a coherent receiver using injection locking. A sample of the incoming signal is taken though an optical isolator to lock the slave laser to its frequency and phase. The output of the slave laser is then combined coherently to the incoming signal, producing a beat signal at the photodetector terminals. One disadvantage of this kind of system is that a part of the incoming optical signal has to be used to injection lock the slave laser before detection takes place, reducing sensitivity.

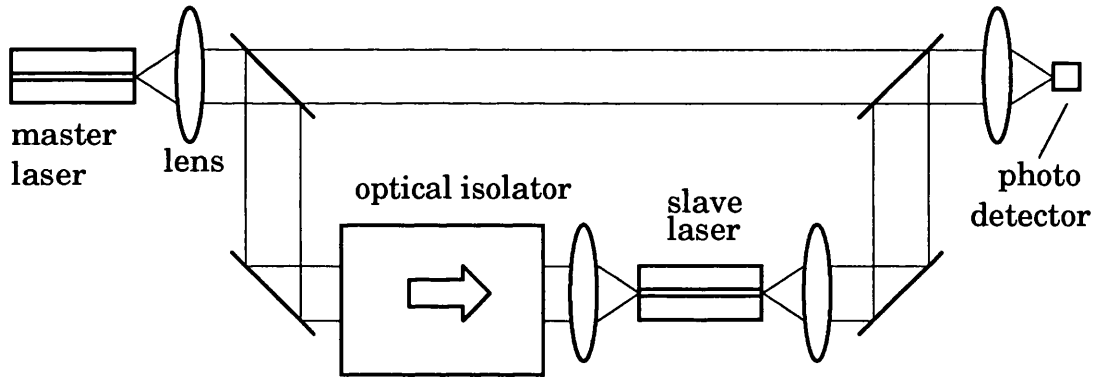

Figure 1.3.4: Diagram of a coherent receiver using injection locking.

1.3.3- Other technologies

Direct modulation can be used for optical carrier generation by using mode-lock techniques to generate a comb of optical frequencies. However, it has the disadvantage of having the frequency offset between carriers fixed to the laser mode space of the laser.

Integrated-optic frequency translators can be used to introduce a frequency shift to an optical carrier. This can be done by using single side band (SSB) modulation techniques [Izutsu 81] [Culshaw 81], in which the side band becomes the new offset optical signal. Other devices are based on an electrooptic effect associated with a propagating microwave field to offset an incoming optical carrier by the frequency of the microwave signal used [Désormière 90].

1.4- OPLL critical parameters

Because most of the phase noise spectrum of the beat signal is used by the control loop, the loop bandwidth has to be wide enough to cover the main frequency range of this noise. The principal critical parameters in the OPLL design are:

- *Laser linewidth*: The main source of noise is the phase noise originated in the lasers used in the system. The extension of the spectrum of this noise is given by the laser linewidth, considering Lorezian lineshape.
- *Loop bandwidth*: When wide linewidth lasers are used, a wide bandwidth loop is required to track the phase noise.
- *Loop delay time*: The loop propagation delay time limits the bandwidth of the system and it is a particularly important factor when wide linewidth lasers and wide bandwidth loop filters are used.

These factors and the relationship between them will be studied quantitatively in Chapter 2 of the thesis.

The implementation of OPLLs in opto-electronic integrated circuit OEIC form will only be possible in the future if semiconductor lasers are used. As these lasers normally possess wide linewidth, wide bandwidth loops need to be used. The effect of the loop delay time is expected to be minimised by its decrease due to the reduction in size brought about by integration.

1.5- Historical Background

1.5.1- Experimental work

The use of phase-lock techniques at optical frequencies has been limited in the past by a series of technological problems. The most important factor has been the unavailability of suitable optical sources. Problems of wideband phase noise, frequency instability and tunablity were the main obstacles to the use of laser sources as slave lasers in OPLLs. In this introduction a brief review of the OPLL experiments reported is presented.

The first OPLL experiment reported was a homodyne system [Leeb 82] using water cooled CO_2 lasers operating single moded at 10.6 μm and tuned by a combination of an internal electro-optic frequency modulator and a piezoelectric (PZT) mounted

mirror. The use of semiconductor laser diodes would make the tuning system simpler and faster, as they could be directly tuned by current. Nevertheless, wideband phase noise prevented their use. The first experiment using semiconductor lasers [Steele 83] applied weakly coupled external cavities to the laser diodes in order to narrow their linewidths. In this heterodyne system, locking was obtained only for short periods due to acoustic frequency jitter and thermal drift affecting the external cavities. The same kind of experiment was done without intentional optical feedback [Richards 85]. However, the loop was not completely stable due to the large amount of phase noise and operation was only obtained over a short period of time.

Homodyne OPLLs were reported later using piezoelectric tuned HeNe lasers [Malyon 84] and $LiNbO_3$ modulator tuned external cavity semiconductor lasers locked to a HeNe laser [Malyon 86]. Heterodyne systems with an offset frequency of 5MHz using HeNe lasers were also achieved [Hall 87]. Solid state Nd:YAG ring lasers operating at 1320nm pumped by laser diodes were used in a homodyne OPLL presenting a natural frequency f_n=36kHz [Kazovsky 89 and 90] and f_n=10kHz [Schöpflin 90]. The same technique was also used for heterodyne loops [Williams 89], with f_n=36kHz and offset frequency of 4GHz [Atlas 90], and f_n=50-100kHz and offset frequency of 12GHz [Wale 91].

Improved external cavity semiconductor lasers were used in a heterodyne OPLL at a 250MHz offset, presenting a natural frequency f_n of the order of 300kHz [Harrison 89] and in a homodyne system with f_n of about 100kHz [Kahn 89]. External cavity three electrode DFB lasers were also used in a homodyne system with 22ns loop delay time and f_n=605kHz [Noriamtsu 90]. Another way of narrowing the linewidth of semiconductor lasers was to employ optical feedback from external high finesse resonators. This technique was used in heterodyne OPLLs with 25MHz offset frequency and f_n=263kHz [Shin 90] and with 20ns loop delay [Telle 90].

In all the experiments mentioned before, very narrow linewidth lasers were used (below 200kHz). This allowed the use of long loop delay times (of the order of 20ns) and low values of loop natural frequency (less than 700kHz). However, as shown theoretically in Chapter 2, relatively wide linewidth lasers (order of MHz) could be used [Ramos 90], provided that the loop delay time was kept low (order of ns) and the loop natural frequency was high (above 10MHz). Very recently, a homodyne OPLL using semiconductor lasers was reported [Kourogi 91], where the slave laser was operated without external cavity and locked to a narrow linewidth laser (150kHz) through a fast and wide bandwidth loop. A 134MHz loop bandwidth was employed with a loop delay time of 1ns.

In Chapter 5, the first heterodyne OPLL experiment using semiconductor lasers without external cavities or other linewidth narrowing methods is described. This is also the heterodyne OPLL with the widest natural frequency (20MHz) and lowest delay time (3ns) [Ramos 92].

1.5.2- Theoretical work

As previous experimental work was done using very narrow linewidth lasers, it was not clear what the maximum value of phase noise was which would still allow the loop to lock. This limit depends strongly on the value of the loop bandwidth, as the phase noise suppression effect within the loop bandwidth is affected. Another important factor is the propagation delay time of the loop, which has great influence on the loop performance and stability, as it also limits the loop bandwidth. There was then the need for developing a theoretical study in order to understand better the influence of the adverse noise characteristics of lasers on OPLL systems.

The first step was to identify the main sources of noise in the system and relate the phase noise to a parameter of quality of locking, such as the phase error variance [Armor 79]. Following this analysis, attempts were made to optimise the design of OPLLs [Hodgkinson 85]. The same approach for optimisation was used and linewidth limits were set for a given bit error rate (BER) [Kazovsky 86]. The influence of the loop propagation delay time was then considered [Grant 87]. A modified first order loop was shown to be more suitable for OPLLs with large phase noise [Steele 88].

However, it was not clear how the system would behave near the limit of stable operation and what the conditions for locking were. There was not a distinct method by which the designer could easily establish a relationship between the loop delay time, the loop gain, the loop filter bandwidth and the laser linewidth, in order to search for the best compromise between these factors. There was also the need to study the possibility of implementing OPLLs in the form of opto-electronic integrated circuits (OEICs), which would drastically reduce the total loop delay time, but would imply that wide linewidth semiconductor lasers without external cavities needed to be used. Different criteria for evaluating the loop performance were also necessary, as the wideband phase noise involved could invalidate linear approximations previously made. This design method, introduced more recently [Ramos 90], is described in Chapter 2 of the thesis, where the use of different loop orders is studied and a new stability criterion is introduced. A new design criterion based on the average time

between cycle slips is also introduced, together with a full discussion on the loop performance.

1.6- Structure of the Thesis

The first objective of this thesis is to demonstrate that commercial OPLLs can be feasible in the future by understanding their limitations, modelling the system and setting design guide lines. The second objective is to build an OPLL in the laboratory.

Chapter 2 presents the theoretical analysis of the OPLL. The block diagram and transfer functions of both homodyne and heterodyne OPLLs are presented and the main sources of noise are identified. Then discussions on the loop filter design and the loop stability are introduced for a non zero loop propagation delay time. Methods of evaluating the loop performance are shown and a cycle slip criterion is established to determine loop parameters during design.

Chapter 3 concentrates on the design of the optical section of the OPLL experiment. Some comments are made on how the optical mixing is carried out, followed by a discussion on optical isolation and an evaluation of the amount of optical misalignment tolerable in order to obtain effective optical mixing. The main characteristics of the double quantum well lasers (DQW) used in the final experiment are presented. As part of this characterisation, the FM response of a DQW laser is measured

Chapter 4 discusses the design of the electrical part of the OPLL, starting by giving an overview of the loop circuit, followed by a description of the phase detector. A design of the phase error amplifier (which is the loop filter) is presented, showing how a split path technique is used to reduce delay time effects. Finally, the temperature control system design is described.

Chapter 5 shows the final OPLL experiment, using the ideas and techniques detailed in the previous chapters. The measured performance is presented, followed by the parameters calculated from the measurements and a comparison to the theoretical predictions. This experiment demonstrates for the first time a stable heterodyne OPLL using semiconductor lasers without external cavities or any other linewidth narrowing process.

Chapter 6 presents a summary of the main conclusions from this project and gives suggestions for future work.

References:

Armor, J.B., Robinson, S., "Phase-lock control considerations for coherently combined lasers", Appl. Opt., 1979, 18(18), pp. 3165-3175.

Atlas, D.A., Kazovsky, L.G., "2 Gbit/s PSK heterodyne communication system using optical phase-locked loop", Electronics Letters, 1990, 26(14), pp. 1030-1032.

Benjamin, R., Zaglanikis, C. D. and Seeds, J. A., "Optical Beam Former for Phased Arrays with Independent Control of Radiated Frequency and Phase", Electronics Letters, vol. 26, n. 22, 1990, pp. 1853-1855.

Culshaw, B. and Wilson, M. G. F., "Integrated Optic Frequency Shifter Modulator", Electronics Letters, vol. 17, 1981, pp. 135-136.

Désormière, B., Maerfeld, C. and Desbois, J., " An Integrated Optic Frequency Translator for Microwave Lightwave Systems", Journal of Lightwave Technology, vol. 8, n. 4, April 1990, pp. 506-513.

Fernando, P. N., Fake, M. and Seeds, A. J., "A Novel Approach to Optical Frequency Synthesis in Coherent Lightwave Systems", Proceedings of SPIE, O/E Fibres, vol. 1372, 1990, pp. 152-163.

Fernando, P. N., Ramos, R. T. and Seeds, A. J., "Optical Carrier Synthesis in Coherent Lightwave Systems", IEE Colloquium on Sources for Coherent Optical Communication, digest n. 1991/013, London, 18 January 1991, pp. 12/1-12/7.

Fioretti, A., Neri, E., Forcesi, S., Gree, A., E., Fernando, P. N., Labrujere, A. C., Koning, O. J., Bekooij, J. P., Veith, G., Shmuck, H., "Technology Aspects of a Coherent Optical M.A.N.", Proceedings of SPIE, vol. 1175, 1989, pp. 182-195.

Gardner, F.M.: Phaselock Techniques, (Wiley, New York, 2nd Ed., 1979).

Gliese U., Christensen, E. L. and Stubkjær, K. E., "Laser Linewidth Requirements and Improvements for Coherent Optical Beam Forming Networks in Satellites", IEEE Journal of Lightwave Technology, vol. 9, n. 6, June 1991, pp. 779-790.

Grant, M.A., Michie, W.C., Fletcher, M.J.: "The performance of optical phase locked loops in the presence of nonnegligible loop propagation delay", J. Lightwave Tech., 1987, LT5, pp. 592-597.

Harrison, J. and Mooradian, A., "Linwidth and Offset Frequency Locking of External Cavity GaAlAs Lasers", Journal of Quantum Electronics, vol. QE-25, n. 6, June, 1989, pp.1152-1155.

Hall, J. L., Sheng, M. L., Kramer, G., "Principles of Phase-Locking: Application to Internal Mirror He-Ne Lasers Phase-Locked via Fast Control of the Discharge Current", Journal of Quantum Electronics, vol. QE-23, n. 4, April, 1987, pp.427-437.

Hodgkinson, T.G.: "Phase locked loop analysis for pilot carrier coherent optical receivers", Electronics Letters, 1985, 21, pp. 1202-1203.

Izutsu, M., Shikama, S. and Sueta, T., "Integrated Optical SSB Modulator/Frequency Shifter", IEEE Journal of Quantum Electronics, vol. QE-17, n. 11, November, 1981, pp. 2225-2227.

Kahn, J.M., Kasper, B. L. and Pollock, K. J., "Optical Phaselock Receiver with Multigigahertz Signal Bandwidth", Elect. Lett., 1989, vol. 25, n. 10, pp. 626-628.

Kahn, J.M., "1 Gbit/s PSK homodyne transmission system using phase-locked semiconductor lasers", Photonics Tech. Lett.,1989, vol. 1(10), pp.340-342.

Kazovsky, L. G., "Performance Analysis and Laser Linewidth Requirements for Optical PSK Heterodyne Communications Systems", J. Lightwave Tech., vol. LT-4, n. 4, April 1986, pp. 415-425.

Kazovsky, L.G., Atlas, D.A., "A 1320 nm experimental optical phase-locked loop", Photonics Tech. Lett., 1989, vol. 1(11), pp.395-397.

Kazovsky, L.G., Atlas, D.A., "A 1320 nm experimental optical phase-locked loop: performance investigation and PSK homodyne experiments at 140 Mb/s and 2 Gb/s", J. of Lightwave Tech, 1990, 8(9), pp.1414-1425.

Keiser, G., "Optical Fibre Communications", McGraw-Hill, 1991.

Kobayashi, S. and Kimmura, T., "Injection Locking Characteristics of an AlGaAs Semiconductor Laser", IEEE Journal of Quantum Electronics, vol. QE-16, n. 9, September 1980, pp. 915-917.

Kourogi, M., Shin, C.H., Ohtsu, M., "A 134MHz bandwidth homodyne optical phase-locked-loop of semiconductor laser diodes", Photonics Tech. Lett., 1991, vol. 3(3), pp.270-272.

Leeb, W.R., Philip, H.K., Scholtz, A.L., Bonek, E.: "Frequency synchronization and phase locking of CO_2 lasers", Appl. Phys. Lett.,1982, vol. 41(7), pp.592-594.

Lidoyne, O., "Bruit de Phase et Modulation d'un Laser a Semi-Conduteur Synchronise; Applications aux Telecommunications", Doctor degree thesis, Ecole Nationale Supérieure des Télécommunications, Paris, France, 1991.

Malyon, D.J., "Digital fibre transmission using optical homodyne detection", Elect. Lett., 1984, vol. 20(7), pp.281-283.

Malyon, D.J., Smith, D.W., Wyatt, R.: "Semiconductor laser homodyne optical phase locked loop", Elect. Lett., 1986, 22(8), pp.421-422.

Norimatsu, S., Iwashita, K., Noguchi, K., "10 Gbit/s optical PSK homodyne transmission experiments using external cavity DFB LDs", Elect. Lett., 1990, vol. 26(10), pp.648-649.

Norimatsu, S., Iwashita, K., Sato, K., "PSK optical homodyne transmission detection using external cavity lasers diodes in Costas loop", Photonics Tech. Lett., 1990, 2(5), pp.374-376.

Ramos, R.T., Seeds, A.J., "Delay, linewidth and bandwidth limitations in optical phase-locked loop design", Elect. Lett., 1990, vol. 26(6), pp.389-391.

Ramos, R.T., Seeds, A.J., "Fast Heterodyne Optical Phase-Lock Loop Using Double Quantum Well Laser Diodes", Elect. Lett., 1992, vol. 28, n.1, pp.82-83.

Richards (page 107)

Shin, C.H., Ohtsu, M., "Heterodyne optical phase-locked loop by confocal Fabry-Perot cavity coupled AlGaAs lasers" Photonics Tech. Lett., 1990, 2(4), pp.297-300.

Shin, C.H., Ohtsu, M., "Optical Phase-Locking Expeirments by Confocal Fabry-Perot Cavity Coupled Semiconductor Lasers", Third Optoelectronics Conference (OEC'90) Technical Digest, July, 1990, Makuhari Messe.

Scholtz, A.L., Leeb, W.R., Flatscher, R. and Philip, H.K., "Realization of a 10-μm Homodyne Receiver", Journal of Lightwave Technology, vol. LT-5, n. 4 April, 1987, pp. 625-632.

Schöpflin, A., Kugelmeier, S., Gottwald, E., Ffelicio, D., Fischer, G., "PSK optical homodyne system with nonlinear phase-locked loop", Elect. Lett., 1990, 26(6), pp.395-396.

Steele, R.C., "Optical phase locked loop using semiconductor laser diodes", Elect. Lett., 1983, vol. 19, pp.69-71.

Steele, R.C., Creaner, M.J., Walker, G.R., Walker, N.G.: "Optical PSK transmission experiment at 565Mbit/s incorporating an endless polarization control system", Proceedings of SPIE Components for Fiber Optics Applications and Coherent Lightwave Communications, Boston, 1988, vol. 988, pp. 302-309.

Telle, H.R., Li, H., "Phase-Locking of Laser Diodes", Electronics Letters, 1990, vol. 26, n. 13, pp.858-859.

Wagner, S. S. and Kobrinski, "WDM Applications in Broadband Telecommunication Networks", IEEE Communications, March 1989, pp. 22-30.

Wale, M.J., Holliday, M.G., "Microwave signal generation using optical phase locked loops", Workshop A Proceedings, European Microwave Conference, Stuttgart, 1991, pp. 77-82.

Williams, K.J., Golberg, L., Esman, R.D., Dagenais, M. and Weller, J.F., "6-34 GHz offset phase locking of Nd:YAG 1319 nm nonplanar ring laser", Elect. Lett., 1989, vol. 25, pp.1242-1243.

Chapter 2

Optical Phase-Lock Loop Theory

2.1- Introduction

As the ability to obtain stable single mode laser radiation developed during the early 1980s, the translation of phase lock techniques in use at microwave frequencies to optical frequencies was slowly made possible. Some OPLL experiments started to be reported, all using very narrow linewidth lasers (order of 100kHz or less). This was achieved using gas lasers like CO_2 and HeNe, solid state lasers like YAG lasers and semiconductor lasers using external cavity optical feedback or electrical feedback. A full review of the OPLL experiments and theoretical work was presented in Chapter 1.

In this Chapter we extend previous analysis [Grant 87] [Steele 88] to include finite loop propagation delay together with photodetector shot noise, and derive design criteria for OPLLs as a function of the loop parameters. First, the block diagram and transfer functions of both homodyne and heterodyne OPLLs are presented and the main sources of noise are identified. Then discussions on the loop filter design and the loop stability are introduced for a non zero loop propagation delay time. Methods of evaluating the loop performance are shown and a cycle slipping criterion is established to determine loop parameters during design. Finally, the conclusions are summarised.

2.2- Block Diagram and Transfer Functions

2.2.1- Homodyne case:

The block diagram of a basic Phase-Locked Loop (PLL) is shown in Figure 2.2.1. The master signal $y_m(t)$ and the slave oscillator signal $y_s(t)$ are given by:

$$y_m(t) = \mathrm{A}\ \sin(\omega_m t + \phi_m(t)) \qquad 2.2.1$$

$$y_s(t) = \mathrm{B}\ \cos(\omega_s t + \phi_s(t)) \qquad 2.2.2$$

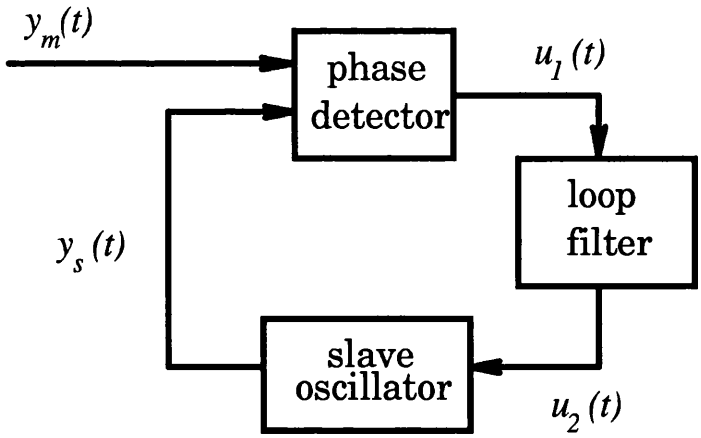

Figure 2.2.1: Block diagram of a general phase-lock loop.

Where A and B are the amplitudes, ω_m and ω_s are the angular frequencies and $\phi_m(t)$ and $\phi_s(t)$ are the phases of master and slave oscillator signals respectively.

Considering first that the master and slave signals have the same frequency, the signal after the phase detector $u_1(t)$, for a sinusoidal phase detector, would be:

$$u_1(t) = k_d \sin[\phi_m(t) - \phi_s(t)] \qquad 2.2.3$$

Where k_d is the phase detector gain. If $f(t)$ is the impulse response of the loop filter and k_g represents the gain of this filter, $u_2(t)$ will be given by the convolution of $u_1(t)$ with $f(t)$ as follow:

$$u_2(t) = k_g\,[u_1(t) * f(t)] \qquad 2.2.4$$

Using a tunable slave oscillator which has its output frequency dependent on the amplitude of the input signal, the output phase $\phi_s(t)$ will be:

$$\frac{d\phi_s(t)}{dt} = k_s\, u_2(t) \qquad 2.2.5$$

Where k_s is the slave oscillator gain. Using equations (2.2.4) and (2.2.5):

$$\frac{d\phi_s(t)}{dt} = k \sin[\phi_m(t) - \phi_s(t)] * f(t) \qquad 2.2.6$$

Where k is the total gain, given by:

$$k = k_d \, k_g \, k_s \tag{2.2.7}$$

For small amounts of phase error (phase error variance lower than $\pi/2\text{rad}^2$), it is possible to use a linearised model of the phase detector:

$$\frac{d\phi_s(t)}{dt} = k\,[\phi_m(t) - \phi_s(t)] * f(t) \tag{2.2.8}$$

Using Laplace transformation in order to pass to the frequency domain:

$$s\,\Phi_s(s) = K\,[\Phi_m(s) - \Phi_s(s)]\,F(s) \tag{2.2.9}$$

The loop transfer function is defined as:

$$H(s) = \frac{\Phi_s(s)}{\Phi_m(s)} = \frac{K\,F(s)}{s + K\,F(s)} \tag{2.2.10}$$

For the phase error given by:

$$\Phi_e(s) = \Phi_m(s) - \Phi_s(s) \tag{2.2.11}$$

One can write:

$$1 - H(s) = \frac{\Phi_e(s)}{\Phi_m(s)} = \frac{\Phi_m(s) - \Phi_s(s)}{\Phi_m(s)} = \frac{s}{s + K\,F(s)} \tag{2.2.12}$$

Figure 2.2.2 shows the block diagram of a homodyne optical phase-locked loop. The master laser and the slave laser operate at the same optical frequency while the photodetector works as a phase detector. In this case the phase detector gain has the same value of the photodetector gain k_p, given by:

$$k_p = 2\,R\,\sqrt{P_m\,P_s} \tag{2.2.13}$$

Where P_m and P_s are the optical powers from the master and slave lasers respectively which are mixed at the photodetector and R is the photodetector responsivity.

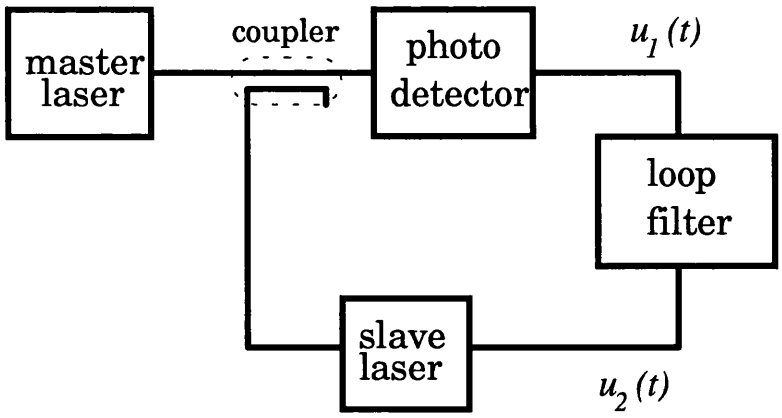

Figure 2.2.2: Homodyne optical phase-lock loop.

2.2.2- Heterodyne case:

Figure 2.2.3 shows the block diagram of a heterodyne OPLL. In this case, the optical frequencies of master and slave lasers are separated by a reference value ω_r .

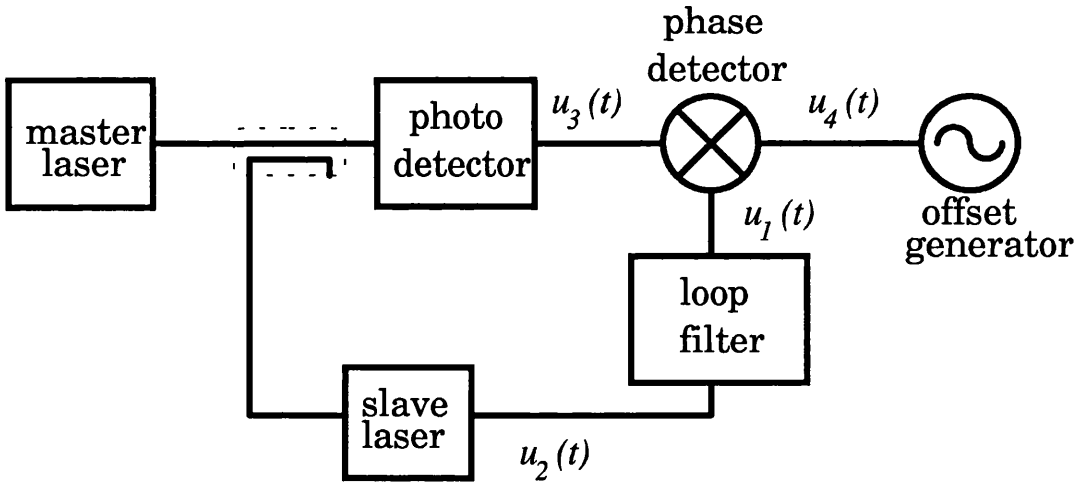

Figure 2.2.3: Heterodyne optical phase-lock loop.

The photodetector produces a signal centred on ω_r , $u_3(t)$:

$$u_3(t) = k_p \sin[\omega_r t + \phi_m(t) - \phi_s(t)] \qquad 2.2.14$$

In Chapter 3 it is shown how this relation can affected by misalignment of the two wavefronts. Assuming the system is locked, a microwave mixer operating as a phase detector gives the phase error signal $u_1(t)$ against a continuous single frequency reference $u_4(t)$ of amplitude C:

$$u_4(t) = \mathrm{C}\cos[\omega_r t + \phi_r(t)] \qquad 2.2.15$$

$$u_1(t) = k_p\, k_d \sin[\phi_m(t) - \phi_s(t) - \phi_r(t)] \qquad 2.2.16$$

Where k_d is a constant of the phase detector. In this case, the total gain k must include k_d and k_p as follows:

$$k = k_d\, k_p\, k_g\, k_s \qquad 2.2.17$$

The new phase error is given by:

$$\Phi_e(s) = \Phi_m(s) - \Phi_s(s) - \Phi_r(s) \qquad 2.2.18$$

2.3- Sources of Noise

Looking at the block diagram of a heterodyne OPLL, Figure 2.2.3, it is possible to identify the major sources of noise:

-phase noise of the master laser signal.
-phase noise of the slave laser signal.
-photodetector shot noise.
-phase noise of the offset reference signal.
-master and slave laser amplitude noise.
-other noise generated in some of the OPLL building blocks such as frequency mixers, wideband amplifiers, the phase detector and dc bias circuits.

In the analyses shown in this chapter, only the main sources of noise will be taken into account as they restrict the design of the system. The use of balanced receivers can reduce the effect of the intensity noise [Patzak 89], which is normally small (relative intensity noise between -140 and -150dB/Hz). For this reason and the fact that it can not be compensated by the action of OPLL, the intensity noise will not be considered in the analysis. It is possible to estimate the contribution of each of these noise sources towards the phase error Φ_e by using the loop transfer function as follows [Ohtsu 92]:

$$\Phi_e(s) = \left[N_m(s) - N_s(s) - N_r(s)\right]\left[1 - H(s)\right] + \left[N_{sn}(s)\right]\left[H(s)\right] \qquad 2.3.1$$

Where N_m is the master phase fluctuation, N_s is the slave laser phase fluctuation and N_r offset reference oscillator phase fluctuation. N_{sn} is the phase translated fluctuation due to the detector shot noise, which is given by multiplying the electrical shot noise by the phase detector constant. Figure 2.3.1 shows a block diagram of the linearised model of the heterodyne OPLL indicating the main sources of noise.

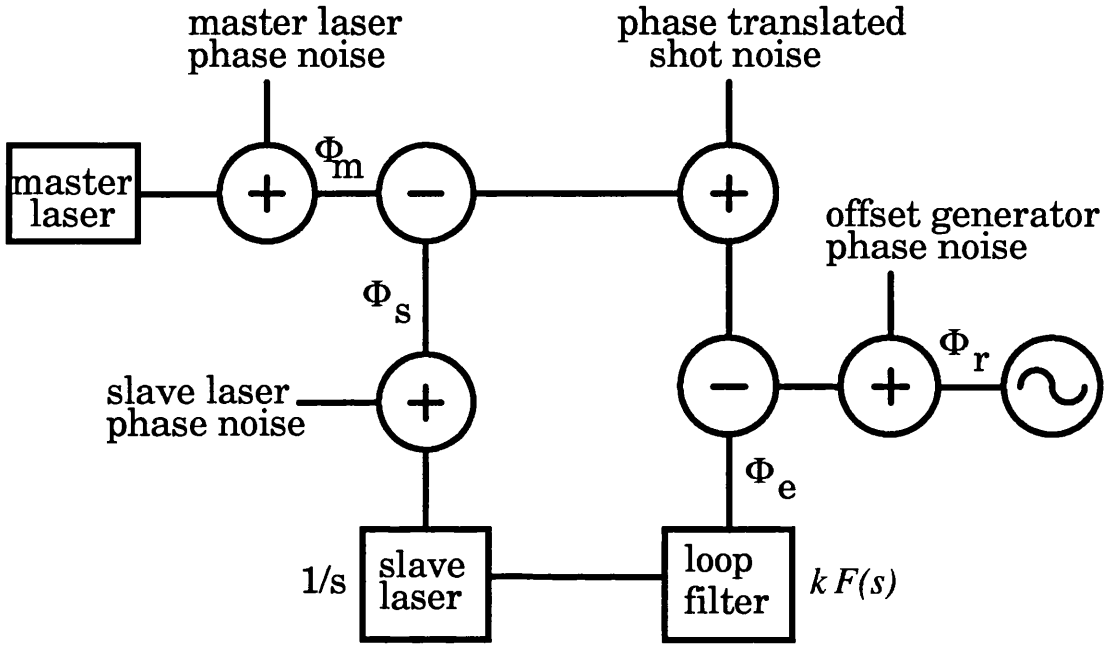

Figure 2.3.1: Block diagram of the OPLL indicating the main sources of noise.

The behaviour of the main sources of noise will be given by the double sided spectra of the master laser phase noise (S_m), slave laser phase noise (S_l) and detector shot noise (S_{sn}).

From now on, the phase noise of the offset frequency generator will not be taken into account since it is usually much smaller than the first three noise sources (the linewidth of a reference signal generator operating at a few GHz would not be expected to exceed 100Hz, while the laser linewidths are of the order of MHz). Other minor sources of noise are also neglected.

2.3.1- Laser Phase Noise

The phase noise introduced by both the master and slave lasers is the most important factor influencing the performance of an OPLL. The gain and bandwidth of the loop has to be tailored mainly according to the spectrum of the laser phase noise. If the noise bandwidth of the lasers is large, then wide loop bandwidth is required. The laser phase noise is here analysed in terms of frequency noise (FM noise).

Semiconductor laser FM noise usually consists of several components [Yamamoto 83] [Ohtsu 92]. The first main component is the frequency fluctuation originating from spontaneous emission resulting in white FM noise. The line *a* in Figure 2.3.2 represents the spectral density of such noise.

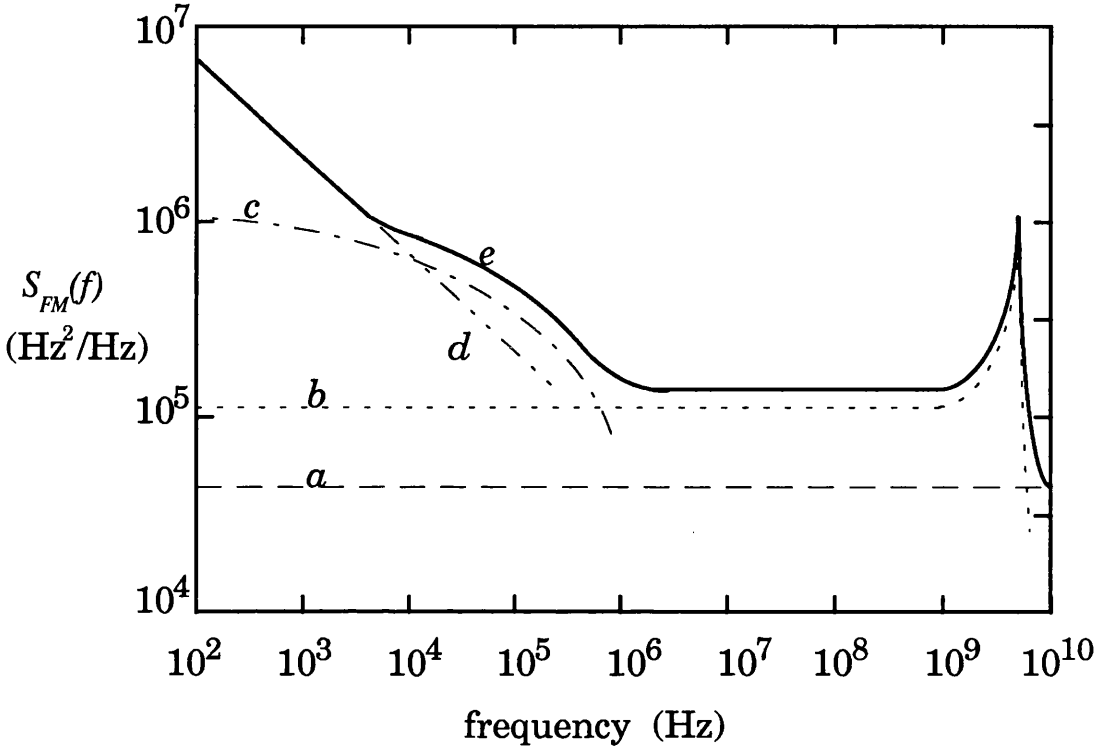

Figure 2.3.2: Schematic representation of the spectral density of a single mode semiconductor laser FM noise (e). The different components are due to:

a- spontaneous emission resulting in white FM noise.

b- fluctuation of the carrier density.

c- slow component due to self heating.

d- flicker noise or 1/f noise.

The second intrinsic source of noise is the fluctuation of the carrier density, represented by the curve *b* in Figure 2.3.2. This frequency noise is due to the variations of the refractive index of the device waveguide caused by the fluctuation of the carrier density, which is optically pumped by the spontaneous emission. The ratio between the spectral density of noise due to the fluctuation of the carrier density and due to spontaneous emission is normally represented by α^2, where α is the linewidth enhancement factor [Henry 82]. This factor is of the order of 2 to 9 and depends on the construction of each particular laser such as the waveguide structure and the material of the active medium. A peak appears in the spectral density of the carrier density

fluctuation noise at the relaxation oscillation frequency, normally above 1GHz, which depends on the carrier life time, the photon life time and the ratio between the injection current and the threshold current. The frequency noise (FM noise) and the intensity noise (IM noise) are correlated to each other via the carrier density fluctuation.

An additional component at low frequencies is originated by the drift of the longitudinal mode frequency, represented by the curve *c* in Figure 2.3.2. This slowly fluctuating component is due to self heating by the current variations induced by the carrier density fluctuation. Also at low frequencies, flicker noise or $1/f$ noise is present, represented by the curve *d* in Figure 2.3.2. One possible origin of the $1/f$ noise is carrier mobility fluctuation [Ohtsu 84]. Finally, the line *e* in Figure 2.3.2 represents the spectral densities of the FM noise $S_{FM}(f)$ [$Hz^2 \cdot Hz^{-1}$] [Yamamoto 83], which is related to the phase noise $S_{PH}(f)$ [$rad^2 \cdot Hz^{-1}$] by:

$$\frac{S_{FM}(f)}{f^2} = S_{PH}(f) \qquad 2.3.2$$

An analytical approximation for the spectral density of the FM noise is given by [Ohtsu 92] [$(rad/s)^2/Hz$]:

$$S_{FM}(f) = \frac{\delta f_{ST}}{\pi} + \frac{\delta f_{ST}}{\pi} \frac{\alpha^2 f_{FR}^4}{(f_{FR}^2 - f^2)^2 + (\gamma_e / 2\pi)^2 f^2} + \frac{\xi}{f} \qquad 2.3.3$$

Where δf_{ST} is the linewidth of the laser due to spontaneous emission given by the Schawlow-Townes's formula, α is the linewidth enhancement factor, f_{RF} is the resonance frequency, γ_e the damping constant of the laser, and ξ is the magnitude of the flicker noise.

Among the components of the laser FM noise, the low frequency components like the flicker noise are normally readily tracked with an OPLL as it usually is fast enough to track such slow frequency fluctuations. The effect of the resonance peak is not critical if the bandwidth of the OPLL system is not wider than this resonance frequency. In this case, it is sufficient to consider only the white component of the laser FM noise in the expression of the phase noise. The single sided spectral density of the master and slave laser phase noise can be approximated by [Grant 87] [Hodgkinson 85] [Steele 88]:

$$S_m(f) = \frac{\delta f_{mt}}{\pi f^2} \qquad [\text{rad}^2/\text{Hz}] \qquad 2.3.4$$

$$S_s(f) = \frac{\delta f_s}{\pi f^2} \qquad [\text{rad}^2/\text{Hz}] \qquad 2.3.5$$

Where δf_{mt} and δf_s are the FWHM linewidth of the master and slave lasers respectively. When the values of the laser linewidth are measured experimentally, not only is the spontaneous emission noise taken in account, but the effect of the carrier density fluctuations and the low frequency fluctuations are included, as the actual value of the linewidth is used.

2.3.2- Detector Shot Noise

Shot noise arises from the optical detection process due to the quantum nature of light. The spectral density of the shot noise is given by (neglecting the dark current):

$$S_{sna}(f) = 2\,e\,R\,(P_m + P_s) \qquad [\text{A}^2/\text{Hz}] \qquad 2.3.6$$

Where e is the electronic charge and R is the photodetector responsivity. The shot noise can be translated in terms of phase noise using equation (2.2.3):

$$P_{u_1}(s) = k_d^2\,[\Phi_m(s) - \Phi_s(s)] + S_{sn}(s) \qquad 2.3.7$$

Where P_{u1} is the power spectrum of the u_1 signal and k_p is the photodetector gain, given by:

$$k_p = 2\,R\sqrt{P_m\,P_s} \qquad 2.3.8$$

The phase translated shot noise spectral density for the linearised OPLL model is given by:

$$S_{sn}(f) = \frac{S_{sna}(f)}{k_p^2} = \frac{e\,(P_m + P_s)}{2\,R\,P_m\,P_s} \qquad [\text{rad}^2/\text{Hz}] \qquad 2.3.9$$

For heterodyne systems, the photodetector generates shot noise as given by $S_{sna}(f)$. However, the contribution of the shot noise is doubled because the phase locking is carried out with a heterodyne signal [Ohtsu 92]. In an heterodyne OPLL, using only an

analogue phase comparator, the spectral density of the phase translated shot noise is given by:

$$S_{sn}(f) = \frac{e\,(P_m + P_s)}{R\,P_m\,P_s} \qquad [\text{rad}^2/\text{Hz}] \qquad 2.3.10$$

2.4- The Loop Filter

In this section, different kinds of loop filter are analysed, corresponding to different types of PLLs: the first order, the modified first order and the second order loop.

2.4.1- First order loop

The first order loop is the most simple of the systems, containing a loop filter with the following transfer function:

$$F(s) = 1 \qquad 2.4.1$$

and a gain *k*. The open loop transfer function is given by:

$$G(s) = \frac{k}{s} F(s) \qquad 2.4.2$$

The Bode diagram of this system is given in Figure 2.4.1

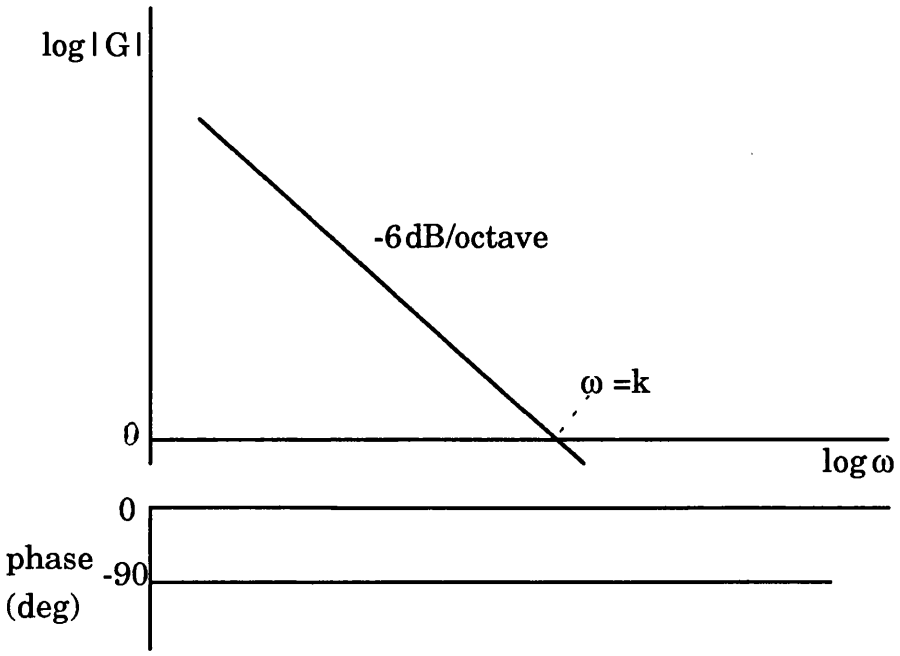

Figure 2.4.1: Bode diagram of the open loop transfer function G(jω) of a first order loop.

First order loops are not normally used because only the gain of the loop can be modified by the designer to adjust the characteristics of the system. The loop bandwidth can not be controlled independently form the loop gain and often large gain and narrow bandwidth are required for good tracking.

2.4.2- Modified first order loop

The modified first order loop contains a loop filter with the following transfer function:

$$F(s) = \frac{1}{s T_1 + 1} \qquad 2.4.3$$

Where the time constant T_1 is related to the filter cut-off frequency f_c by:

$$T_1 = \frac{1}{2\pi f_c} \qquad 2.4.4$$

This loop filter is basically an amplifier with a finite bandwidth given by f_c . The modified first order loop can be seen as a more realistic version of the ideal first order loop, where the filter only provides gain. In this case, the format of the loop transfer function is given by:

$$H(s) = \frac{k F(s)}{s + k F(s)} = \frac{\frac{k}{T_1}}{s^2 + \frac{s}{T_1} + \frac{k}{T_1}} \qquad 2.4.5$$

Strictly speaking, this kind of loop qualifies as a second order loop, as the denominator is of second degree. However, it is best regarded as a modified first order loop as its behaviour is similar to the first order loop [Gardner 79]. The loop natural frequency and damping factor are then given by:

$$\omega_n = \sqrt{\frac{k}{T_1}} \qquad 2.4.6$$

$$\zeta = \frac{1}{2}\frac{1}{T_1 \omega_n} = \frac{1}{2}\sqrt{\frac{1}{T_1 k}} \qquad 2.4.7$$

As there are only two parameters available (the amplifier gain and the cut-off frequency) and three loop parameter specifications to be met (k, ω_n and ζ), the loop parameters cannot be adjusted independently. If the gain is large and the bandwidth is small, the loop can become badly underdamped and the transient response will be poor [Gardner 79]. For the OPLL, wide bandwidth is generally an objective to improve laser phase noise suppression.

Figure 2.4.2 shows the Bode diagram of the open loop transfer function $G(j\omega)$ of a modified first order loop. It shows that adequate phase margin can easily be achieved in a high gain and wide bandwidth systems.

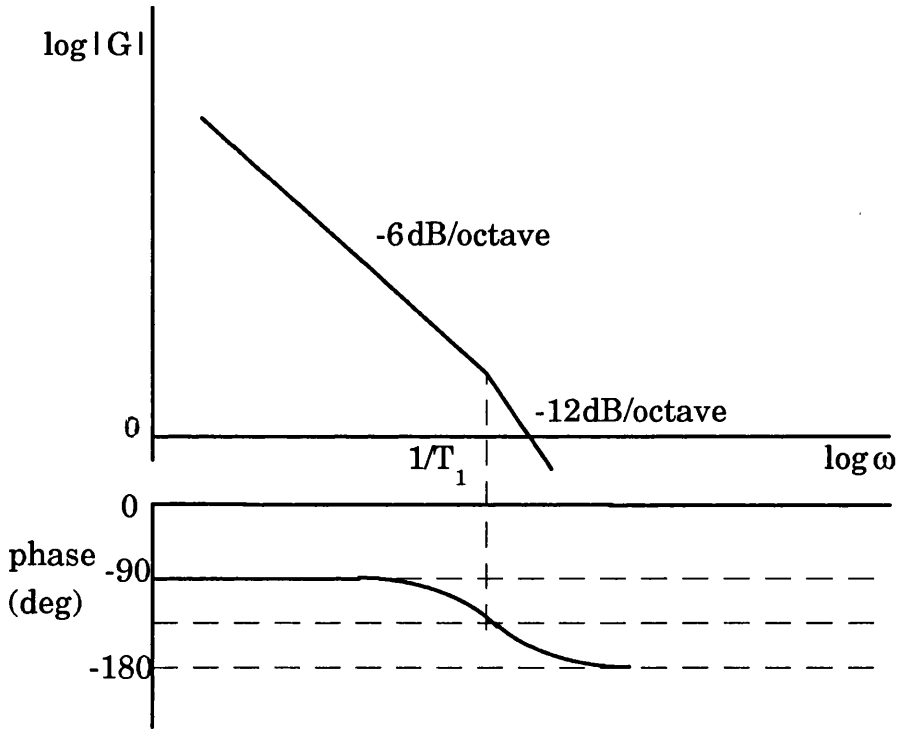

Figure 2.4.2: Bode diagram of the open loop transfer function G(jω) of a modified first order loop.

2.4.3- Second order loop

The most commonly used type of loop in phase-lock applications is the second order loop, in which a first order filter is used as the second pole is provided by the integration arising from the voltage-frequency conversion at the slave oscillator. The transfer function of such a filter is given by [Gardner 79]:

$$F_2(s) = \frac{1 + s\,T_2}{s\,T_1} \qquad 2.4.8$$

Second order loops are normally preferred due to the ability to alter the dynamic response by varying the loop parameters. The extra pole in the feedback loop gives good tracking of frequency drifts and the dynamic phase tracking can be adjusted to suit the application. The format of the loop transfer function is given by:

$$H(s) = \frac{k\,F(s)}{s + k\,F(s)} = \frac{\omega_n^2 + 2\,\zeta\,\omega_n\,s}{s^2 + 2\,\zeta\,\omega_n\,s + \omega_n^2} \qquad 2.4.9$$

Where k is the loop gain, ω_n is the loop natural frequency and ζ is the damping factor. For the second order loop, ω_n and ζ are given by:

$$\omega_n = \sqrt{\frac{k}{T_1}} \qquad 2.4.10$$

$$\zeta = \frac{T_2\,\omega_n}{2} \qquad 2.4.11$$

It is possible to adjust the loop natural frequency and the damping independently by varying the values of T_1 and T_2 . Figure 2.4.3 shows the Bode diagram of the open loop transfer function $G(j\omega)$ of an ideal second order loop.

However, when wide bandwidth is required, the finite bandwidth of the amplifiers and other components of the loop can cause phase lag and attenuation, negating the phase lead effect of the proportional gain part of the filter [Steele 88] as shown in Figure 2.4.4.

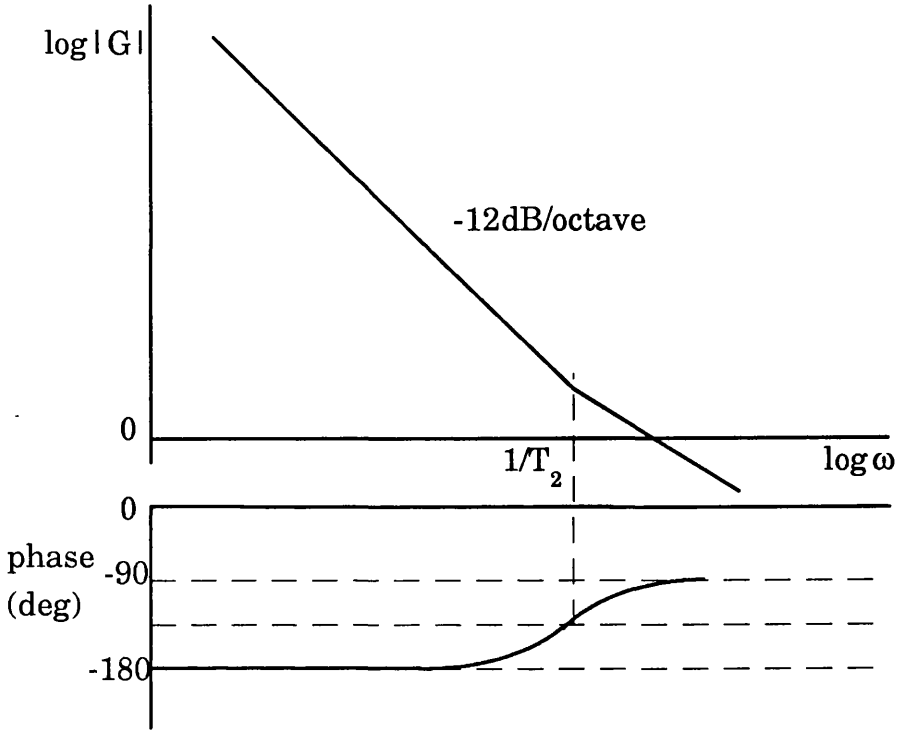

Figure 2.4.3: Bode diagram of the open loop transfer function G(jω) of an ideal second order loop.

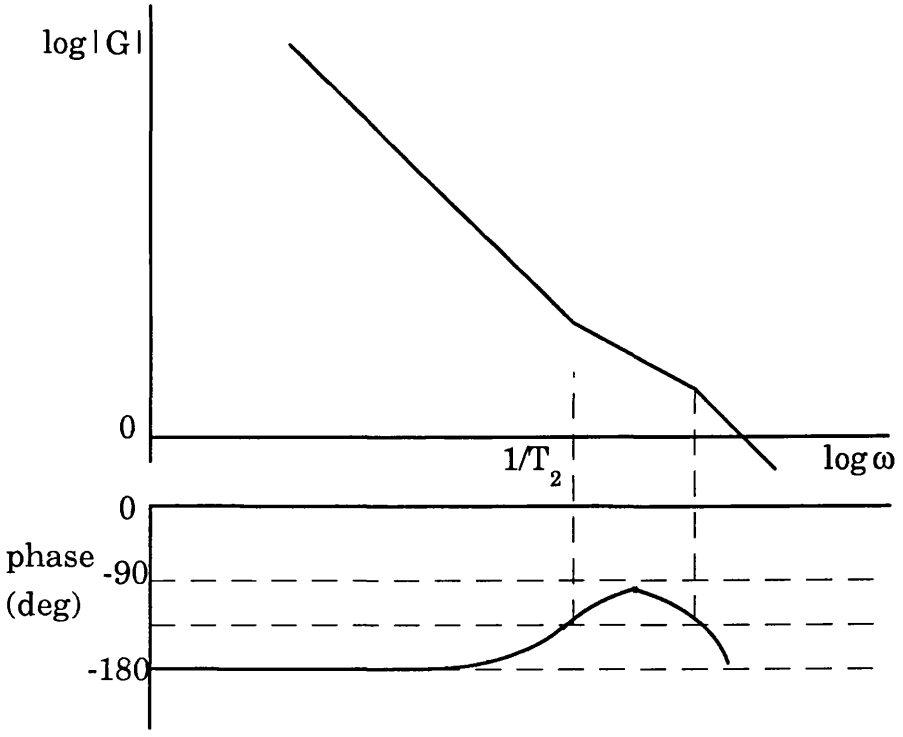

Figure 2.4.4: Bode diagram of the open loop transfer function G(jω) of second order loop with an extra time constant.

2.4.4- Third order loop

Third order loops are used in some PLL applications, being found more useful if the loop filter contains two cascaded integrators [Gardner 79]. The loop transfer function of such a system in given by:

$$H(s)=\frac{k\,F(s)}{s+k\,F(s)}=\frac{k\,(s^2+a_2\,s+a_3)}{s^3+k\,(s^2+a_2\,s+a_3)} \qquad 2.4.12$$

The Bode diagram of the open loop response is shown in Figure 2.4.5.

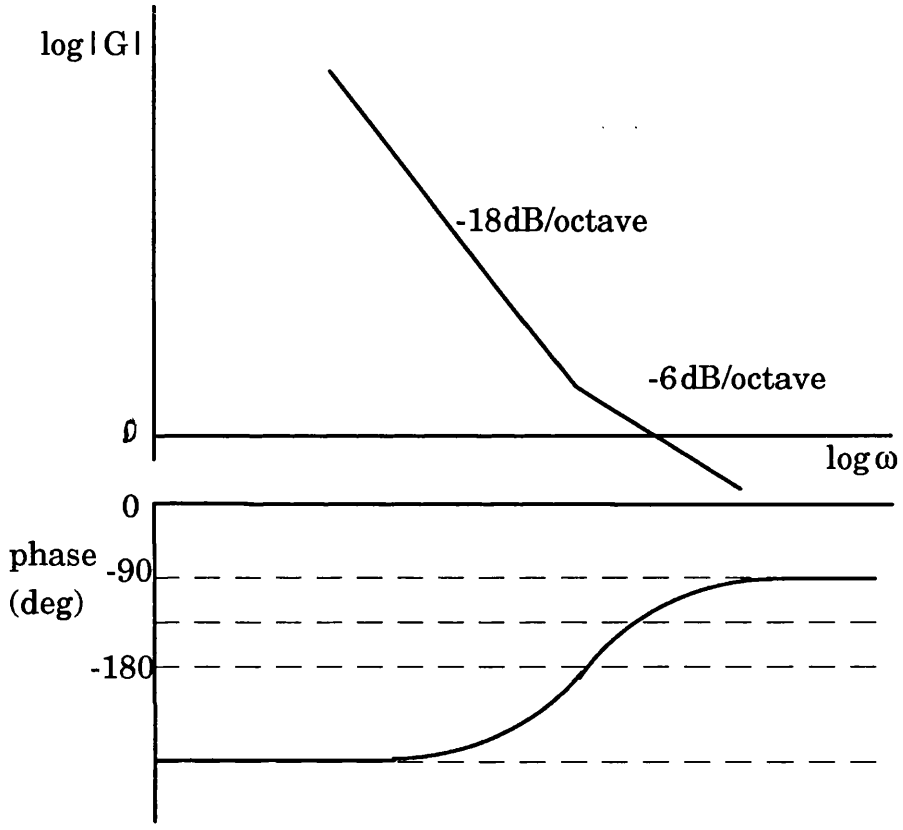

Figure 2.4.5: Bode diagram of the open loop transfer function G(jω) of a third order loop.

2.4.5- Comparison of loop filters

In radio and microwave frequencies applications of phase-lock techniques, the loop bandwidth is normally kept narrow to improve the tracking capabilities of the system

[Gardner 79]. As in first order loops, a reduction in loop bandwidth is invariably accompanied by a reduction of loop gain, they are not widely used due to their poor tracking ability. Second or third order loops can have high dc gains and narrow bandwidths thus improving the tracking and making them preferable.

However, in optical phase-lock loops using semiconductor lasers, wideband loops are necessary in order to handle the wideband phase noise from the lasers due to their wide linewidth. The use of wide bandwidths nevertheless can increase the effect of parasitic circuit elements, which can often cause a loop intended to be of a certain order to be actually of much higher order.

In real systems, amplifiers and other loop components have restricted bandwidth which could present a problem. One other concern is that the slave laser oscillator may not behave as a perfect integrator, as assumed so far. The real frequency modulation response of the slave laser can also introduce unexpected poles into the final transfer function. Loop delay time is another factor which can limit the loop bandwidth. In these situations, the extra poles introduced by the finite bandwidth of the loop components can reduce the phase margin of the system and make the loop unstable.

This plus being more difficult to stabilise, makes the use of third and higher order loops not very attractive for use in OPLLs. Also, the closed loop parameters of third and higher order active networks tend to be very sensitive to changes of gain and circuit components [Gardner 79]. First order loops can become modified first order loops when wide bandwidths are used, due to the bandwidth limitation of the components.

Modified first order loops and second order loops are then the best option for the construction of an OPLL using semiconductor lasers. For the experiment described in Chapter 5, the filter used is basically an amplifier with a given bandwidth making the system a modified first order loop. This decision was taken in order to obtain better control of the system stability, by improving control over the phase margin of the loop. The bandwidth limitations of practical loops make the use of a modified first order loop often preferable for OPLLs using other than very narrow (kHz) linewidth lasers [Steele 88]. This decision proved to be wise as the limitations imposed by the slave laser FM response brought the behaviour of the loop closer to that of a second order loop.

2.5- Loop delay time and Stability

2.5.1- Loop delay time:

So far the analysis presented has assumed negligible loop propagation delay time. However, for critically designed OPLLs when wide linewidth lasers are used and wide loop bandwidth is required, the assumption of zero time delay may result in instability problems. Roughly speaking, this assumption is not considered safe if the linewidths of the sources involved are above 500kHz [Grant 87]. Delay time can limit the maximum loop bandwidth and therefore affect the loop noise performance. In order to take the influence of the loop propagation delay time into account, a new variable T_d is introduced which represents the overall delay time of the loop, both optical and electrical. The Laplace transform of a time translation T_d is given by:

$$L\{\delta(t-T_d)\} = e^{-sT_d} \qquad 2.5.1$$

Where $\delta(\ )$ is the dirac function. As the system is considered linear, the various components of the loop delay can be combined together in one term and modelled as shown in the block diagram in Figure 2.5.1.

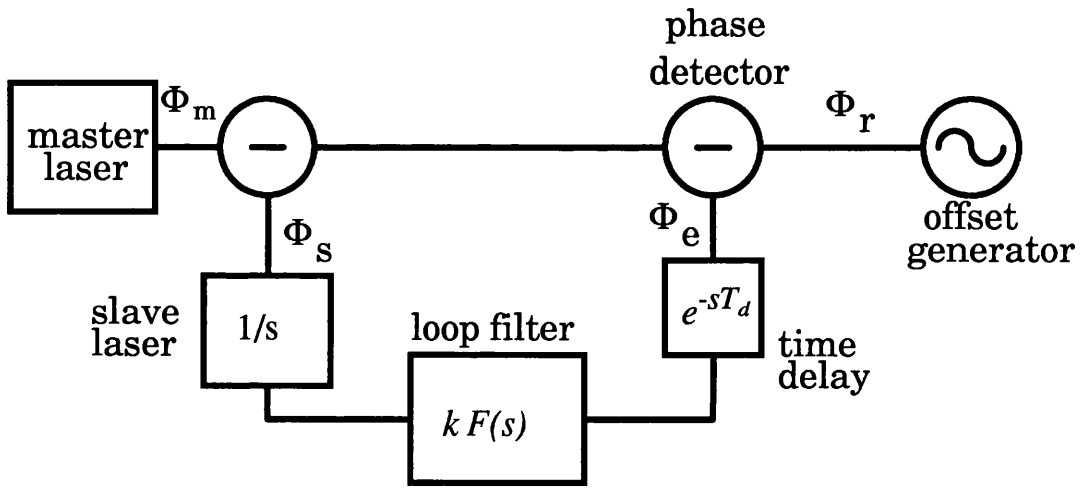

Figure 2.5.1: Block diagram of a heterodyne OPLL including a propagation delay time.

The new loop transfer function is then given by:

$$H(s) = \frac{k\,F(s)\,e^{-sT_d}}{s + k\,F(s)\,e^{-sT_d}} \qquad 2.5.2$$

2.5.2- Loop stability:

The primary concern of any control system designer is to avoid instabilities of the system which can result in oscillations and therefore loss of control. As an OPLL is basically an closed loop control system, stability conditions have to be set to assure proper operation. Loop delay time is an important factor to be considered when the loop stability is studied, as it modifies the phase of the open loop response towards reducing the phase margin.

One way of achieving stability is to calculate the values of the critical parameters of the loop for which the system starts to oscillate and then keep a safe margin from these critical values.

Modified first order loop:

It is possible to set the limits on loop stability by finding the critical value of ω for stability. This approach can be used to establish a stability criterion for a modified first order loop considering the effect of the loop propagation delay time. It is possible to consider the effect of this delay by including it into the open loop transfer function as follow:

$$G(s)=\frac{k}{s}\,\frac{e^{(-s\,T_d)}}{s\,T_1+1} \qquad 2.5.3$$

Where T_d is the total loop delay time. It is possible to calculate the maximum gain for a stable system by finding the critical angular frequency ω_{cr} , where the phase of the open loop transfer function crosses -π radians:

$$\frac{\pi}{2}+\omega_{cr}\,T_d+\tan^{-1}(\omega_{cr}\,T_1)=\pi \qquad 2.5.4$$

Using the following approximation: ($\omega_{cr}\,T_1<0.4$ for an error of less than 5%):

$$\tan^{-1}(\omega_{cr}\,T_1)\cong\omega_{cr}\,T_1 \qquad 2.5.5$$

The critical angular frequency ω_{cr} is given by:

$$\omega_{cr}=\frac{\pi}{2\,(T_d+T_1)} \qquad 2.5.6$$

As the open loop gain at this frequency must be less than one:

$$\frac{k}{\omega_{cr}} \frac{1}{\sqrt{1+(\omega_{cr} T_1)^2}} \leq 1 \qquad 2.5.7$$

The critical gain for a stable system k_{cr} can be calculated as:

$$k_{cr} = \omega_{cr} \sqrt{1+(\omega_{cr} T_1)^2} \qquad 2.5.8$$

A reduction of 10dB in loop gain is introduced to obtain a loop damping factor of 0.707 [Ward 81]. Thus, the final expression for the maximum gain of the system is:

$$k_m = \frac{\pi}{2\sqrt{10}\,(T_d + T_1)} \sqrt{1+\left(\frac{\pi T_1}{2\,(T_d + T_1)}\right)^2} \qquad 2.5.9$$

Figure 2.5.2 shows a plot of this equation, giving the maximum gain for a stable system k_m on a logarithmic scale for different values of loop delay time T_d in ns against the loop filter cut-off frequency $f_c = 1/(2\pi T_1)$, in GHz.

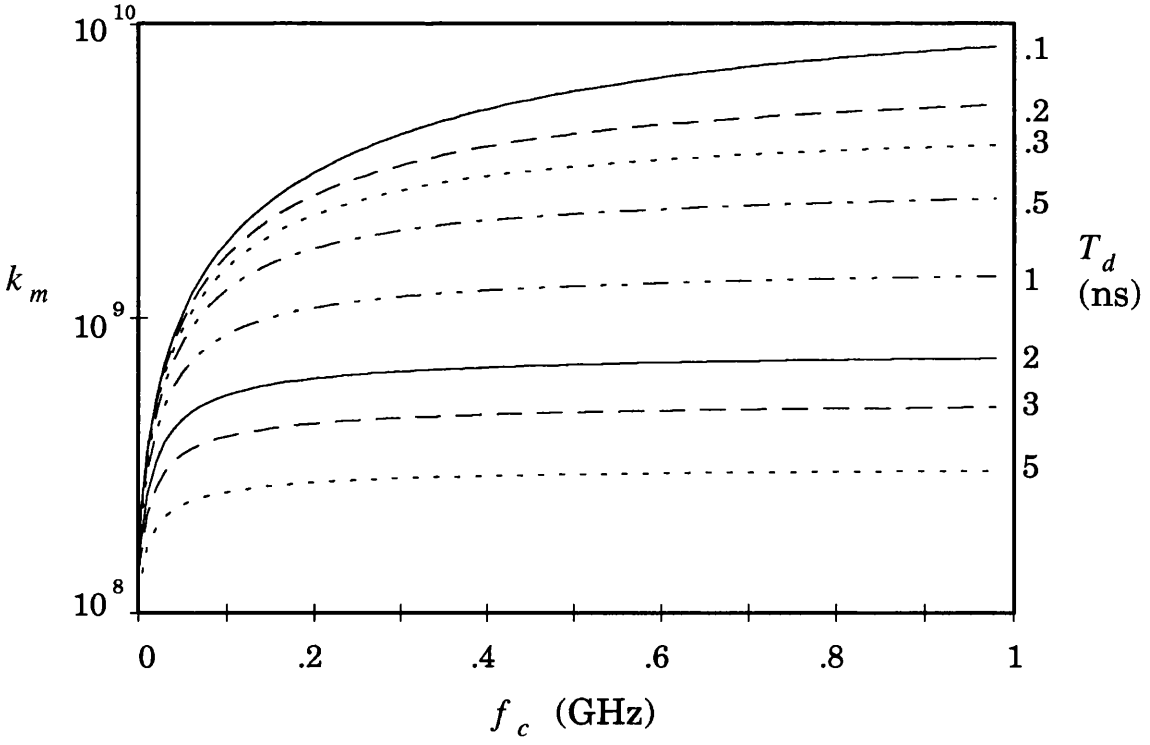

Figure 2.5.2: Maximum gain k_m (given by equation 2.5.9) for different values of loop delay time T_d against the loop filter cut-off frequency f_c.

Second order loop:

Considering the use of ideal components (infinite bandwidth amplifiers), it is possible to set the limits on loop stability by finding the critical value of ω for stability [Grant 87]. The presence of loop delay time changes the open loop transfer function from the original second order loop expression to:

$$G(s) = \frac{k\, e^{(-s\,T_d)}}{s} \frac{s\,T_2 + 1}{s\,T_1} \qquad 2.5.10$$

The system becomes no longer a second order loop and the definitions of loop natural frequency and damping factor are not valid [Kuo 87]. However, it is possible to define new parameters called relative natural frequency and relative damping factor as the natural frequency and damping factor of the loop when the effect of loop delay time is neglected:

$$\omega_{no} = \sqrt{\frac{k}{T_1}} \qquad 2.5.11$$

$$\zeta_o = \frac{T_2\,\omega_n}{2} \qquad 2.5.12$$

The open loop phase response (equation 2.5.10) reaches π rad at the critical frequency ω_{cr} given by:

$$\pi + \omega_{cr}\,T_d - \tan^{-1}(\omega_{cr}\,T_2) = \pi \qquad 2.5.13$$

For the gain to be less then 1 at this frequency:

$$\frac{\omega_{no}^2}{\omega_{cr}^2}\sqrt{1 + (\omega_{cr}\,T_2)^2} \le 1 \qquad 2.5.14$$

The condition which satisfies both equations is derived in Appendix 1, giving:

$$\omega_{no}\,T_d < \frac{\tan^{-1}\left(2\zeta_o\sqrt{2\zeta_o^2 + \sqrt{4\zeta_o^4 + 1}}\right)}{\sqrt{2\zeta_o^2 + \sqrt{4\zeta_o^4 + 1}}} \qquad 2.5.15$$

Making $\zeta_o = 0.707$:

$$\omega_{no} T_d < 0.736 \qquad 2.5.16$$

Substituting the value of ω_{no} , it is possible to calculate the critical value of gain allowed for a second order loop to be stable:

$$k_{cr} < 0.541 \frac{T_1}{T_d^2} \qquad 2.5.17$$

At the limit of the condition shown above, the loop operates in a critical situation, close to oscillation, making the real damping different form the value given by ζ_o . Again a 10dB decrease in gain has to be introduced to keep a safe margin from the critical value and to assure a damping factor above 0.707. The maximum gain is then given by:

$$k_m = \frac{k_{cr}}{\sqrt{10}} = 0.171 \frac{T_1}{T_d^2} \qquad 2.5.18$$

Figure 2.5.3 shows the variation of k_m/T_1 with the loop delay time. This illustrates the strong restrictions imposed on the loop gain by the presence of loop delay in order to keep the system stable.

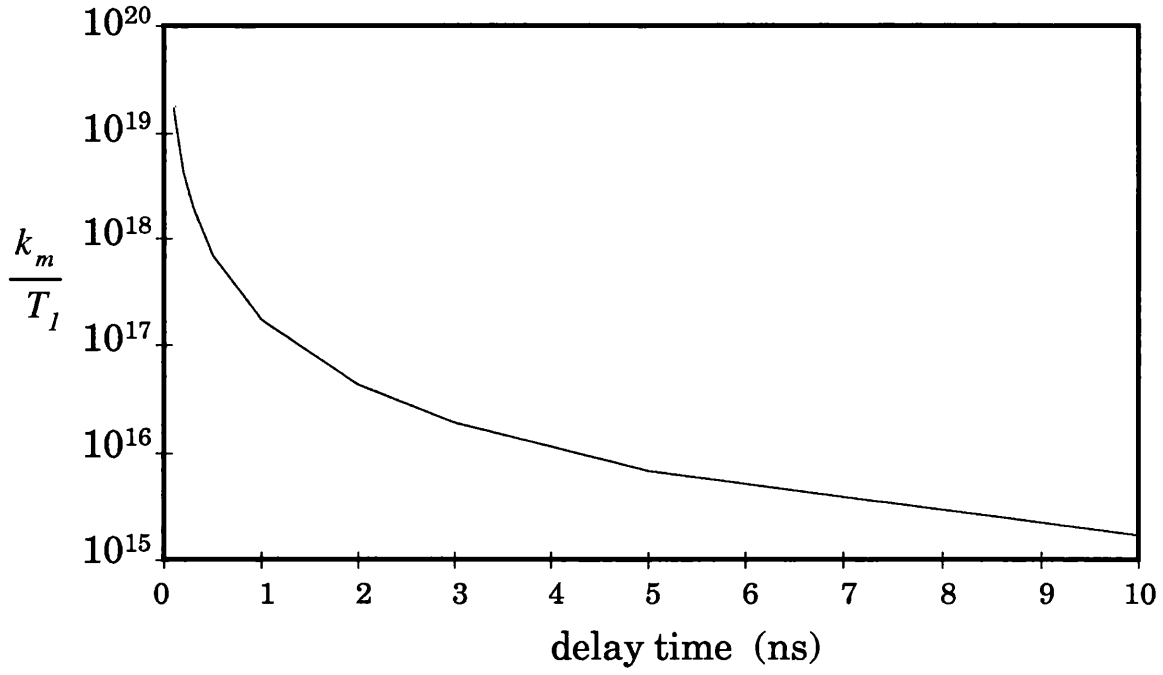

Figure 2.5.3: k_m/T_1 with the loop delay time for ζ_o=0.707.

However, it is possible to calculate k_m/T_1 for other values of ζ_o. Figure 2.5.4 show the variation of k_m/T_1 with the delay time for three different values of relative damping factor.

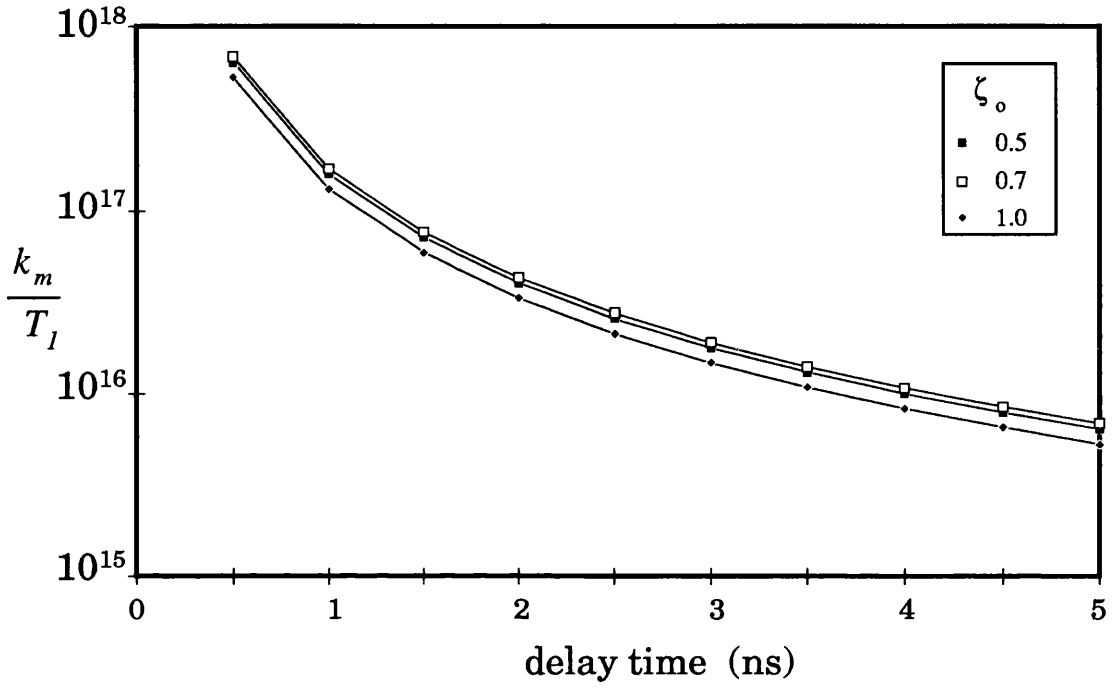

Figure 2.5.4: k_m/T_1 with the loop delay time for a second order loop for several values of relative damping factor.

2.6- Loop Performance

In order to design an OPLL, it is essential to relate the loop parameters to the overall performance of the system. For this reason, it is necessary to establish a criterion through which it is possible to measure the performance of the loop. In this section, three different criteria are considered: The spectrum of the phase error signal, the phase error variance and the average time between cycle slips.

The first criterion, the spectrum of the phase error signal (S_e), depends on the interpretation of a graph. However, it gives more information about the behaviour of the loop and can help in the design and optimisation of the system. The phase error variance (σ^2), is the most commonly used criterion and is useful since it gives in a single number the amount of phase noise still present in the phase error signal. The last criterion, the average time between cycle slips (T_{av}), is closely related to the phase

error variance, giving an easier understanding physical meaning to the parameter. As it takes into account the non linearity of the phase detector transfer function, this criterion is more suitable for dealing with loops having large amounts of phase noise, close to the linear limits. T_{av} can be used to establish the conditions for the loop to lock, at the beginning of the OPLL design. The employment of T_{av} first proposed in [Ramos 90] has already been used in [Fernando 90] and [Gliese 91].

2.6.1- Phase error signal spectrum

It is relatively easy to measure the spectral density of the phase error signal from an OPLL, as it is only necessary to connect a spectrum analyser to the output of the phase detector. This measurement is very important because from it all the other performance parameters can be abstracted. Thus it is desirable to be able to predict the shape of this spectrum.

The phase error for the loop, including phase noise of the optical signals and photodetector shot noise, can be taken from equation (2.3.1):

$$\begin{aligned}\Phi_e(s) = &\left[N_m(s) - N_s(s)\right]\left[1 - H(s)\right] \\ &+\left[N_{sn}(s)\right]\left[H(s)\right]\end{aligned} \qquad 2.6.1$$

The spectrum of the phase error $S_e(f)$ can be calculated by using the phase noise spectrum of each source of noise given in section 2.3:

$$\begin{aligned}S_e(f) = &\left[S_m(f) + S_s(f)\right]\left[\left|1 - H(j2\pi f)\right|\right]^2 \\ &+\left[S_{sn}(f)\right]\left[\left|H(j2\pi f)\right|\right]^2\end{aligned} \qquad 2.6.2$$

Where $H(j2\pi f)$ is the closed loop frequency response of the OPLL, $S_{sn}(f)$ is the detector shot noise and $S_m(f)$ and $S_s(f)$ are the double sided spectra of the master and slave lasers phase noise. It is assumed that the offset frequency source phase noise can be made small relative to the laser phase noise.

Using equation 2.6.2 it is possible to estimate the spectrum of the phase error signal S_e by substituting the expressions of the master and slave lasers phase noise spectrum, shot noise and the loop transfer function. Substituting the expressions of $S_{sn}(f)$, $S_m(f)$ and $S_s(f)$ given in Section 2.3 into equation (2.6.2):

$$S_e(f) = \frac{\delta f_{mt} + \delta f_s}{\pi} \left| \frac{1 - H(j2\pi f)}{f} \right|^2 + \frac{e\,(P_m + P_s)}{R\,P_m\,P_s} |H(j2\pi f)|^2 \qquad 2.6.3$$

Figures 2.6.1*a* and *b* show S_e and the spectrum of the phase noise of the lasers S_l (which is the sum of the spectrum of the master and slave lasers). The summed linewidth is fixed at 5MHz and the loop delay time at 3ns. Figure 2.6.1(a) corresponds to a modified first order loop in which the loop filter cut-off frequency is 500MHz. Figure 2.6.1(b) corresponds to a second order loop.

The first curve of S_e was plotted using the value of loop gain k_m when the value of the critical gain k_{cr} was divided by $10^{1/2}$ (which is 3.16) introducing a reduction of 10dB to the critical gain in order to keep the loop damping factor above 0.707. The second curve uses half of k_{cr} , the third curve uses $k_{cr}/1.5$ and the last curve uses k_{cr}. Note that as the gain k is increased and gets closer to its critical value, the spectrum of the phase error signal starts peaking at frequencies close to the loop natural frequency. For values of loop gain above the critical, this peaking tends towards infinity and the loop starts to oscillate.

Comparing Figure 2.6.1 (a) and (b), it can be seen that the second order loop presents much lower phase noise at low frequencies due to the integrator in the loop filter, while the modified first order loop presents finite low frequency phase noise. However, the modified first order loop displays lower phase noise levels at frequencies near the loop natural frequency and allow the use of wider loop bandwidth before it becomes unstable.

One way of estimating the loop bandwidth is to find the frequency at which the spectrum of the phase error for the locked loop becomes higher than the free-running phase error signal spectrum. In other words, the frequency where S_e crosses S_l, as indicated in Figure 2.6.1(a) and (b) (in this case, at about 24MHz and 22MHz for the first curve of each (a) and (b) plots respectively). However for high values of loop gain, when the damping factor is low, the loop natural frequency is more easily determined, what can be done by observing the peaking frequency of the phase error signal spectrum.

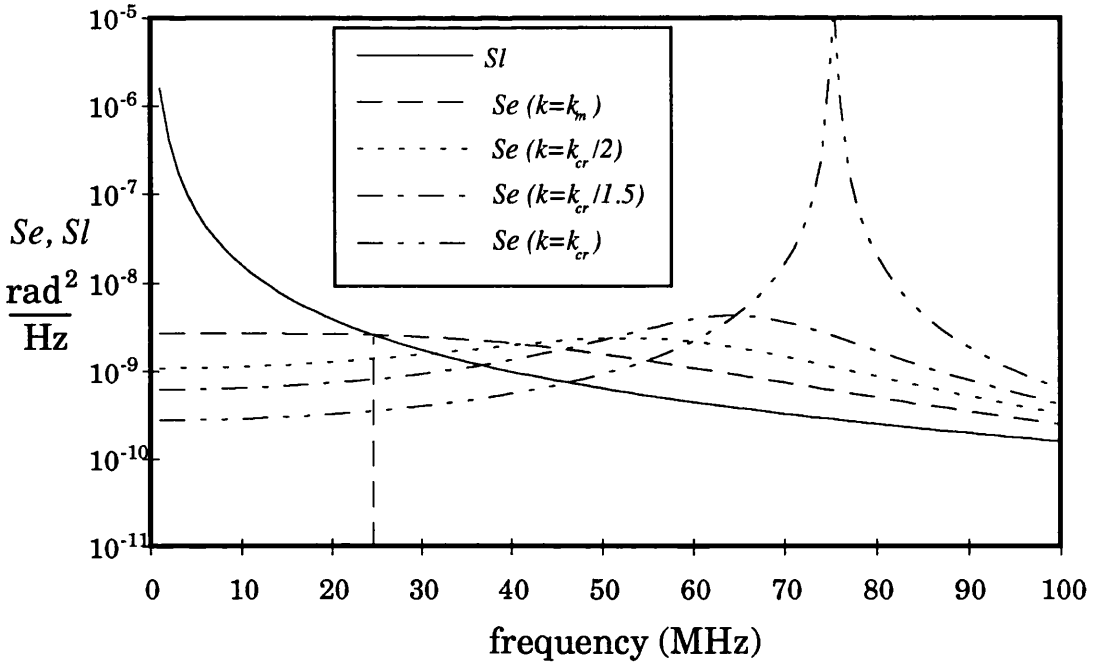

Figure 2.6.1(a): Spectrum of the phase error signal S_e for a modified first order loop for several values of loop gain. The summed spectrum of the phase noise of the lasers S_l is also shown.

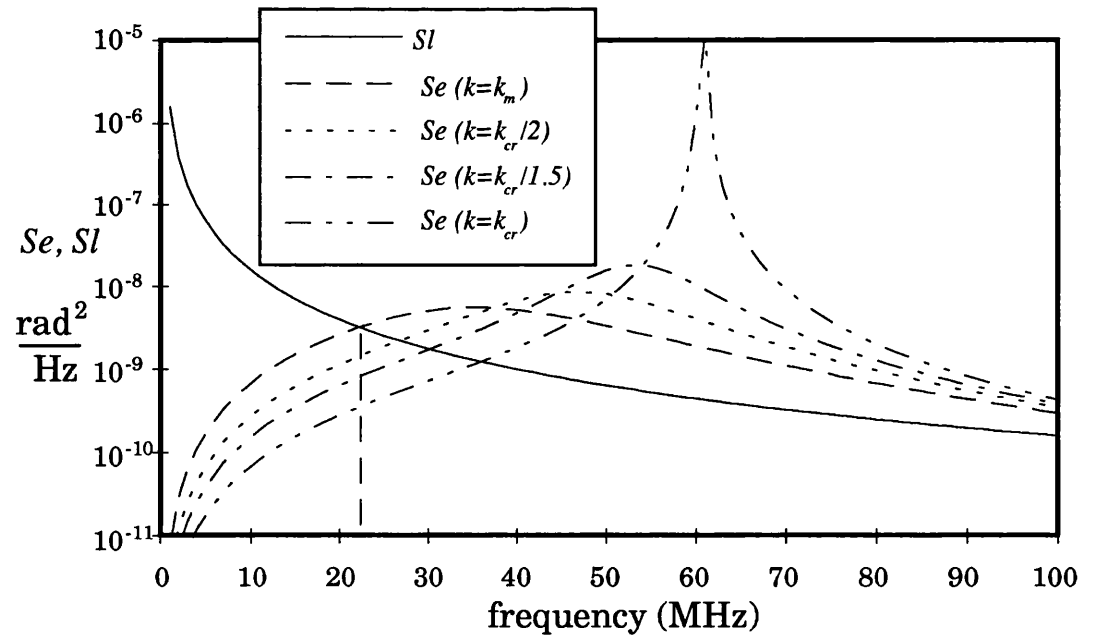

Figure 2.6.1(b): Spectrum of the phase error signal S_e for a second order loop for several values of loop gain. The summed spectrum of the phase noise of the lasers S_l is also shown. ζ_o=0.707.

This modelling, however, does not take into account the non uniform frequency response of loop components such as the phase detector and the slave laser FM response, which can introduce significant changes to the graphs in Figure 2.6.1. The slave laser FM response was considered to be flat for all frequencies in the analysis so far. However, this is not the case for most current tuned semiconductor laser sources, as will be discussed in Chapter 3.

In Section 2.5.2 it was shown how to calculate the maximum gain k_m in a second order loop for different values of relative damping factor. Figure 2.6.2 show the spectrum of the phase error signal *Se* using k_m for ζ_o = 0.5, 0.707 and 1.0, and for the free running case *Sl*.

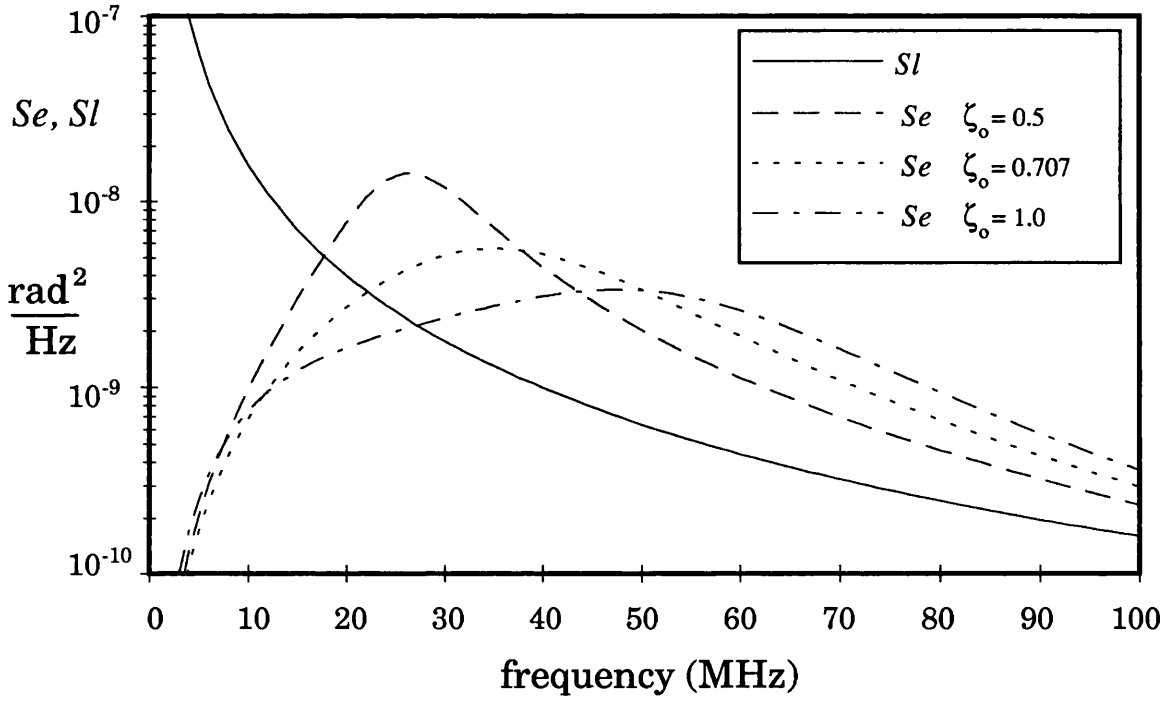

Figure 2.6.2: Spectrum of the phase error signal S_e for a second order loop for several values of relative damping factor. The summed spectrum of the phase noise of the lasers S_l is also shown.

2.6.2- Beat signal spectrum

In order to know the spectral shape of the detected beat signal between the master and slave lasers in a heterodyne OPLL, some approximations are made to simplify the calculations. The phase error signal coming from the phase error amplifier is injected into the slave laser which is tuned accordingly so that the error is minimised. This is equivalent to saying that the slave laser is frequency modulated by the phase error signal. Assuming that the modulation index β is small enough, $\beta<0.2$, it is possible to make the so called narrow band FM approximation. In this approximation it is assumed that for each frequency of the input signal spectrum there is a corresponding component at the output proportional to the modulation index. The details of this approximation are given in Appendix 2, where the expression to estimate the detected power spectral density of the beat signal $S_b(\omega)$ from the phase error spectrum $S_e(\omega)$ is derived, given by:

$$S_b(\omega) = 4\, r_l\, R^2\, A^2\, I_1\, I_2 \frac{k_\omega^2(\omega)}{k_d^2} \frac{S_e(\omega)}{\omega^2} \qquad 2.6.4$$

Where r_l is the photodetector load resistance, R is the photodetector resposivity A is the photodetector illuminated area, I_1 and I_2 are the optical intensity of the slave and master lasers, $k_\omega(\omega)$ is the frequency response of the slave laser and k_d is the phase detector gain.

Assuming the frequency response of the slave laser is uniform for all frequencies and equal to a constant k_ω , the spectrum of the beat signal will be proportional to the spectrum of the error signal divided by ω^2. Figures 2.6.3(a) and (b) show such spectrum for a modified first order loop (a) and for a second order loop (b) (ζ_o=0.707) respectively. The summed linewidth is fixed at 5MHz and the loop delay time at 3ns. For each case, several values of gain were used as in Figure 2.6.1. A normalised resolution bandwidth of 1Hz is assumed.

Figure 2.6.4 shows the estimation of the beat signal spectra S_e/ω^2 for a second order loop, for three different values of relative damping factor, ζ_o=0.5, 0.707 and 1.0, using the value of k_m/T_1 calculated as in Section 2.5.2 for each value of ζ_o.

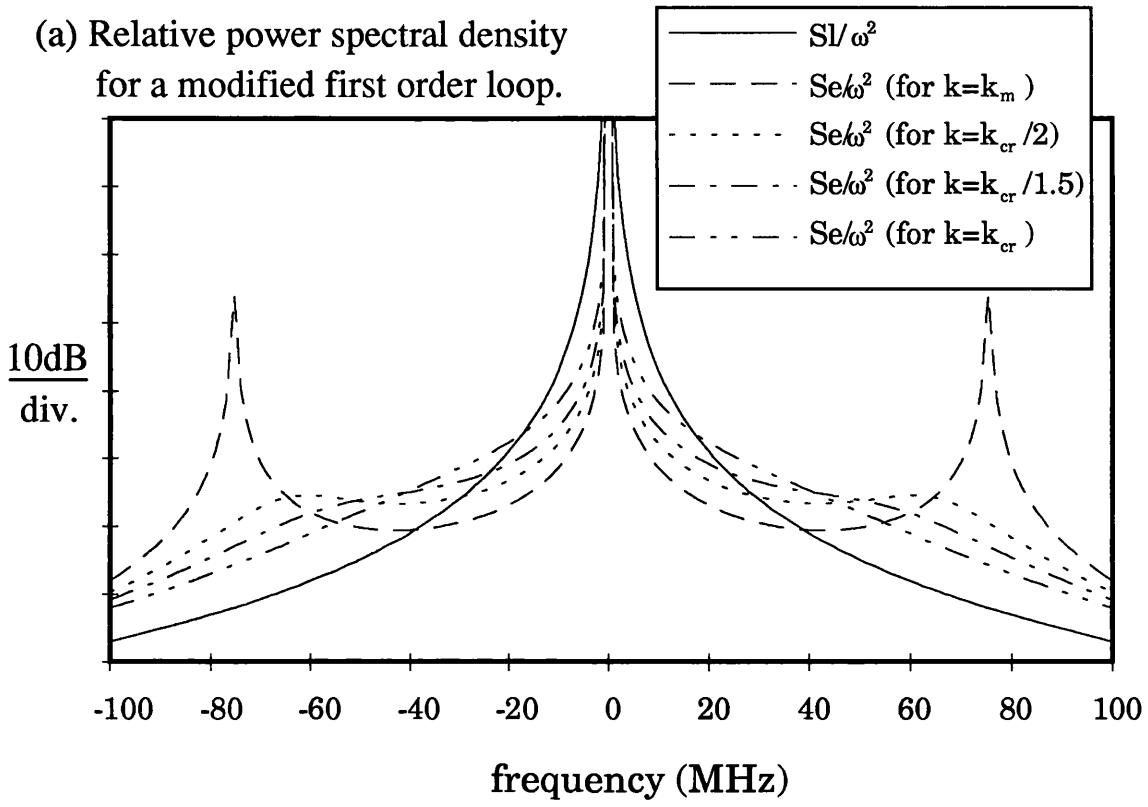

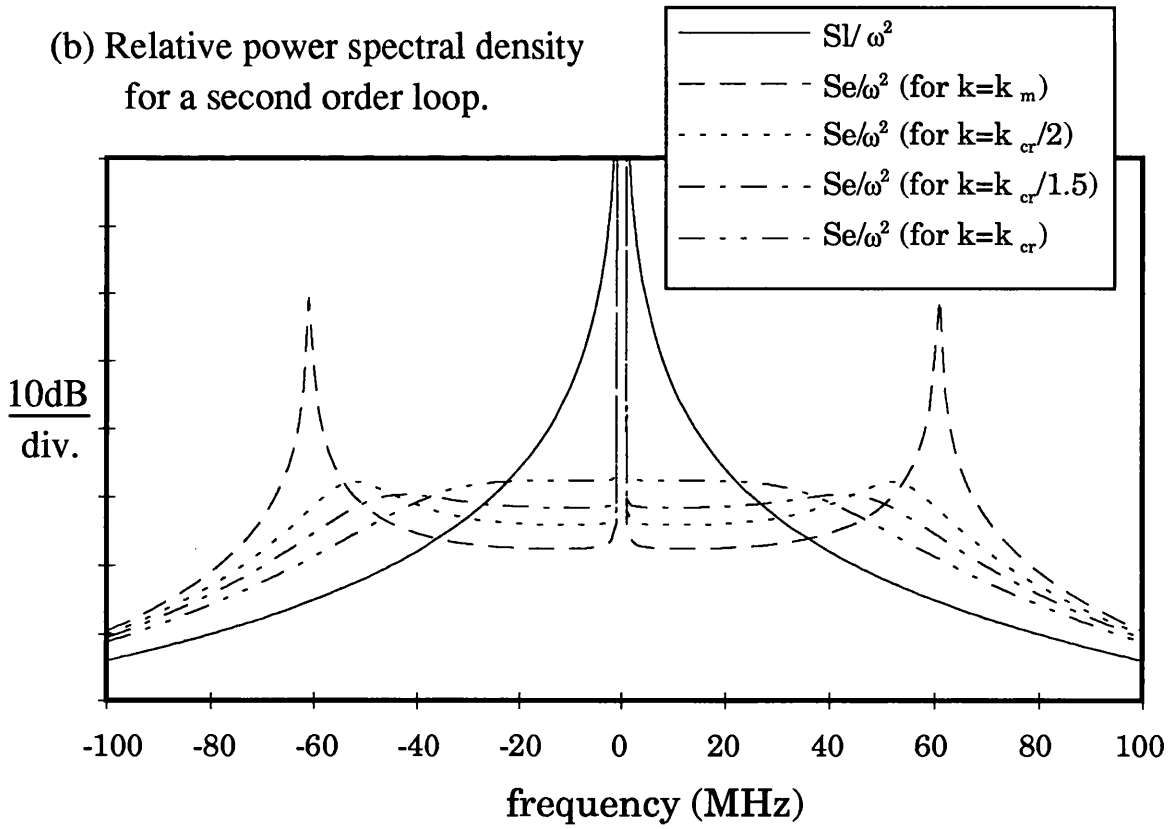

Figure 2.6.3: Estimation of the beat signal spectra for several values of loop gain: (a) for a modified first order loop and (b) for a second order loop, ζ_o=0.707.

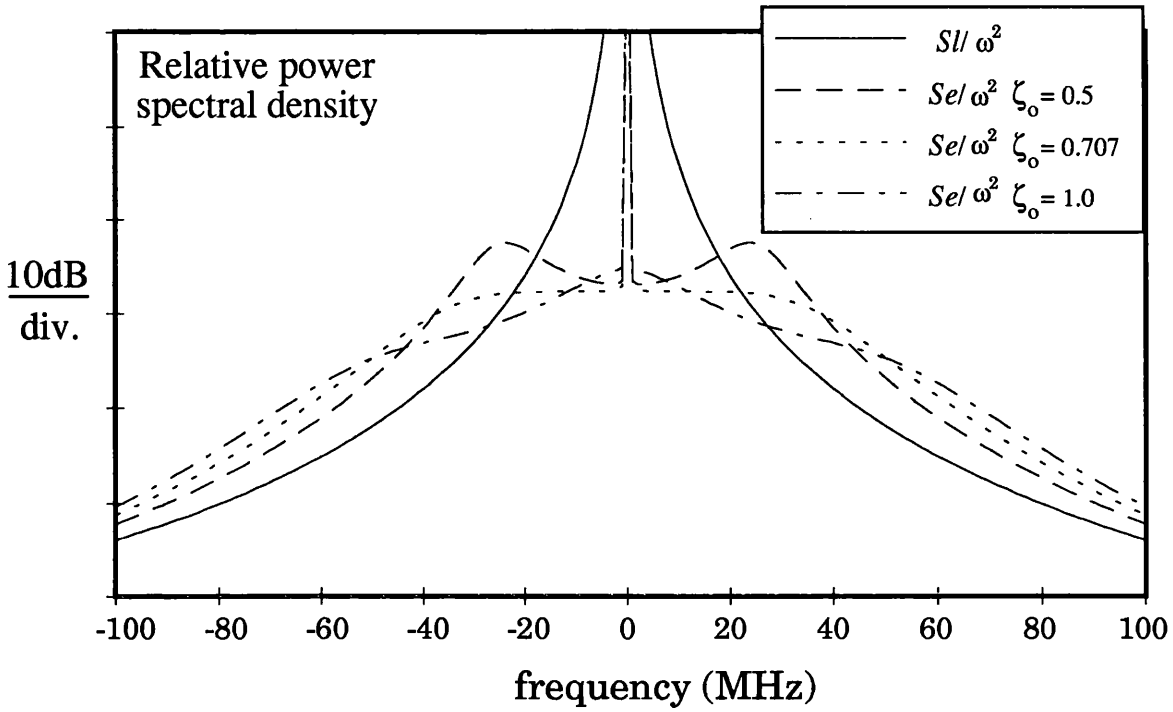

Figure 2.6.4: Estimation of the beat signal spectra for several values of relative damping factor for a second order loop.

2.6.3- Phase error variance

The variance is a statistical parameter which gives the average value of the square of the deviation of a variable in relation to its mean value. It is normally used as a measure of the spread of a distribution. It is very convenient to use this parameter to evaluate the quality of phase locking, as it is possible to calculate the variance of the error signal relative to its ideal value (zero radians). In order to estimate the phase error variance theoretically, it is necessary first to establish an expression for the phase error signal and relate it to different sources of noise in the loop.

As the spectral density of the squared phase error $S_e(f)$ is already the distribution of the square of the deviation of the phase, the variance of the phase error can be calculated by the integration of $S_e(f)$ over the whole spectrum, giving the following expression [Hodgkinson 85] [Grant 87] [Ohtsu 92]:

$$\sigma^2 = \int_0^\infty [S_m(f) + S_s(f)]\,[|1 - H(j2\pi f)|]^2\, df + \int_0^\infty [S_{sn}(f)]\,[|H(j2\pi f)|]^2\, df \qquad 2.6.5$$

Substituting the expressions for $S_{sn}(f)$, $S_m(f)$ and $S_s(f)$ given in section 2.3 into equation (2.6.3):

$$\sigma^2 = \frac{\delta f_{mt} + \delta f_s}{\pi} \int_0^\infty \left| \frac{1 - H(j2\pi f)}{f} \right|^2 df + \frac{e(P_m + P_s)}{R P_m P_s} \int_0^\infty |H(j2\pi f)|^2 df \qquad 2.6.6$$

From this equation two integrals can be isolated: I_p given by:

$$I_p = \int_0^\infty \left| \frac{1 - H(j2\pi f)}{f} \right|^2 df \qquad 2.6.7$$

and the loop noise bandwidth B_n, given by:

$$B_n = \int_0^\infty |H(j2\pi f)|^2 df \qquad 2.6.8$$

Equation (2.6.6) can be rewritten:

$$\sigma^2 = \frac{\delta f \, I_p}{\pi} + \frac{e(P_m + P_s) B_n}{R P_m P_s} \qquad 2.6.9$$

Where δf is the summed linewidth:

$$\delta f = \delta f_{mt} + \delta f_s \qquad 2.6.10$$

Where δf_{mt} and δf_s are the FWHM linewidth of the master and slave lasers respectively. Figure 2.6.5 shows the phase error variance for a modified first order loop as function of the loop filter cut-off frequency for several values of loop delay time, plotted using numerical integration to obtain I_p and B_n. The value of the loop gain is the maximum k_m for each point. In Figure 2.6.5(a) the summed linewidth is fixed at 5MHz, while in Figure 2.6.5(b) two sets of graphs are given for 2 and 10MHz summed linewidth. The values of R=0.35, P_m=1μW and P_s=1μW were fixed to reduce the number of variables for the graphs in this chapter.

From Figure 2.6.5, it is possible to see that the influence of the loop delay time on the overall loop performance becomes considerably stronger when wide bandwidth filters are used, as the lines corresponding to each value of delay diverge from each other

with an increase of f_c. If the summed linewidth is 10MHz and the loop filter bandwidth is below 5MHz, the phase error variance reaches the critical value of 2.46rad^2 ($\pi^2/4$ rad^2), unless narrower linewidth lasers are used (as shown in Figure 2.6.5(b)). Above this critical value the loop is considered out of lock, though good locking requires phase error variances of the order of 0.01rad^2 , as explained in Section 2.6.

It is important to notice that the value of phase error variance goes down sharply with increasing loop bandwidth until a certain value of f_c (in this case about 100MHz), above which σ^2 becomes less and less sensitive to f_c. Above this specific value of f_c, the influence of the laser phase noise towards the deterioration of the loop performance is overtaken by the influence of the detector shot noise. This behaviour can be explained by the expression for the phase error variance, as the component containing the contribution of the lasers phase noise is multiplied by $|1-H(j2\pi f)|^2$, while the shot noise is multiplied by $|H(j2\pi f)|^2$. So, an increase of loop bandwidth tends to suppress the influence of the laser phase noise, but at the same time it allows more shot noise into the system. Theoretically it would be possible to operate using a loop with an optimum bandwidth, however in practice this value of f_c would be prohibitively high as the phase noise generated by the lasers is normally much larger than the shot noise.

Figure 2.6.6(a) gives the phase error variance of a modified first order loop as function of the loop delay time for several values of loop filter cut-off frequency, where maximum loop gain k_m is calculated for each point and the summed linewidth is fixed at 5MHz. It shows that there is an almost linear relation between the phase error variance and loop delay time for the loop design. Figure 2.6.6(b) shows the phase error variance for a second order loop as function of loop delay time for relative damping factor ζ_o= 0.5, 0.707 and 1.0. It was also obtained by using numerical integration to obtain I_p and B_n and maximum value of the loop gain k_m for each point. As the value of the phase error variance can be changed by varying the integration interval of I_p and B_n , an interval of ten times the natural frequency is used.

Considering the curves in Figure 2.6.6(a) and (b) to be linear, it is possible to calculate the inclination of these curves which gives the degradation rate of the phase error variance with the loop delay time. This rate is about 0.057rad^2/ns for the modified first order loop curves and 0.08rad^2/ns for the ζ_o= 0.707 second order loop curve, 0.076rad^2/ns for the ζ_o= 0.5 and 0.062rad^2/ns for the ζ_o= 1.0 curve. This means that the curves in Figure 2.6.6(b) are steeper than those in Figure 2.6.6(a), indicating that second order loops are more sensitive to changes of loop delay time than modified first order loops. For second order loops, lower sensitivity to delay time is observed when the system is critically damped (ζ_o=1).

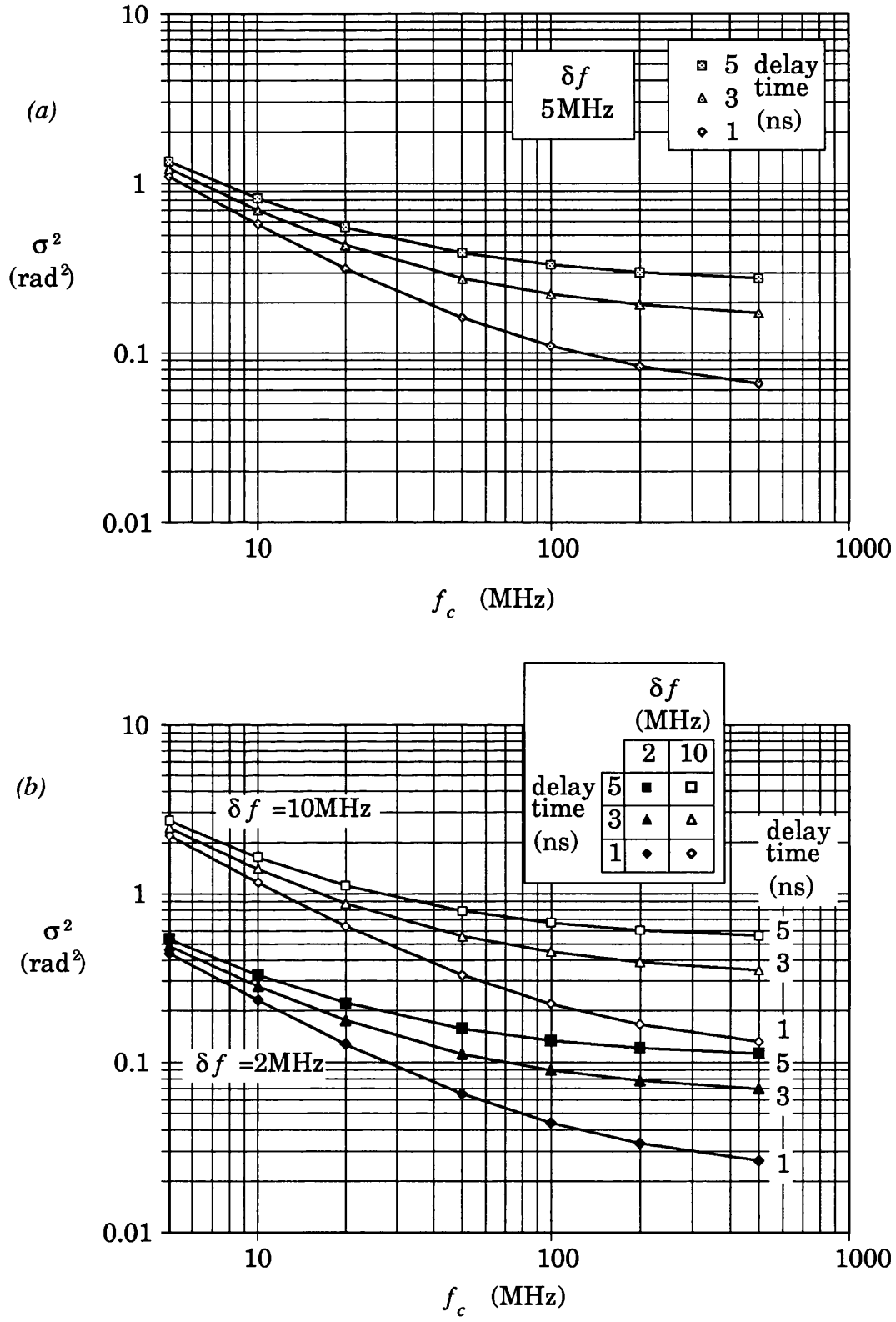

Figure 2.6.5: Phase error variance for a modified first order loop as function of the loop filter cut-off frequency for several values of loop delay time (maximum loop gain k_m for each point):
(a) Summed linewidth δf= 5MHz; (b) Summed linewidth δf= 2 and 10MHz.

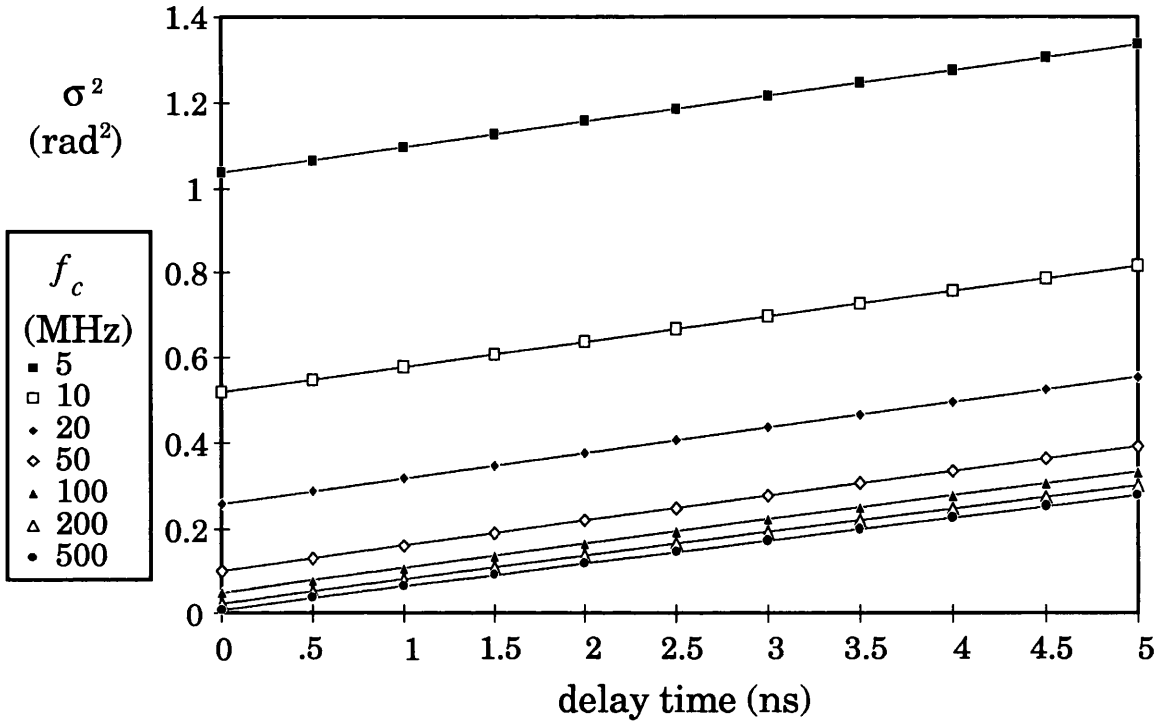

Figure 2.6.6(a): Phase error variance for a modified first order loop as function of the loop delay time for several values of loop filter cut-off frequency (maximum loop gain k_m for each point).

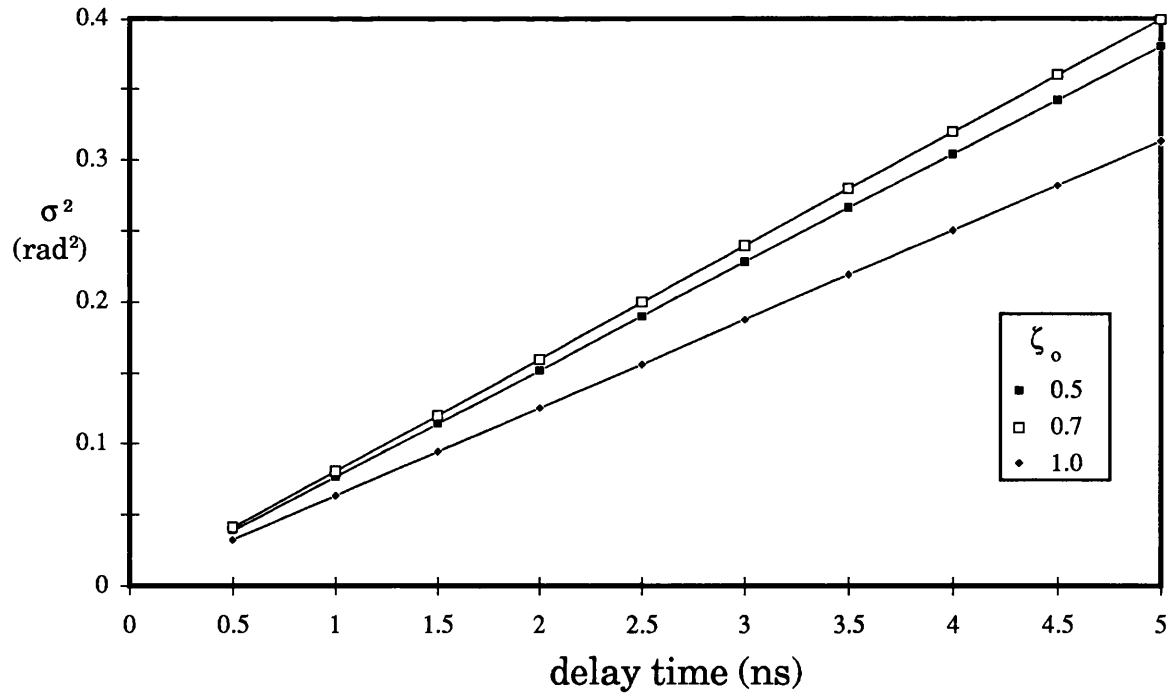

Figure 2.6.6(b): Phase error variance for a second order loop as function of the loop delay time for several values of relative damping factor (maximum loop gain k_m for each point).

From Figure 2.6.6(b) it is possible to see that a change in relative damping factor has the effect of changing the influence of the loop delay time on the phase error variance. Figure 2.6.7 shows how the phase error variance varies with ζ_o for a fixed loop delay time of 3ns, where the maximum loop gain k_m is calculated for each point and the summed linewidth is fixed at 5MHz. the phase error variance is seen not to be a strong function of ζ_o. However, a marginally better performance can be achieved when the system is critically damped (ζ_o=1).

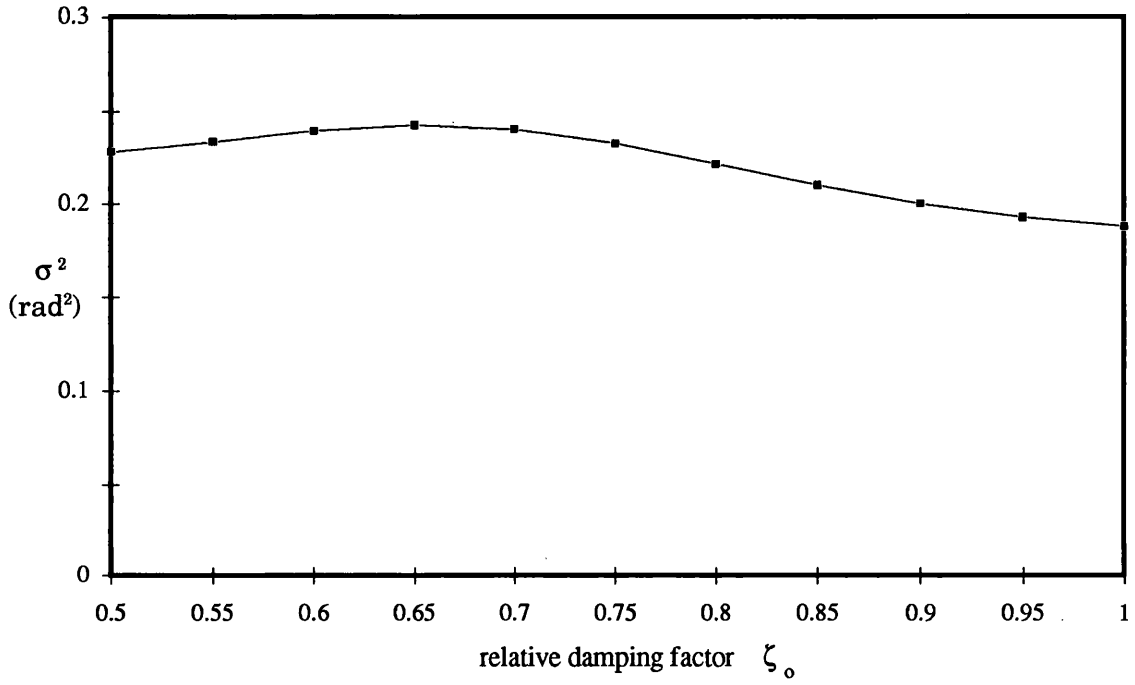

Figure 2.6.7: Phase error variance as function of ζ_o. Loop delay time 3ns, summed linewidth 5MHz, maximum loop gain k_m is calculated for each point.

2.6.4- Cycle slipping criterion

It is important to remember that at the beginning of this chapter an approximation was made by considering the transfer function of the phase detector to be linear. However, the response of the normally used analogue phase detector is sinusoidal as given by Equation (2.2.3) and can only be considered linear for small values of phase error. However, for marginally operating OPLLs, the distribution of the phase error can be placed above this limit. Figure 2.6.8 represents the response of an analogue phase detector. For values of phase error above one radian the phase detector can not be considered linear and the efficiency of the phase detection becomes very low. If the phase error is increased even further, around $\pi/2$ radians, the device loses any phase detection capability and the loop drops out of lock. From this moment, two things can happen: The loop can acquire lock again coming back to the same sector of the phase

detector transfer function or it can skip a whole cycle of the sinusoidal response and return to lock at another sector of the curve. This last event is normally called *cycle slip*.

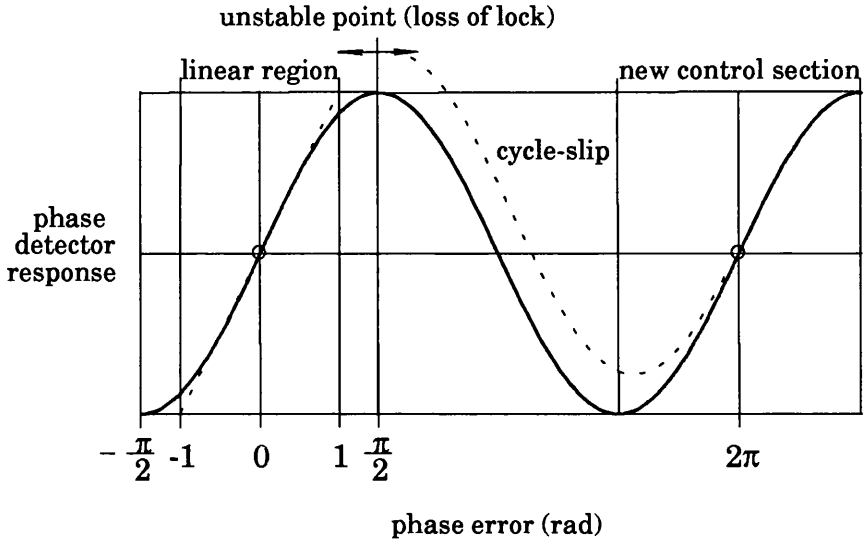

Figure 2.6.8: Response of an analogue phase detector.

If the performance of the loop is good, presenting a low value of phase error variance, cycle slips are not very likely to occur. Nevertheless, if the phase error variance is about 1rad^2, cycle slips will occur frequently and for values of σ^2 above $\pi^2/4\text{rad}^2$ the cycle slips would happen so often that the system would be considered completely out of lock.

There is a finite probability that a noise-induced phase excursion will throw the loop out of lock causing the slave laser to slip one or more cycles. The average time between such events, assuming zero mean phase error, can be approximated by [Gardner 79]:

$$T_{av} \cong \pi \frac{e^{\left[\frac{2}{\sigma^2}\right]}}{4\,B_n} \qquad 2.6.11$$

Figure 2.6.9 gives a graph of T_{av} (on log scale) against the loop delay time using the values of phase error variance shown before when the summed linewidth was fixed at 5MHz, for a modified first order loop (a) and a second order loop (b). Note that for loop filter bandwidths above 100MHz, in Figure 2.6.9(a), there is a dramatic variation of the average time between cycle slips with the loop delay time, as it can drop from 10 years to 1 second due to a increase of only 1.5 ns of T_d. For the second order loop,

Figure 2.6.9(b), this drop of T_{av} is even more dramatic, as an increase of 1ns (from 0.5 to 1.5ns) can cause a fall of T_{av} from thousands of years to 10ms.

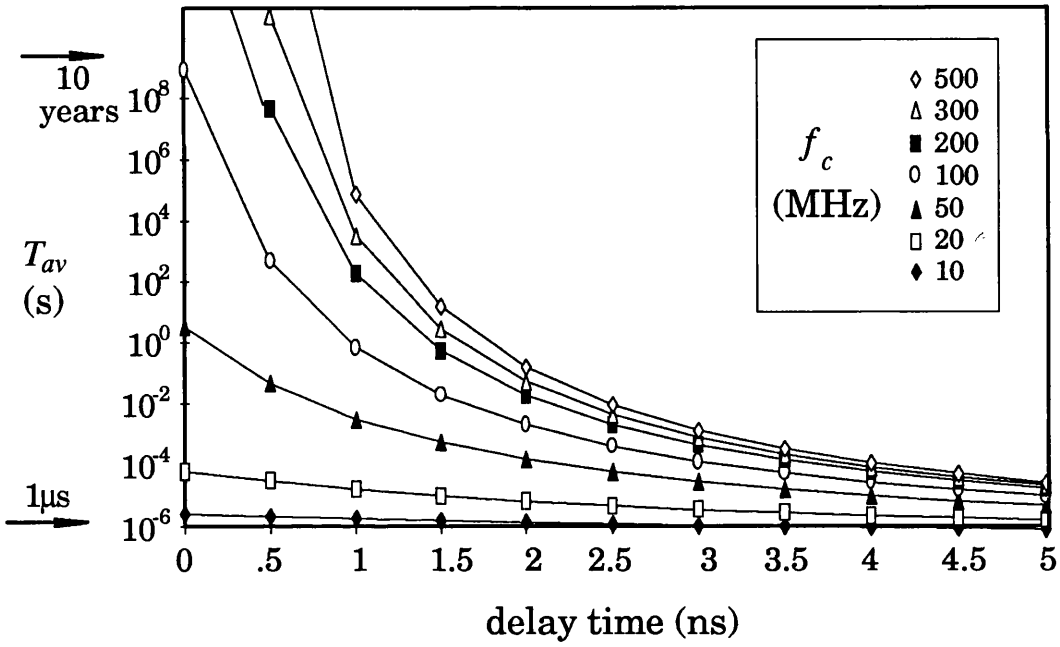

Figure 2.6.9(a) : T_{av} for a modified first order loop against the loop delay time for several values of loop filter cut-off frequency (summed linewidth = 5MHz).

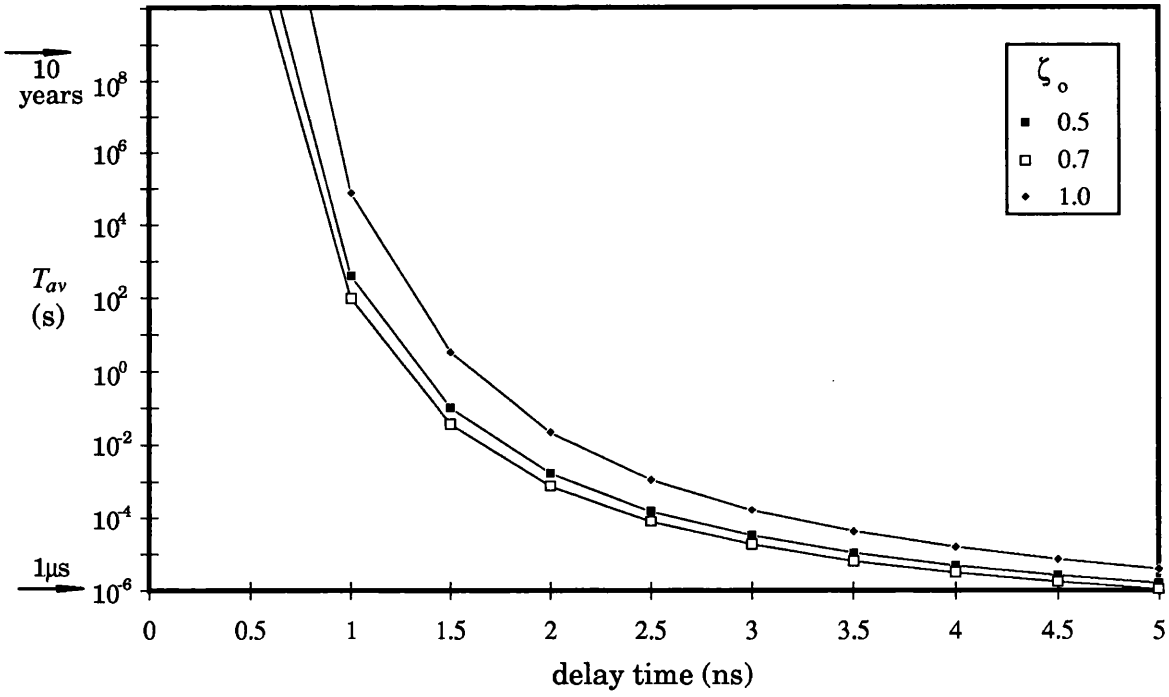

Figure 2.6.9(b): T_{av} for a second order loop against the loop delay time for several values of relative damping factor (summed linewidth = 5MHz).

By combining equation (2.6.19) and (2.6.11), it is possible to calculate the maximum summed linewidth δf_m for which a minimum average cycle slipping interval T_{av} is maintained:

$$\delta f_m = \frac{\pi}{I_p}\left\{\frac{2}{\ln\left[\frac{T_{av}\,4\,B_n}{\pi}\right]} - \frac{e\,(P_m + P_s)\,B_n}{R\,P_m\,P_s}\right\} \qquad 2.6.12$$

Figure 2.6.10 gives the maximum summed linewidth δf_m against the loop delay time when T_{av} is given the value of 10 years (3.15×10^8 seconds), for: (a) modified first order loop (for several values of loop cut-off frequency) and (b) second order loop (for several values of relative damping factor). Note that this requirement can not normally be met if the summed linewidth of master and slave lasers exceeds 10 MHz (even using wide bandwidth loop filters), representing a severe restriction for conventional semiconductor lasers. This suggests that reliable OPLLs could be realised in three ways:

- The use of non-conventional very narrow semiconductor lasers. This is possible by employing linewidth narrowing techniques such as the use of an external cavity or negative electrical feedback. A better option is to make use of newly developed narrow linewidth monolithic semiconductor lasers, such as long cavity distributed feedback (DFB) lasers and quantum well (QW) lasers.
- The use of very low loop delay time. This can be achieved by reducing the physical size of the assemblage, through the integration of parts of the OPLL or the whole system.
- A combination of both.

When the OPLL is used for optical frequency synthesis, such as for generating channel offsets in a dense wavelength division multiplexing system, T_{av} can be a very useful parameter to describe the performance of the system. The criterion of minimum average time between cycle slips of 10 years was established to provide reliable operation in practical systems [Ramos 90]. This same criterion was used to establish laser linewidth requirements (as show above) for OPLLs employed in coherent optical beam forming networks in satellites [Gliese 91].

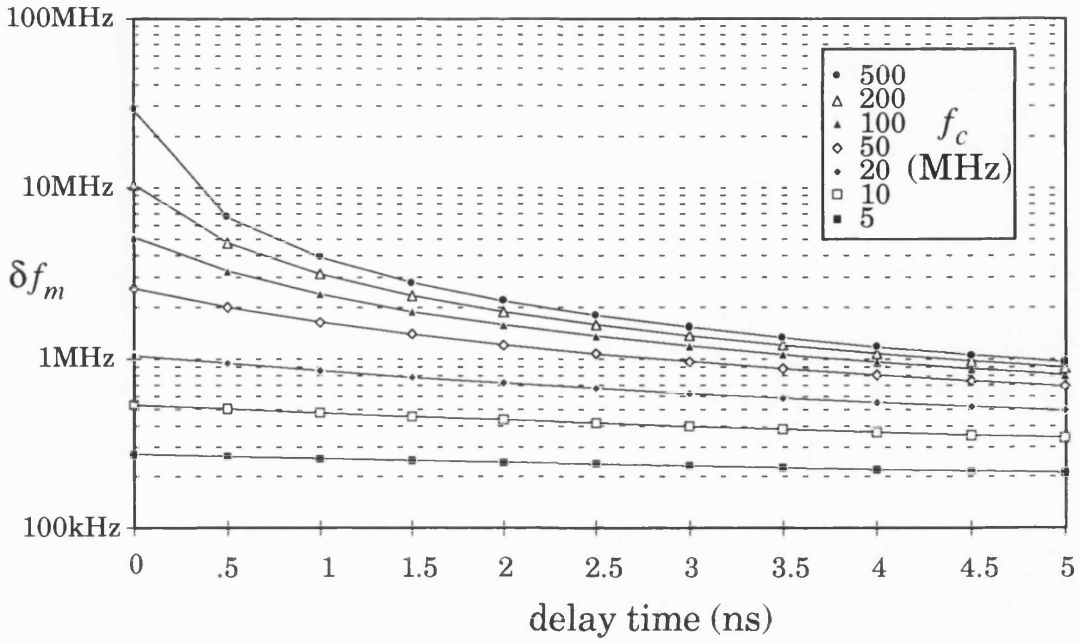

Figure 2.6.10(a) : Maximum laser summed linewidth against the loop delay time for several values of loop filter cut-off frequency for a modified first order loop (T_{av}=10years).

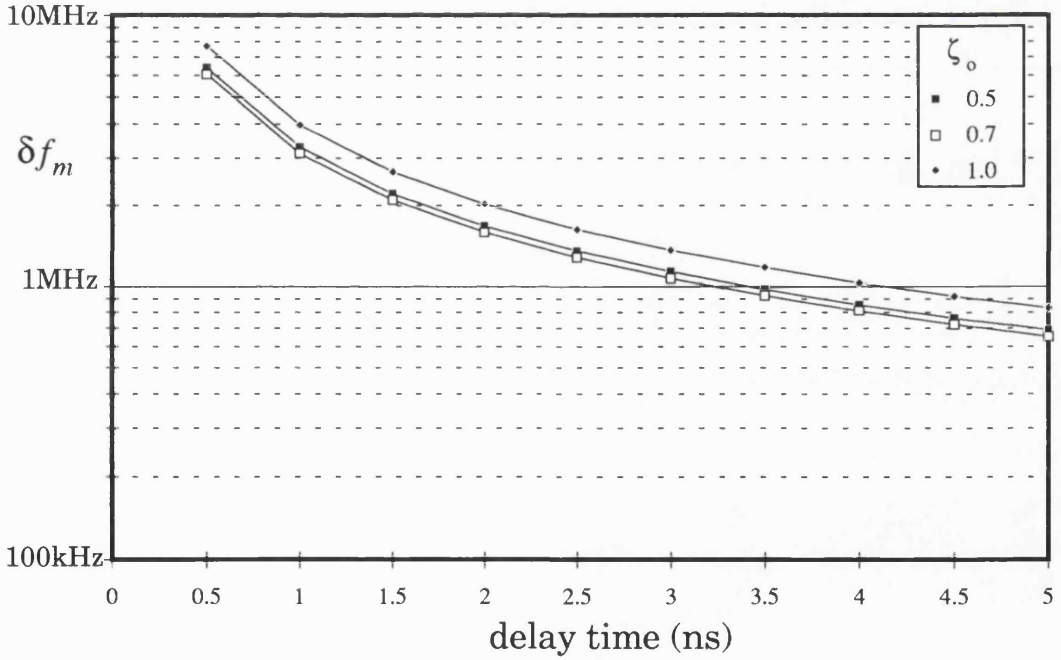

Figure 2.6.10(b) : Maximum laser summed linewidth against the loop delay time for a second order loop for several values of relative damping factor (T_{av} = 10 years).

However, if the OPLL is used as phase demodulator in a PSK system, the effect of cycle slips on the performance of the system can be translated in terms of the contribution of this phenomenon towards the over all bit error rate *BER* of the receiver. When the loop is unlocked (cycle slipping state), the probability of bit error occurring is 0.5 [Wolejsza 76] [Kazovsky 86]. The cycle slip contribution to bit error rate BER_{cs} can be estimated by:

$$BER_{cs} \cong \pi \frac{e^{\left[-\frac{\pi}{2\sigma^2}\right]}}{4} \qquad 2.6.13$$

Note that BER_{cs} does not take into account the error due to phase jitter without cycle slips. Figure 2.6.11 shows the behaviour of BER_{cs} against the loop delay time, when the laser summed linewidth is fixed at 5MHz for: (a) a modified first order loop (for several values of loop filter cut-off frequency) and (b) a second order loop (for several values of relative damping factor). For a modified first order loop, reasonable values of BER_{cs} are achievable if loop filter bandwidths above 100MHz are used, when the dependence of BER_{cs} on the loop delay time is very sharp.

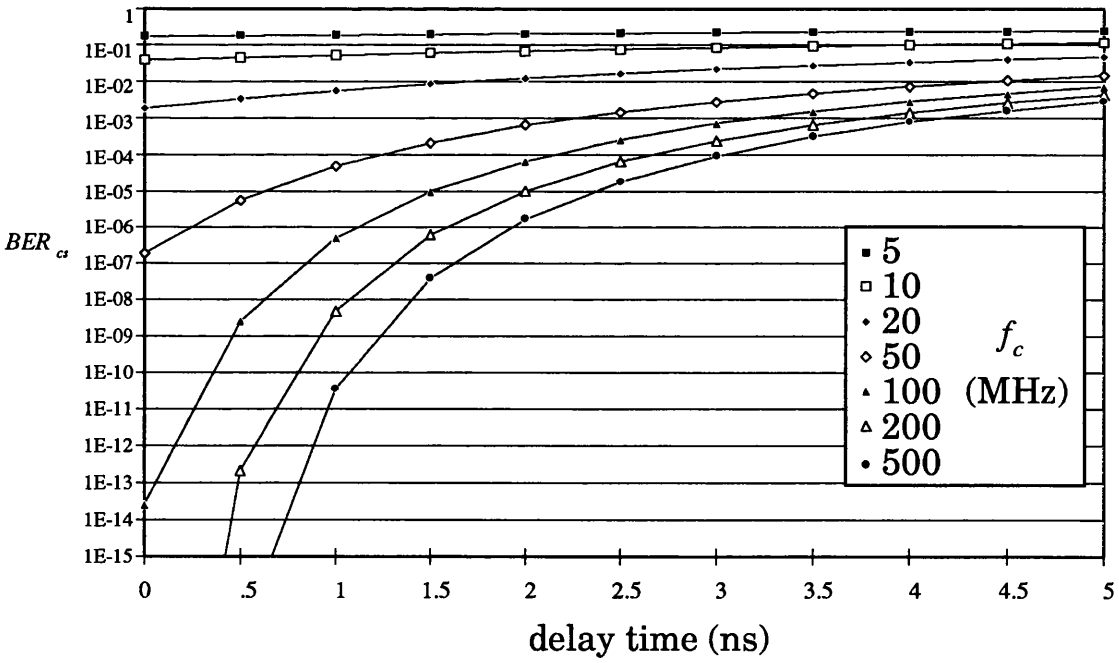

Figure 2.6.11(a) : BER_{cs} against the loop delay time for several values of loop filter cut-off frequency for a modified first order loop when the laser summed linewidth is fixed at 5MHz.

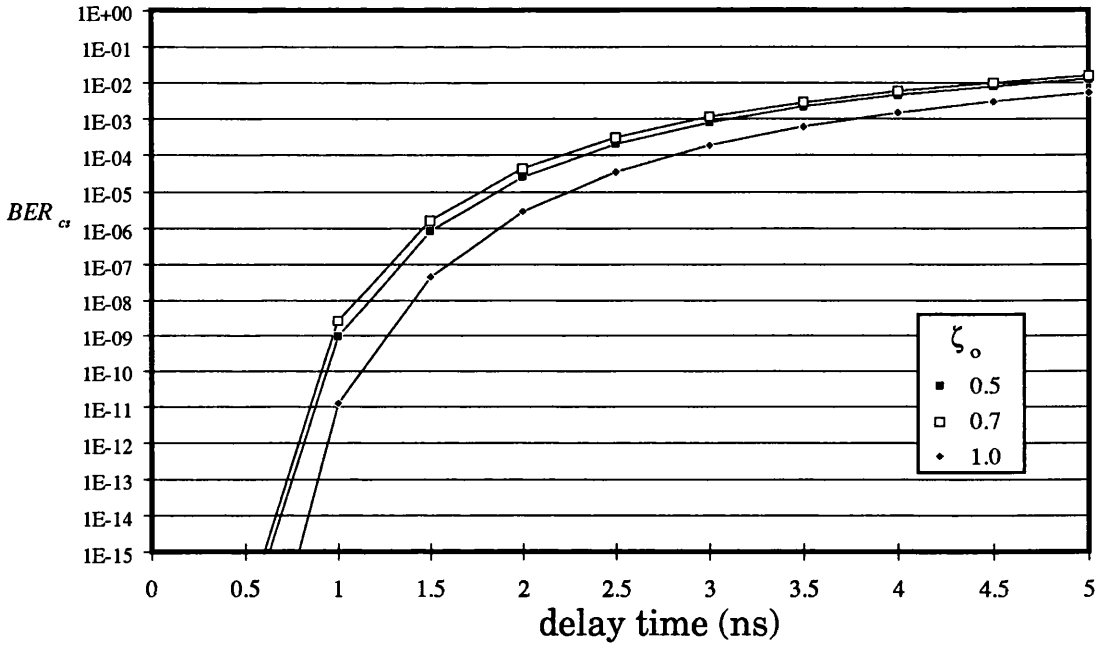

Figure 2.6.11(b) : BER_{cs} against the loop delay time for a second order loop for several values of relative damping factor, when the summed linewidth is fixed at 5MHz.

Again, the maximum value of summed linewidth can be calculated for a given limit value of BER_{cs}, as given below:

$$\delta f_m = \frac{\pi}{I_p}\left\{\frac{-\pi}{2\ln\left[\frac{4\,BER_{cs}}{\pi}\right]} - \frac{e\,(P_m + P_s)\,B_n}{R\,P_m\,P_s}\right\} \qquad 2.6.14$$

Figure 2.6.12 gives the maximum summed linewidth δf_m against the loop delay time when BER_{cs} is 10^{-10}, for: (a) a modified first order loop (for several values of loop filter cut-off frequency) and (b) a second order loop (for several values of relative damping factor). Note that this criterion is looser than that used before (T_{av} = 10 years), allowing wider linewidth lasers to be used.

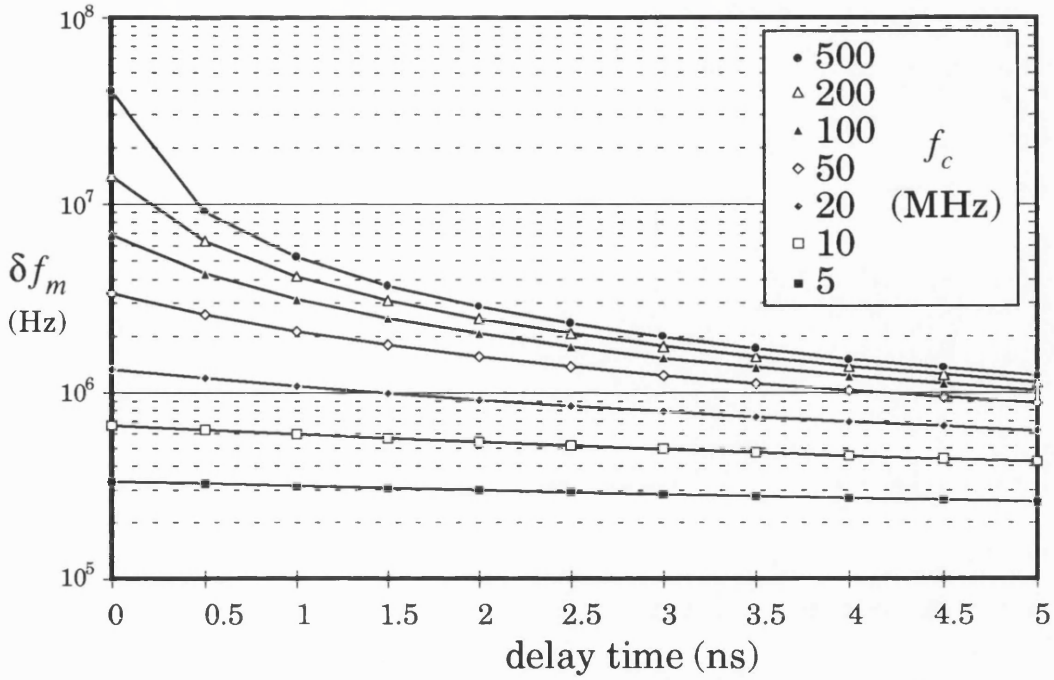

Figure 2.6.12(a) : Maximum summed linewidth δf_m against the loop delay time for a modified first order loop, for several values of loop cut-off frequency, when BER_{cs} is given the value of 10^{-10}.

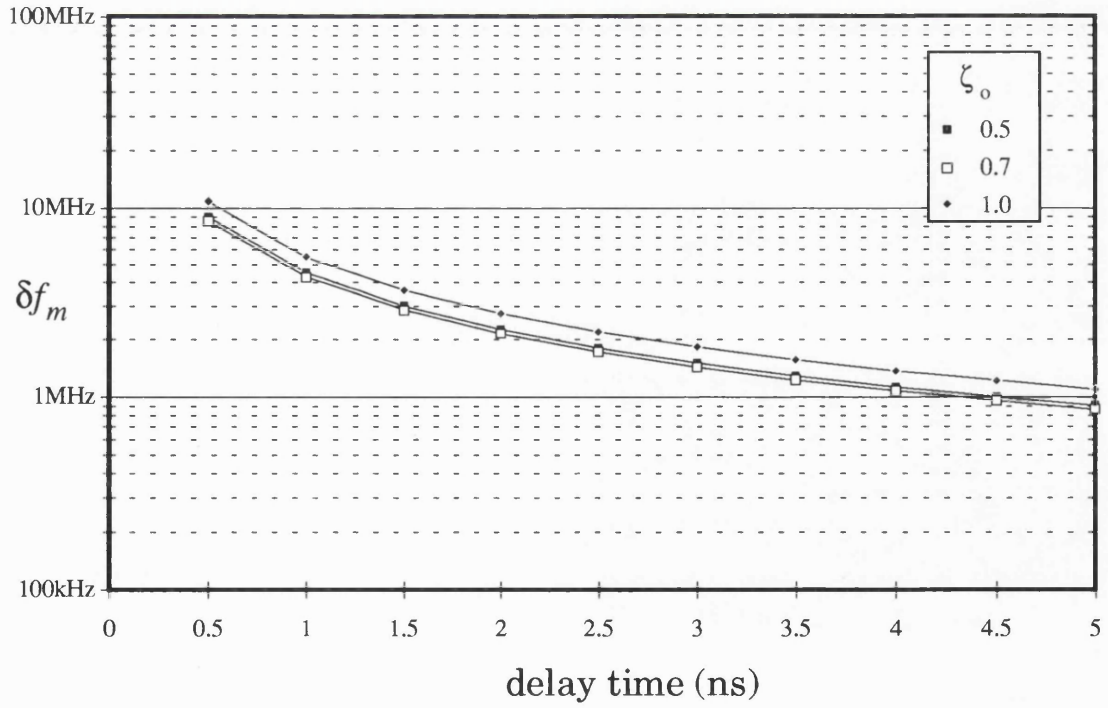

Figure 2.6.12(b) : Maximum summed linewidth δf_m against the loop delay time for a second order loop for several values of relative damping factor, when BER_{cs} is given the value of 10^{-10}.

2.7- Conclusion

2.7.1- Main conclusions

A review of previous theoretical studies has been presented, followed by the basic OPLL theory. The main sources of noise have been identified and their effects studied. The loop filter design has been discussed, showing different loop orders. It was concluded that modified first order and second order loops were the most likely to meet the requirements of an OPLL using semiconductor lasers. It was also decided to use a modified first order loop for the final experiment.

The influence of the loop delay time on the loop stability was studied and stability conditions were set for both modified first order and second order loops. The relation between loop parameters was established to allow loop design. The main loop parameters involved are: lasers linewidth, loop gain, loop filter bandwidth and loop delay time.

The loop performance was first analysed by predicting the shape of the phase error signal and the beat signal, showing that it is possible to obtain wider loop bandwidth if modified first order loops are used. The phase error variance was then calculated and the effect of the loop delay time was observed. It was found that second order loops are more sensitive to variations of delay time than modified first order loops. For second order loops, the phase error variance was found to be a weak function of ζ_o. However, a marginally better performance can be achieved when the system is critically damped (ζ_o=1)

Finally, the loop performance was examined by calculating the average time between cycle slips, which was noticed to be a strong function of loop delay time. The maximum summed linewidth allowed to keep the average time between cycle slips above 10 years was calculated, also including the loop delay time. Loop delay has been shown to impose severe restrictions on this maximum linewidth. The contribution of the cycle slips towards the total bit error rate was calculated and the maximum summed linewidth allowed to keep this contribution below 10^{-10} was also calculated. The T_{av} >10 years criteria was seen to be compatible with the normal digital communication criteria, as it is harder to achieve than the $BER<10^{-9}$ criteria. The advantage of the cycle slip criteria introduced here is that it is based on a parameter of the loop itself, making it useful for all OPLL applications.

2.7.2- Discussion

The optical path length equivalent to a delay time of 1, 2 and 3 ns in a medium of refractive index 1.5 would be 0.2, 0.4 and 0.6 metres respectively. When optical fibre or bulk optics are used, it is difficult to obtain a system with a path length less than 0.5 metre, seriously restricting the performance of the loop when the summed linewidth is of the order of MHz. The use of integrated optics systems will allow the commercial development of these kind of OPLLs in the future. The use of monolithic microwave integrated circuits (MMICs) in the electrical part of the system would also help to reduce the total loop delay time, improving the loop performance.

If the loop delay time is kept at 0.5ns the system would require lasers with a maximum summed linewidth of 7MHz (500MHz filter bandwidth assumed) for a modified first order loop or 6MHz for a second order loop. Such a loop would be difficult, although possible, to realise with commercially available DFB lasers, but should be straight-forward with current tuned external cavity lasers [Mellis 88]. The recently reported monolithic tunable lasers with sub-MHz linewidths [Kotaki 89] should permit use of the OPLL offset frequency generation scheme in future systems. The tuning speed restrictions of plasma effect tuning, as used in most tunable semiconductor lasers, can be modelled, approximately, by adjusting f_c. To overcome this problem multi section lasers [Yamazaki 85] or even reverse bias tuned quantum well structures [Cai 89] could be used as slave lasers.

References

Cai, B., Seeds, A. J., Rivers, A., and Roberts, J. S.: "Multiple quantum well-tuned GaAs/AlGaAs laser", Electronics Letters, 1989, 25, pp.145-146.

Fernando, P. N., Fake, M. and Seeds, A. J., "A Novel Approach to Optical Frequency Synthesis in Coherent Lightwave Systems", SPIE O/E Fibers, 1990, San Jose, USA, pp. 152-163.

Gardner, F.M.: Phaselock Techniques, (Wiley, New York, 2nd Ed., 1979).

Gliese, U., Christensen, E. L. and Stubkajær, K. E., "Laser Linewidth Requirements and Improvements for Coherent Optical Beam Forming Networks in Satellites", J. Lightwave Tech., vol. 9, n. 6, June 1991, pp. 779-790.

Grant, M.A., Michie, W.C., Fletcher, M.J.: "The performance of optical phase locked loops in the presence of nonnegligible loop propagation delay", J. Lightwave Tech., 1987, LT5, pp. 592-597.

Henry, C. H., "Theory of Linewidth of Semiconductor Laser", J. Quantum Electronics, vol. QE-18, n. 2, 1982, pp. 259-264.

Kotaki, Y., Ogita, S., Matsuda, M., Kuwahara, and Y., Ishikawa, H.: "Tunable, narrow-linewidth and high-power l/4-shifted DFB laser", Electronics Letters, 1989, 25, pp. 990-991.

Kuo, B., "Automatic Control System", Prentice-Hall International Editions, Fifth Edition, 1987.

Mellis, J., Al-Chalabi, S. A., Cameron, K. H., Wyatt, R., Regnault, J. C., Devlin, W. J., and Brain, M. C.: "Miniature packaged external-cavity semiconductor laser with 50GHz continuous electrical tuning range", Electronics Letters, 1988, 24, pp. 988-989.

Ohtsu, M. and Kotajima, S., "Derivation of the Spectral Width of a 0.8 m AlGaAs Laser Considering 1/f Noise", Japanese J. Applied Physics, vol. 23, n. 6, June, 1984, pp. 760-764.

Ohtsu, M., "Highly Coherent Semiconductor Lasers", Artech House, 1992.

Patzak (next page)

Ramos, R. T. and Seeds, A. J., "Delay, Linewidth and Bandwidth Limitations in Optical Phase-Locked Loop Design", Electronics Letters, 1990, 26, pp. 389-391.

Steele, R.C., Creaner, M.J., Walker, G.R., Walker, N.G.: "Optical PSK transmission experiment at 565Mbit/s incorporating an endless polarization control system", Proceedings of SPIE Components for Fiber Optics Applications and Coherent Lightwave Communications, Boston, 1988, vol. 988, pp. 302-309.

Ward, C. J.: "Delay reduction techniques in phase-locked loop amplifiers", Electronics Letters, 1981, 17, pp. 253-255.

Wolejsza, C. J., "Effects of Oscillator Phase Noise on PSK Demodulation", COMSAT Tech. Rev., vol. 6, n. 1, 1976, pp. 107-125.

Yamamoto, Y., Saito, S. and Mukai, T., "AM and FM Quantum Noise in Semiconductor Lasers-Part II: Comparison of Theoretical and Experimental Results for AlGaAs Lasers", IEEE Journal of Quantum Electronics, vol. QE-19, n. 1, January, 1983, pp. 47-58.

Yamazaki, S., Emura, K., Shikada, M., Yamaguchi, M. and Mito, I, "Realisation of Flat FM Response by Directly Modulating a Phase Tunable DFB Laser Diode", Electronics Letters., 1985, vol. 21, n. 7, pp. 283-285.

Blanchard, A., "Phase-locked loops", John Wiley & Sons, 1976.

Okoshi, T. and Kikuchi, K., "Coherent optical fiber communications", KTK Scientific Publishers, Tokyo, 1988.

Patzak, E. and Langenhorst, R., "Sensitivity degradation of conventional and balanced 3×3 port phase diversity DPSK receivers due to thermal and local oscillator intensity noise", Electronics Letters, 1989, vol. 25, n. 8, pp. 545-547.

Chapter 3

Optical Design

3.1- Introduction

Due to the limitations imposed on the maximum delay time, the physical size of the OPLL has to be reduced to a minimum. This limitation determines the kind of optical arrangement used and the characteristics of each component in the system. As was suggested at the end of Chapter 2, the ideal solution would be the use of an optoelectronic integrated circuit (OEIC) in which the physical dimensions could be kept sub-millimetric. Although almost all of the loop components have already been demonstrated to be able to be integrated, this technology is still not readily available and the integration of devices such as optical isolators remains a difficulty.

OEIC technology is advancing rapidly and it will make possible the production of reliable OPLLs in the near future. Some very recent work [Koch 91] [Charles 92] has been done in the direction of integrating laser, optical waveguide and couplers, which are the main components of OPLLs. For our experiment, however, discrete components have to be used, making the design very critical.

This chapter concentrates on the design of the optical section of the OPLL experiment. Some comments are made on how the optical mixing is carried out, followed by a discussion on optical isolation and an evaluation of the amount of optical misalignment tolerable in order to retain an effective optical mixing. Quantum well lasers are introduced and the main characteristics of the double quantum well lasers used in the final experiment are presented.

3.2- Optical combining

The initial idea was to use an optical fibre coupler for combining the signals from the master and slave lasers, as illustrated in Figure 3.2.1. However, for efficient optical mixing at the detector surface, both signals need to be presented with the same polarisation state. The use of fibre optics would introduce the problem of adjusting the polarisation of these two signals, since fibres do not normally keep the state of polarisation of the signal. The use of a polarisation control system would be necessary [Steele 88] which would increase the complexity of the system and introduce an undesirable extra delay to the loop. As the polarisation of reflected beams would also

be modified by the fibre, a Faraday rotation optical isolator, which blocks reflections with any polarisation state, would be required. Furthermore, the use of a fibre coupler would introduce a relatively longer optical path length due to its physical length, its refractive index and the need for Faraday rotation optical isolators, introducing a prohibitive delay time into the loop. Delays well above 5ns could be expected, requiring sub-MHz linewidth lasers, as was discussed in Chapter 2 (Figure 2.6.7). It would also introduce severe losses in launching the radiation into single mode fibre. It was therefore decided to use a beam splitter cube to combine the laser outputs, as shown in Figure 3.2.2, instead of an optical fibre coupler.

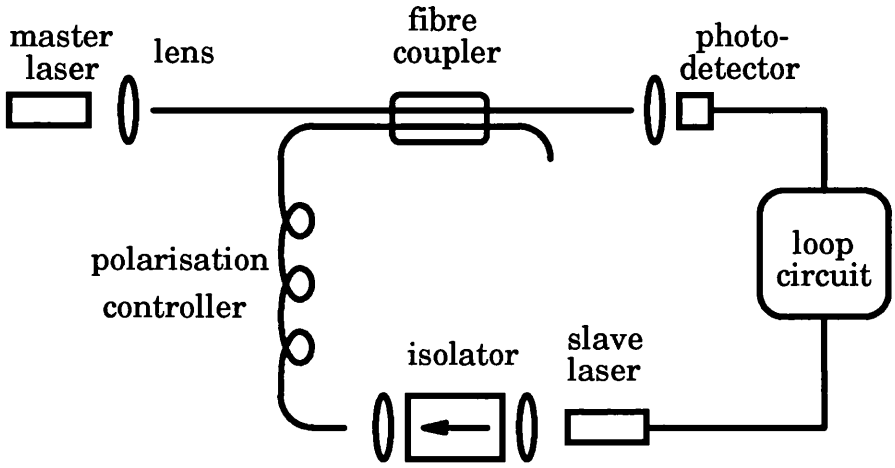

Figure 3.2.1: Block diagram of an OPLL using optical fibre.

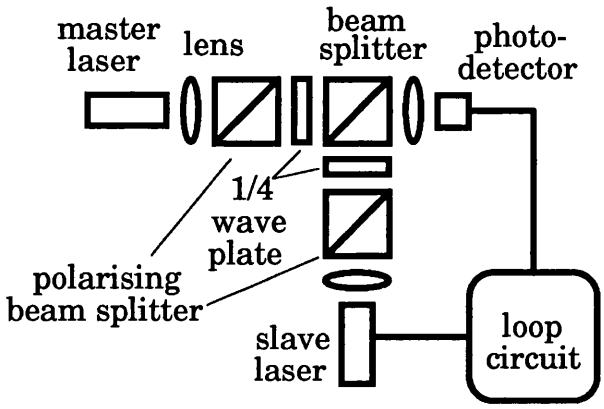

Figure 3.2.2: Block diagram of an OPLL using bulk optics.

This solution can be used in the laboratory, but it presents some problems which are undesirable for commercial applications. Firstly, it is still too big as loop delay time is unlikely to be lower than 1ns with this kind of arrangement. It does not solve the

problem of polarisation sensitivity if the signal from the master laser is brought through an optical fibre. It requires fine optical alignment, as will be seen in section 3.4. It is sensitive to vibrations and temperature fluctuations. Most of these problems could be solved by the use of an OEIC.

3.3- Optical isolation

Commercial optical isolators are based on the Faraday rotation effect. A polariser is placed at the input in order to allow only a linearly polarised beam to pass through the isolator. This beam is coupled into a high birefringence crystal under a constant magnetic field given by a permanent magnet to provide a 45° rotation on the signal polarisation due to the Faraday effect. A second polariser at the output is positioned 45° relative to the first one as shown in Figure 3.3.1.

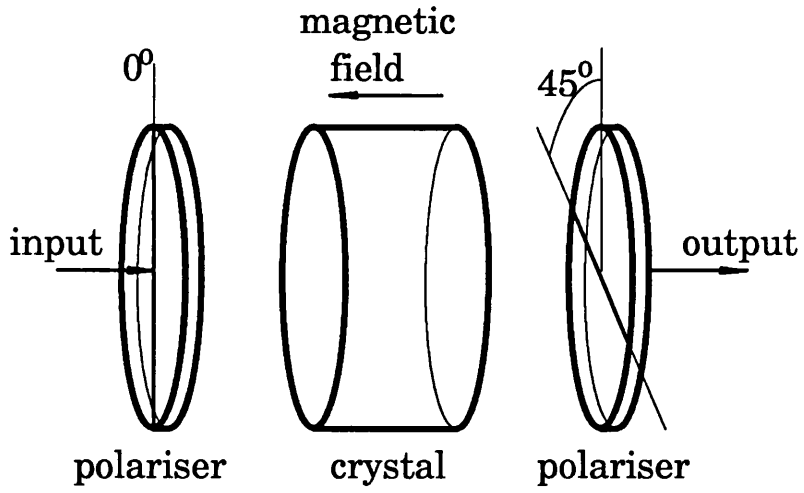

Figure 3.3.1: Faraday rotation isolator.

Faraday rotation isolators are very effective for protection against reflections, providing about 30 dB isolation and blocking any reverse signal independent of its state of polarisation. However, long crystals are needed to provide enough rotation at 830 nm, making the effective optical path length through the isolator of the order of 180 mm. Some isolators use shorter crystals, but the beam is passed through the crystal several times resulting in the same effective optical path length. For these reasons, Faraday rotation isolators are only used outside the loop to prevent reflections from the monitoring instruments (optical spectrum analyser and scanning Fabry Perrot interferometer) disturbing loop operations.

For use inside the loop another kind of isolator can be used, made of a combination of a polariser and a quarter-wave plate, as shown in Figure 3.3.2. A polariser at the input provides a linear polarised beam with a 45° offset from the main axis of a quarter-wave plate which transforms the polarisation of the signal into circular polarisation. If the signal is reflected back, the quarter-wave plate re-transforms its polarisation into linear, but now at 90° relative to the input polariser which blocks the reflected beam. This kind of isolator provides protection against simple reflections, but is ineffective against reflection after transmission through optical fibres since they change the state of polarisation of the guided signal. However it can be used inside the loop where there is no fibre, avoiding the long delays of a Faraday isolator. In the OPLL experiment it is desirable to use the same kind of isolation for the master and slave lasers, in order to match both polarisation states for optical mixing.

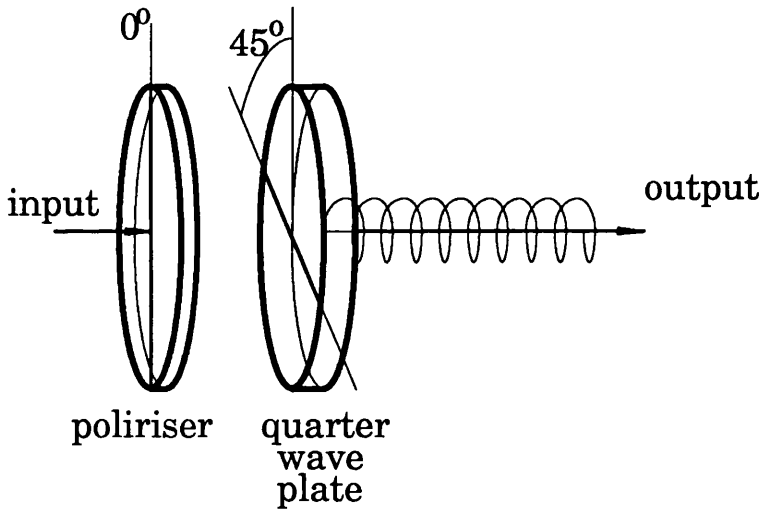

Figure 3.3.2: Isolator using quarter-wave plate and polariser.

3.4- Alignment

The use of a beam splitter brings the problem of alignment. Both beams must have coincident wavefronts in order to produce optical mixing at the detector. This section analyses the influence of a misalignment angle between the wavefronts on the heterodyning process [Richards 85]. Figure 3.4.1 shows a diagram representing the wavefronts of two electrical fields, e_1 and e_2 , incident on the square active area of a photodiode of side l.

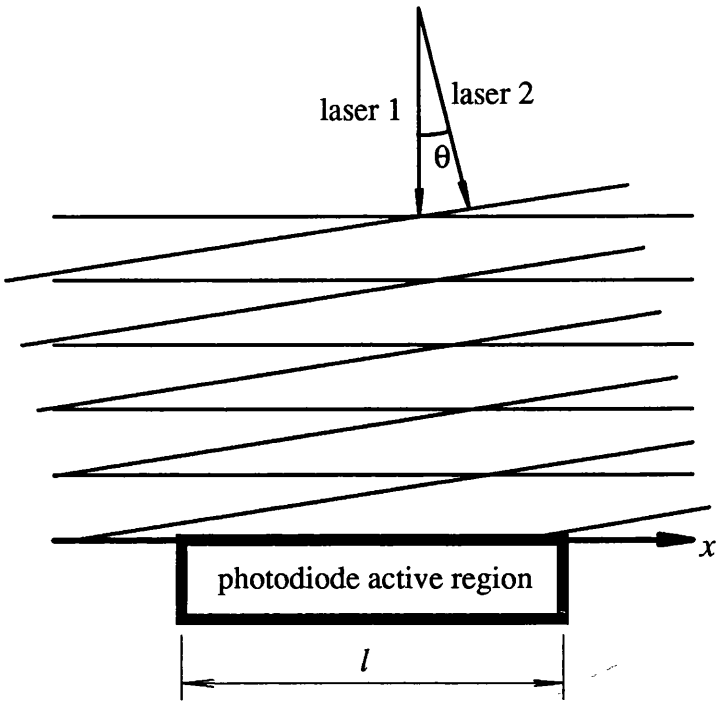

Figure 3.4.1: Diagram of the wavefronts of two misaligned lasers inciding on a photodetector active region.

The misalignment angle is given by θ. The electrical fields in the x direction are given by:

$$e_{1x} = E_1 \cos(\omega_1 t + \phi_1) \qquad 3.4.1$$

$$e_{2x} = E_2 \cos\theta \cos(\omega_2 t + \phi_2 - \beta_x) \qquad 3.4.2$$

Where E_1 and E_2 are the maximum amplitude of the electrical fields, ω_1 and ω_2 are their angular frequencies, ϕ_1 and ϕ_2 their phases and β_x is the phase constant in the x direction of the laser 2, given by:

$$\beta_x = \frac{2\pi}{\lambda_2}\sin(\theta) = \frac{\omega_2}{c}\sin(\theta) \qquad 3.4.3$$

Where λ is the wavelength of e_2. The optical intensity of each signal is given by:

$$I_1 = \frac{(E_1/\sqrt{2})^2}{\eta} \qquad 3.4.4$$

$$I_2 = \frac{(E_2/\sqrt{2})^2}{\eta} \qquad 3.4.5$$

Where η is the characteristic impedance of the medium. Rewriting:

$$E_1 = 2\sqrt{\eta I_1} \qquad 3.4.6$$

$$E_2 = 2\sqrt{\eta I_2} \qquad 3.4.7$$

The total electrical field incident on the detector surface is:

$$e_t = e_{1x} + e_{2x} \qquad 3.4.8$$

The total optical intensity is then:

$$\begin{aligned} I_t = (e_t)^2/\eta = 2\big[& I_1 + I_2\cos^2(\theta) + \\ & + 2\sqrt{I_1 I_2}\cos(\theta)\cos((\omega_1 - \omega_2)t + \phi_1 - \phi_2 + \beta_x x) + \\ & + I_1\cos(2\omega_1 t + 2\phi_1) + I_2\cos^2(\theta)\cos^2(2\omega_2 t + 2\phi_2 - 2\beta_x x) + \\ & + 2\sqrt{I_1 I_2}\cos(\theta)\cos((\omega_1 + \omega_2)t + \phi_1 + \phi_2 - \beta_x x)\big] \end{aligned} \qquad 3.4.9$$

Appendix 3 shows the derivation of equation 3.4.9.

Considering a photodetector with a square surface of side l, the photo current at the photodetector terminals is given by:

$$i_p = R\,l\int_l \frac{I_t}{2}\,dx \qquad 3.4.10$$

Where R is the photodetector responsivity. The last three terms of the expression of e_t are not taken in account, since i_p cannot have components at optical frequencies. Thus:

$$\begin{aligned} I_t = & Rl[I_1 + I_2\cos^2(\theta)] + \\ & + 2Rl\sqrt{I_1 I_2}\cos(\theta)\cos[(\omega_1 - \omega_2)t + \phi_1 - \phi_2 + \beta_x x] \end{aligned} \qquad 3.4.11$$

$$i_p = Rl[I_1 + I_2\cos^2(\theta)] +$$

$$+2Rl\sqrt{I_1 I_2}\cos(\theta)\left(\frac{\sin\left(\beta_x \frac{l}{2}\right)}{\beta_x \frac{l}{2}}\right)\cos((\omega_1 - \omega_2)t + \phi_1 - \phi_2) \qquad 3.4.12$$

which can be split into a dc component i_{dc} and a signal component i_{sig} :

$$i_{dc} = Rl[I_1 + I_2\cos^2(\theta)] \qquad 3.4.13$$

$$i_{sig} = 2Rl\sqrt{I_1 I_2}\cos(\theta)\left(\frac{\sin\left(\beta_x \frac{l}{2}\right)}{\beta_x \frac{l}{2}}\right)\cos((\omega_1 - \omega_2)t + \phi_1 - \phi_2) \qquad 3.4.14$$

When the photodetector is loaded with a resistance r_l , the dissipated power is given by:

$$P_{dc} = r_l(i_{dc})^2 = r_l R^2 l^2 [I_1 + I_2\cos^2(\theta)]^2 \qquad 3.4.15$$

$$P_{sig} = r_l\left(\frac{i_{sig}}{\sqrt{2}}\right)^2 = 2r_l R^2 l^2 I_1 I_2\cos^2(\theta)\left(\frac{\sin\left(\beta_x \frac{l}{2}\right)}{\beta_x \frac{l}{2}}\right)^2 \qquad 3.4.16$$

Where I_{sig} is the maximum amplitude of i_{sig}. For:

$$\beta_x = \frac{2\pi}{\lambda_2}\sin\theta \qquad 3.4.17$$

The final expression relating P_{sig} and θ is:

$$P_{sig} = 2r_l R^2 l^2 I_1 I_2 \cos^2(\theta) \left(\frac{\sin\left(\frac{\pi l}{\lambda_2}\sin\theta\right)}{\frac{\pi l}{\lambda_2}\sin\theta} \right)^2 \qquad 3.4.18$$

The photodetector used in the experimental work was a GEC high speed GaAs PIN photodiode, which has a responsivity of 0.35A/W @ 830nm and l=30μm. Assuming I_1 and I_2 are both constants, it is possible to relate P_{sig} to θ. Figure 3.4.2 shows the loss inflicted on $P_{sig}(\theta)$ in dB in relation to $P_{sig}(0)$, the signal power when there is no misalignment, against the misalignment angle θ. From the graph, a misalignment of 1° would penalise the signal power by 6.8dB, while the 3dB penalty angle would be 0.7°.

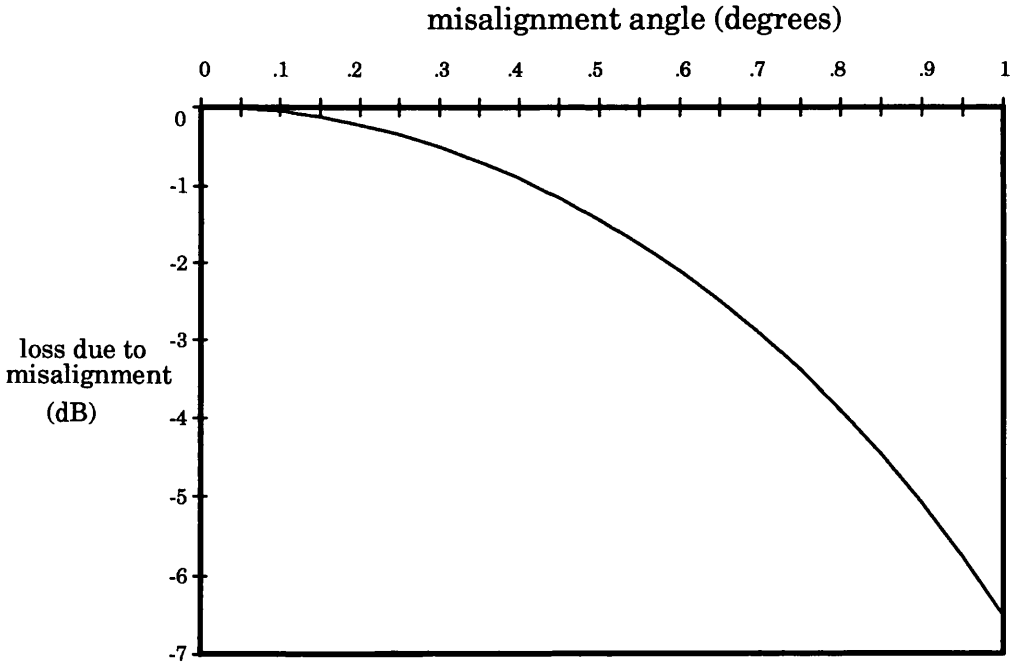

Figure 3.4.2: Degradation of the signal power with misalignment.

Figure 3.4.3 shows the procedure used for aligning the lasers. A screen is positioned at a distance of 60 cm from the beam splitter where the two beams are combined. When the two spots are no more than 1mm apart, the misalignment angle is less than 0.1°, what gives a penalty of less than 0.07dB.

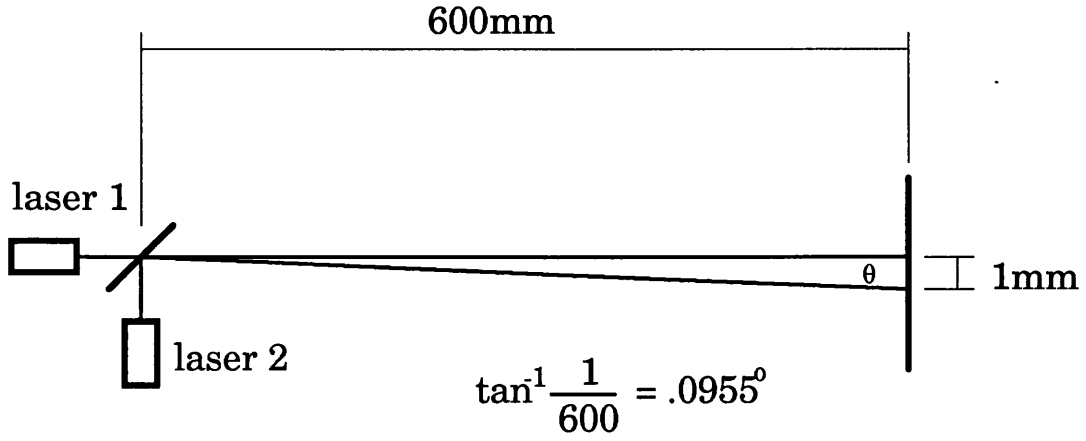

Figure 3.4.3: Procedure for laser alignment.

3.5- Quantum well lasers

3.5.1-The double quantum well laser

Two double quantum well separated confinement heterostructure (DQW-SCH) metal clad ridge waveguide GaAs/AlGaAs laser diodes are used as master and slave lasers in the final OPLL experiment described in Chapter 5 (Northern Telecom/STC LT40-82) [Garrett 87] [Daniel 89]. The same principles seen in the sections 3.6.2 and 3.6.3 can be applied here as the two wells are placed far enough from each other so that there is no coupling between them. Under this condition, each well can be treated as an individual well. The second quantum well is added in order to increase the output optical power of the device and to improve optical confinement.

The DQW-SCH lasers are grown by metal organic chemical vapour deposition (MOCVD), where the two undoped GaAs quantum wells are incorporated into an $Al_XGa_{1-X}As$ central region which is sandwiched between cladding layers of $Al_yGa_{1-y}As$ of higher Al concentration. These devices have threshold currents of about 25mA and optical power output of 14mW at 40mA bias current. Output power of 175 mW is achievable with these devices for continuos wave operation with single spatial mode [Daniel 89]. The front facet has an Alumina coating resulting in a 5% reflectivity while the back facet has an Aluminium coating with 90% reflectivity. Due to the low reflectivity of the coated front facet, these lasers are sensitive to optical reflections and suitable optical isolation must be added for stable operation. Figure 3.5.1 shows the schematic diagram of a DQW-SCH metal-clad ridge waveguide laser, having a 600 μ m long Fabry Perot cavity.

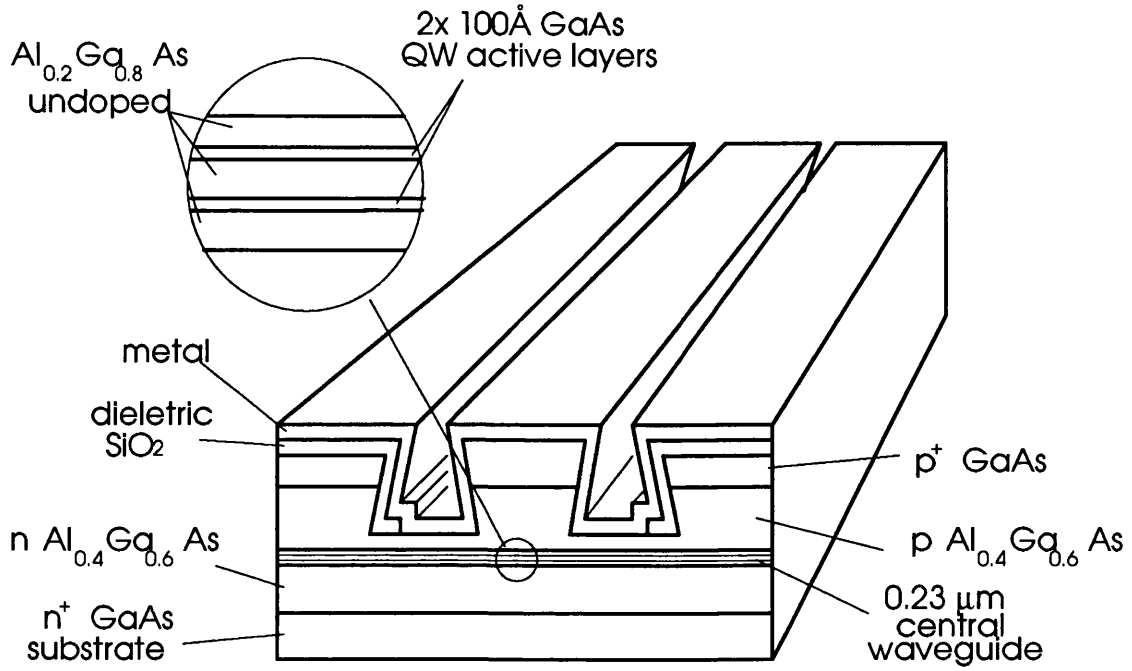

Figure 3.5.1: Schematic diagram of a DQW-SCH metal-clad ridge waveguide laser.

Figure 3.5.2 shows the output optical power as a function of injected current for a new device and for the same device after one month. Note there is a substantial increase on the value of the threshold current (from 25 to 39mA). The nature of this ageing is not fully understood, but could be caused by imperfections of the bounding of the laser chip on the heat sink producing overheating.

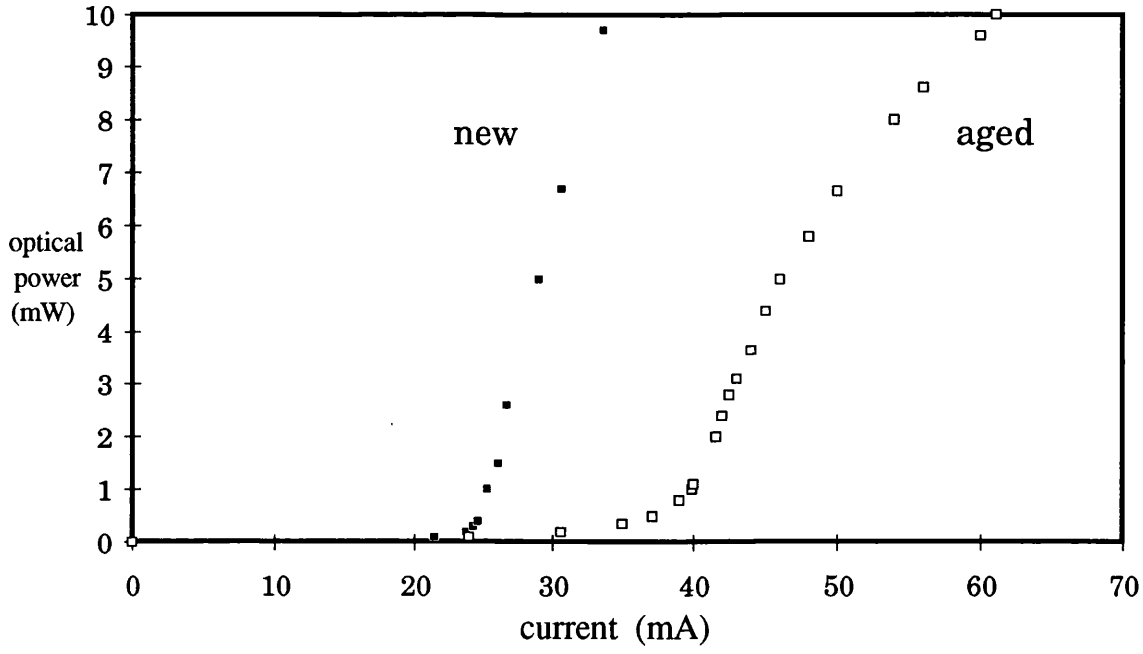

Figure 3.5.2: Output optical power as function of injected current

3.5.2- Spectral characteristics

The spectrum of the lasers was observed using an optical spectrum analyser (Anritsu MS9001B1 0.6-1.75μm) showing single mode operation at about 840nm as shown in Figure 3.5.3. However, this kind of equipment is not suitable for measuring the linewidth of the lasers, owing to its limited resolution. A self homodyne technique was used therefore for this purpose. Figure 3.5.4 shows the arrangement used.

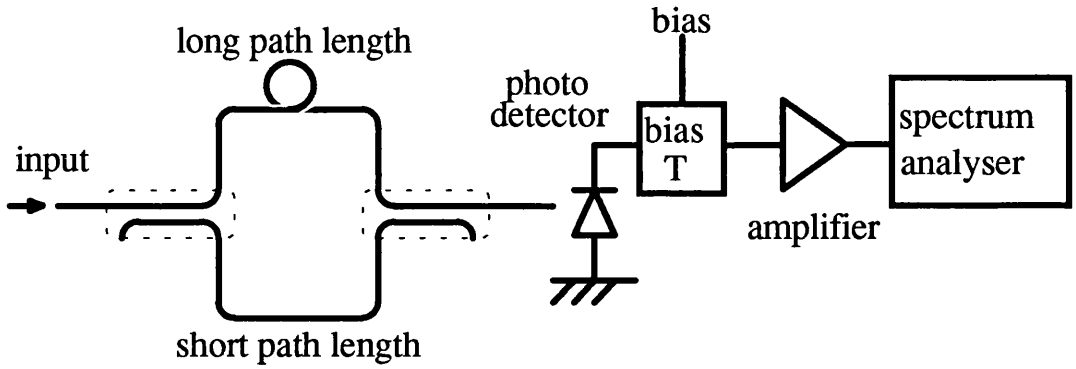

Figure 3.5.4: Diagram of the set up for the linewidth measurement using self homodyne techniques.

The input optical signal is divided into two different paths, one longer than the other, with a difference of optical path length above the coherence length s_c of the laser [Okoshi 80]. In this way, the two signals are uncorrelated when they are recombined at the output, destroying any interferometric effect from the optical mixing. This brings the spectrum of the laser to zero frequency where it can be seen by using a low frequency spectrum analyser. The coherence length s_c for a Lorentzian line shape is given by [Braga 89]:

$$s_c = \frac{c}{n \pi \delta f} \qquad 3.5.1$$

For a laser linewidth of δf=2.5 MHz, the speed of light c=3x10^{8}m/s and the refractive index of the medium n=1.5, the coherence length s_c would be 25.5 m. In the experiment, an 1km length of optical fibre was used for the long path arm, giving a resolution of less than 100 kHz and ensuring the decorrelation of the signals at the photodetector. Figure 3.5.5 shows the linewidth of the DQW-SCH laser against the inverse of laser output optical power.

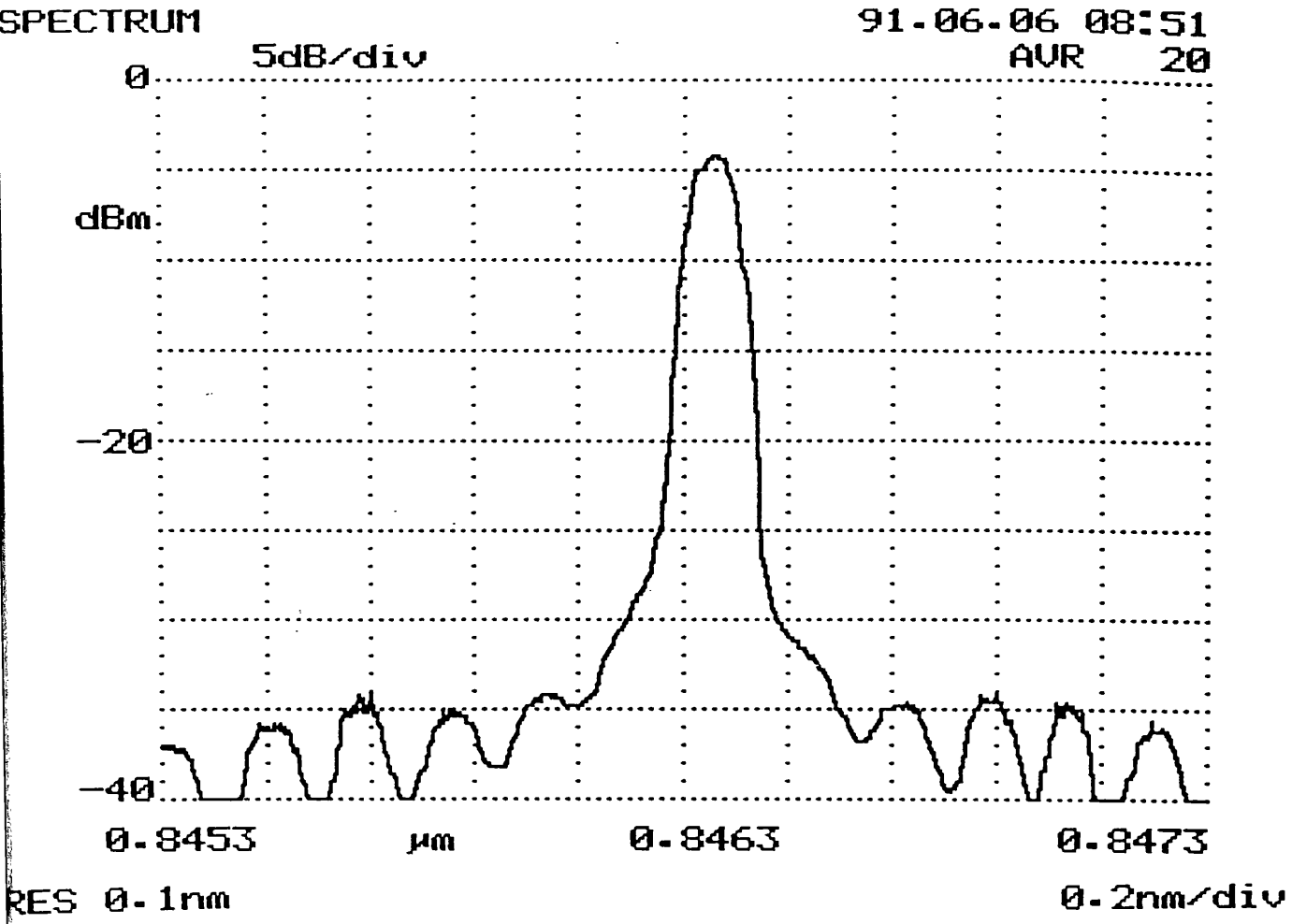

Figure 3.5.3: Spectrum of a DQW laser.

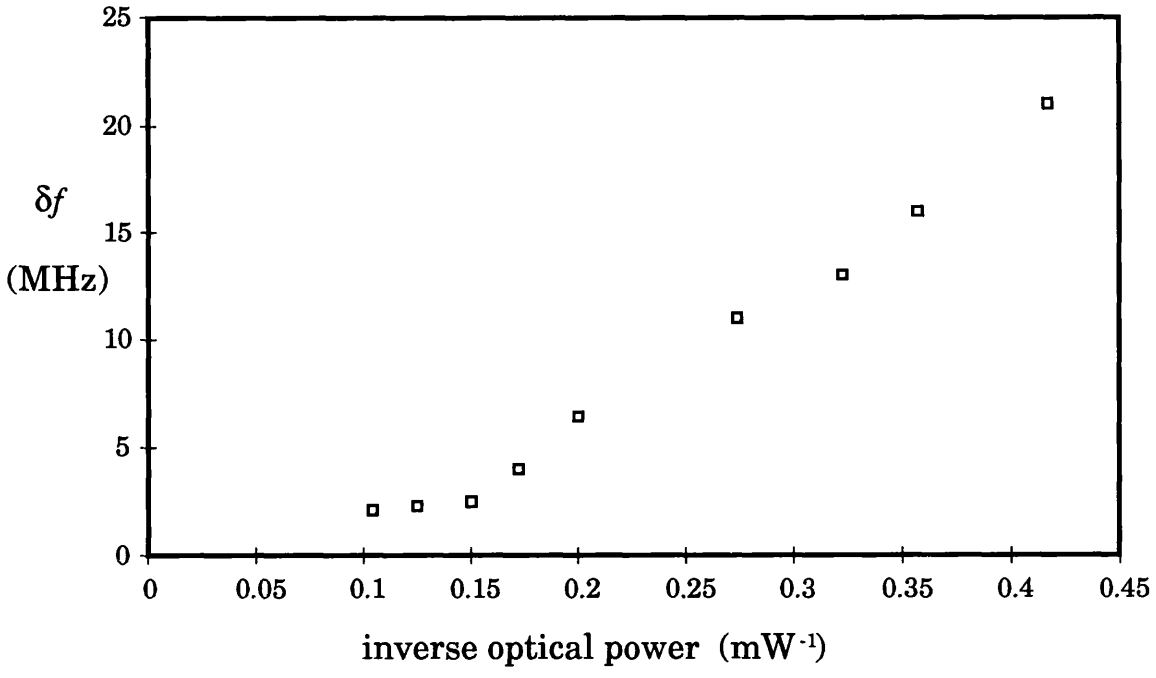

Figure 3.5.5: Linewidth of the DQW-SCH laser against the inverse of output optical power.

Note that the laser linewidth is proportional to the inverse of the optical power P_O (which is proportional to I_I), as given by:

$$\delta f = \frac{R_{sp}}{4\pi P_o}(1+\alpha^2) \qquad 3.5.2$$

Where R_{sp} is the spontaneous rate, which is proportional to the cavity gain and to the degree of inversion, and α is the linewidth enhancement factor [Henry 86]. Quantum well lasers present the benefit of a reduced value of α in the range of 2 to 3 against 5 to 6 in conventional semiconductor lasers [Yariv 89]. The linewidth of about 2.5MHz for currents above 40 mA was also measured by heterodyning two free running lasers.

3.5.3- Laser frequency modulation response measurement

The performance of an OPLL depends strongly on the bandwidth of the loop used, as was seen in Chapter 2. This dependency is particularly critical for narrow loop bandwidths. When wideband components are used in the loop, the frequency

modulation (FM) response of the slave laser becomes the limiting factor on the loop bandwidth. Measuring the FM response of the laser is therefore important in estimating the performance of the system. The area of the FM response curve of most importance is at low frequencies, as dc tuning is necessary to track of the master laser drift.

In this region, the dominant tuning mechanism is the thermal effect. As not all the pump power is converted into light emission, both spontaneous and stimulated emission, some of this power is wasted in the form of heat. When the injection current of the laser diode is modulated this power varies and so does the temperature of the device. The speed of this temperature variation depends basically on the thermal capacitance of the device and the thermal resistance between the device and the heat sink. It also depends on the thermal structure of the laser diode which is normally complicated. The temperature variation creates a change of the device optical length, which is closely related to the laser operating wavelength, producing frequency modulation. Experimentally, a variation of 1% in the total device optical length is expected for each °C [Cai 92].

One method of measuring the FM response of a laser diode is to measure the electrical transmission characteristics of the device together with an interferometric frequency discriminator using a network analyser. This method is described in this section and it was used to measure the low frequency part of the FM response of a DQW laser, (0-100MHz) which corresponds to the region normally dominated by the thermal effect.

For frequencies above 100MHz, the dominant effect in the tuning mechanism is the carrier density effect. A variation in injected current through the laser active region produces an alteration of the density of carriers (electrons and holes), which causes a change in the refractive index through plasma and band filling effects. A second method of measuring the FM response was used above 100MHz, which uses the relative size of the sidebands on the optical spectrum created by the modulation. These sidebands are observed using heterodyne techniques.

Principle:

The optical frequency discriminator produces a voltage at its output which is proportional to the frequency of the input optical signal. Optical frequency discriminators can be built using several kinds of interferometric systems like Fabry-

Perrot, Michelson or Mach-Zehnder interferometers. In this experiment, a Mach-Zehnder interferometer using a high birefringence optical fibre was used as an optical frequency discriminator.

Figure 3.5.6 shows a diagram of an all fibre Mach-Zehnder interferometer. The input optical signal is split into two different path with different optical path length and combined at the output.

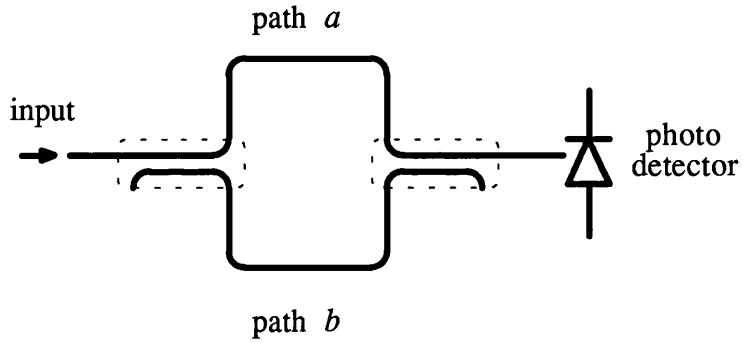

Figure 3.5.6: Diagram of an all fibre Mach-Zehnder interferometer.

The electrical fields of the signals coming from the paths *a* and *b* are given by:

$$e_a = 2\sqrt{\eta\, in_a}\cos(\omega t) \qquad 3.5.3$$

$$e_b = 2\sqrt{\eta\, in_b}\cos[\omega (t+\Delta)] \qquad 3.5.4$$

Where in_a and in_b are the intensity of the two signals, ω is the optical frequency of the input signal, η is the characteristic impedance of the medium and Δt is the propagation time difference between the two optical path lengths. The photo current at the photodiode terminals is given by equation 3.5.5 which is derived in Appendix 5.

$$i_p = \frac{R\,A}{2} in_t = R\,A\left[in_a + in_b + 2\sqrt{in_a\, in_b}\cos(\omega\,\Delta t)\right] \qquad 3.5.5$$

Note that i_p cannot have components in optical frequencies. Figure 3.5.7 shows a graph of equation (3.5.5) as function of $\omega\,\Delta t$.

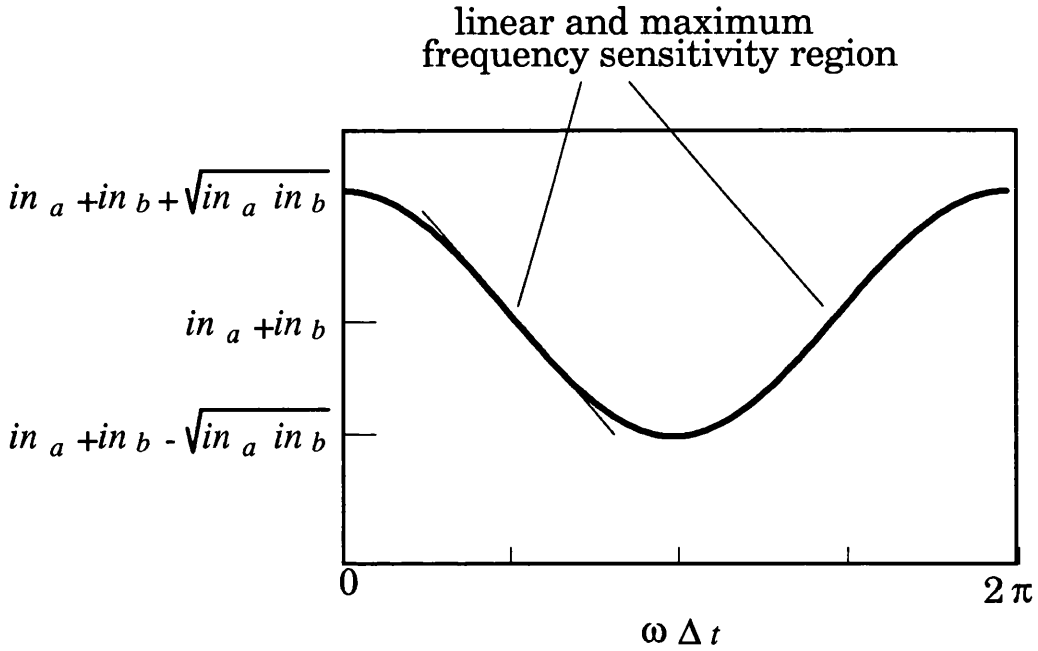

Figure 3.5.7: Graph of equation 3.5.5 as function of $\omega\,\Delta t$.

When the input signal is frequency modulated, ω can be described by :

$$\omega(t) = \omega_o + k_w\, a(t) \qquad 3.5.6$$

Where ω_o is the centre optical frequency k_w is the frequency modulation constant in rad·s^{-1}·V^{-1} and $a(t)$ is the modulating signal. The value of Δt can be adjusted in order to obtain maximum frequency sensitivity by making:

$$\Delta t\ \omega_o = \frac{3\pi}{2} + \mathrm{n}\,2\pi \qquad 3.5.7$$

or

$$\Delta t\ \omega_o = \frac{\pi}{2} + \mathrm{n}\,2\pi \qquad 3.5.8$$

Where n is an integer. The photo currents obtained when the conditions above are met, i_{p1} and i_{p2} ,are given by:

$$i_{p1} = R\,A\left[in_a + in_b + 2\sqrt{in_a\ in_b}\ \sin(k_w\ a(t)\,\Delta t)\right] \qquad 3.5.9$$

or

$$i_{p2} = R\,A\left[in_a + in_b - 2\sqrt{in_a\ in_b}\ \sin(k_w\ a(t)\,\Delta t)\right] \qquad 3.5.10$$

Equations (3.5.9) and (3.5.10) correspond to the conditions (3.5.7) and (3.5.8) respectively. If one of these conditions is met and:

$$k_w\, a(t)\, \Delta t \leq 1\,\text{rad} \qquad 3.5.11$$

it is possible to linearise the response of the frequency discriminator as:

$$i_{p1} = R\, A\left[in_a + in_b + 2\sqrt{in_a\, in_b}\, k_{fd}\, k_w\, a(t)\right] \qquad 3.5.12$$

or

$$i_{p2} = R\, A\left[in_a + in_b - 2\sqrt{in_a\, in_b}\, k_{fd}\, k_w\, a(t)\right] \qquad 3.5.13$$

Where k_{fd} is the frequency discriminator gain. Equations (3.5.12) and (3.5.13) correspond to the conditions (3.5.7) and (3.5.8) respectively. However, when the laser is directly modulated, its optical intensity is modulated as well as its optical frequency. In order to obtain the frequency response of the laser $k_w(\omega)$, it is necessary to eliminate the effect of the intensity modulation.

Assuming the intensity level to be the same at the arms a and b of the interferometer, and the modulation frequency f_m to be much smaller than the free spectral range of the interferometer:

$$f_m << \frac{1}{\Delta t} \qquad 3.5.14$$

it is possible to say that $in \cong in_a \cong in_b$, equations (3.5.12) and (3.5.13) become:

$$i_{p1} = 2\, in\, R\, A\left[1 + k_{fd}\, k_w\, a(t)\right] \qquad 3.5.15$$

and

$$i_{p2} = 2\, in\, R\, A\left[1 - k_{fd}\, k_w\, a(t)\right] \qquad 3.5.16$$

making:

$$i_p = \frac{i_{p1} - i_{p2}}{i_{p1} + i_{p2}} \qquad 3.5.17$$

resulting in:

$$i_p = k_{fd}\, k_w\, a(t) \qquad 3.5.18$$

Using equation (3.5.18), it is possible to estimate the frequency response of the laser by measuring the magnitude and phase of i_{p1} and i_{p2}.

High Birefringence fibre Mach-Zehnder interferometer:

Because the signal wavelength is extremely short compared to the total length of the arms, all fibre Mach-Zehnder interferometers are very sensitive to variations in environmental conditions such as temperature, pressure, vibrations, etc. This is the reason for their being widely used in fibre optic sensor systems. Several methods of stabilising this kind of interferometer have been proposed [Ramos 89], though they complicate the design of the system.

In a High Birefringence fibre Mach-Zehnder interferometer (Hi-Bi MZI), instead of using two different fibres for the two arms of the interferometer, only one hi-bi fibre is used which presents different refractive index for two orthogonal polarisation directions. Figure 3.5.8 shows the experimental arrangement.

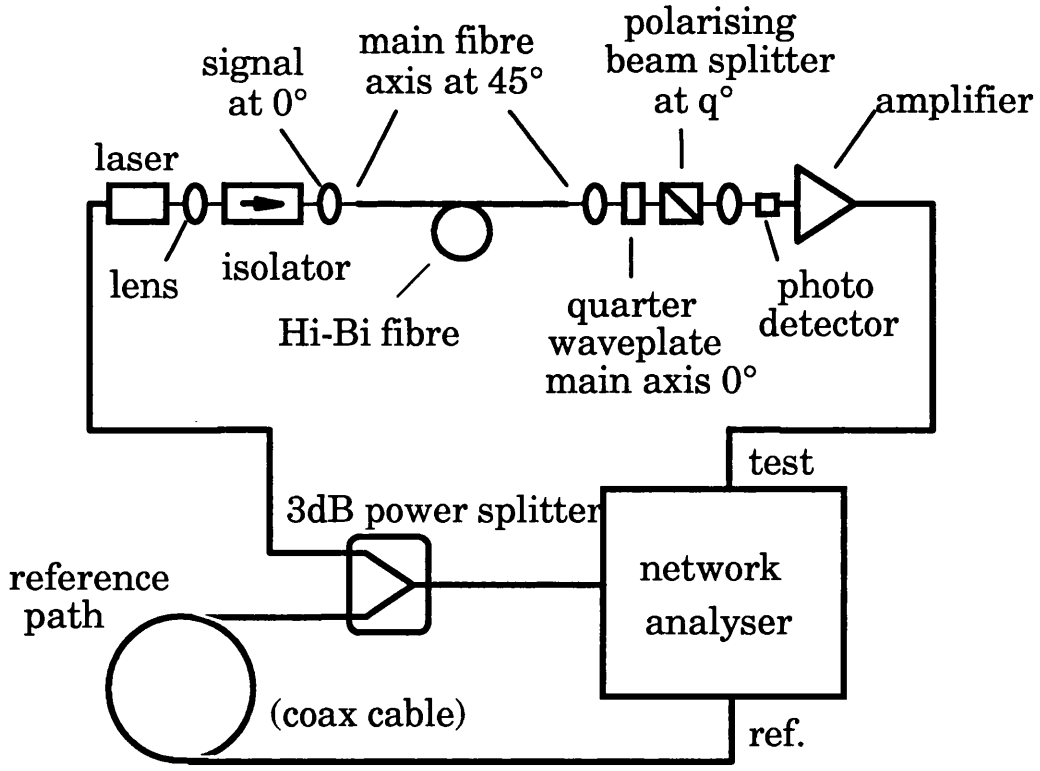

Figure 3.5.8: Diagram of the experiment used to measure the frequency response of the laser.

The input signal is split into these two orthogonal polarisation directions. As the propagation time through the fibre is different for each polarisation direction, at the output of the fibre a time delay Δt is introduced between the two signals. When these signals are combined, the system works as a Mach-Zehnder interferometer with two distinct path lengths. Because only one fibre is used to transmit both signals, each arm of the interferometer is equally affected by the environment, which makes the system less sensitive to fluctuations on temperature. In this way it is possible to avoid the need for stabilisation schemes.

A quarter wave plate is placed at the Hi-Bi fibre output, with its main axis positioned 45° from the main axis of the fibre, in order to recombine the two signals. It is possible to adjust the phase difference between the two signals by varying the angle of the last polarising beam splitter in relation to the quarter wave plate [Cai 92].

The Hi-Bi fibre used has a beat length (l_b) of 1 mm, so that every millimetre of fibre introduces a $\lambda/2$ shift between the signal polarised in the fast and the slow direction. In this case, the propagation time difference between the two optical path lengths Δt is given by:

$$\Delta t = \frac{l_f \lambda n}{2c} \qquad 3.5.19$$

Where l_f is the fibre length which is 34m for this case, λ is the wavelength, here 840nm, n is the fibre refractive index, here approximated to 1.5, and c is the speed of light in vacuum. This results in a Δt of 71.4ps (Δt^{-1}=14GHz), which is enough to meet the condition given by equation 3.5.14. The value of Δt can be easily adjusted by changing the angle of the polarising beam splitter θ [Cai 92]. In this way, it is possible to modify the value of Δt in order to obtain maximum frequency sensitivity, meeting the conditions given by equations (3.5.7) and (3.5.8).

A network analyser (HP4195A 10Hz-500MHz) was used to measure phase and magnitude of i_{p1} and i_{p2} for each frequency and a program was written to calculate i_p. Initially, the FM response of a Hitachi HPL1400 (for a current of 70mA) was measured, as shown in Figure 3.5.9. Also plotted are the measurements made using other techniques by [Welford 85] [Olesen 82 and Jacobsen 82] for the same laser type. The agreement is seen to be satisfactory in verifying the validity of the present method.

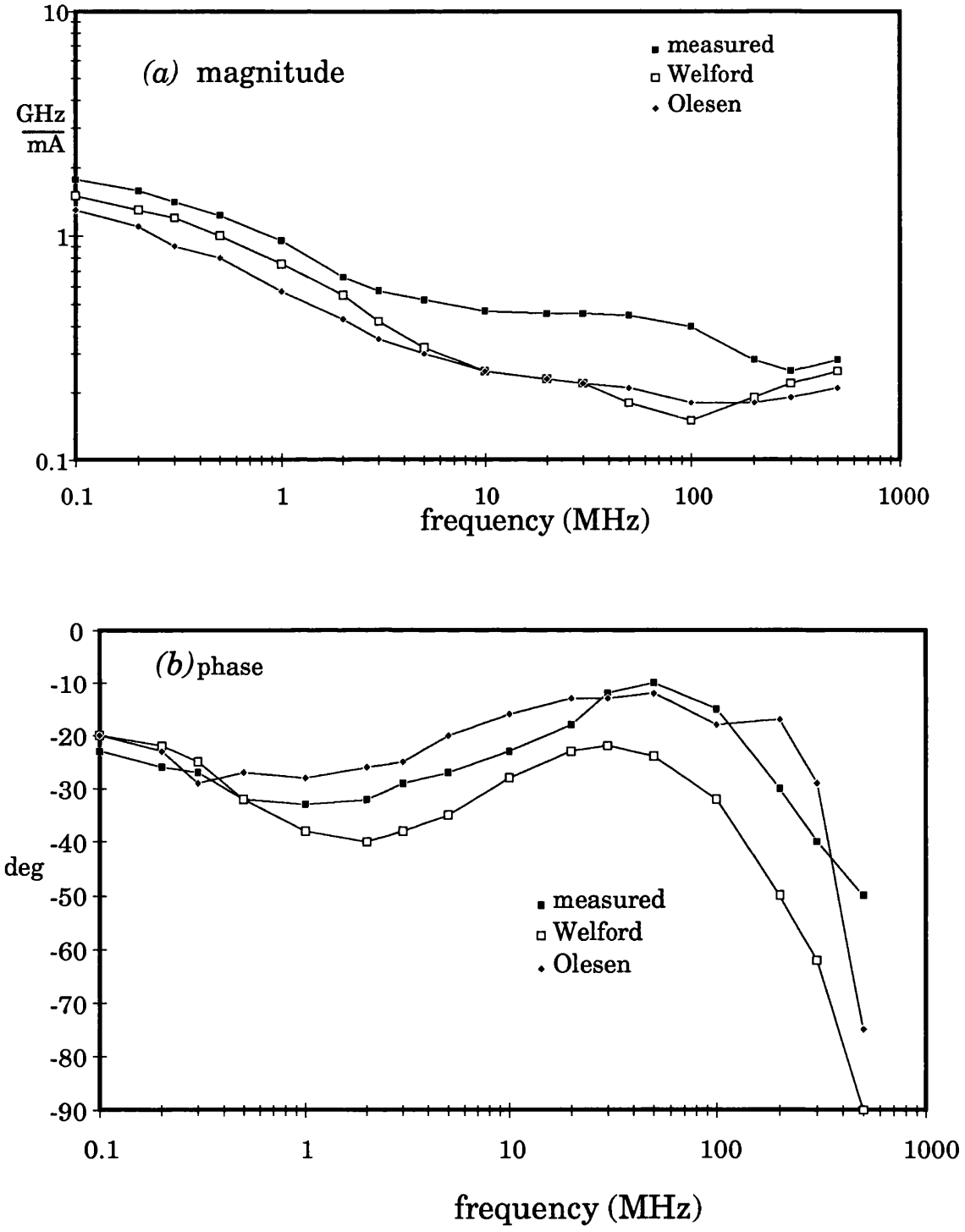

Figure 3.5.9: Magnitude (a) and phase (b) of i_p for a HLP1400 laser, (proportional to its frequency response).

Figure 3.5.10 shows the graphs of magnitude and phase of $i_p/a(t)$ for a DQW-SCH laser, which are proportional to its FM response. The dc frequency modulation constant of 3.75GHz/mA could be measured using a scanning Fabry Perot interferometer and was used to calibrate the curve.

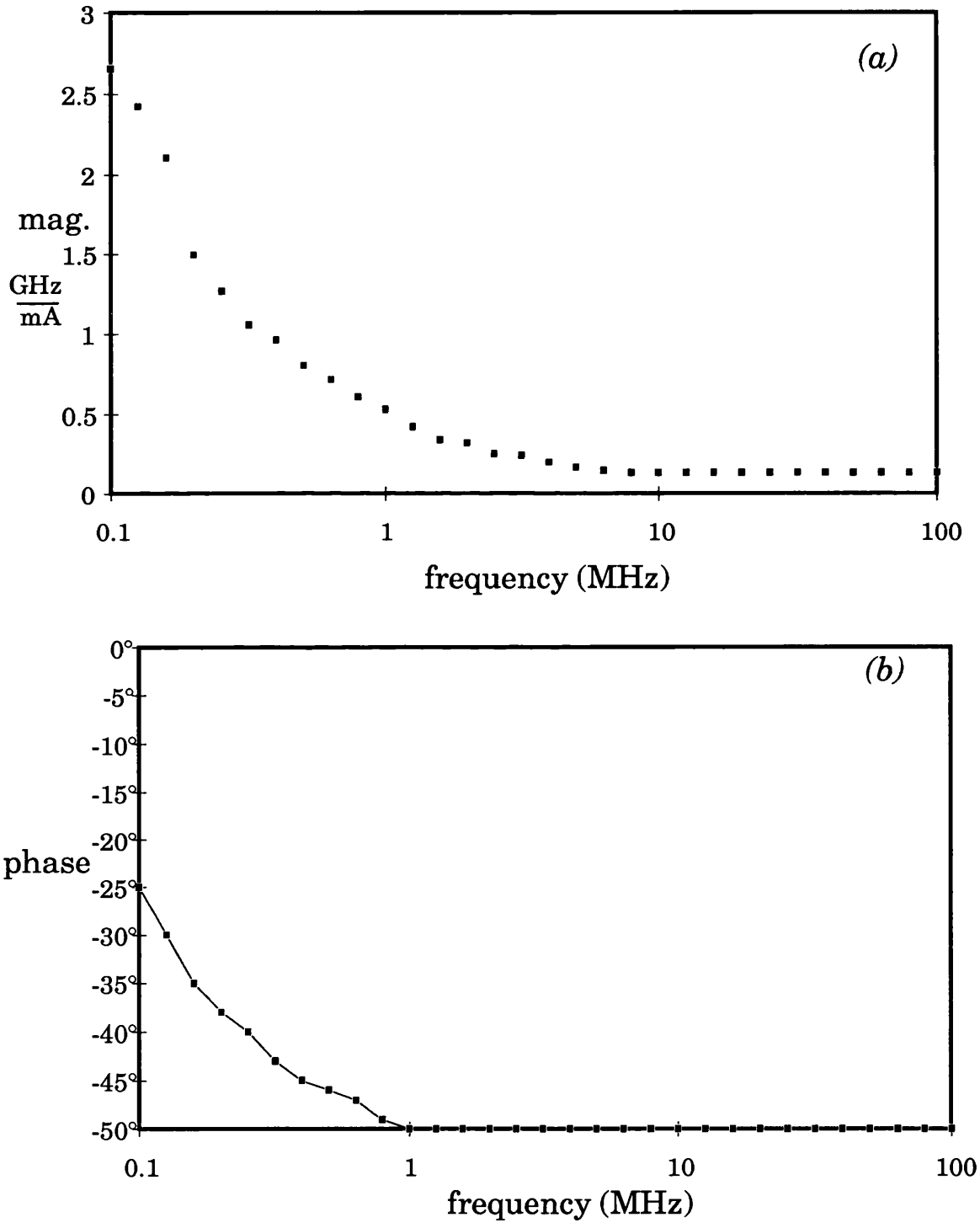

Figure 3.5.10: Magnitude (a) and phase (b) of a DQW-SCH laser FM response.

From Figure 3.5.10(a) it is possible to see that the low frequency response due to thermal effect limits the laser tuning to frequencies below 6MHz. For frequencies above 100MHz, the FM response of the DQW laser becomes too low to be measured with the hi-bi fibre interferometer, as better sensitivity is required. Therefore, a different method was used to measure the laser response for frequencies higher than 100MHz. Two DQW lasers were heterodyned using the arrangement described in Chapter 5 and the beat signal was observed using a microwave spectrum analyser. One of the lasers was then modulated generating side bands, as shown in Figure 3.5.11. The normalised power spectrum of a frequency modulated signal is given by Figure 3.5.12, where $J_n(\beta)$ is the Bessel function of first kind and order n, f_o is the centre frequency and β is the modulation index given by:

$$\beta = \frac{k_f \, A}{f_m} \qquad 3.5.20$$

Where k_f is the modulation constant, A is the modulating signal amplitude and f_m is the modulating signal frequency.

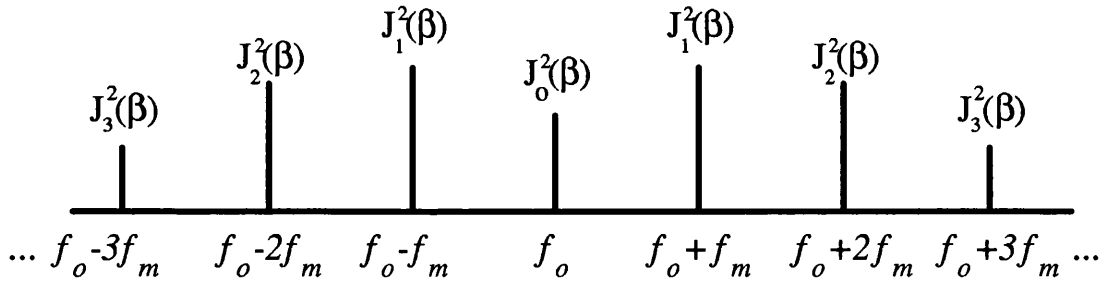

Figure 3.5.12: Normalised power spectrum of a frequency modulated signal.

The ratio between the side bands sizes is calculated and compared to a table of Bessel functions to determine the value of β for each value of modulation frequency. In this way it was possible to obtain the FM response shown in Figure 3.5.13. Note that in Figure 3.5.11 the hold maximum function of the spectrum analyser was used for a few seconds to minimise the error due to low frequency jitter of the beat signal. For this reason this method could not be used for measurements below 50MHz as the accuracy would be compromised. This method does not allow measurement of the phase of the FM response unlike the frequency discriminator method.

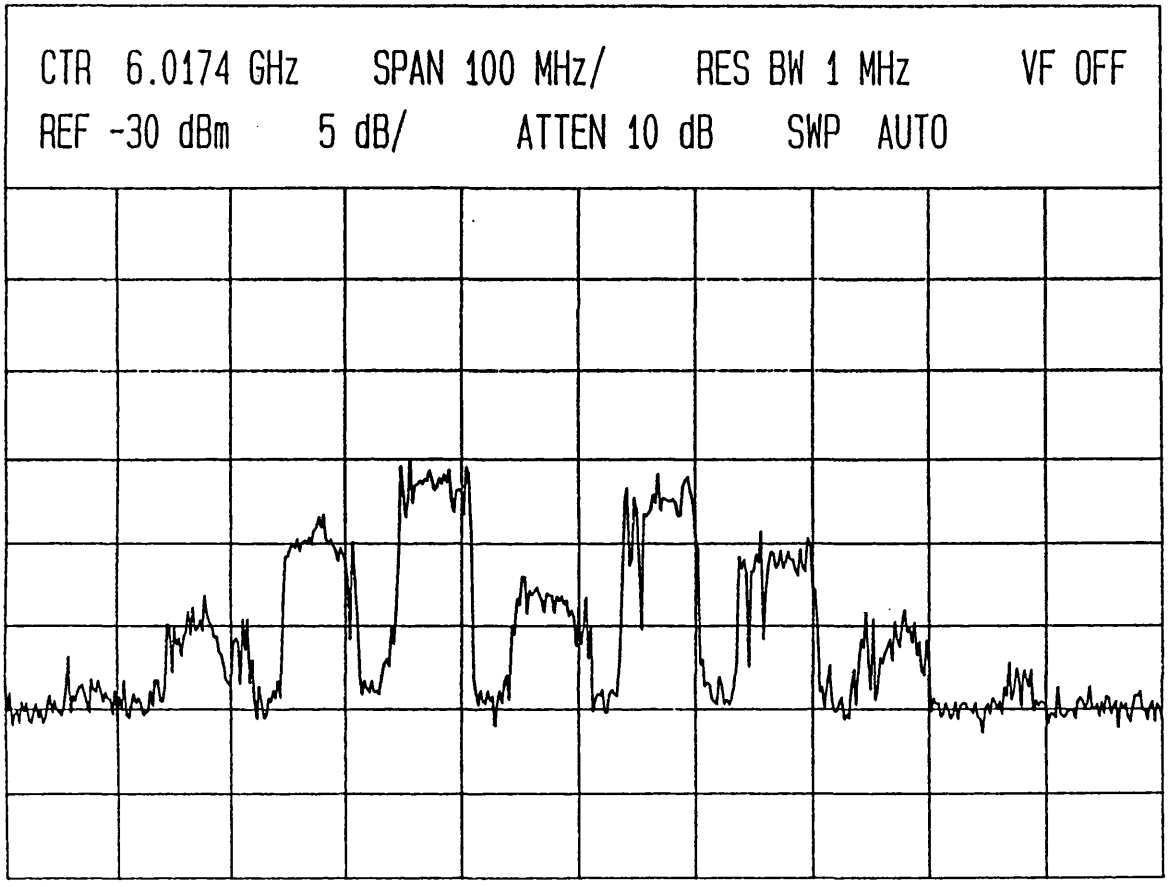

Figure 3.5.11: Spectrum of the heterodyne signal when one of the lasers is modulated.

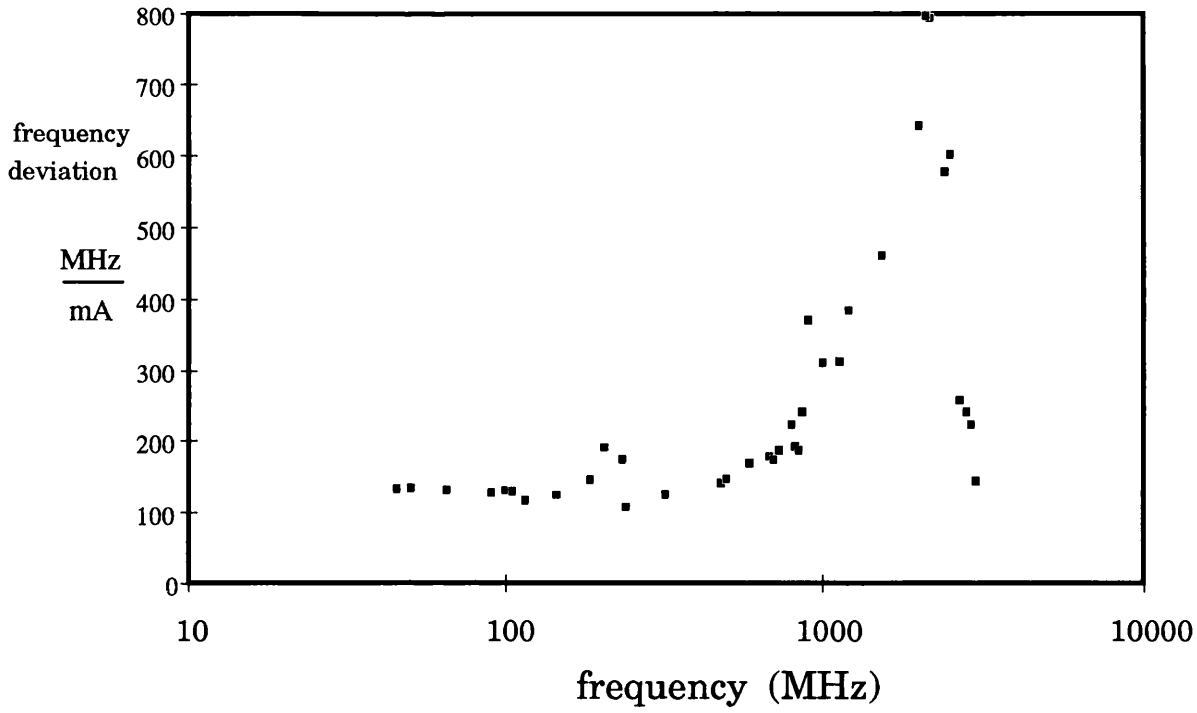

Figure 3.5.13: Magnitude of a DQW-SCH laser FM response using heterodyne method.

Over this frequency range, the dominant effect in the tuning mechanism is the carrier density effect. Note that the FM response of this laser peaks at about 2GHz. This peak is due the resonance frequency of the carriers and photons, which changes the relation between the injected current and carrier density. The value of this resonance frequency depends on the carrier and photon life time and the relative pumping level [Cai 92] [Kobayashi 82].

3.5.4- Discussion

In this chapter, the optical arrangement for the final experiment (described in Chapter 5) was studied. The use of bulk optics was found preferable to fibre optics in order to keep the loop delay time to its minimum. A combination of quarter-wave plates and beam splitters were found to be useful as optical isolators as they present shorter optical path lengths than Faraday rotation effect isolators at the 830 nm region. The optical mixing and the influence of misalignments were also studied.

The possibility of the use of optoelectronic integrated circuit (OEIC) in OPLLs in the future makes the use of external cavity lasers very unattractive, as they cannot be integrated. Although they offer narrow linewidths, external cavity lasers are very sensitive to vibrations and temperature fluctuations. They are also difficult to tune

continuously, restricting their use in OPLLs (Appendix 4 gives information on the external cavity laser experiments). For these reasons, the final experiment described in Chapter 5 was done using DQW-SCH lasers without external cavities.

The use of QW lasers in OPLLs is very attractive due to their narrow linewidth, which is a critical factor in the OPLL design, and to the possibility of integration of the slave laser into an integrated system. However, the FM response of the DQW lasers available can limit the loop bandwidth and severely restrict the loop performance. Using the equations given in Chapter 2 and assuming that a modified first order loop presenting a 6MHz cut-off frequency filter (which is roughly the frequency when the thermal effect becomes negligible for the DQW laser FM response), a 1.044rad^2 phase error variance would be expected. Despite being well below the $\pi^2/4$ rad^2 limit for achieving locking, a short time between cycle slips of 670 ns would be expected. However, the non uniform slave laser FM response is likely to alter the loop order and a better simulation using the FM response would be more accurate [Richards 85].

References

Braga, E. L., "Building and analysis of a high resolution Interferometer, implemented in fibre optics, using self-homodyne process", Master thesis, Department of Electrical Engineering, State University of Campinas, UNICAMP, Brazil, 1989.

Cai, B., "Electronic Tuning of Semiconductor Lasers with Quantum Well Devices", Ph.D. thesis, Department of Electronic and Electrical Engineering, University College London, 1992.

Charles, P. M., Williams, P. J., Wood, A. K., Ogden, R. and Carter, A. C., "OEICs for WDM Tranceiver Modules Fabricated by Reactive Ion Etching on Semi-Insulating Substrate", Electronics Letters, vol. 28, n. 12, 1992, pp. 1084-1085.

Daniel, D.R., Buckley, D., Garrett, B., "Quantum well ridge waveguide lasers optimised for high power single spatial mode applications", Proc. SPIE, Los Angeles, 1989, vol.1043, p.61.

Garrett, B., Glew, R.W., "Low-threshold, high-power zero-order lateral-mode DQW-SCH metal-clad rigid waveguide (AlGa)As/GaAs lasers", *Elect. Lett.*, 1987, vol.23, pp. 371-373.

Henry, C. H., "Phase Noise in Semiconductor Lasers", J. Lightwave Tech., vol. LT-4, n. 3, March 1986, pp. 298-311.

Jacobsen, G., Olesen, H., Birkedahl, F. and Tromborg, B., "Current/Frequency-Modulation Characteristics for Directly Optical Frequency-Modulated Injection Lasers at 830nm and 1.3μm", Electronics Letters, vol. 18, n. 20, 1982, pp. 874-876.

Kobayashi, S., Yamamoto, Y., Ito, M. and Kimura, T., "Direct Frequency Modulation in AlGaAs Semiconductor Lasers", IEEE Journal of Quantum Electronics, vol. QE-18, n. 4, April, 1982, pp. 582-595.

Koch, T. L. and Koren, U., "Semiconductor Photonic Integrated Circuits", IEEE Journal of Quantum Electronics, vol. QE-27, n. 3, March, 1991, pp. 641-653.

Okoshi T., Kikuchi, K. and Nakayama, A., "Novel Method for High Resolution Measurement of Laser Output Spectrum", Electronics Letters, vol. 16, n. 16, 1980, pp. 630-631.

Olesen, H. and Jacobsen G., "Phase Delay between Intensity and Frequency Modulation of a Semiconductor Laser", Proceedings of the 8th European Conference in Optical Communications, September, paper B IV-4, pp. 291-295.

Ramos, R.T., Conforti, E., "Stabilization of an all fibre Mach-Zehnder interferometer for optical telemetry applications", International Microwave Symposium, Sao Paulo, Brazil, 1989.

Ramos, R.T., Seeds, A.J., "Delay, linewidth and bandwidth limitations in optical phase-locked loop design", *Elect. Lett.*, 1990, 26(6), pp.389-391.

Richards F. P.: "Microwave signal transmission on optical links", Ph.D. thesis, Department of Electronic and Electrical Engineering, University College London, 1985.

Steele, R.C., Creaner, M.J., Walker, G.R., Walker, N.G.: "Optical PSK transmission experiment at 565Mbit/s incorporating an endless polarization control system", Proceedings of SPIE Components for Fiber Optics Applications and Coherent Lightwave Communications, Boston, 1988, vol.988, pp. 302-309.

Steele, R.C., "Optical phase locked loop using semiconductor laser diodes", Elect. Lett., 1983, 19, pp.69-71.

Yariv, A., "Quantum well semiconductor lasers are taking over", IEEE Circuits and Devices Magazine, November 1989, pp. 25-28.

Welford, D., and Alexander, S. B., "Magnitude and Phase Characteristics of Frequency Modulation in Direct Modulated GaAlAs Semiconductor Diode Lasers", J. of Lightwave Technology, vol. LT-3, n. 5, October, 1985, pp. 1092-1099.

Chapter 4

Electrical Design

4.1- Introduction

The performance of the optical phase-locked loop (OPLL) is closely related to the loop gain, loop bandwidth and the total loop propagation delay time, as discussed in Chapter 2. Therefore, the design of the loop circuit is dictated by these restricting factors.

The loop gain and bandwidth depends on the frequency response of all the loop components, mainly the photodetector response, the FM response of the slave laser, which was discussed in Chapter 3, and the phase detector gain. A microwave amplifier and active loop filter are included to provide extra gain necessary in the loop. The loop bandwidth is required to be as wide as possible, since wide linewidth lasers are used. Despite all the efforts to keep the loop filter bandwidth as wide as 500 MHz in the electronic circuit, the total bandwidth is limited by the laser frequency response, as will be shown in Chapter 5. Finally, the loop delay time has to be kept to the minimum possible, though its bandwidth limiting effect is also diminished by the bandwidth limitation imposed by the laser FM response.

In this chapter, the design of the electrical part of a modified first order OPLL is outlined, starting by giving an overview on the loop circuit, followed by a description of the phase detector used. The design of the phase error amplifier (loop filter) is presented, showing how a split path technique was used to overcome delay restrictions in dc coupled amplifiers. Finally, the temperature control system design is described.

4.2.- The Loop configuration

Figure 4.2.1 shows the electrical configuration for a heterodyne OPLL. As a heterodyne OPLL is required, the first step in the design of the loop circuit is to define the value of the offset frequency, which can be chosen depending on the particular application of the system. If the OPLL is used as an optical frequency synthesiser [Fernando 90], the offset frequency would give the optical carrier spacing. If used as a coherent receiver, the value of the offset frequency would select a given channel

among a comb of optical carriers. The experiment described here is not aimed at any specific application of OPLLs. The value of the offset frequency selected was 6 GHz, which is a reasonable value for most of the applications. However, due to the wide bandwidth of the microwave components used, the value of the offset frequency could be changed from 5 to 7 GHz simply by tuning the offset generator.

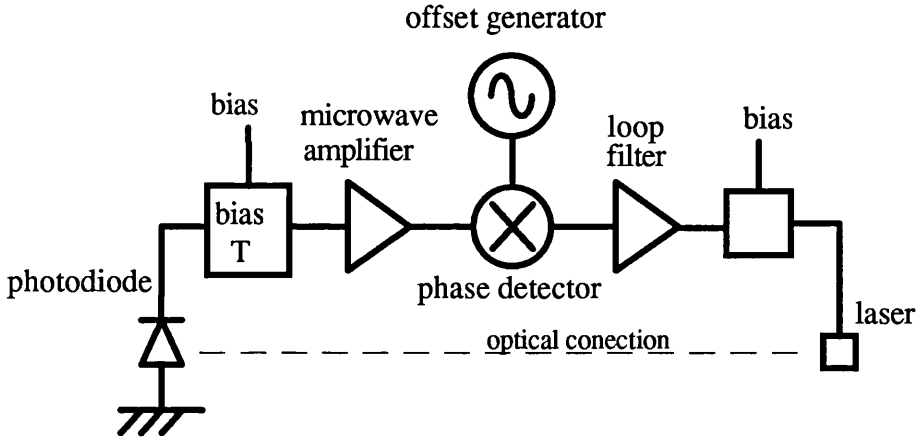

Figure 4.2.1: Diagram of the electrical configuration.

The first component of the loop circuit is the photo detector whose bandwidth could restrict the total loop bandwidth. The detector bandwidth is inversely proportional to its capacitance which depends on the device area. Smaller area normally results in wider bandwidth, though the use of a small area detector can complicate the optical alignment. However, the angular misalignment tolerance for efficient optical mixing is improved by using small area photodetectors as seen in Chapter 3. The detector selected was an ultra high speed GaAs ITO Schottky photo diode (GEC Y-35-5252-22) with a bandwidth of 18 GHz when reverse biased at 5V. It has an active area of 470μm^2 and is mounted on an SMA connector, which was found to be convenient for high frequency operation. The responsivity was 0.35 A/W in the 830 nm wavelength region. A bias circuit was built and fed using a battery to avoid ripple noise from power suppliers.

A microwave amplifier is placed just after the photo diode because the beat signal was found to be too weak (of the order of -40 dBm) to be efficiently discriminated by the phase detector. This low power level is mainly due to difficulties with alignment and optical coupling. The amplifier used was a WJ6882-812 (Watkins-Johnson) with a gain of 20 dB and bandwidth from 2 to 8 GHz.

4.3- The phase detector

The ideal phase detector produces a voltage at its output terminal which is proportional to the phase difference between its two input signals. However, practical devices present non-linear response which can be approximated as linear for small values of phase shifts. Although several kind of phase detectors are available for low frequency operation, the use of double balanced mixers has been the most attractive solution at GHz frequencies. These devices have sinusoidal responses which can be considered linear for phase errors below 1 radian.

In the experiment described in Chapter 5, a double balanced mixer (Watkins Johnson WJ-M14) was used as the phase detector. This device was chosen for its wide bandwidth around 6 GHz (the offset frequency selected): LO input from 4 to 9 GHz, RF input from 4 to 8 GHz and the IF output from DC to 2 GHz.

The sinusoidal response of this device was measured using the set up shown in Figure 4.3.1a, while Figure 4.3.1b shows the device characteristic. For this measurement, the LO drive power was 7 dBm which provides the best phase sensitivity [WJ data book]. A trombone delay line was used to adjust the phase difference between the two inputs, while the output was loaded with a resistance of 50Ω to avoid impedance mismatches at high frequencies, despite the efficiency loss introduced by this low impedance.

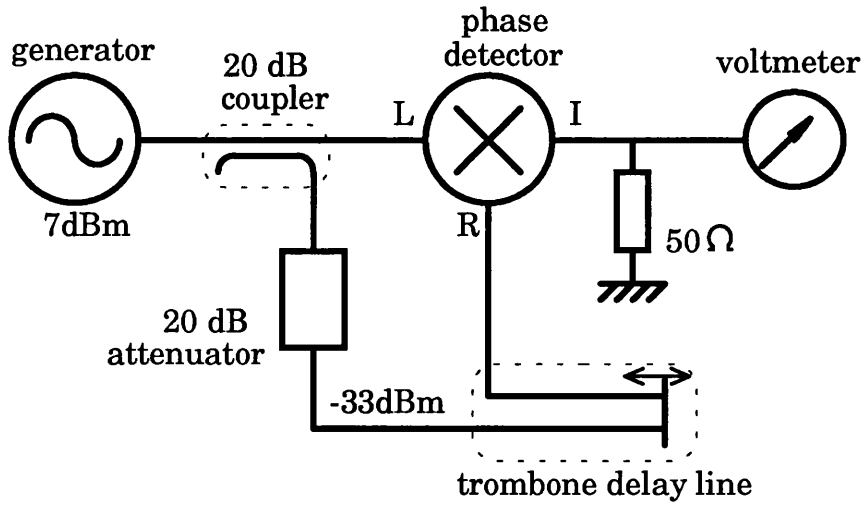

Figure 4.3.1a: Diagram of the set up for measuring the response of the phase detector.

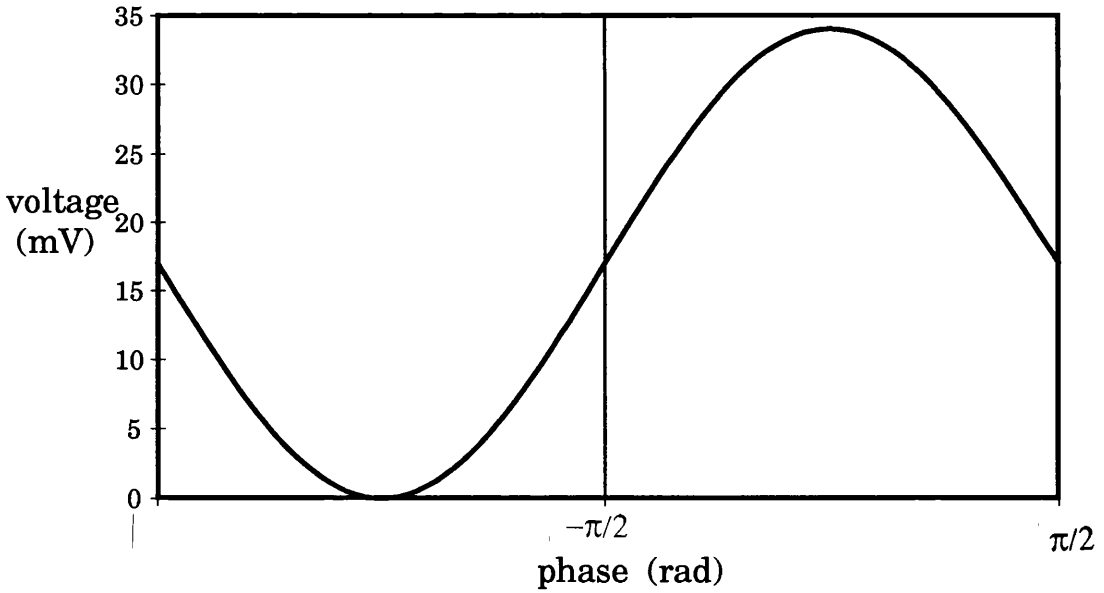

Figure 4.3.1b: Response of the phase detector.

However, the response of the phase detector depends strongly on the power level of the input signals, which makes it possible to change the sensitivity of the device by changing the power of the LO input signal. This provides an effective way of adjusting the total loop gain by altering the output power of the offset generator. So, it was necessary to measure the response of the phase detector for several values of LO and RF levels. A different set up was necessary for this measurement once the voltage levels were too low to be detected by available voltmeters. Figure 4.3.2a shows the arrangement used, while Figure 4.3.2b plots the power level at the IF port against that at the RF port for several different LO port levels.

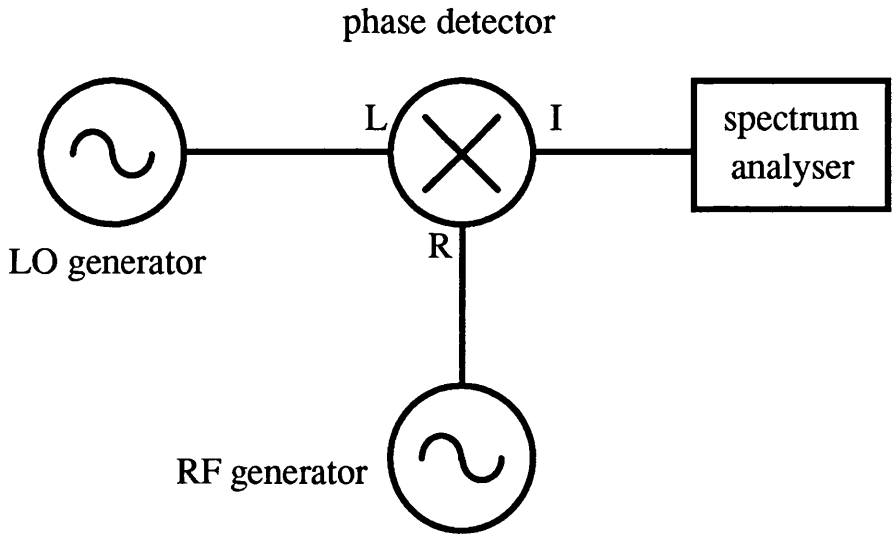

Figure 4.3.2a: Diagram of the set up for measurement of the power levels at the phase detector ports.

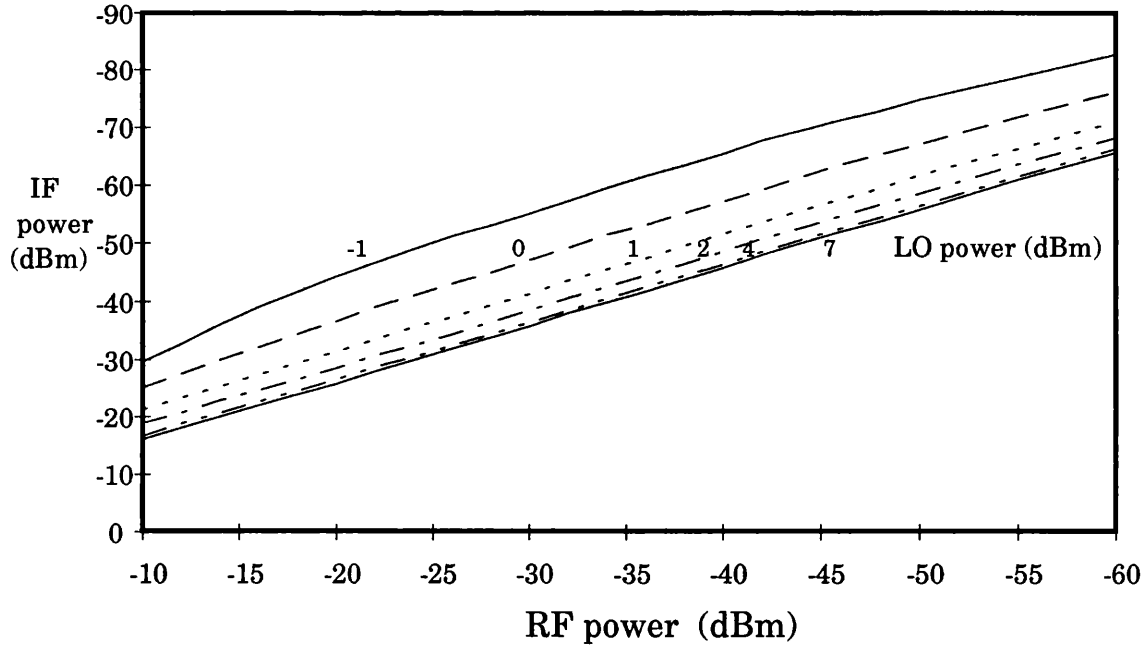

Figure 4.3.2b: Plot of the power levels at the phase detector ports.

With this data it is possible to calculate the phase detector gain k_d for several levels of LO signal power, by calculating the maximum voltage excursion V_{max} for each value of IF power level in dBm I_{dBm} over a load resistance r_l=50Ω. As the inclination of a sinusoid can be considered 1 for low values of phase error, k_d is given by V_{max} (in V/rad)

$$k_d = \sqrt{2\, r_l\, 10^{\left(\frac{I_{dBm}}{10}\right)}\, 10^{-3}} \qquad 4.3.1$$

The response of the phase detector is considered linear for small variations of the phase error (up to about 1rad) around the point of quadrature where the phase difference between the two input signals is π/2 rad. Figure 4.3.3 shows the phase detector gain (k_d) against RF power for several values of LO power.

From the graph, it is possible to see that the sensitivity of k_d with LO power variations above 4dBm is too low to affect to total loop gain significantly. Therefore, LO power levels between -1dBm and 4dBm have to be used if an adjustment of the phase detector gain is required in order to change the loop gain. For RF power levels of about -40dBm, this range would give a gain variation from 0.2 to 1.4mV/rad, equivalent to 8.5dB variation in the total loop gain. By performing the heterodyne experiment described in Chapter 5, it was seen that power levels of about -40 dBm are expected at the RF port. So a k_d of 0.8mV/rad was used for the circuit design (corresponding to a LO power of 1dBm).

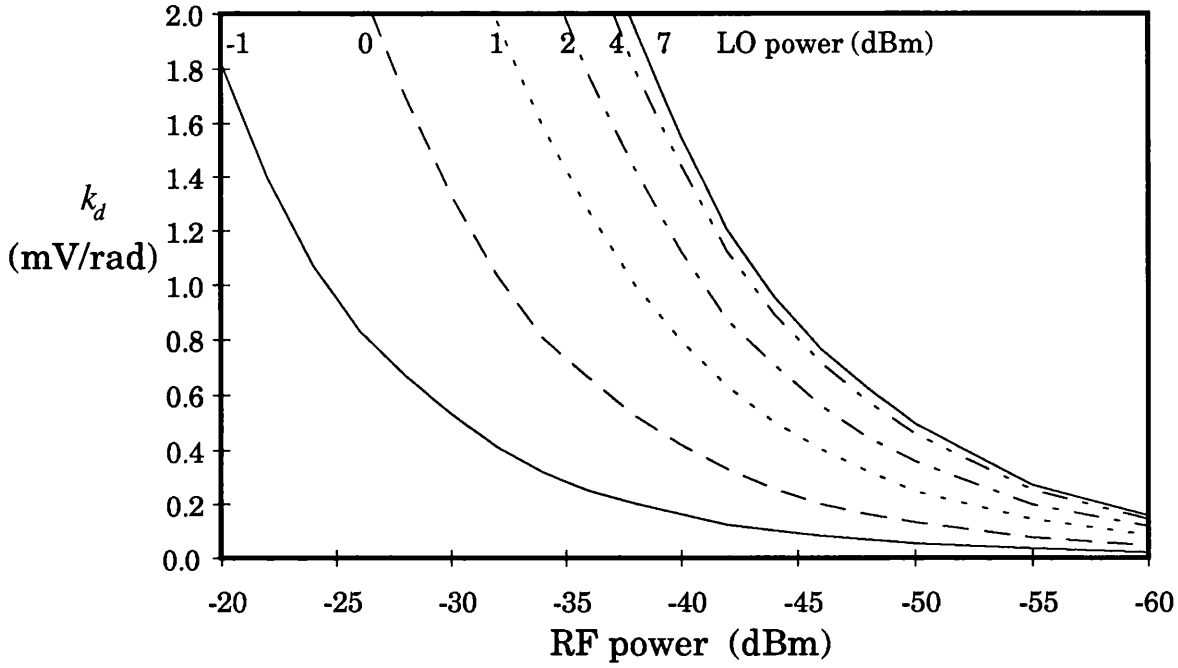

Figure 4.3.3: Plot of the phase detector gain (k_d) against the RF power for several values of LO power .

4.4.- Phase error amplifier

4.4.1- Introduction

The phase error amplifier is basically a modified first order loop filter and it is the most critical element of the electronic design. As was seen in Chapter 2, a wide loop filter bandwidth allows the use of relatively wide linewidth lasers in OPLLs, as long as the total loop delay time is kept low. The phase error amplifier has also to be DC coupled. Wide bandwidth and DC coupled amplifiers are not commonly available and are difficult to design. This section describes the design and construction of a 20 dB gain amplifier which has uniform magnitude and phase from 0 to 500 MHz.

Previous work has been done on fast acquisition loops [Ward 81], in which microwave PLLs were used as translation loops in active phased array radar systems. In this case, rapid lock-up capability is required if the radiated pulse spectrum is not to be degraded by locking transients. Further work suggested a solution based on the use of wide bandwidth dc-coupled amplifiers in the loop [Ward 83]. To achieve this, a split path configuration was proposed.

Baseband communication systems have also required dc-coupled amplifiers with constant gain and linear phase to achieve a constant group delay. Kahlert et al [Kahlert 89] also proposed the use of a split path technique and built a hybrid integrated dc-coupled amplifier with a gain-bandwidth product of 40 GHz.

The design of a dc-coupled wideband amplifier for lightwave test instrumentation has also been considered [Miller 91]. In this case, dc-coupling is required to display the absolute levels of a time domain waveform and to be able to determine extinction ratio. In addition, the average optical power can be determined from the dc level. The solution adopted was a split path amplifier similar to the one presented here.

4.4.2- Split path amplifier principle

Delay through microwave components is usually defined purely by the electrical path length, with physical size as a limiting factor. However, because of the necessary bias circuitry, microwave broadband amplifiers do not allow dc-coupling [Ward 83] [Kahlert 89]. The configuration of split path amplification [Ward 81] solves the problem by employing the technique of routing the high frequency (HF) and the low frequency (LF) part of the signal to amplifiers each best suited to the range of frequencies involved, followed by addition of the output signals. In this way, amplifier delay time for high frequencies can be reduced to below 0.5 ns [Ward 83] while maintaining operational amplifier accuracy at low frequencies. Figure 4.4.1 shows the block diagram of a split path amplifier.

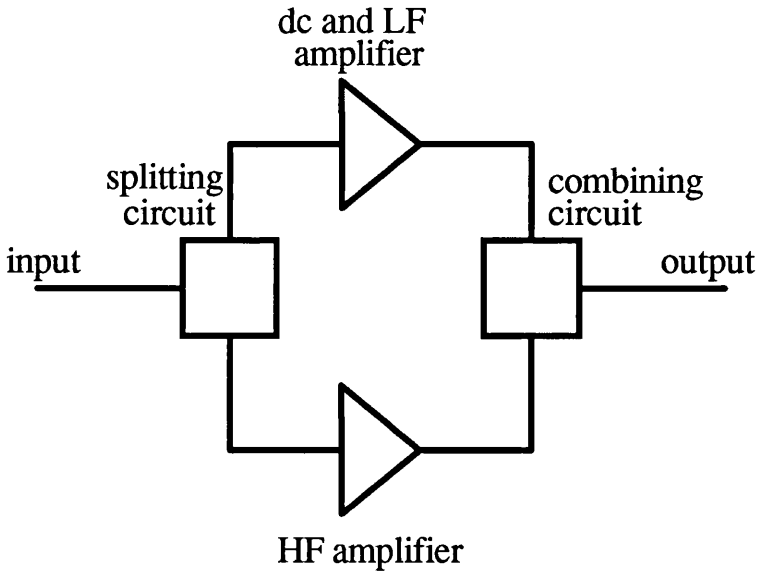

Figure 4.4.1: Block diagram of a split path amplifier.

The ideal operation of the two amplifiers in the neighbourhood of the crossover is shown in Figure 4.4.2 *a* and *b* by a polar and frequency response plot of the response of both amplifiers [Miller 91].

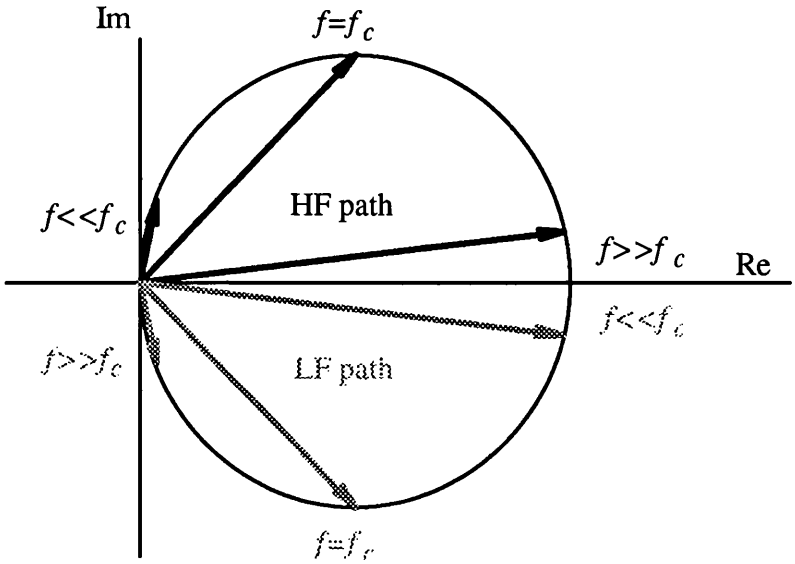

Figure 4.4.2a: s plane plot of ideal operation of the low frequency and high frequency amplifiers near the crossover frequency.

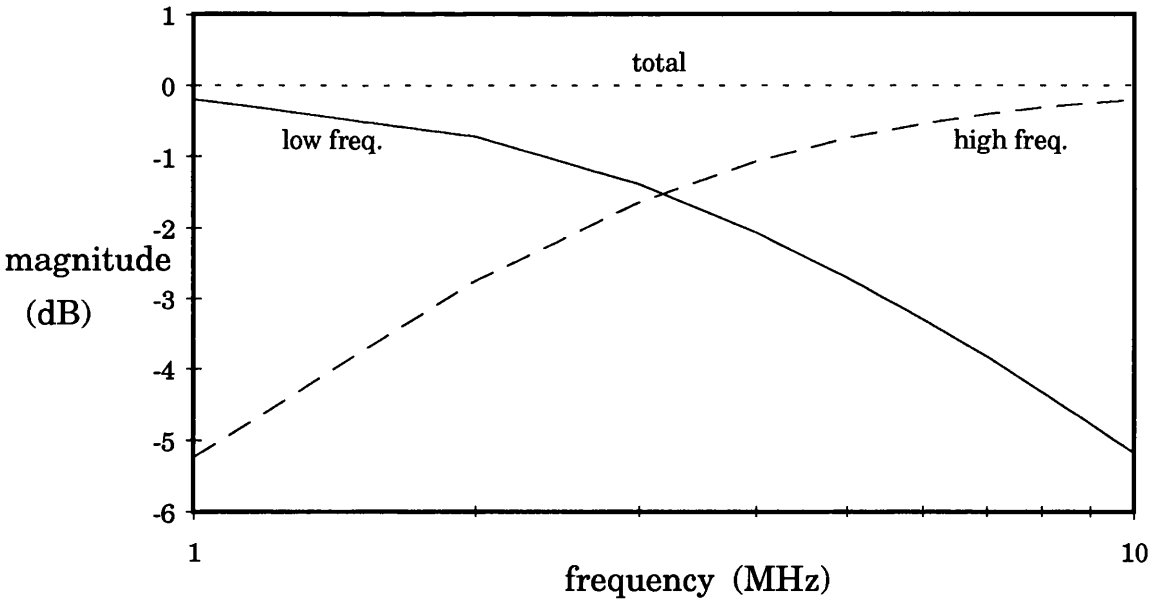

Figure 4.4.2b: Frequency response plot of ideal operation of the low frequency and high frequency amplifiers near the crossover frequency.

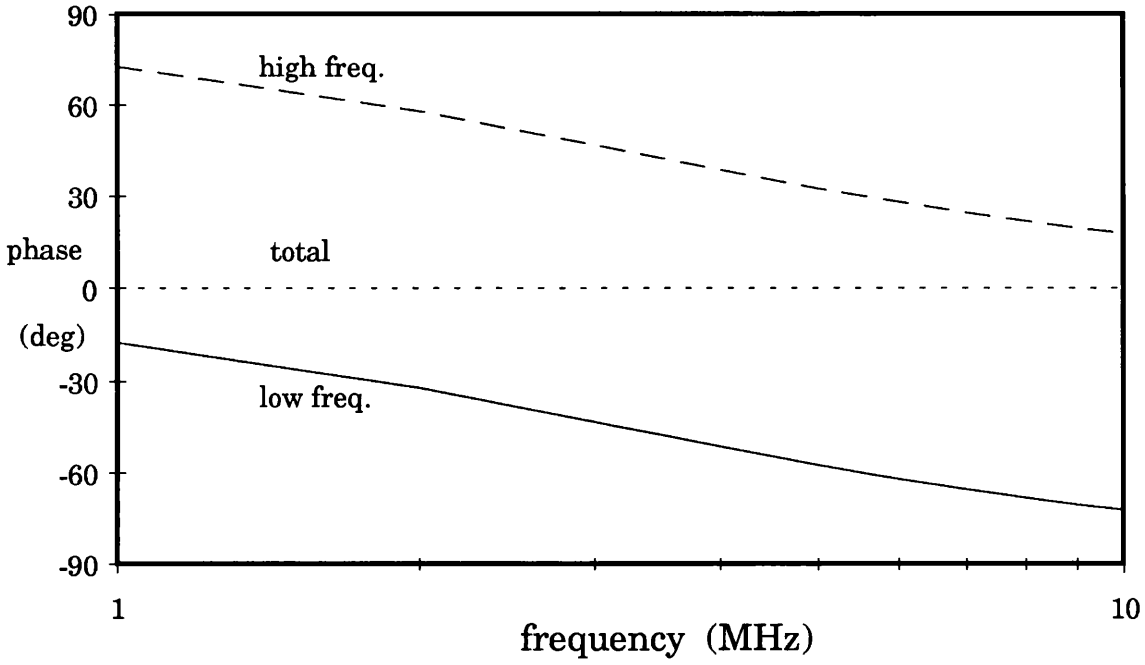

Figure 4.4.2b: Phase of the frequency response plot of ideal operation of the low frequency and high frequency amplifiers near the crossover frequency.

Well below the crossover frequency, the high frequency path has 90 degrees of phase lead and essentially zero amplitude, while the low-frequency path has zero degrees of phase and unity amplitude. At the crossover frequency, both paths have vectors that are complex conjugates and sum to produce a vector of unity amplitude with zero degrees of phase. Well above the crossover frequency the low frequency path has 90 degrees of phase lag and essentially zero amplitude, while the high-frequency path has zero degrees of phase and unity amplitude. A well-behaved crossover frequency response characteristic is important for good time-domain performance for signals that have a spectral content in the neighbourhood of the crossover frequency.

The objective is to achieve flat amplitude and phase response for the total amplifier, as shown in Figure 4.4.2b. The two amplifiers work as a low pass and high pass first order active filter with exactly the same value of cut-off frequency. If there is a frequency mismatch, any difference between the two cut-off frequencies, the total amplifier response loses its flatness as shown in the frequency response plot in Figure 4.4.3.

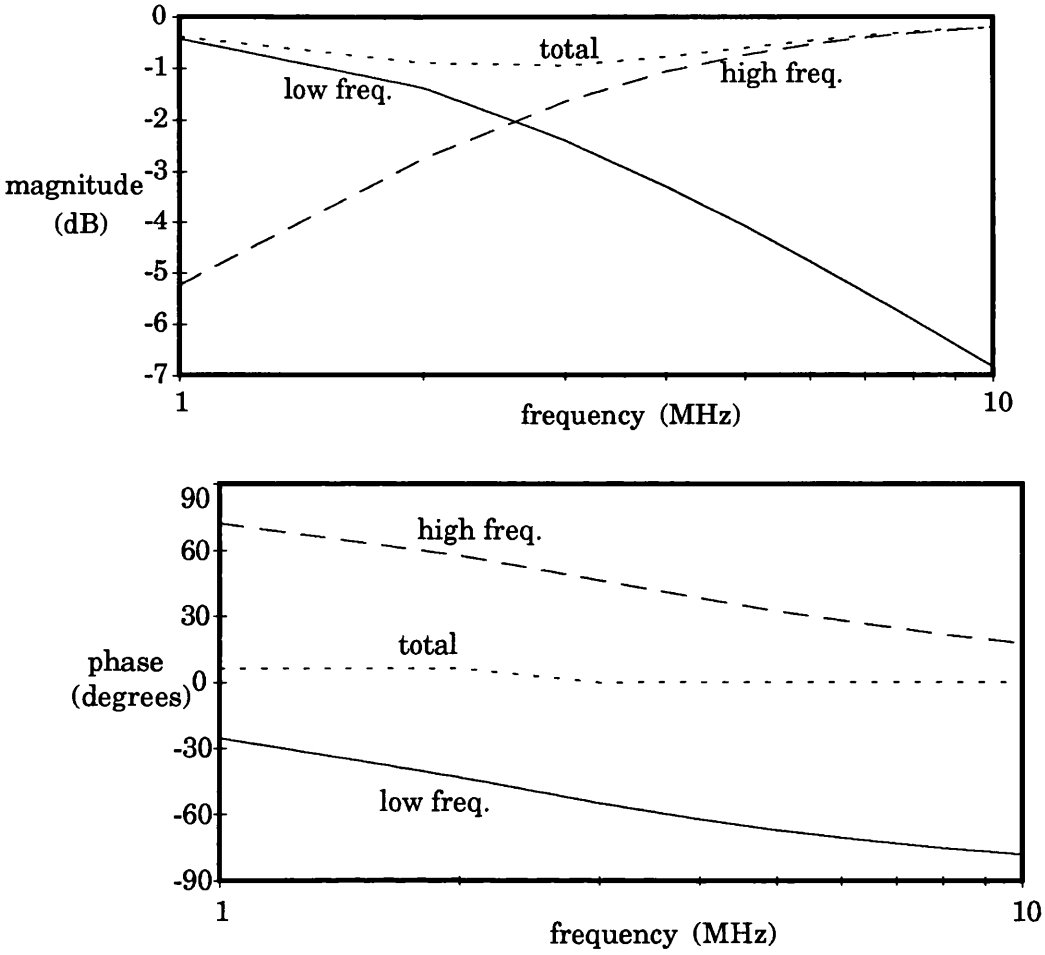

Figure 4.4.3: Frequency response plot of the operation of the low frequency and high frequency amplifiers near the crossover frequency when they do not present the same cut-off frequency.

4.4.3- Split path amplifier circuit

In this section, the design of each block of the split path amplifier is discussed and the circuit diagrams presented. The four circuits shown here correspond to the four blocks of Figure 4.4.1. The value of the crossover frequency was chosen to be 3.2 MHz, which corresponds to an RC time constant given by 50 Ω and 1 nF. Figure 4.4.4 shows the complete circuit diagram of the split path amplifier, divided into four parts.

High frequency amplifier:

Two monolithic microwave amplifiers Avantek MSA 0135 were used in cascade. They present 50 Ω input and output impedance, an upper cut-off frequency of 700 MHz and a lower cut-off frequency dependent on the coupling capacitors between stages. The two 47 nF capacitors used bring the lower cut-off frequency well below

the crossover frequency. Good bias decoupling circuits were found essential for the stable operation of the amplifier.

DC and low frequency amplifier:

The NE 5539 high speed operational amplifier was used as the DC and low frequency amplifier. Due to its wide bandwidth (gain bandwidth product of 1.2 GHz) and high slew rate (600 V/μs), this amplifier presents uniform response from dc to well above the crossover frequency (40 MHz). Gain and offset adjust control were added to a non-inverting configuration.

Splitting circuit:

The function of this circuit is to keep the input impedance of the total amplifier constant (50 Ω) throughout its bandwidth and fix the cut-off frequency of the low frequency amplifier. The 50 Ω input impedance is maintained by introducing a π circuit into the high frequency path, while a 470 Ω resistance keeps the impedance of the low frequency path high enough not to interfere with the total input impedance. The cut-off frequency of the low frequency amplifier can be adjusted by a variable capacitor.

Combining circuit:

The output impedance is kept at 50 Ω by a T junction which provides two 50 Ω outputs, one for the laser and the other for the spectrum analyser. The lower crossover frequency of the HF amplifier is given by the 1 nF coupling capacitor at the output and 50 Ω. A transistor diode voltage shift circuit is added to the LF path to match the output voltage of the amplifier to the voltage of the biased laser. A 200 Ω divider maintains the LF path output impedance constant and high in relation to the HF output path.

Total result:

Figure 4.4.5 shows the frequency response plot corresponding to the total split path amplifier response. Its behaviour at the crossover frequency is uniform to within 0.1 dB and the total bandwidth achieved covers from dc to 700 MHz with a gain over 20 dB.

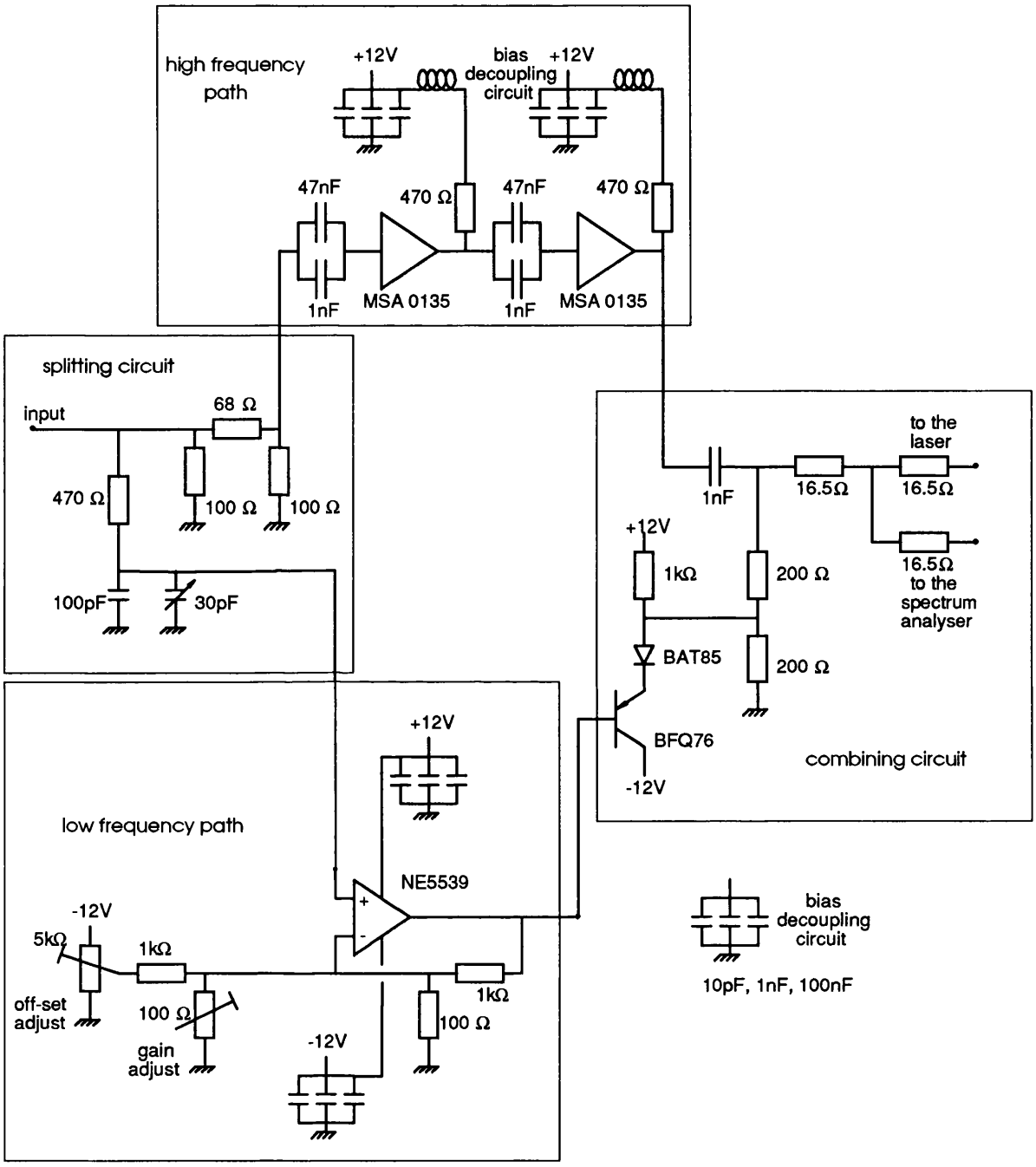

Figure 4.4.4: Diagram of the split path amplifier built.

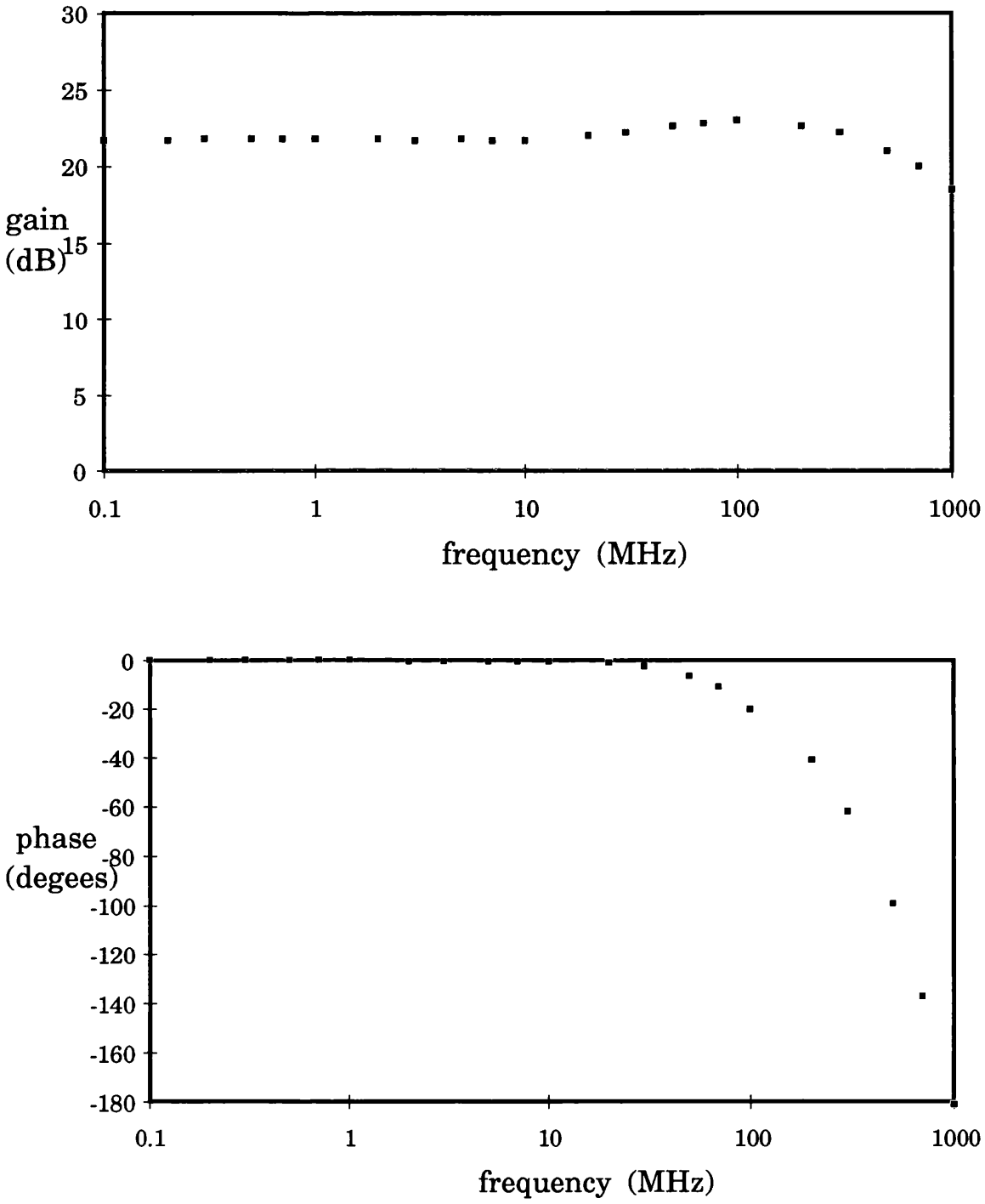

Figure 4.4.5: Frequency response plot of the total split path amplifier.

4.5- Temperature Control

4.5.1- Introduction

The laser diode characteristics, including the emission wavelength, optical power and lifetime, depend on the operating temperature of the device. In the case of the optical phase locked loop, fluctuations in temperature would cause wavelength variations which would bring the system out of lock. Typically, single-mode GaAlAs lasers have a frequency/temperature tuning slope of 20 GHz/K [Okoshi 80] within certain limits of temperature variations, beyond which a mode jump is expected.

Temperature stabilisation of 0.1 to 0.005 C has been reported [Matthews 85] [Pezolet 83] [Saito 81], utilising different techniques such as the use of a temperature controlled water flux [Pezolet 83] or a temperature controlled heat sink [Kikuchi 81] to improve the stability. The use of closed chambers to avoid temperature fluctuations [Esman 85] is another common method.

By analysing the equivalent thermal circuit of the mounting and finding the thermal transfer function, it is possible to measure its main time constant and build a circuit to control its temperature. No water flux nor sealed chambers were found to be necessary to achieve temperature stability better than 10mK over periods above half an hour in an uncontrolled laboratory environment.

4.5.2- Transfer function

Figure 4.5.1 shows schematically the mounting associated with the laser. ΔT is the temperature difference between the laser and ambient and q_o is the thermal power pumped by the Peltier heat pump. As the heat sink is a block of aluminium screwed to the optical table, its thermal resistance is small enough to be neglected, so the heat sink temperature is practically the same as the ambient temperature.

Figure 4.5.2 shows the equivalent thermal circuit. C_t is the thermal capacitance of the laser mounting and is given basically by its size, R_t is the thermal resistance between the laser mounting and the ambient, given basically by the geometry of the mounting and its fixing screw material and diameter. From the circuit:

$$q_o = \frac{\Delta T}{R_t} + C_t \frac{\mathrm{d}}{\mathrm{dt}} \Delta T \qquad 4.5.1$$

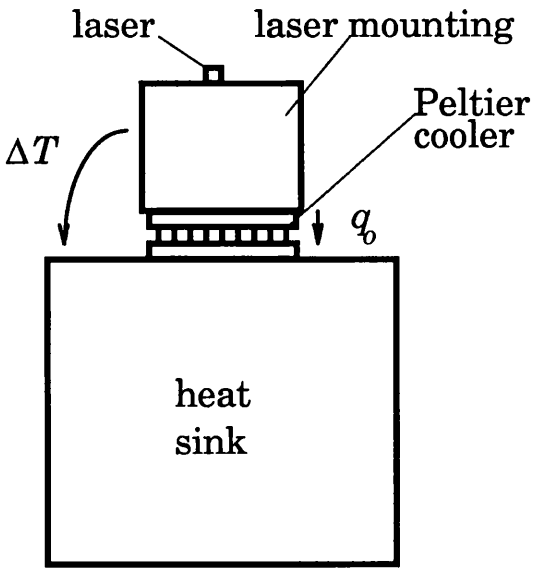

Figure 4.5.1: Laser mounting diagram.

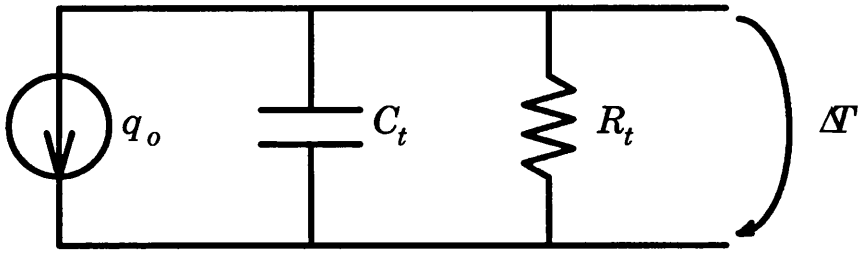

Figure 4.5.2: Equivalent thermal circuit.

The Laplace transform of equation (4.5.1) is:

$$Q_o(s) = \frac{1}{R_t}\Delta T(s) + s\,C_t \cdot \Delta(s) \qquad 4.5.2$$

and the transfer function is:

$$\frac{\Delta T(s)}{Q_o(s)} = \frac{1}{\frac{1}{R_t} + C_t\,s} = \frac{R_t}{1+\tau_t\,s} \qquad 4.5.3$$

Where τ_t is the thermal time constant of the system, given by:

$$\tau_t = R_t \cdot C_t \qquad 4.5.4$$

4.5.3- Thermal time constant measurement

A thermistor connected to a resistance bridge was put into a hole in the laser mounting to measure the temperature. A potentiometer in another arm of the bridge sets the reference temperature while an operational amplifier amplifies the error signal. Figure 4.5.3 shows the diagram of the sensor and error signal amplifier circuit.

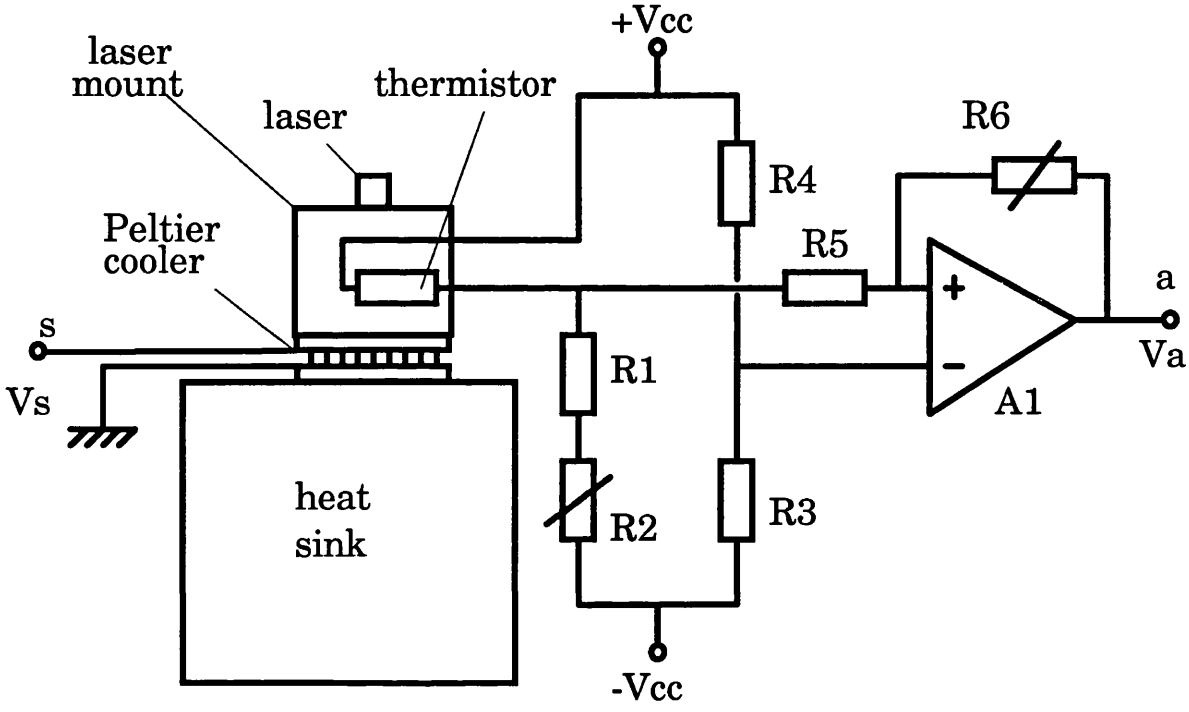

Figure 4.5.3: Diagram of the sensor and error signal amplifier circuit (components values in Appendix 6).

A small voltage source V_s, less than 0.3V, was connected to the Peltier cooler in series with a switch generating a step function $v_s(t)$. The expected behaviour of the thermal system from equation 4.5.3 is:

$$V_a = k \frac{V_s}{s} \frac{R_t}{1+\tau_t s} \qquad 4.5.5$$

Where k is a constant which depends on the sensitivity of the temperature sensor, the amplifier gain and the Peltier cooler efficiency. Note that the thermistor, the bridge circuit and the Peltier cooler transfer functions are considered linear for small variations. Equation 5.5.5 can be rewritten:

$$V_a = k V_s R_t \left(\frac{1}{s} - \frac{\tau_t}{1+\tau_t s}\right) \qquad 4.5.6$$

with an inverse Laplace transform:

$$v_a(t) = k\, v_s\, R_t\, (1 - \tau_t\, e^{(\frac{-t}{\tau_t})}) \qquad 4.5.7$$

Figure 4.5.4 shows a plot of this function. If Δv_a is the difference between the final and initial value of $v_a(t)$, τ_t is taken to $v_a(t)$ to reach 63.2% of Δv_a . A X-Y recorder was used to plot $v_a(t)$ and measure τ_t.

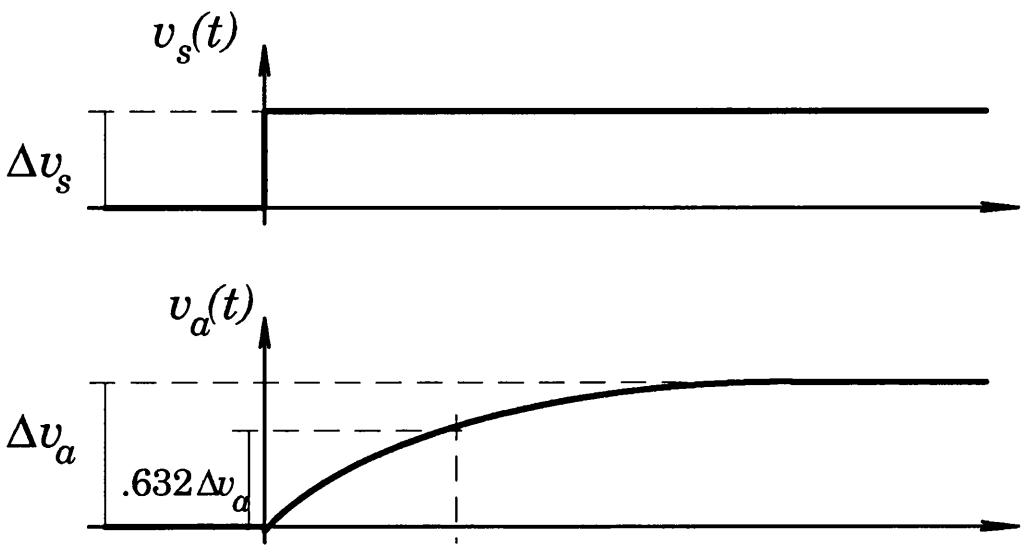

Figure 4.5.4: Step function response of the laser mounting.

In the case of the laser mounting used in the experiments, the time constant was measured to be 24 seconds.

4.5.4- Control Circuit

In order to minimise the steady-state error, the control filter transfer function incorporates an integration. A proportional integral (PI) controller was chosen, the transfer function of which is given by:

$$P(s) = T_i + \frac{1}{s} = \frac{T_i + 1}{s} \qquad 4.5.8$$

The best value of T_i is $T_i = \tau_t$, when zero and pole cancel each other. Figure 4.5.5 shows the basic circuit of a PI filter.

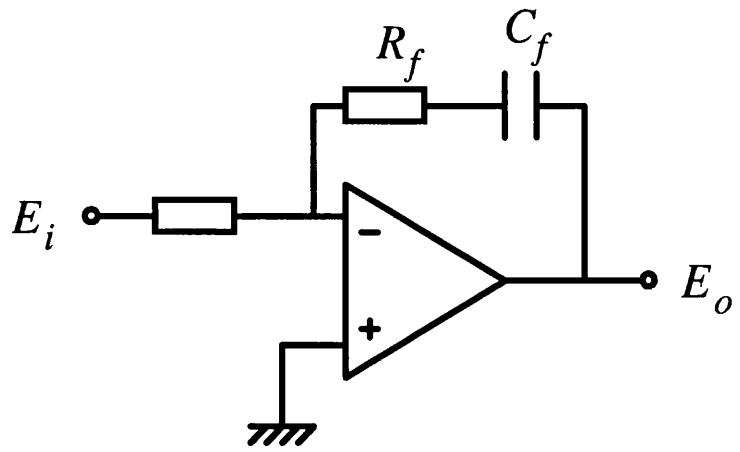

Figure 4.5.5: Basic circuit of a PI filter.

Its transfer function is:

$$\frac{E_o}{E_i} = -\frac{1}{R_i C_f s}(s R_f C_f + 1) \qquad 4.5.9$$

where:

$$T_i = R_f C_f \qquad 4.5.10$$

As the Peltier thermoelectric cooler can use relatively high power, mainly when the system is switched on or a major disturbance occurs, a push-pull type amplifier is added to the circuit, as shown in Figure 4.5.6. A small capacitor C2 was included for high frequency stabilisation.

4.5.5- Results

Figure 4.5.7 shows the temperature variation of the laser mounting during a period of 15 minutes. A plastic box covering the whole set up was placed to avoid air currents flowing around the laser. This was measured by monitoring the error signal using a X-Y recorder from a separated circuit similar to the one shown in Figure 4.5.3 using a second thermistor, all isolated from the temperature control system.

Stability better than 10mK over periods of more than half an hour, in an uncontrolled laboratory environment, was achieved using this simple method. Later experiments showed that the heterodyne signal between two lasers without external cavities was stable in its frequency (varying about 100MHz over a period of 5 minutes), showing that their temperature stabilisation was satisfactory.

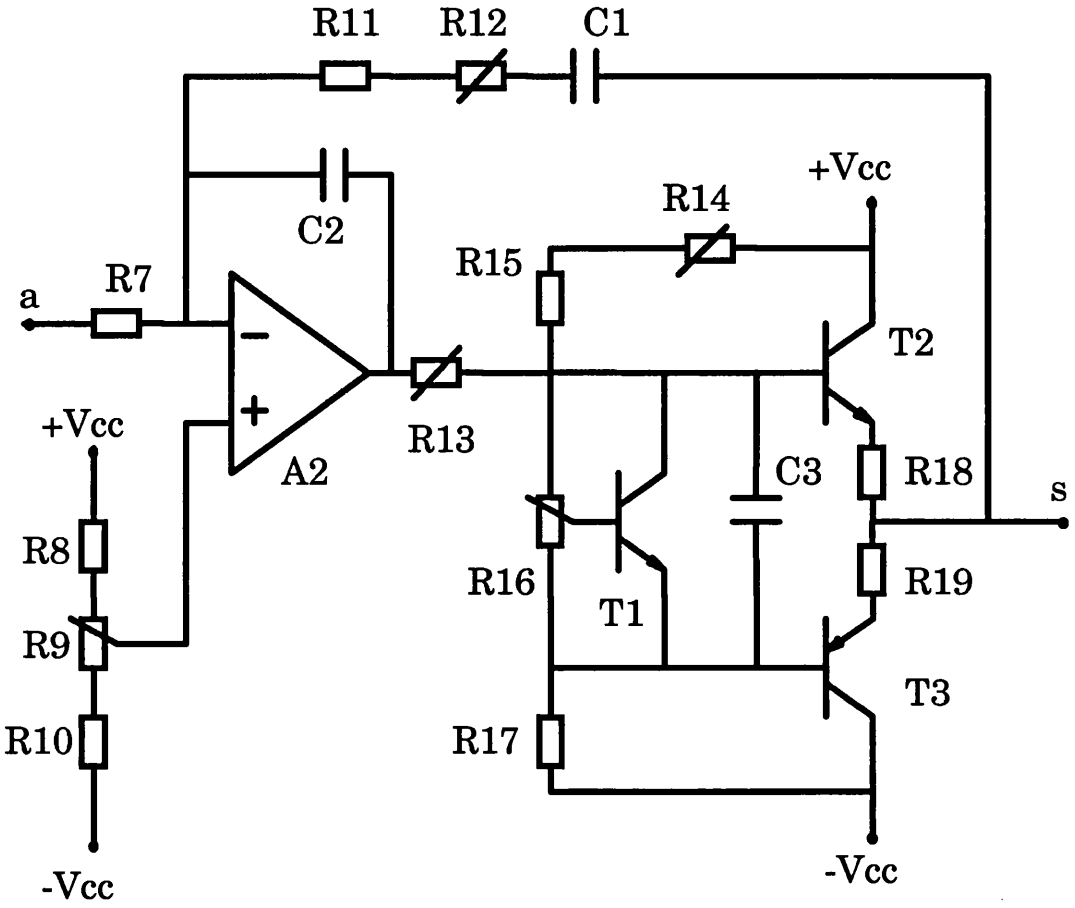

Figure 4.5.6: PI controller used (components values in Appendix 6).

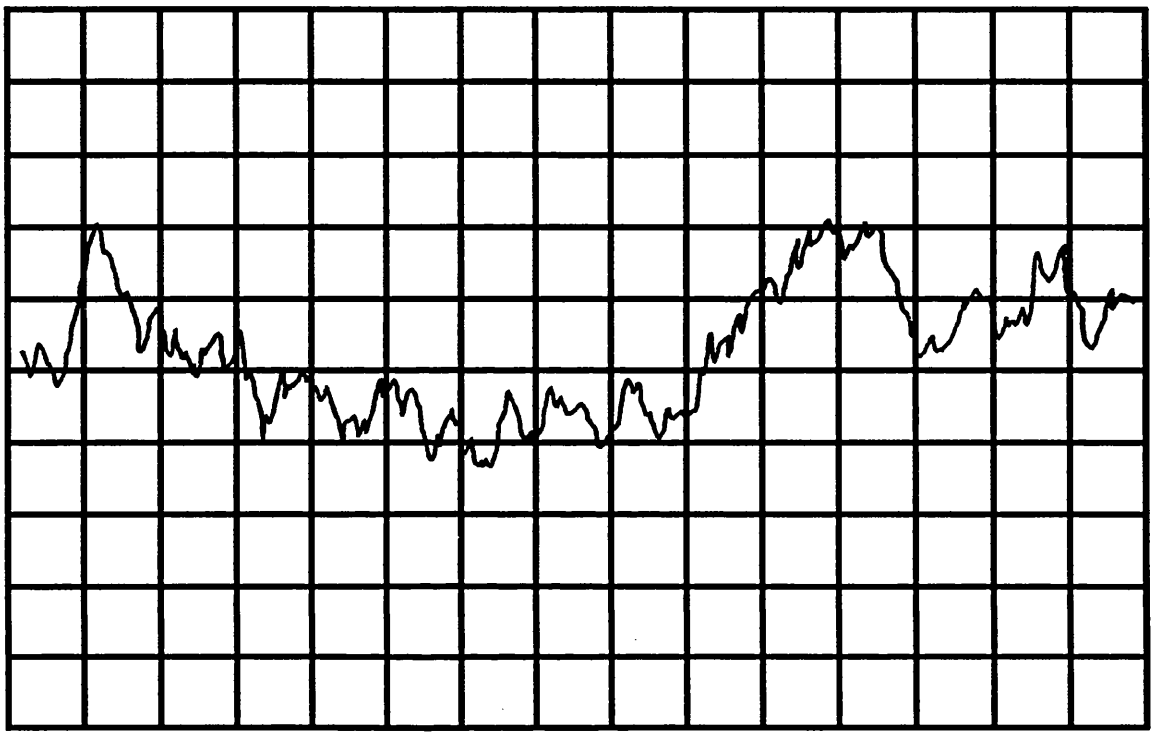

Figure 4.5.7: Temperature variation of the laser mounting during a period of 15 minutes when the control system is in use.

References

Esman, R. D., Rode, D. L., "100-μk Temperature Controller", Rev. Sci. Instrum. Vol 54, No 10, pp 1368-70, October 1985.

Fernando, P.N., Fake, M., Seeds, A.J., "A novel approach to optical frequency synthesis in coherent lightwave systems", SPIE O/E Fibers 1990, Sao Jose, pp.152-163.

Johnson, L. A., "Controlling Temperature of Diode Lasers and Detectors Thermoelectrically", Laser and Optronics, pp 109-114, April 1988.

Kahlert, J., Piscalar, W., Mulombe, N., "DC-12.3 GHz broadband amplifier", Electronics Letters, vol. 25, n. 21, 1989, pp. 1463-1465.

Kikuchi, K., Okoshi, T., Kawanishi, S., "Achievement of a mHz Frequency Stability of Semiconductor Lasers by Double-Loop AFC Scheme", Electronics Letters, Vol 17, No 15, pp 515-6, 23 July 1981.

Matthews, M. R., Cameron, K.H., Wyatt, R., Devlin, W.J., "Packaged Frequency-Stable Tunable 20kHz Linewidth 1.5μm InGaAsP External Cavity Laser", Electronics Letters, Vol 21, pp 113-115, 31 January 1985.

Miller, C. M., Collins, R, A., "A broadband, general-purpose instrumentation lightwave converter", Hewlett-Packard Journal, 1991, pp. 51-57.

Ogata, K., "Modern Control Engineering", Prentice-Hall, 1970.

Okoshi, T., Kikuchi, K., "Frequency Stabilisation of Semiconductor Lasers for Heterodyne-Type Optical Communication Systems", Electronics Letters, Vol 16, No 5, pp 179-181, 28 February 1980.

Pezolet, M., Boulr, B., Bourque, D., "Thermoelectrically Regulated Sample holder for Raman Spectroscopy", Rev. Sci. Instrum. Vol 54, No 10, pp 1364-67, October 1983.

Saito, S., Yamamoto, Y., Kimura, T., "Optical FSK Heterodyne Detection Experiments Using Semiconductor Laser Transmitter and Local Oscillator", IEEE J. of Quantum Electronics, Vol QE.17, No 6, pp 935-941, June 1981.

Vegte, J.V., "Feedback Control Systems", Prentice-Hall, 1986.

WJ RF and microwave components designers' handbook, Watkins-Johnson company, 1990-1991.

Ward, C.J., "Delay reduction techniques in phase-locked loop amplifiers", Electronics Letters, vol. 17, n. 7, 1981, pp.253-255.

Ward, C.J., Forrest, J.R., "Fast acquisition phase-locked loops for frequency agile pulsed radar systems", IEE Proceedings, vol. 130, Pt. H, n. 7, December 1983, pp. 489-494.

Chapter 5

OPLL Experiment

5.1- Introduction

In this chapter, the first OPLL using both master and slave lasers without any line narrowing devices is reported. It is the first heterodyne system using semiconductor lasers without external cavities or other linewidth narrowing method. Moreover, it presents the highest natural frequency and the lowest delay time of the OPLLs so far reported, excepted for the homodyne loop of [Kourogi 91]. It is also the first to use quantum well lasers in this kind of systems.

In Chapter 2 it was seen that severe restrictions on laser linewidth and loop delay time need to be imposed, if a reliable OPLL is to be built. In Chapter 3, the design of the optical part of the loop was detailed, giving some options for keeping the loop delay time to a minimum and for choosing optical sources. Chapter 4 was focused on the design of the electrical part of the loop, showing how it is possible to overcome some of the problems of gain, bandwidth and temperature stability. In this chapter, these results are assembled in order to build an heterodyne OPLL. The target of our experiments is to achieve heterodyne optical phase-lock with a phase error variance below 1.5 rad^2, given the difficulties presented in the previous chapters.

5.2- Heterodyne System

Figure 5.2.1 shows a block diagram of the basic system assembled in the laboratory for mixing the master and slave laser signals. Most of the details of the optical set up used are covered in Chapter 3.

The laser mounts also hold microstrip circuits to provide the bias current, avoiding great limitation of the system bandwidth. The photodetector used is an ultra high speed GaAs ITO Schottky photo diode (GEC Y-35-5252-22) with a bandwidth of 18GHz and the microwave amplifier has a gain of 20dB from 2 to 8 GHz (Watkins-Johnson WJ6882-812).

A optical spectrum analyser (Anritsu MS9001B1 0.6-1.75μm) was used to observe the spectrum of the lasers to allow them to be tuned to the desired frequencies. However,

the maximum resolution of the instrument is 0.1nm, equivalent to about 44GHz at 830nm, which is insufficient for the fine frequency adjustment required. A scanning Fabry-Perot interferometer is therefore added to the measurement system, having a plate spacing of about 5mm, giving a 30 GHz free spectral range, to provide the resolution required. Fine frequency setting is then obtained by observing the beat signal on a microwave spectrum analyser.

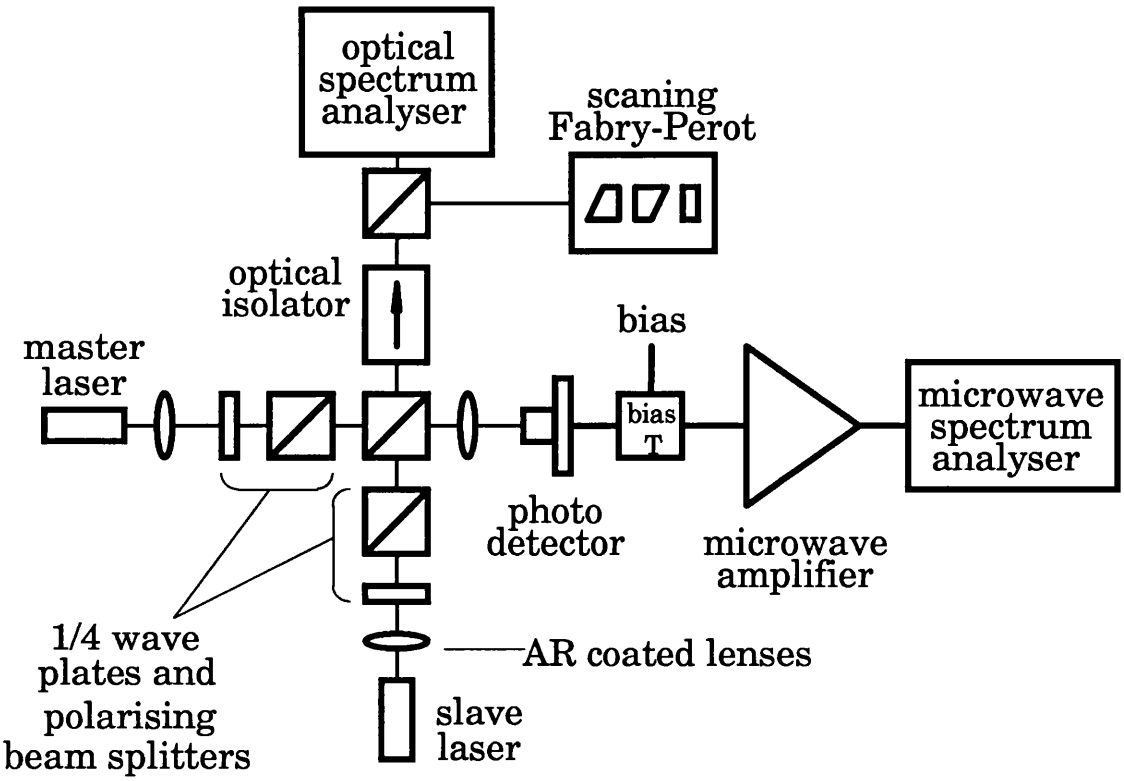

Figure 5.2.1: Block diagram of the basic system assembled in the laboratory for mixing the master and slave laser signals.

5.3- Heterodyne Results

Initially, two Hitachi HLP1400 laser diodes were tuned to oscillate 7.8GHz apart, producing a beat signal at the photodetector terminals centred on this frequency. Figure 5.3.1 shows the spectrum of this signal. Assuming the two lasers have equal Lorentzian linewidths, the linewidth of each laser corresponds to half of the linewidth of the beat signal, giving a laser linewidth of 40MHz. The central frequency of the beat signal was very stable, varying about 100MHz over a period of 5 minutes. This would correspond to a temperature stability of 50mK, assuming the frequency variation rate of 20GHz/K, proving the effectiveness of the temperature control.

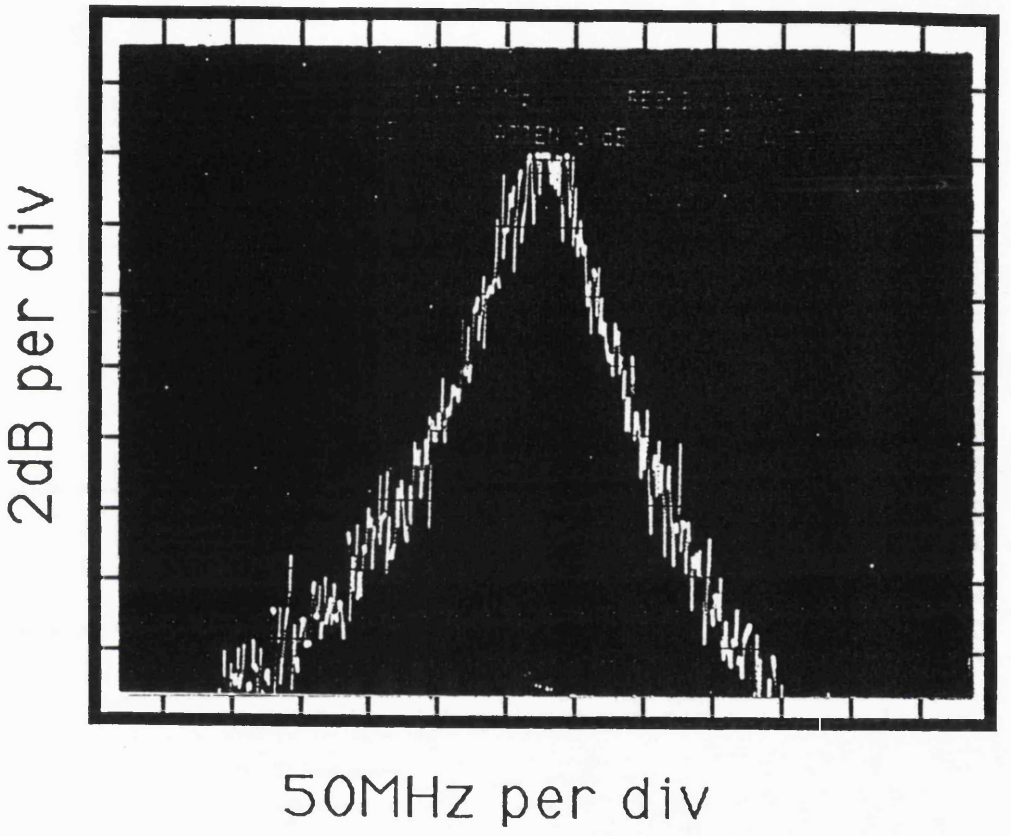

Figure 5.3.1: Spectrum of the beat signal of two HLP1400 laser diodes. Central frequency 7.8GHz, reference -48dBm, resolution bandwidth 1MHz.

The FM response of the HLP1400, presented in Chapter 3, would limit the open loop bandwidth to about 100MHz. Using this value of f_c and a loop delay time of 3ns, it is possible to estimate that the phase error variance σ^2 would be 3.58rad^2, employing the equations given in Chapter 2. This value is above $\pi^2/4$, meaning that it would not be possible to obtain stable phase lock. The average time between cycle slips T_{av} would then be 30ns. In order to bring the value of σ^2 below $\pi^2/4$, the loop delay time would have to be 1.5ns (resulting in σ^2=2.22rad^2, T_{av}=26ns). Even if an integrated system was used and the delay time of 0.5ns achieved, the phase error variance would still be quite high, 1.28rad^2 (T_{av}=65ns). However, it was not possible to reduce the loop delay time below 3ns with the set up available.

Experiments using external cavities to reduce the linewidth of the HLP1400 lasers were carried out and are described in Appendix 4. These confirmed the environmental sensitivity of such systems.

To achieve narrower linewidth from monolithic lasers, two double quantum well (DQW) metal clad ridge waveguide GaAs/AlGaAs laser diodes (Northern Telecom STC LT40-82) were then used [Garret 87] [Daniel 89]. The characterisation of these devices was discussed in Chapter 3. Their linewidths are about 2.5MHz, measured by heterodyning two free running lasers or by self homodyne techniques. This value of linewidth is narrow enough to allow good performance phase locking, as seen in Chapter 2.

5.4- Closed Loop Measurements

The experimental arrangement used for a heterodyne OPLL is shown in Figure 5.4.1. In a heterodyne OPLL the master and slave lasers oscillate at different frequencies producing a beat signal at the terminals of the photodetector at this offset frequency as before. This signal is then amplified and a phase detector compares the phase of the beat signal with that of the reference signal, thus generating the phase error signal.

The loop filter is a dc to 700MHz 20dB uniform gain split path amplifier as described in Chapter 4. The directional coupler and the phase detector also have wide bandwidths, operating from 4 to 8 GHz. For an offset frequency between 5 and 7GHz, the loop bandwidth depends mainly on the loop delay time and the FM response of the laser diode. This loop can then be regarded as a modified first order loop. The loop gain can be adjusted by changing the offset generator output power, which changes the phase detector gain as seen in Chapter 4. Slight loop gain adjustment can also be

obtained by varying the photodetector bias voltage. The total loop delay time was estimated to be 3ns, of which 0.35ns was due to optical path length, 1.5ns to the electrical path length, 0.55ns to the phase error amplifier and the rest due to delays introduced by the other microwave components.

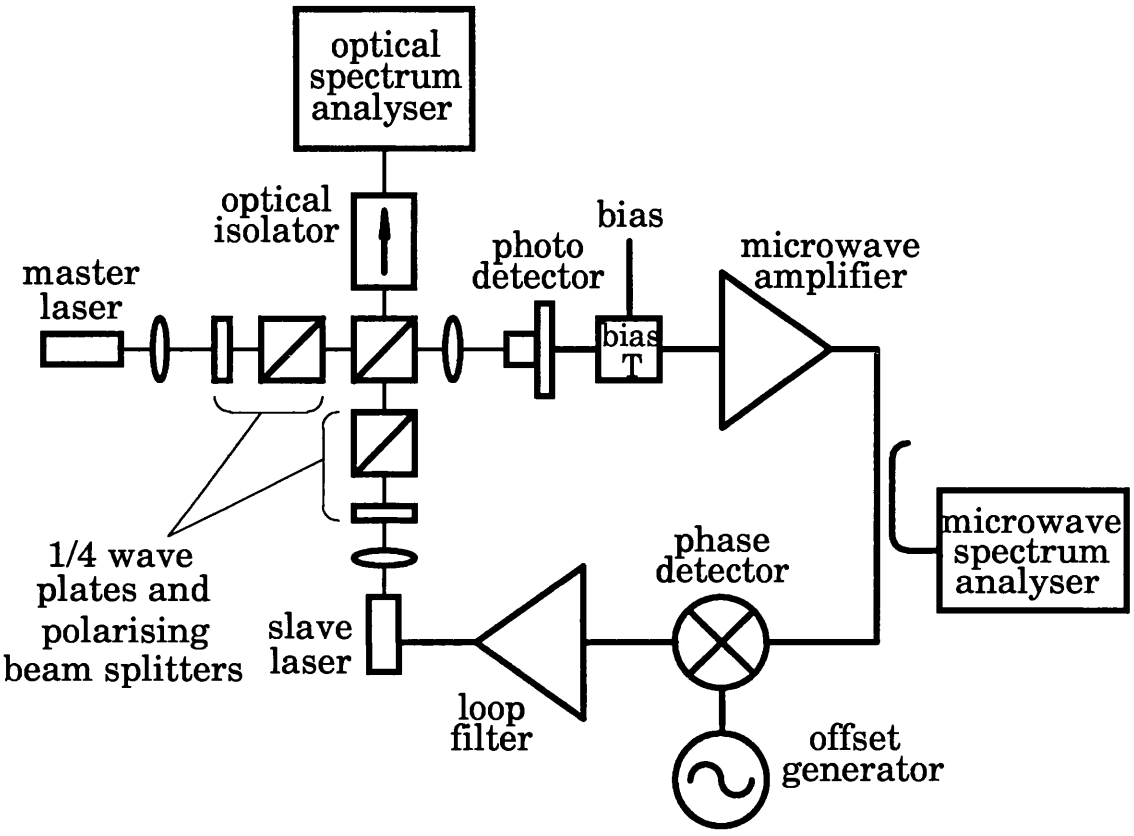

Figure 5.4.1: Block diagram of the heterodyne OPLL built.

Locking is observed by tuning one of the lasers until the beat signal is about 20MHz from the offset frequency, when it falls into lock. Figure 5.4.2 shows the spectrum of the beat signal when locking is achieved. The linewidth of the central peak in the plot is limited by the resolution bandwidth of the spectrum analyser (minimum of 300Hz), but would be expected to be similar to that of the frequency synthesiser used to generate the offset frequency. Phase noise suppression occurs over a band of about ±20MHz around the offset frequency. This bandwidth depends on the value of the loop gain.

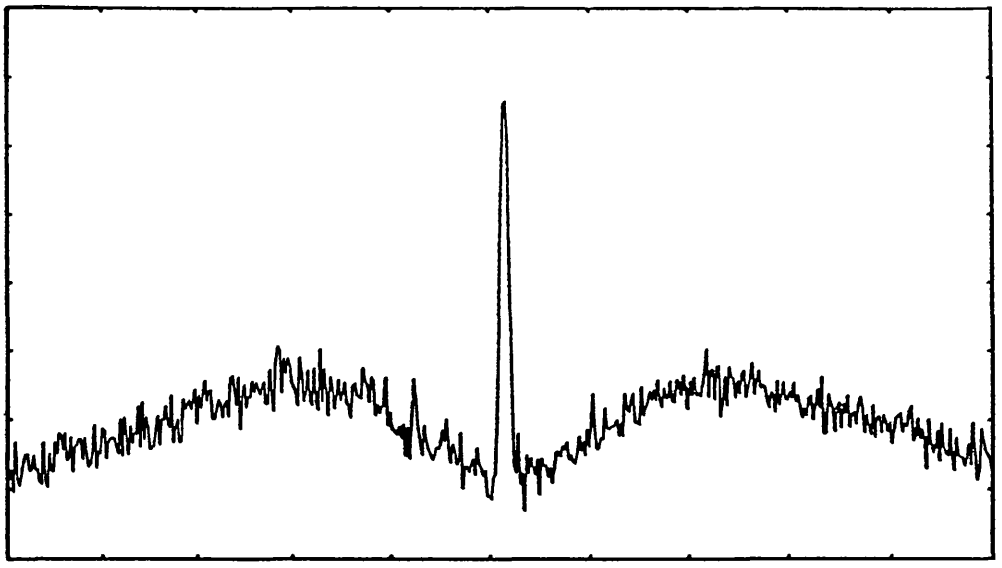

Figure 5.4.2: Spectrum of the beat signal when locking is achieved. Reference -5dBm, 5dB/div, centre frequency 5.1GHz, 10MHz/div. Resolution bandwidth 300kHz.

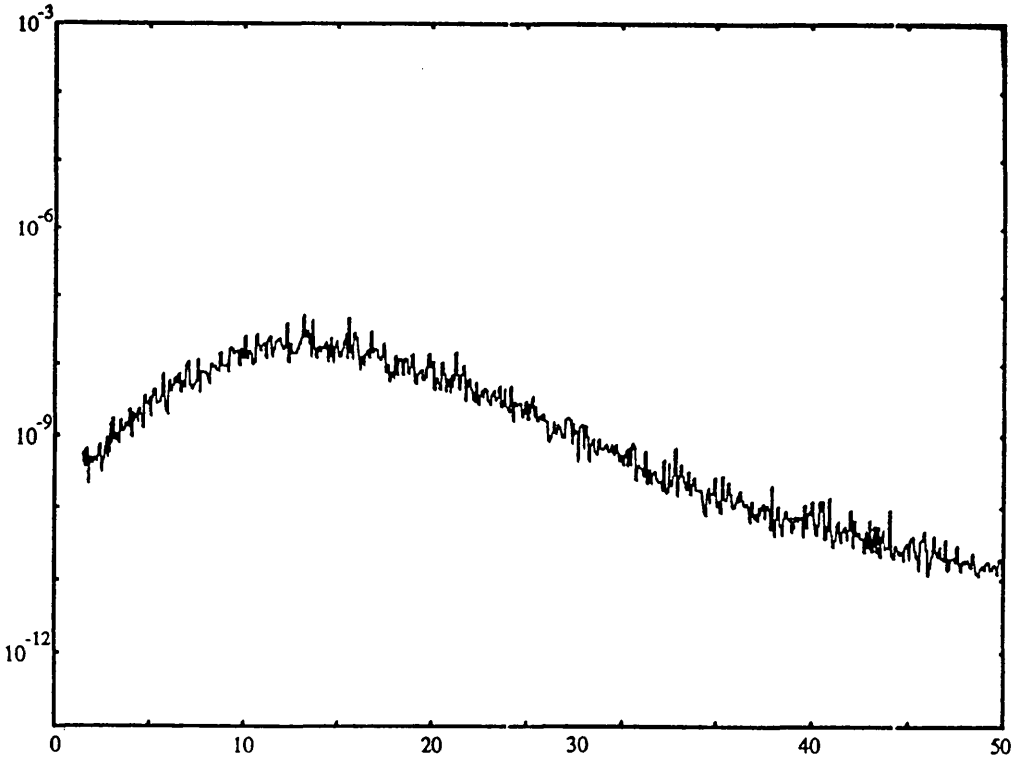

Figure 5.4.3: Spectrum of the phase error signal in rad²/Hz. Frequency in MHz.

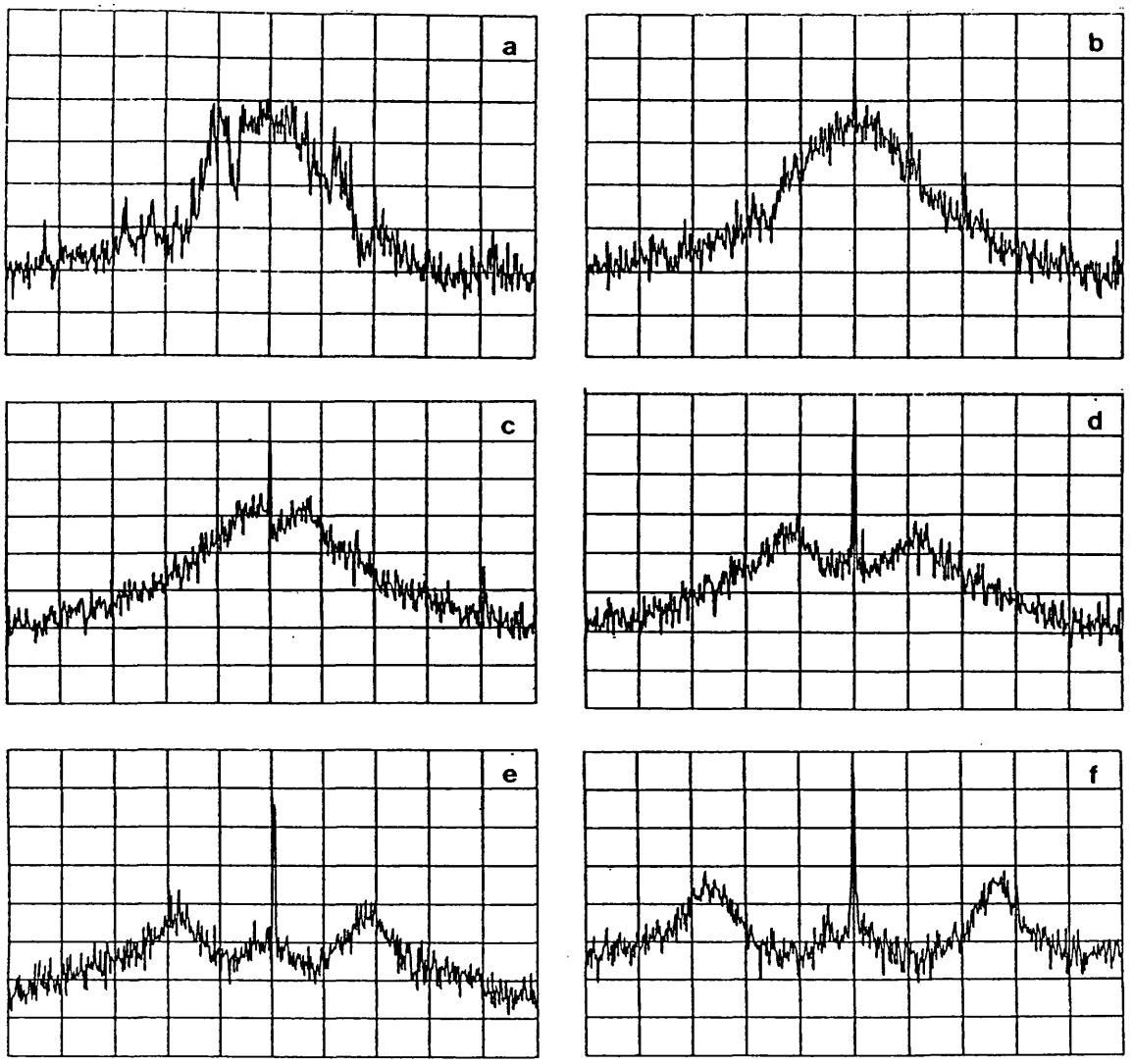

Figure 5.4.4: Sequence of beat signal spectrum for increasing values of loop gain. Reference -30dBm, 5dB/div, centre frequency 6GHz, 5MHz/div. Resolution bandwidth 100kHz.

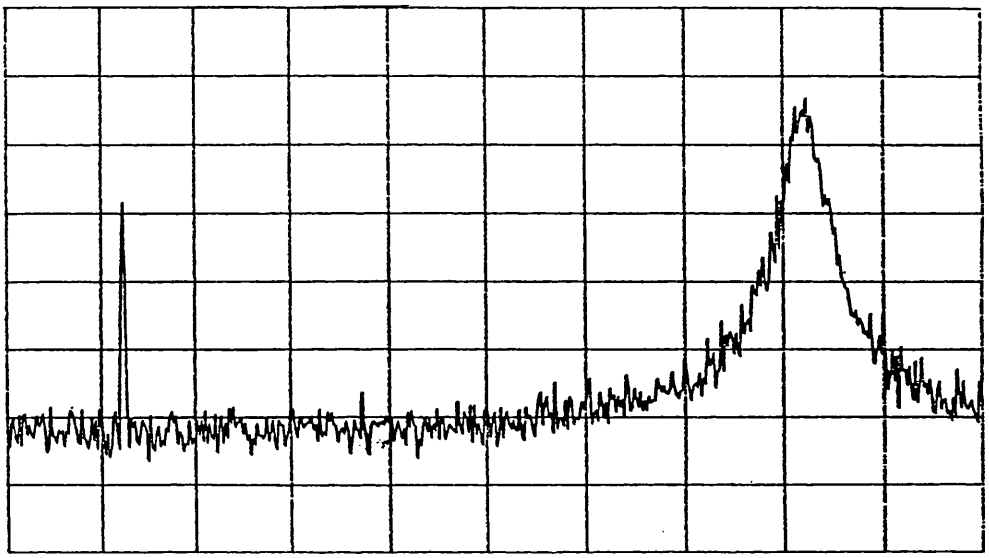

Figure 5.4.5: Spectrum of the beat signal under false locking condition. Reference -35dBm, 5dB/div, centre frequency 6GHz, 20MHz/div. Resolution bandwidth 300kHz.

When the offset generator is swept over 5MHz the beat signal follows it, retaining its spectral shape. Phase-lock was achieved for several different values of offset frequency from 5 to 7GHz. Figure 5.4.3 shows the spectrum of the phase error signal, measured at the slave laser terminals. By observing this signal it is possible to say that the loop bandwidth is about 15MHz, probably limited by the FM response of the laser diode.

Figure 5.4.4 shows a sequence of plots from the microwave spectrum analyser giving the beat signal spectrum for several increasing values of loop gain. In Figure 5.4.4(a) the loop gain is too low to provide any phase locking and the beat signal drifts across the screen. In Figure 5.4.4(b) the gain is kept to a minimum to achieve phase locking, enough to make the frequency of the beat signal very stable. In Figure 5.4.4(c) and (d) the gain is gradually increased resulting in the widening of the phase noise suppression region, corresponding to the controlled bandwidth of the loop. In Figures 5.4.4(e) and (f) the gain starts to become too high, resulting in a decrease of damping factor to values below ζ=0.707. At this stage the noise starts to peak at the loop natural frequency. For loop gain values beyond the one used in Figure 5.4.4(f), the loop becomes unstable and phase lock is lost. When this happens, the loop falls into a false lock and the beat signal is dragged to frequencies different from that of the offset generator. Figure 5.4.5 gives the spectrum of the beat signal under false locking conditions. The beat signal is at a stable frequency which can be slightly tuned by varying the loop gain. This kind of frequency lock was obtainable at about 150MHz above or below the offset generator frequency.

5.5- Comparison with Theory

It is possible to estimate the phase error variance from the experimental results by integrating the phase error signal spectrum. The phase error variance σ^2 corresponding to Figures 5.4.3 was estimated to be 1.02rad^2 by the integration of the phase error signal spectrum over a measurement bandwidth of 500MHz.

Figure 5.5.1 shows how the phase error variance changes when different values of measurement bandwidth are tried. Looking at this plot, it is possible to see that about 83% of the phase noise still in the loop is concentrated at the first 50MHz and 95.6% in the first 100MHz.

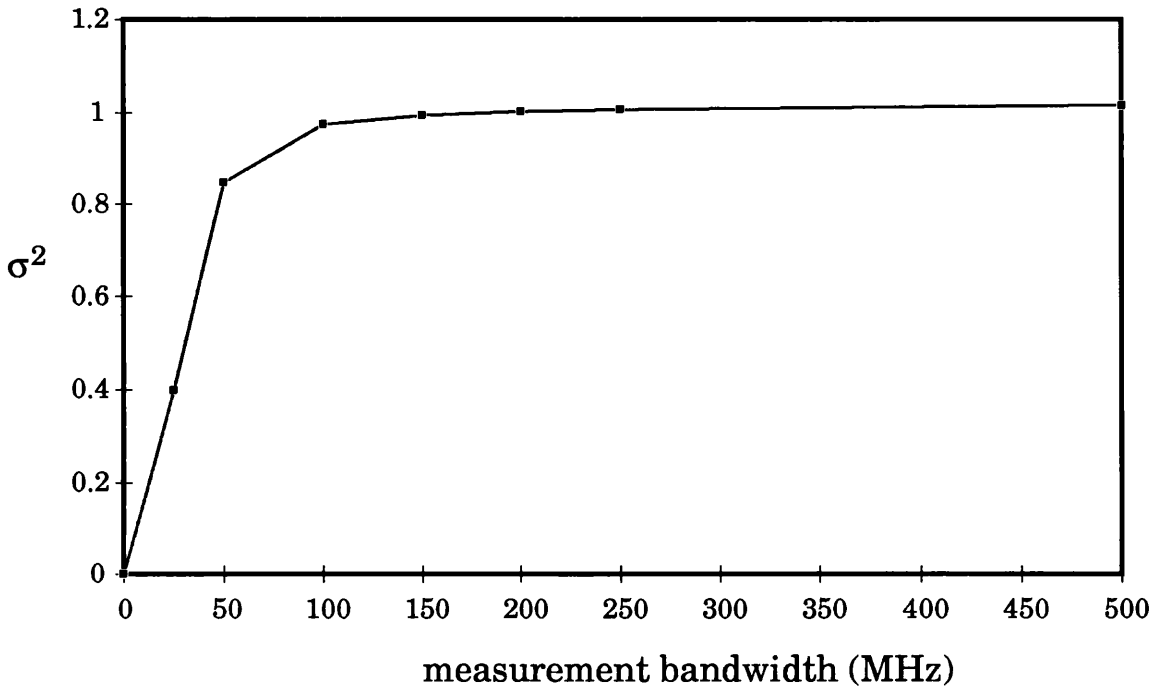

Figure 5.5.1: Phase error variance σ ² against measurement bandwidth.

This performance is inferior to that expected for a loop using a 500MHz bandwidth filter, as seen in Chapter 2. The total loop bandwidth of about 15MHz, given by the peaking of the phase error spectrum (Figure 5.4.3), is also different from that expected in Chapter 2. As all the electronic components of the loop have wide bandwidth, the restricting factor was the limited FM response of the slave laser diode.

The FM response of this laser, seen in Chapter 3, limits the open loop bandwidth to a maximum of about 6MHz, due to the thermal response of the laser. For a loop delay time of 3ns, a phase error variance of 1.04rad² would be expected, corresponding to an average time between cycle slips of 670ns. In the same situation, the phase error variance of 1.02rad² measured experimentally corresponds to an average time between cycle slips of 700ns.

The complex FM response of the slave laser measured in Chapter 3 can be used to give a better prediction of the phase error spectrum. Figure 5.5.2 shows such a spectrum using the same values of gain used in Figure 2.6.1. Note that the effect of the limited frequency response bandwidth of the slave laser is a drastic reduction of the total loop bandwidth. Figure 5.5.3 shows the approximation of the spectrum of the beat signal, assuming the slave laser modulation is small, as derived in Chapter 2 (vertical scale not calibrated and assuming 1Hz resolution bandwidth). Figure 5.5.4 shows the spectrum of the measured phase error variance and the calculated one from Figure

5.5.2 which best fits, corresponding to a loop gain of 4.787×10^8 which corresponds to the calculated critical gain.

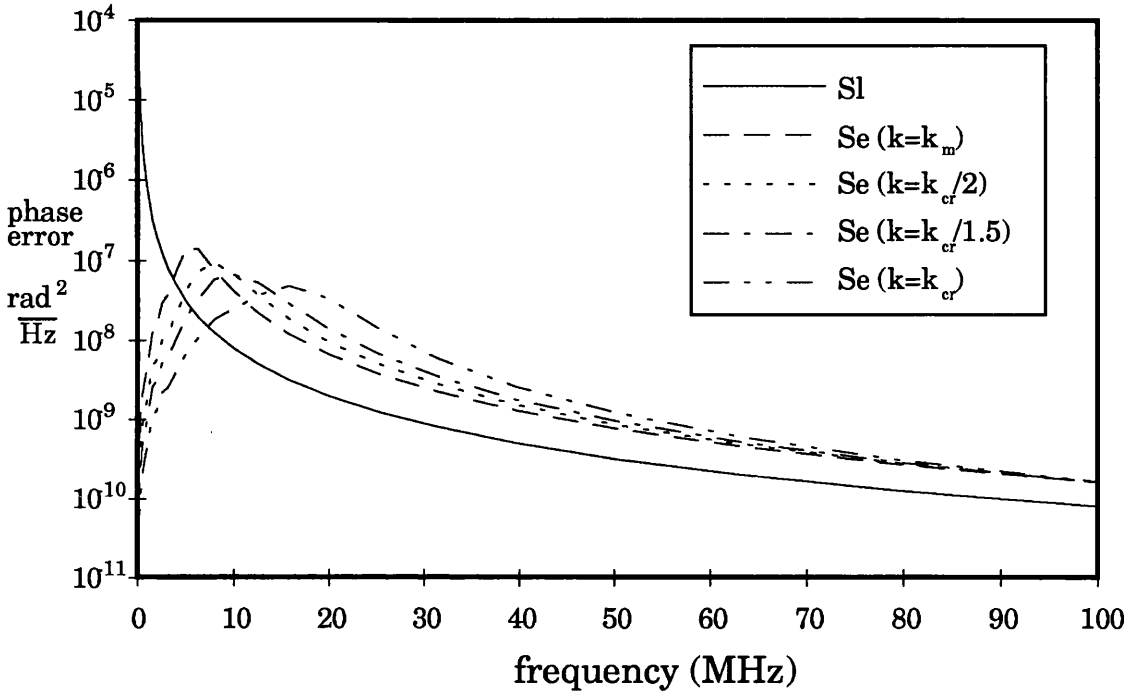

Figure 5.5.2: Calculated phase error spectrum including the FM response of the slave laser.

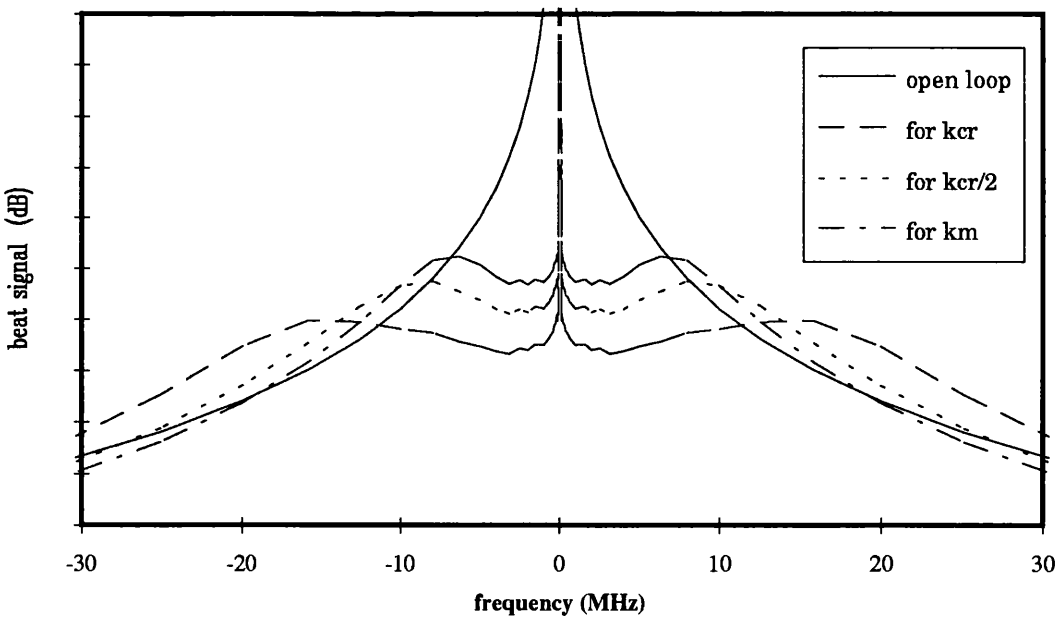

Figure 5.5.3: Approximation of the relative spectrum of the beat signal S_e/ω^2 for several values of loop gain (as seen in Section 2.6.2).

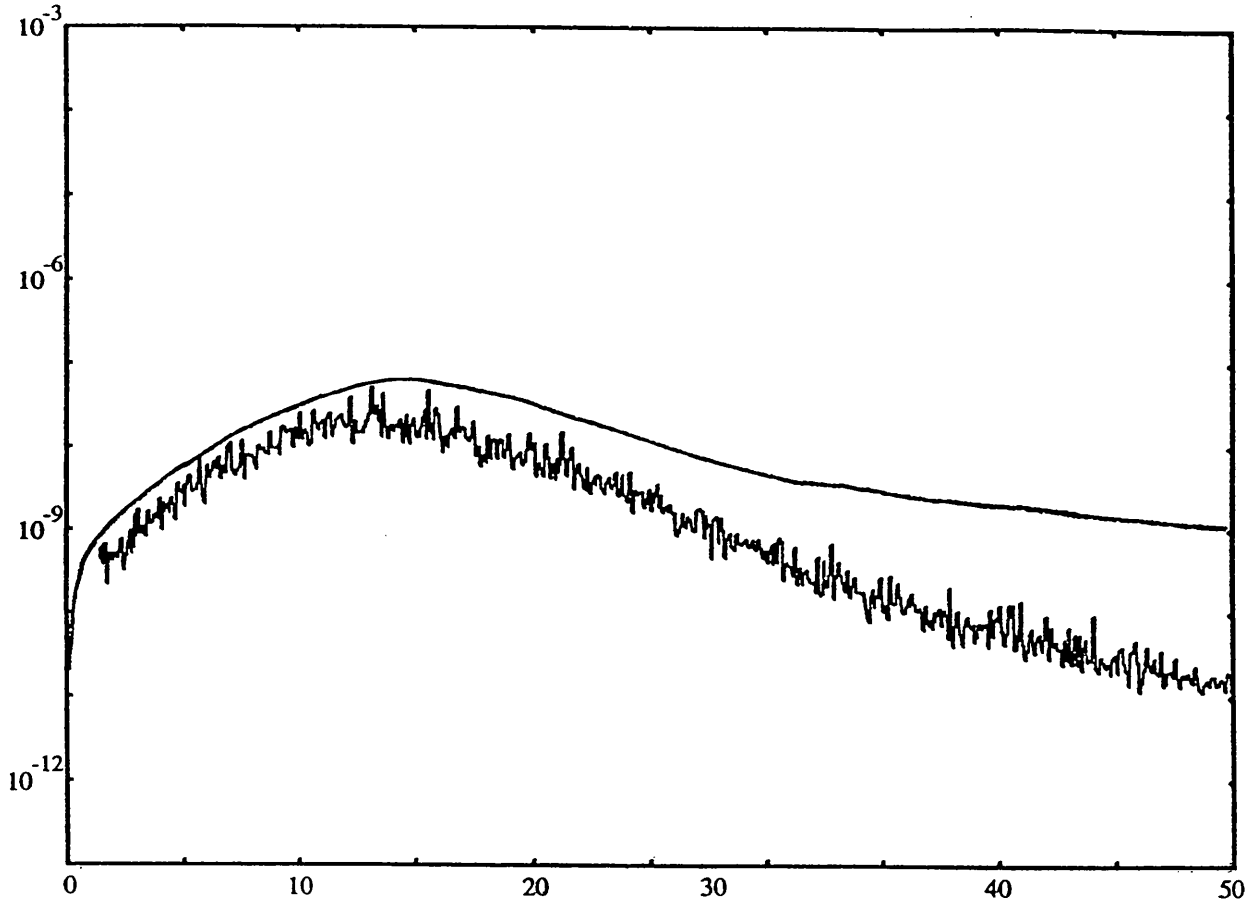

Figure 5.5.4: Calculated and measured phase error spectrum in rad²/Hz, frequency in MHz.

The difference between the two curves in Figure 5.5.4 is mainly due to the poor resolution of the FM response measurement, in particular for frequencies above 10MHz, and to ageing of the lasers between measurements.

Figure 5.5.3 shows the effect of increasing the loop gain on the beat signal spectrum, which accords with the experimental results (Figure 5.4.4). Good agreement is also observed between the measured and calculated curve in Figure 5.5.4, where both curves peaking at the same frequency.

The phase error variance of around $1rad^2$, which was measured and calculated here, is still too high for commercial systems. However great improvement would be expected if a slave laser with better tunability is used. Solving this problem, the next limitation would be the loop delay time which limits the loop bandwidth. The integration of the system could then reduce the delay time and improve even further the performance of the loop.

5.6- Discussion

The first OPLL using both master and slave lasers without any line narrowing devices has been realised. Quantum well lasers were used for the first time in this kind of system, in the highest natural frequency and lowest delay time heterodyne OPLL reported. It is the first heterodyne system using semiconductor lasers without external cavities or any linewidth narrowing method.

This experiment confirms theoretical calculations predicting that OPLLs can be built using relatively wide linewidth lasers (order of MHz), by restricting the loop delay time and maximising the loop bandwidth. It also demonstrates that optical frequency synthesis is possible at any offset frequency within the boundaries set by the microwave components. From the point of view of practical applications the experiment shows that OPLLs can be constructed with lasers of linewidth values that might be realisable from sources monolithically integrated in OEIC form. The short loop delay obtainable with this approach suggests that convenient optical frequency synthesis blocks could be produced, having many applications in coherent optical communication systems.

The main limitation on loop bandwidth in our work was due to the current tuning response of the laser diode. One option to overcome this limitation is the use of a passive network to equalise the FM response using an electrical filter [Alexander 85] or electrical feedback [Swanson 91]. Although this flattens the response, it severely compromises the FM sensitivity and also introduces extra delay into the loop, becoming an unattractive solution. Another option would be the use of multi section lasers as a way of obtaining flat FM response and increased loop bandwidth. Long cavity multi-electrode DFB lasers with 500kHz linewidth and flat FM response of

400MHz/mA up to 1GHz have already been reported [Twu 90]. Three electrode lasers have been studied theoretically [Coldren 87] and experimentally [Pedersen 90] with similar characteristics.

Reverse bias multiple quantum well (MQW) tuning techniques [Cai 89] could provide a good solution for the slave laser tuning problem. In this case, an extension of the laser cavity is added containing a MQW structure and tuning is achieved by changing the refractive index of this material by varying the reverse bias voltage, altering the optical cavity length.

References:

Alexander, S. B. and Welford, D., "Equalisation of Semiconductor Diode Laser Frequency Modulation with a Passive Network", Electronics Letters, vol. 21, n. 9, 1985, pp. 361-362.

Cai, B., Seeds, A.J., Rivers, A., Roberts, J.S., "Multiple quantum well tuned GaAs/AlGaAs laser", Elect. Lett., 1989, vol. 25, pp. 145-146.

Coldren, L. A. and Corzine, S. W., "Continuously-Tunable Single-Frequency Semiconductor Lasers", Journal of Quantum Electronics, vol. QE-23, n. 6, June 1987, pp. 903-908.

Daniel, D.R., Buckley, D., Garrett, B., "Quantum Well Ridge Wavegide Lasers Optimised for High Power Single Mode Applications", Proc. SPIE, Los Angeles, 1989, vol. 1043, pp. 61.

Garrett, B., Glew, R.W., "Low-threshold, high-power zero-order lateral-mode DQW-SCH metal-clad rigid wavegide (AlGa)As/GaAs lasers", Elect. Lett., 1987, vol. 23, pp. 371-373.

Kourogi, M., Shin, C.H., Ohtsu, M., "A 134MHz bandwidth homodyne optical phase-locked-loop of semiconductor laser diodes", Photonics Tech. Lett., 1991, vol. 3(3), pp.270-272.

Nielsen T. N., Storkfelt, N., Gliese, U., Mikkelsen, B., Durhuus, T., Stubkær, K. E., Fernier, B., Leblond, F. and Accard, A., "Pure Phase Modulation by the Use of a Two-Electrode Semiconductor Optical Amplifier", Technical Digest of the 2nd Topical

Meeting on Optical Amplifiers and Their Applications, 1991, Boulder, Colorado, USA, Post Deadline Paper PdP8.

Pedersen, R. J. S., Gliese, U., Broberg, B. and Nilsson, S., "Characterization of a 1.5μm Three-Electrode DFB Laser", Proceedings of the 16th European Conference on Optical Communications, 1990, Amsterdam, Netherlands, vol. 1, pp. 279-282.

Ramos, R.T., Seeds, A.J., "Delay, linewidth and bandwidth limitations in optical phase-locked loop design", Elect. Lett., 1990, vol. 26(6), pp.389-391.

Ramos, R.T., Seeds, A.J., "Fast Heterodyne Optical Phase-Lock Loop Using Double Quantum Well Laser Diodes", Elect. Lett., 1992, vol. 28, n.1, pp.82-83.

Steele, R.C., Creaner, M.J., Walker, G.R., Walker, N.G.: "Optical PSK transmission experiment at 565Mbit/s incorporating an endless polarization control system", Proceedings of SPIE Components for Fiber Optics Applications and Coherent Lightwave Communications, Boston, 1988, vol. 988, pp. 302-309.

Swanson E. A., Alexander, S. B. and Bondurant, R. S., "Wideband Frequency Noise Reduction and FM Equalization in AlGaAs Lasers Using Electrical Feedback", Optics Letters, vol. 16, n. 18, 1991, pp. 1403-1405.

Twu, Y., Wang, S. J., Kuo, C. Y., Wynn, C. D., Brown, R. L., Gruezke, L. A., Strege, K. E., Lin, M. S., Dutta, N. K., "Long-Cavity, Multi-electrode DFB Lasers fro Coherent FSK Systems", Electronics Letters, vol. 26, n. 11, 1990, pp. 708-710.

Wandernoth, B., "20 Photon/bit 565 Mbit/s PSK Homodyne Receiver Using Syncronisation Bits", Electronics Letters, vol. 28, n. 4, 1992, pp. 387-388.

Ward, C.J., "Delay reduction techniques in phase-locked loop amplifiers", Elect. Lett., 1981, vol. 17, pp. 253-255.

Chapter 6

Conclusions

6.1- Main results

This thesis had two main objectives. The first was to develop a theory to understand the OPLL limitations, to make a model of the system and to set design guide lines. The second was to build an OPLL using semiconductor lasers without line narrowing in the laboratory and characterise it. Both objectives were fulfilled bringing new contributions to the field.

6.1.1- OPLL Theory

A model of the OPLL was made and the main sources of noise were identified. The loop delay time was considered and new stability conditions were set. Performance parameters were analysed and the shape of the phase error signal spectrum was predicted. A design criterion based on the average time between cycle slips was adopted [Ramos 90]. The criterion set here, of an average time between cycle slips of 10 years, was found to be compatible with bit error rate criteria used for coherent receiver applications with the advantage of serving other applications.

A complete comparison between the performance of modified first order loops and second order loops was made for the first time, revealing that the modified first order loop is a good option if a wide bandwidth loop and long delay time are used, as it is less sensitive to loop delay. This was the first analysis of modified first order OPLLs to include loop delay time.

6.1.2- OPLL Experiment

Quantum well lasers were used in an OPLL for the first time. The first reported OPLL using both master and slave lasers without external cavity or any other linewidth narrowing technique was built and characterised [Ramos 92]. It is also the heterodyne OPLL with the widest reported loop bandwidth.

In order to achieve the main results, a series of elaborate techniques were used: A technique to control the laser temperature was developed, achieving temperature stability better than 10 mK for more than an hour without the use of sealed chambers.

A method of measuring the FM response of the DQW laser was developed using a hi-bi fibre and a procedure to cancel the effect of the amplitude modulation was also produced. Split path loop amplifiers were used to minimise loop delay.

6.2- Discussion

The first question to be answered at the beginning of this project was what design conditions would have to be met in order to achieve phase locking with wide linewidth sources. To answer this question it was necessary to establish how good the locking would have to be and then look for the conditions to achieve this specification. The first and the most natural of the loop performance parameters is the variance of the phase error and the first idea was to set a value of maximum phase error variance as a specification criteria. However, with wide linewidth sources, the probability of phase excursions taking the loop out of lock also needs to be considered.

Another criterion which could be used is the bit error rate (*BER*) in a digital communication system. In this way, the OPLL would be assumed to be part of the receiver of a PSK link and a limit of *BER* would be set. This approach is only reasonable if the OPLL is used in a digital communication system, as *BER* is not a parameter of the loop itself and it loses its significance when the loop is used for other applications. The establishment of a specification criterion which could be used by OPLL designers independent of the application and with a good physical meaning was clearly missing in the literature.

The criterion which best seems to meet the requirements for a single parameter defining loop performance is the average time between cycle slips (T_{av}). It is a parameter of the loop which can be used for all OPLL applications and has a clear physical meaning - it gives the time interval expected between momentary losses of lock. Its main advantage over the phase error variance is that it takes into account the sinusoidal response of the phase detector.

The average time between cycle slips was found to be a strong function of the loop delay time, which is a very important factor influencing the loop performance. T_{av} can vary from a few nanoseconds to 10 years with a 1ns variation in delay time, as shown in Chapter 2. A criterion of T_{av}>10 years was adopted. This criterion was also found to be reasonable compared to the *BER* criterion. The criterion set here of an average time between cycle slips of 10 years has subsequently been used by other research groups to assist the design of OPLLs for use in phased array antennas [Gliese 91].

The main concern of a control loop designer is to assure the stability of the system. The stability conditions for modified first order loops and second order loops were established. It was found that the maximum recommended gain should be 10 dB below the critical gain (above which the loop becomes unstable) to assure acceptable values of damping factor.

The next important decision for the designer is to choose the order of the loop to be used. The performances which can be achieved by a modified first order loop and a second order loop were compared for several values of loop delay time. It was then found that modified first order loops are less sensitive to loop delay time than second order loops. If a wide bandwidth filter is used, it is possible to obtain better performance with a modified first order loop when the delay time is large. It was also possible to predict the shape of the spectrum of the phase error signal and the beat signal, showing that wider bandwidth loops can be achieved using modified first order than second order loops when they present delay time. This confirms previous suggestions that modified first order loops would be preferable in OPLLs [Steele 88].

From the theory it was possible to see that OPLLs could be built using monolithic semiconductor lasers given that the loop delay time was kept low and the loop bandwidth wide. The best solution would be to build the system in OEIC form. This would also help to reduce costs, making commercially available OPLLs possible.

The second part of the project was dedicated to building and characterising a heterodyne OPLL using semiconductor lasers. The first step was to make a temperature control system to stabilise the lasers temperature and consequently their emission wavelength. A temperature stability better than 10mK was achieved over a period of more than half an hour in an uncontrolled laboratory environment. This was obtained by measuring the thermal constant of the laser mount and using a proportional-integral control loop. This suggests that the deployment of such systems within a controlled telecommunication environment should be straightforward.

A dc coupled wideband amplifier was built to work as the filter of a modified first order loop. A split path technique was used to obtain a uniform response up to 700MHz. The technique appears useful for wideband loops. Problems with alignment and optical isolation were studied and practical solutions were found.

Double quantum well (DQW) lasers were selected as the optical sources for the experimental work. Their linewidths were measured by heterodyning two lasers and by a self homodyne method giving a linewidth of 2.5 MHz, narrow enough for the

experiment. The FM response of the DQW lasers was measured using two methods. Observing the spectrum of the heterodyne signal when one of the lasers was modulated made it possible to measure the FM response at high frequencies. At low frequencies a frequency discriminator using a hi-bi fibre interferometer was used. Despite the FM response of the laser limiting the loop bandwidth, the loop was closed and phase lock achieved. The system was then characterised showing good agreement with expected results. This indicates that the model developed is a useful tool OPLL design.

6.3- Suggestions for further work

The search for a better optical source continues as new semiconductor lasers with narrower linewidths and wider FM responses are frequently reported. A great amount of work is still to be done, mainly in obtaining a wide bandwidth tunable laser with low degree of intensity modulation.

6.3.1- Implementation of the system in OEIC form

This work proves that it is possible to build heterodyne OPLLs using semiconductor lasers without external cavities or other linewidth narrowing methods. The theory developed shows that reducing the total loop delay time can improve the loop performance. This can be achieved by reducing the size of the loop and using components which have wide bandwidths. All these point to the integration of the system in the form of an OEIC (opto-electronic integrated circuit) as a way of improving the loop performance. The implementation of the OPLL in an OEIC would also improve the reliability and reduce production costs, making it possible to have this system commercially available in the future.

Figure 6.3.1 shows a diagram of an OPLL in a planar OEIC structure. The idea is to integrate the slave laser, waveguides, couplers and photodetectors on a single substrate. Very similar structures (without amplifier, mixer and loop filter) have been demonstrated [Hernandez-Gil 89] [Koch 91]. Optical frequency-lock loop has been demonstrated using waveguide detectors [Koch 89]. In this system, no tendency to injection lock due to internal reflections was observed in the circuit, dissipating fears that the absence of optical isolation would make the system unstable.

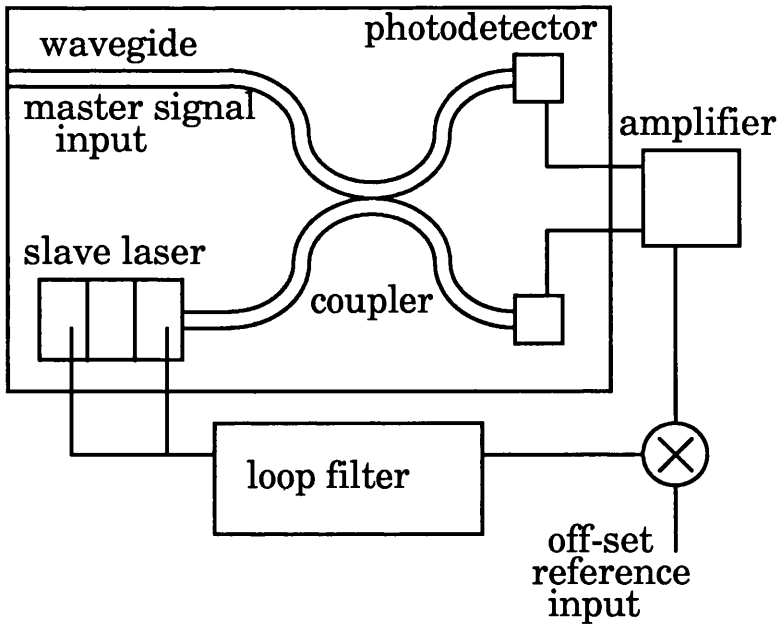

Figure 6.3.1: Diagram of an OPLL in a planar OEIC structure.

Some difficulties still need to be overcome in order to integrate the system. Optical isolation is one of the problems which is difficult to handle in OEICs and therefore requires further research. However, not many obstacles are expected in implementing the rest of the systems as individual components have already proved possible to integrate. When the OPLL is used in coherent receivers, polarisation matching between the master and slave laser signals is also required, which could also cause problems in integration. Integrated-optic polarisation controllers have been demonstrated [Alferness 85] using structures in which a birefringence is introduced in waveguide. This birefringence could be modified in strength and direction according to the voltages applied to the electrodes over the waveguide, making it possible to achieve endless polarisation control [Walker 88].

6.3.2- Monolithic multi-quantum well tuned semiconductor lasers

It has proved possible to make tunable lasers using reverse biased multiple quantum well (MQW) modulators within the laser cavity using an external cavity semiconductor laser [Cai 89]. This may provide a solution for the limitation of the FM response of the slave laser due to the dominance of the thermal effect over other tuning mechanisms when current tuning is used at low frequencies. It also helps to avoid the effect of the photon-electron lifetime resonance at high frequencies.

However, this kind of device needs to be realised in an integrated form. Figure 6.3.2 shows a diagram of a monolithic multi-quantum well tuned semiconductor laser. The

waveguide is divided into two sections: a laser section where the gain is concentrated and a modulator section into which the modulating signal is injected. The difference between this approach and normal double section lasers is that the modulator sector is reverse biased while the laser sector is forward biased. Electrical isolation between the two sections is then necessary to prevent the current flow between the two electrodes. This isolation can be provided by a combination of etching and proton bombardment of the region between the electrodes.

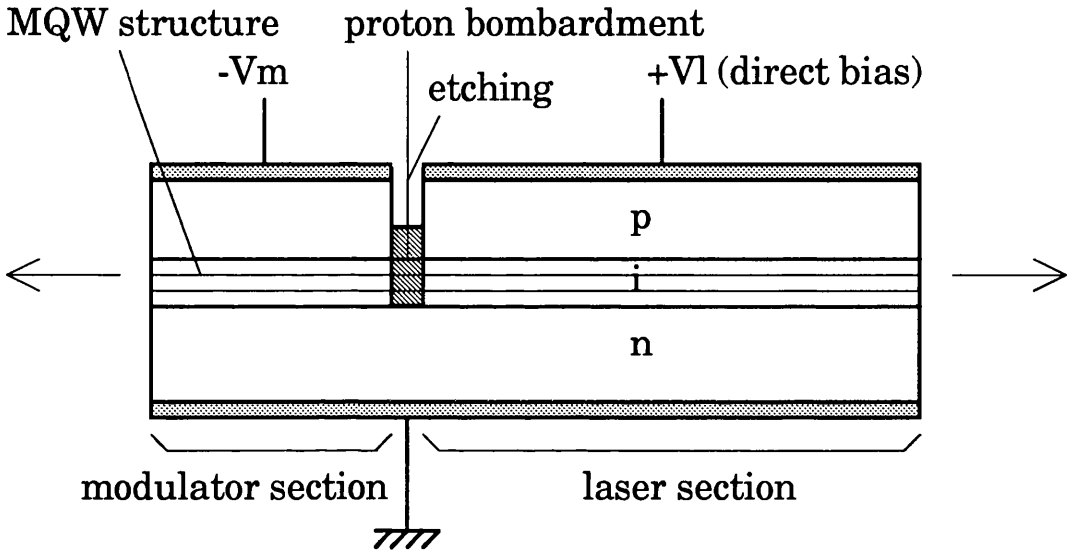

Figure 6.3.2: Diagram of a monolithic multi-quantum well tuned semiconductor laser.

6.3.3- Use of other loop filters

Most of the theoretical study was done using modified first order and second order loops. The experiment used a modified first order loop, although its behaviour was in some ways similar to a second order loop due to the non uniform FM response of the slave laser. However other kinds of loop filters could be considered in the future, once the problem of obtaining a wideband uniform FM response laser has been solved.

One possible solution is the use of split path techniques to achieve second order loops, as illustrated in Figure 6.3.3. Second order loops use filters similar to those used in proportional integral (PI) control systems in which an integrating filter is added in parallel to a proportional filter. The effect of the integration is dominant at low frequencies, while the proportional response takes over at higher frequencies. However, the limited bandwidth of dc coupled low frequency amplifiers can introduce undesirable poles and make the loop unstable. Using the split path technique it is possible to add an ac coupled wideband amplifier to provide gain at high frequencies when the effect of the integration is very low.

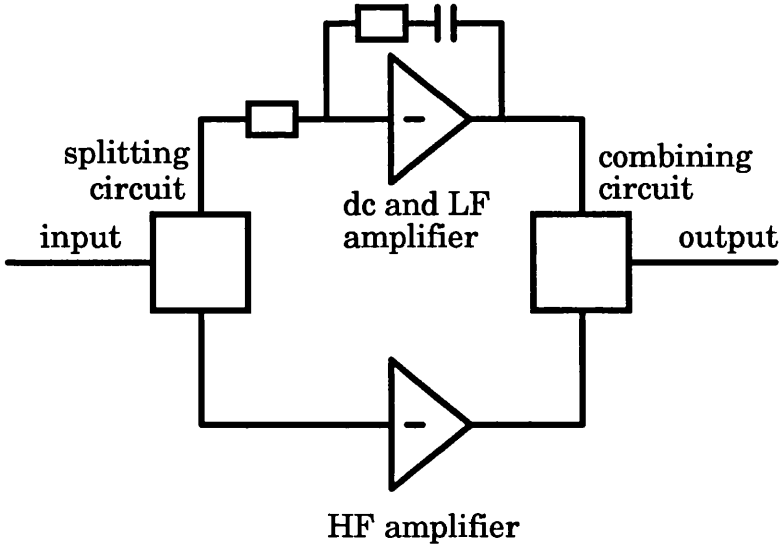

Figure 6.3.3: Block diagram of a split path filter for a second order loop.

Another possible solution could be the use of a passive second order loop. In this case, there would be no active component in the filter which could limit its bandwidth, as shown in Figure 6.3.4. Nevertheless all the loop gain would be then concentrated in the ac coupled amplifier before the phase detector, centred at the offset frequency. One of the problems of using such a configuration would be that the output of the phase detector would have to supply all the necessary current to tune the slave laser.

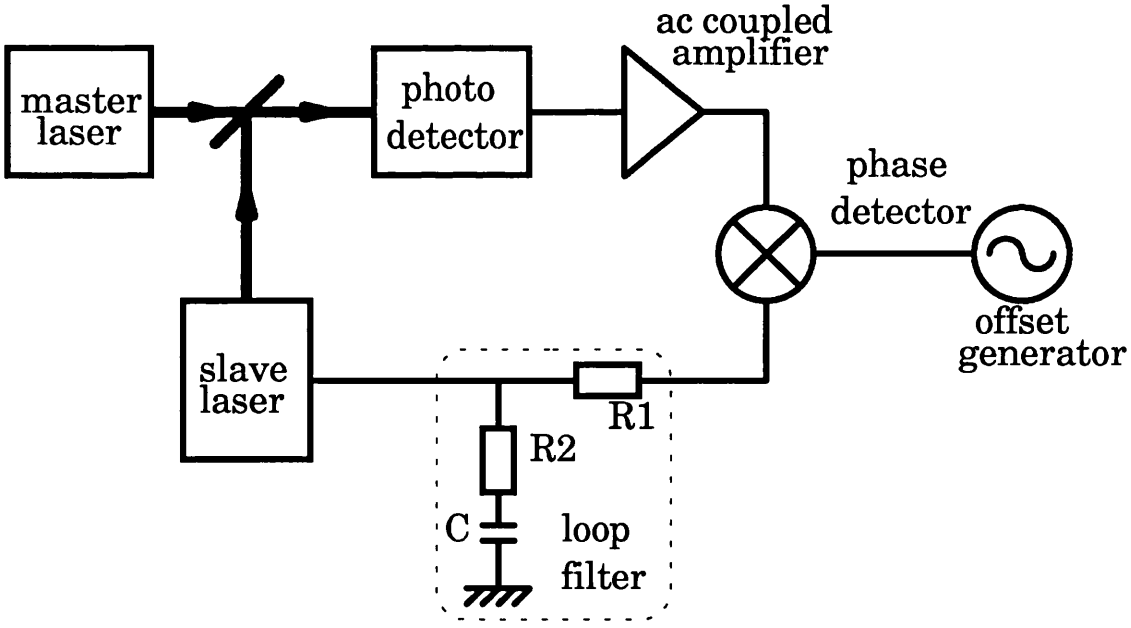

Figure 6.3.4: Block diagram of a heterodyne second order Optical Phase-Lock Loop using passive filter.

6.3.4- Other studies on OPLL performance

Other characteristics of OPLLs are still to be studied, such as the locking acquisition and tracking capabilities. However, these studies would be better performed for each application. The effect of different factors which can influence the loop performance and their dependence on specific applications needs more attention. For example, the effect of the different kinds of modulation used in optical communication links has to be taken into account during the system design. In free space applications, such as inter-satellite optical links, other possible sources of noise and perturbations need to be analysed.

Another study which is needed is the effect of the intensity modulation (IM) of the slave laser when it is tuned. The amount of IM present will depend on the kind of laser and tuning mechanism used by the loop and its influence on the loop performance is still not known. One idea would be to minimise the effect of the intensity modulation by limiting the maximum amplitude of the signal before the phase detector. Another option would be to limit the maximum intensity of the lasers by using an optical intensity limit device. Such a device is still not available and needs further study.

References:

Alferness, R. C. and Buhl, L. L., "Low Loss, Wavelength Tunable, Waveguide Electro-Optic Polarization Controller for λ=1.32μm", Applied Physics Letters, vol. 47, n. 11, December 1985, pp. 1137-1139.

Cai, B., Seeds, A.J., Rivers, A., Roberts, J.S., "Multiple quantum well tuned GaAs/AlGaAs laser", Electronics Letters, 1989, vol. 25, pp. 145-146.

Gliese U., Christensen, E. L. and Stubkjær, K. E., "Laser Linewidth Requirements and Improvements for Coherent Optical Beam Forming Networks in Satellites", Journal of Lightwave Technology, vol. 9, n. 6, June 1991, pp. 779-790.

Hernandez-Gil, F., Koch, T. L., Koren, U., Gnall, R. P. and Burrus, C. A., "Tunable MQW-DBR Laser with Monolithically Integrated GaInAsP/InP Directional Coupler Switch", Electronics Letters, 1989, vol. 25, n. 19, pp. 1271-1272.

Koch, T. L., Koren, U., Gnall, R. P., Choa, F. S., Hernandez-Gil, F., Burrus, C. A., Young, M. G., Oron, M. and Miller, B. I., "GaInAs/GaInAsP Multiple-Quantum-Well

Integrated Heterodyne Receiver", Electronics Letters, 1989, vol. 25, n. 24, pp. 1621-1623.

Koch, T. L. and Koren, U., "Semiconductor Photonic Integrated Circuits", Journal of Lightwave Technology, vol. LT-27, n. 3, March 1991, pp. 641-653.

Ramos, R.T., Seeds, A.J., "Delay, linewidth and bandwidth limitations in optical phase-locked loop design", Electronics Letters, 1990, vol. 26(6), pp.389-391.

Ramos, R.T., Seeds, A.J., "Fast Heterodyne Optical Phase-Lock Loop Using Double Quantum Well Laser Diodes", Electronics Letters, 1992, vol. 28, n.1, pp.82-83.

Steele, R.C., Creaner, M.J., Walker, G.R., Walker, N.G.: "Optical PSK transmission experiment at 565Mbit/s incorporating an endless polarization control system", Proceedings of SPIE Components for Fiber Optics Applications and Coherent Lightwave Communications, Boston, 1988, vol. 988, pp. 302-309.

Walker, N. G., Walker, G. R., Davidson, J., Cunningham, D. C., Beaumont, A. R. and Booth, R. C., "Lithium Niobate Waveguide Polarisation Convertor", Electronics Letters, 1988, vol. 24, n. 2, pp. 103-105.

Walker, N. G., Walker G. R. and Davidson, J., "Endless Polarisation Control Using an Integrated Optic Lithium Niobate Device", Electronics Letters, 1988, vol. 24, n. 5, pp. 266-268.

Appendix 1

Critical frequency for a second order loop
(referred to by section 2.5.2)

This appendix gives the derivation of the equation of the critical frequency for a second order loop.
The open loop transfer function for a second order loop is:

$$G(s) = \frac{k\, e^{(-sT_d)}}{s} \frac{s\,T_2 + 1}{s\,T_1} \qquad \text{A1.1}$$

The phase response reaches π rad at the critical frequency ω_{cr} given by:

$$\pi + \omega_{cr}\, T_d - \tan^{-1}(\omega_{cr}\, T_2) = \pi \qquad \text{A1.2}$$

For the gain to be less then 1 at this frequency:

$$\frac{\omega_{no}^2}{\omega_{cr}^2} \sqrt{1 + (\omega_{cr}\, T_2)^2} \le 1 \qquad \text{A1.3}$$

Considering the gain equal to 1 at the critical frequency, equation A1.3 can be rewritten as:

$$\omega_{no}^2 \sqrt{1 + (\omega_{cr}\, T_2)^2} = \omega_{cr}^2 \qquad \text{A1.4}$$

$$\omega_{cr}^4 - \omega_{cr}^2\, \omega_{no}^4\, T_2^2 - \omega_{no}^4 = 0 \qquad \text{A1.5}$$

For: $x=\omega_{cr}^2$:

$$x^2 - x\, \omega_{no}^4\, T_2^2 - \omega_{no}^4 = 0 \qquad \text{A1.6}$$

The solution for this equation is:

$$x = \frac{\omega_{no}^4\, T_2^2 \pm \sqrt{(\omega_{no}^4\, T_2^2)^2 + 4\, \omega_{no}^4}}{2} \qquad \text{A1.7}$$

Considering only the positive solution:

$$x = \frac{\omega_{no}^4 T_2^2 + \omega_{no}^2 \sqrt{\omega_{no}^4 T_2^4 + 4}}{2} \qquad \text{A1.7}$$

The relative damping factor is given by:

$$\zeta_o = \frac{T_2 \omega_{no}}{2} \qquad \text{A1.8}$$

Isolating T_2 and substituting into equation (A1.7):

$$x = \frac{4\zeta_o^2 \omega_{no}^2 + \omega_{no}^2 \sqrt{16\zeta_o^4 + 4}}{2} \qquad \text{A1.8}$$

$$x = \omega_{no}^2 \left(2\zeta_o^2 + \sqrt{4\zeta_o^4 + 1}\right) \qquad \text{A1.9}$$

The critical frequency is then given by:

$$\omega_{cr} = \omega_{no} \sqrt{2\zeta_o^2 + \sqrt{4\zeta_o^4 + 1}} \qquad \text{A1.10}$$

Equation A1.2 can be rewritten using equation (A1.8):

$$\omega_{cr} T_d = \tan^{-1}\left(\omega_{cr} \frac{2\zeta_o}{\omega_{no}}\right) \qquad \text{A1.11}$$

Substituting this value of critical frequency:

$$\omega_{no} T_d < \frac{\tan^{-1}\left(2\zeta_o \sqrt{2\zeta_o^2 + \sqrt{4\zeta_o^4 + 1}}\right)}{\sqrt{2\zeta_o^2 + \sqrt{4\zeta_o^4 + 1}}} \qquad \text{A1.12}$$

Which is the stability criteria.

Appendix 2

Estimation of the beat signal spectrum using narrow band FM approximation
(referred to by section 2.6.2)

This appendix shows how an estimation of the beat signal spectrum can be made from the phase error spectrum using the narrowband FM approximation.

Suppose that the error signal modulating the slave laser is given by:

$$m(t) = M\cos(\omega_d\, t) \qquad \text{A2.1}$$

Where M is the amplitude and ω_d the frequency of the modulating signal. The instantaneous frequency of the modulated signal is then given by:

$$\omega_i(t) = \omega_o + k_\omega\, M\cos(\omega_d\, t) \qquad \text{A2.2}$$

Where k_ω is the frequency response of the slave laser at the frequency ω_d. As instantaneous frequency and phase are related according to:

$$\omega_i(t) = \frac{d\theta_i(t)}{dt} \qquad \text{A2.3}$$

The instantaneous phase of the modulated signal is given by:

$$\theta_i(t) = \omega_o\, t + \frac{k_\omega\, M}{\omega_d}\sin(\omega_d\, t) \qquad \text{A2.4}$$

The modulation index β is defined as:

$$\beta = \frac{k_\omega\, M}{\omega_d} \qquad \text{A2.5}$$

The modulated signal is then given by:

$$e_1(t) = E_1\cos\left(\omega_o\, t + \beta\sin(\omega_d\, t)\right) \qquad \text{A2.6}$$

Where E_1 is the amplitude of the modulated signal. Using the trigonometric relation:

$$\cos(a+b)=\cos(a)\cos(b)-\sin(a)\sin(b) \qquad \text{A2.7}$$

Equation A2.6 can be rewritten as:

$$e_1(t)=E_1\cos\omega_o t\cos(\beta\sin\omega_d t)-E_1\sin\omega_o t\sin(\beta\sin\omega_d t) \qquad \text{A2.8}$$

For low values of β (β<0.2) the narrowband FM approximation can be made. In this approximation it is assumed that:

$$\sin(\beta\sin\omega_d t)\cong\beta\sin\omega_d t \quad \text{and} \quad \cos(\beta\sin\omega_d t)\cong 1 \qquad \text{A2.9}$$

Thus:

$$e_1(t)=E_1\cos\omega_o t-E_1\beta\sin\omega_o t\sin\omega_d t \qquad \text{A2.10}$$

Using another trigonometric relation:

$$-\sin(a)\sin(b)=\frac{\cos(a+b)-\cos(a-b)}{2} \qquad \text{A2.11}$$

The modulated signal is then given by:

$$e_1(t)=E_1\cos\omega_o t+\frac{E_1\beta}{2}\cos((\omega_o+\omega_d)t)-\frac{E_1\beta}{2}\cos((\omega_o-\omega_d)t) \qquad \text{A2.12}$$

Supposing that all the frequency deviation is concentrated at the slave laser signal and the master laser is producing a single tone signal given by:

$$e_2(t)=E_2\cos((\omega_o+\omega_r)t) \qquad \text{A2.13}$$

Where E_2 is the amplitude of the master signal and ω_r the frequency of the offset generator signal. The total optical intensity is given by:

$$I_t=\frac{(e_1+e_2)^2}{\eta} \qquad \text{A2.14}$$

Where η is the characteristic impedance of the medium. Using the same procedure described in Appendix 3, it is possible to transform equation A2.14 into:

$$I_t(t) = \frac{E_1 E_2}{\eta} \cos\omega_r t + \frac{E_1 E_2 \beta}{2\eta} \cos((\omega_r - \omega_d)t) - \frac{E_1 E_2 \beta}{2\eta} \cos((\omega_r + \omega_d)t) \qquad \text{A2.15}$$

The optical frequency components are neglected as the photodetector cannot answer to them and the dc and low frequency components are also neglected for being blocked by the detector decoupling capacitor. E_1 and E_2 relate to the respective optical intensities I_1 and I_2 as:

$$E_1 = 2\sqrt{\eta I_1} \qquad \text{A2.16}$$

$$E_2 = 2\sqrt{\eta I_2} \qquad \text{A2.17}$$

Thus

$$I_t(t) = 4\sqrt{I_1 I_2} \cos\omega_r t + 2\beta\sqrt{I_1 I_2} \cos((\omega_r - \omega_d)t) - 2\beta\sqrt{I_1 I_2} \cos((\omega_r + \omega_d)t) \qquad \text{A2.18}$$

The photo current produced at the photodetector terminals is given by:

$$I_p = R A I_t \qquad \text{A2.19}$$

The amplitude of each sideband is given by:

$$I_b = 2 R A \sqrt{I_1 I_2}\, \beta \qquad \text{A2.20}$$

Where R is the photodetector responsivity and the A is the photodetector illuminated area. The power associated to each sideband is given by:

$$P_b = r_l I_b^2 = 4 r_l R^2 A^2 I_1 I_2 \beta^2 \qquad \text{A2.21}$$

Where r_l is the photodetector load resistance. Substituting β from equation A2.5:

$$P_b = 4 r_l R^2 A^2 I_1 I_2 k_\omega^2 \frac{M^2}{\omega_d^2} \qquad \text{A2.22}$$

The amplitude of the modulating signal M can be related to the phase error signal θ_e by:

$$M = \frac{\theta_e}{k_d} \qquad \text{A2.23}$$

Where k_d is the phase detector gain. P_b can be rewritten as:

$$P_b = 4\, r_l\, R^2\, A^2\, I_1\, I_2 \frac{k_\omega^2}{k_d^2} \frac{\theta_e^2}{\omega_d^2} \qquad \text{A2.24}$$

Assuming that each point of the modulated signal spectrum corresponds to a point of the modulating signal spectrum, it is possible to reconstruct the power spectrum at the detector terminals $S_b(\omega)$ from the phase error spectrum $S_e(\omega)$ as follows:

$$S_b(\omega) = 4\, r_l\, R^2\, A^2\, I_1\, I_2 \frac{k_\omega^2(\omega)}{k_d^2} \frac{S_e(\omega)}{\omega^2} \qquad \text{A2.25}$$

Where $k_\omega(\omega)$ is the frequency response of the slave laser.

Appendix 3

Derivation of equation 3.4.9

(referred to by Section 3.4)

$$e_t = 2\sqrt{\eta}\left[\sqrt{I_1}\cos(\omega_1 t + \phi_1) + \sqrt{I_2}\cos\theta\cos(\omega_2 t + \phi_2 - \beta_x x)\right] \quad \text{A3.1}$$

The total optical intensity is then:

$$I_t = \frac{(e_t)^2}{\eta} \quad \text{A3.2}$$

$$I_t = 4[\sqrt{I_1}\cos(\omega_1 t + \phi_1) + \sqrt{I_2}\cos\theta\cos(\omega_2 t + \phi_2 - \beta_x x)]^2 \quad \text{A3.3}$$

$$I_t = 4[I_1\cos^2(\omega_1 t + \phi_1) + I_2\cos^2(\theta)\cos^2(\omega_2 t + \phi_2 - \beta_x x) + \\ +2\sqrt{I_1 I_2}\cos(\theta)\cos(\omega_1 t + \phi_1)\cos(\omega_2 t + \phi_2 - \beta_x x)] \quad \text{A3.4}$$

Using the identities:

$$\cos^2 a = \frac{1+\cos(2a)}{2} \quad \text{A3.5}$$

$$\cos(a)\cos(b) = \frac{\cos(a+b)+\cos(a-b)}{2} \quad \text{A3.6}$$

gives:

$$I_t = 2\Big[I_1 + I_2\cos^2(\theta) + \\ +2\sqrt{I_1 I_2}\cos(\theta)\cos((\omega_1 - \omega_2)t + \phi_1 - \phi_2 + \beta_x x) + \\ +I_1\cos(2\omega_1 t + 2\phi_1) + I_2\cos^2(\theta)\cos^2(2\omega_2 t + 2\phi_2 - 2\beta_x x) + \\ +2\sqrt{I_1 I_2}\cos(\theta)\cos((\omega_1 + \omega_2)t + \phi_1 + \phi_2 - \beta_x x)\Big] \quad \text{A3.7}$$

Appendix 4

External cavity lasers and AR coatings

As all the previous experiments published on optical phase-lock loops using semiconductor lasers have used external cavities, a heterodyne system based on external cavity lasers was constructed and tested.

External cavity lasers

The first OPLL experiments reported used gas lasers such as CO_2 [Leep 82] due to their narrow linewidth, making possible the use of the PLL theory already developed for microwave systems. In order to use semiconductor laser diodes it was found necessary to narrow their linewidth, one of the most used methods being the building of external cavities [Steele 83] [Kahn 89] [Norimatsu 90].

Figure A4.1 shows a schematic diagram of an external cavity laser. The idea is to narrow the output linewidth by expanding the resonant laser cavity. Ideally, the whole system should work as a single cavity and an anti-reflection coating (AR coating) is deposited on one of the facets of the laser diode to remove internal cavity reflections. However, in practice it is difficult to obtain a perfect AR coating and the system has to be seen as a double cavity device. As the cavity becomes longer, the mode spacing becomes smaller making it necessary to add a diffraction grating to provide appropriate mode selection. Note that the intra cavity lens has also to be AR coated.

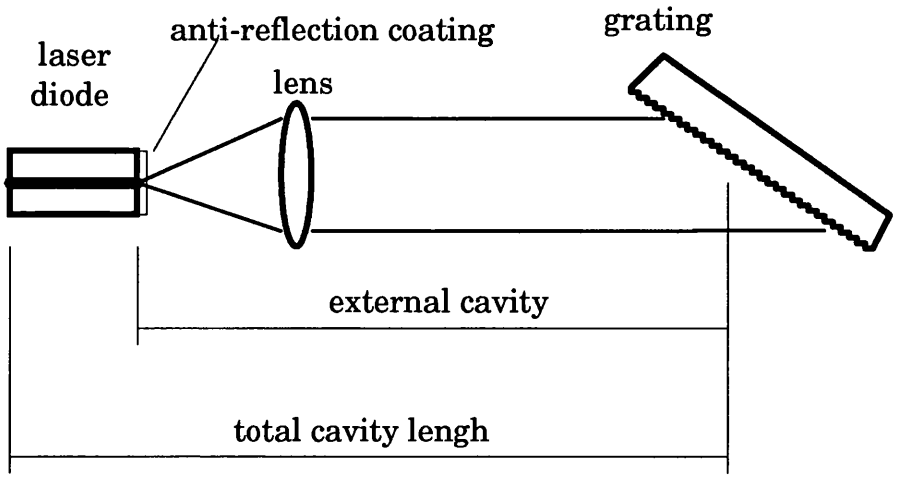

Figure A4.1: Schematic diagram of an external cavity laser.

Anti reflection coatings

Anti reflection coatings were applied to one facet of each laser of the heterodyne system. The most convenient material for the coating was Silicon Monoxide (SiO), due to its refractive index and low evaporating temperature. Figure A4.2 shows a diagram of a quarter wavelength single layer anti-reflection coating, where n_m, n_f and n_o the refractive index of the material, the film and the air and λ is the wavelength. The reflectivity R_f of such a structure is given by [Macleod]:

$$R_f = \left(\frac{n_o - \frac{n_f^2}{n_m}}{n_o + \frac{n_f^2}{n_m}} \right)^2 \qquad \text{A4.1}$$

The refractive index of the material, GaAs, is n_m=3.5 and the refractive index of the film, SiO, is n_f=1.924 at 830nm. The reflectivity in this case would be 0.0785%.

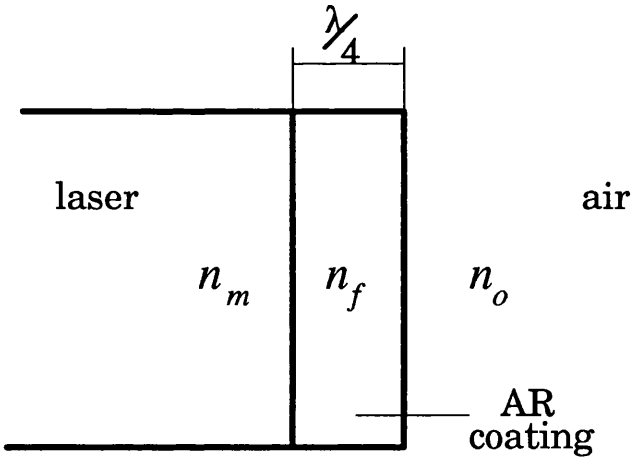

Figure A4.2: Diagram of an anti reflexion coating.

It is important to be able to control the depth of the film in order to achieve a quarter wavelength thickness. For this, the laser was placed inside a vacum chamber (≈50 10^{-6} bar) together with a photodetector facing the laser facet to be coated, but slightly off the main axis, as shown in Figure A4.3.

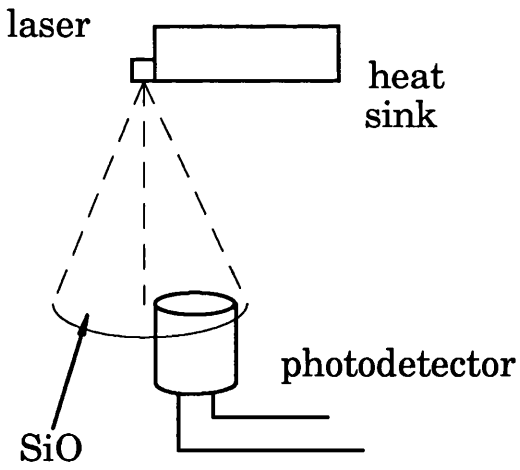

Figure A4.3: Relative position of the laser and detector during evaporation..

The laser was then driven by a low frequency (about 20kHz) sinusoidal forward current which had a minimum value of zero and maximum value below the threshold current. Keeping these values fixed, the amplitude of the resulting emission will be inversely proportional to the reflectivity at the laser's facet. It is important to be sure that only spontaneous emission is present in order to retain this proportionality. The photo current at the photodetector terminals is a maximum when the reflectivity is a minimum, indicating that the evaporation must be stopped.

A lock-in amplifier was used to amplify the photodetector signal and avoid the strong electrical noise from the vacuum pump. The signal frequency was chosen to avoid the mains supply harmonics. An X-Y recorder was used to register the amplitude of the detector signal. Figure A4.4 shows a diagram of the monitoring circuit.

The gain of the amplifier was adjusted as follow: With the laser off, the zero of the X-Y recorder was adjusted. With the laser on the amplifier gain was adjusted until the recorder registered 70% of the final expected position of the pen. Care was taken not to saturate the lock-in amplifier. Figure A4.5 shows the X-Y recorder plot obtained during evaporation.

The reflectivity of the coated facet R_c can be estimated in relation to the reflectivity of the uncoated facet R_u:

$$\frac{\eta_c}{\eta_u} = \sqrt{\frac{R_u}{R_c}\,\frac{(1-R_c)}{(1-R_u)}} \qquad \text{A4.2}$$

Where η_c and η_u are the slopes of the light/current characteristics of the coated and uncoated facets (W/A). Figures A4.6a and A4.6b show the light/current curves of the two lasers after coating for both coated and uncoated facets.

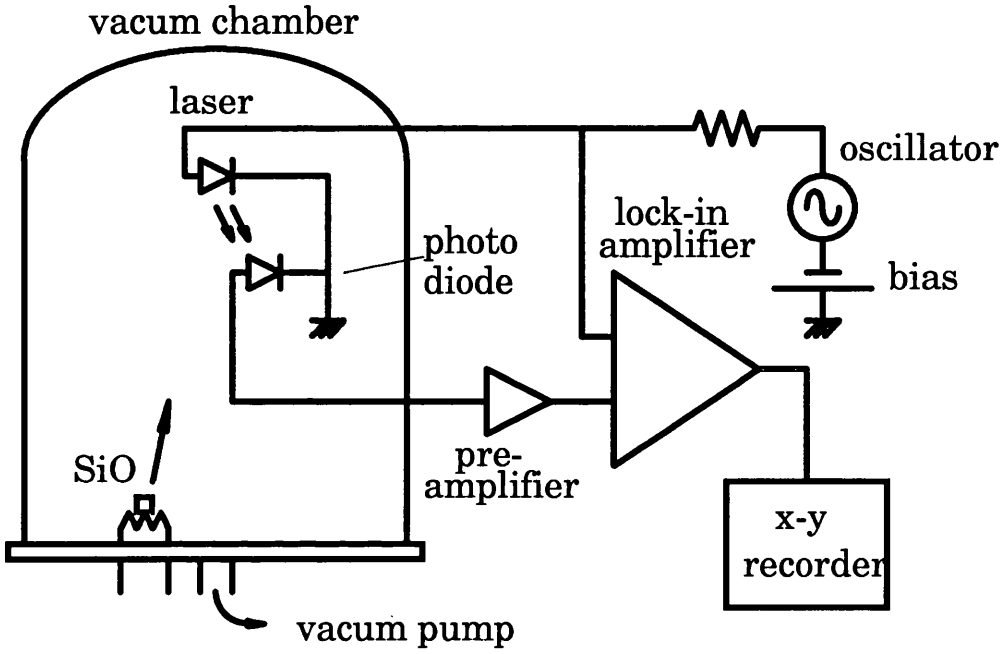

Figure A4.4: Diagram of the coating thickness control circuit.

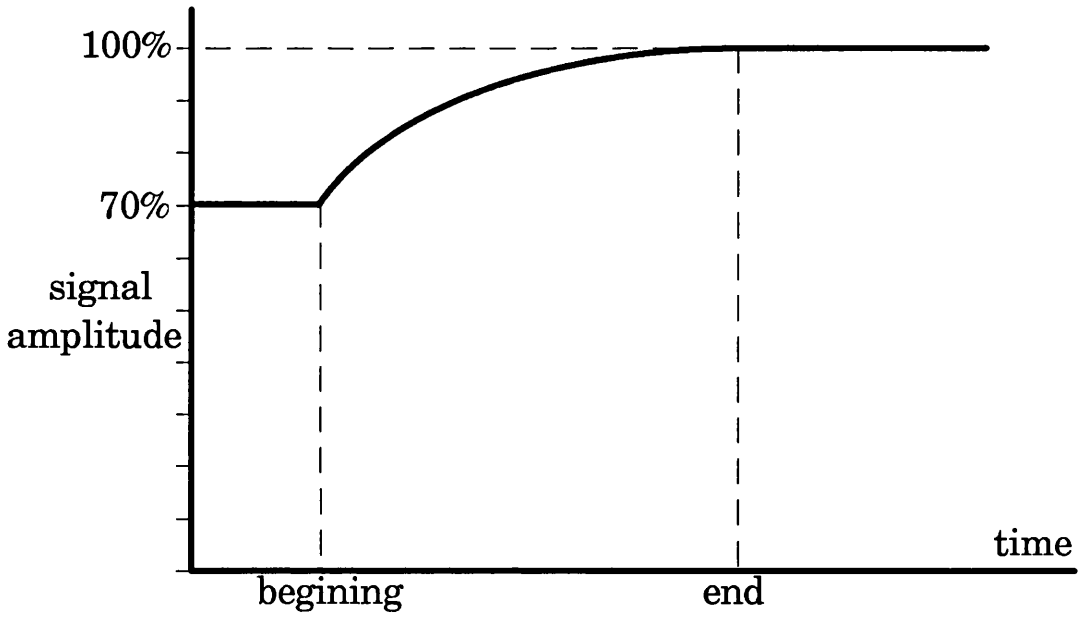

Figure A4.5: X-Y recorder plot during evaporation.

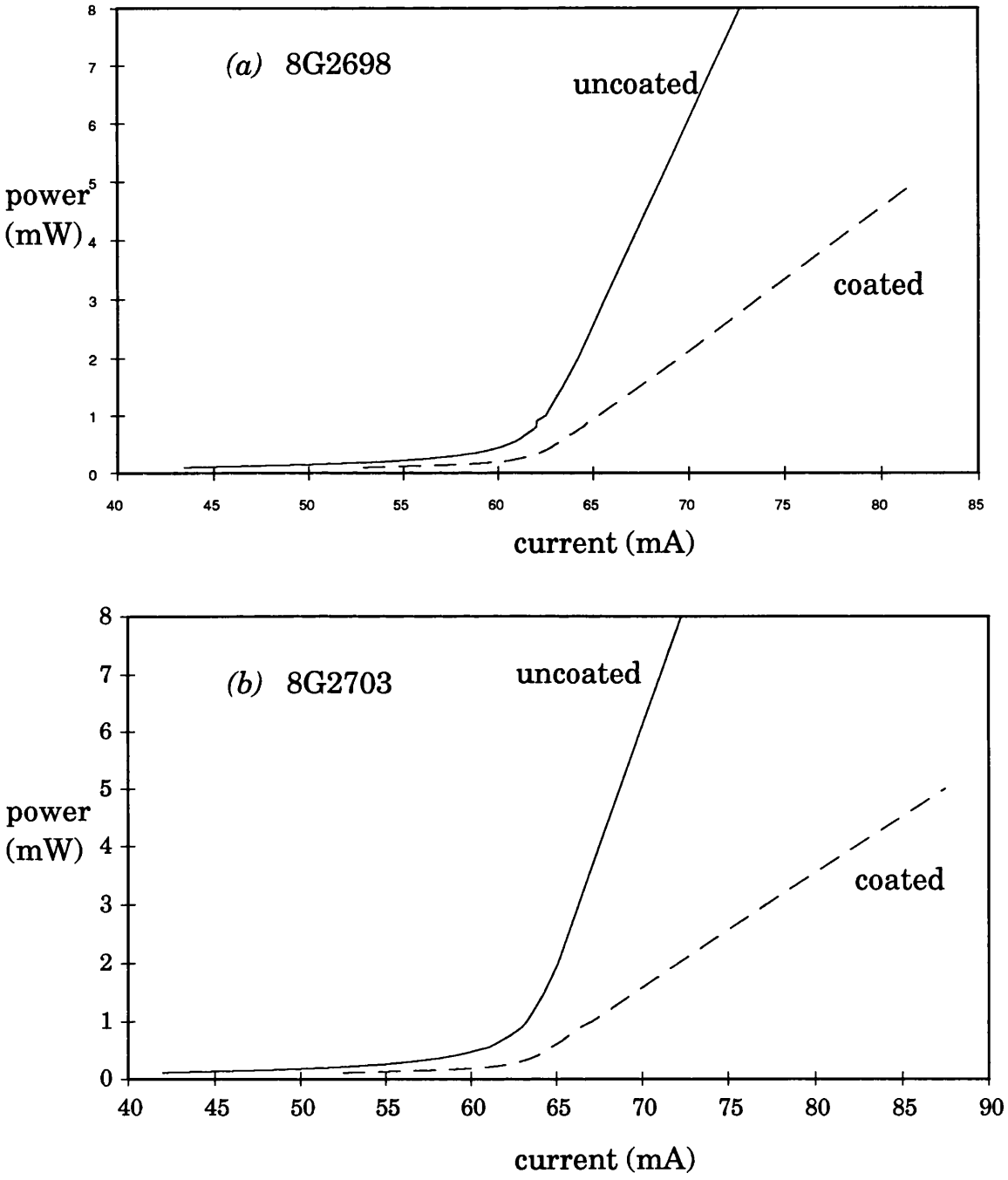

Figures A4.6: Characteristic curve after coating for both coated and uncoated facets for two different lasers.

For R_u=31%, the reflectivities of the coated facet R_c were calculated to be 3.4% and 4.3% for each laser. Using Equation A4.1 again, for a reflectivity of R_f=4% the refractive index of the film would be n=1.53 which is different from the refractive index of SiO (1.924 @ 830nm). It is possible that some contamination of silicon

dioxide SiO_2 occurred. The refractive index of SiO_2 is 1.456 @ 830nm. The refractive index of the film could also be changed by non uniformity of the layer.

External cavity mounting

The reflectivity of the coated facet achieved was 3.4% and 4.1% for the two lasers coated. Two external cavity lasers were assembled, one using a grating and the other using a flat mirror, both being about 50mm long. Precision piezoelectric controlled micro-positioners were used to achieve fine alignment and tuning. The reductions of the threshold current by the addition of the external cavities were 12.2mA and 10.4mA respectively, bringing the threshold current to pre coating levels.

The external cavity laser using a grating as reflector was tuned mechanically and a map of the possible single mode operation wavelengths was made. The influence of internal modes spaced 0.3nm (corresponding to 130GHz at 830nm) from each other was found to be still very strong despite the AR coatings, making it impossible to obtain stable operation at wavelengths in between modes. About 21 modes (7nm) could be selected manually using the micropositioners, from which 10 modes (3nm) could be selected using piezoelectric positioners. Also using the pizoelectric controls, it was possible to select about 10 external modes (spaced 1.6GHz from each other) at each internal mode wavelength. About 1GHz continuous tuning could be achieved at each external mode. Continuous tuning was also achieved by changing the laser diode current with a rate of 100MHz/mA for low frequency variations. The laser mounted with a Fabry Perrot external cavity could only be tuned over 3 internal modes. However, better sensitivity to current tuning was achieved (400MHz/mA). Both external cavity lasers were very sensitive to vibrations and temperature fluctuations.

Continuous tuning over a range of 15nm is possible to obtain [Favre 86] using a mechanical arrangement which makes it feasible to translate and rotate the grating at an exact rate. However, very good AR coating is required (0.01%). The use of miniature packaged external cavity laser [Mellis 88] [Harrison 89] [Kahn 89] can diminish the sensitivity to vibrations and temperature fluctuations.

Heterodyning external cavity lasers

The front facets of the lasers were used for coupling to the external cavities, while the back facets were used to extract the signal from each laser. This brought the problem

of wavefront matching as a complicated wavefront pattern is formed at the back of each laser diode due to reflections of the beam from the heat sink blocks on which the laser chips are mounted. The result was poor efficiency of the optical mixing and low beat signal power (order of -50dBm). As the use of an external cavity also reduces the laser sensitivity to direct current tuning (to about 100MHz/mA), high gain amplifiers would be necessary to obtain reasonable loop gain and hence satisfactory phase lock.

Another drawback of the use of the external cavity solution was its extreme sensitivity to vibrations and acoustic noises. A fixed Fabry Perot interferometer was placed in front of one of the lasers to serve as an optical frequency discriminator and a photodetector at the other side of the interferometer gave a signal proportional to the laser frequency fluctuations. The spectrum of this signal presented strong low frequency noise, peaking at several frequencies corresponding to resonances of the several parts of the mount and the noise of the cooling fans of the measurement equipment in the laboratory. As a result, the spectrum of the beat signal of the two lasers was not stable, presenting fluctuations of up to 50MHz from the central frequency. Figure A4.7 shows the spectrum of the beat signal of two external cavity lasers when the spectrum analyser hold maximum function was used for a couple of minutes to measure the frequency fluctuation range.

The use of external cavities also diminishes the laser sensitivity to temperature tuning, since only the internal cavity is temperature controlled. This makes necessary the use of large temperature offsets (order of 10°C) to provide wavelength matching of the lasers involved in the heterodyne process. For these reasons, an alternative solution to the use of external cavities was considered preferable.

References:

Favre, F., Guen, D. Le, Simon, J. C. and Landousies, B., "External-Cavity Semiconductor Laser with 15nm Continuous Tuning Range", Electronics Letters, vlo. 22, n. 15, 1986, pp. 795-796.

Harrison, J. and Mooradian, A., "Linwidth and Offset Frequency Locking of External Cavity GaAlAs Lasers", Journal of Quantum Electronics, vol. QE-25, n. 6, June, 1989, pp.1152-1155.

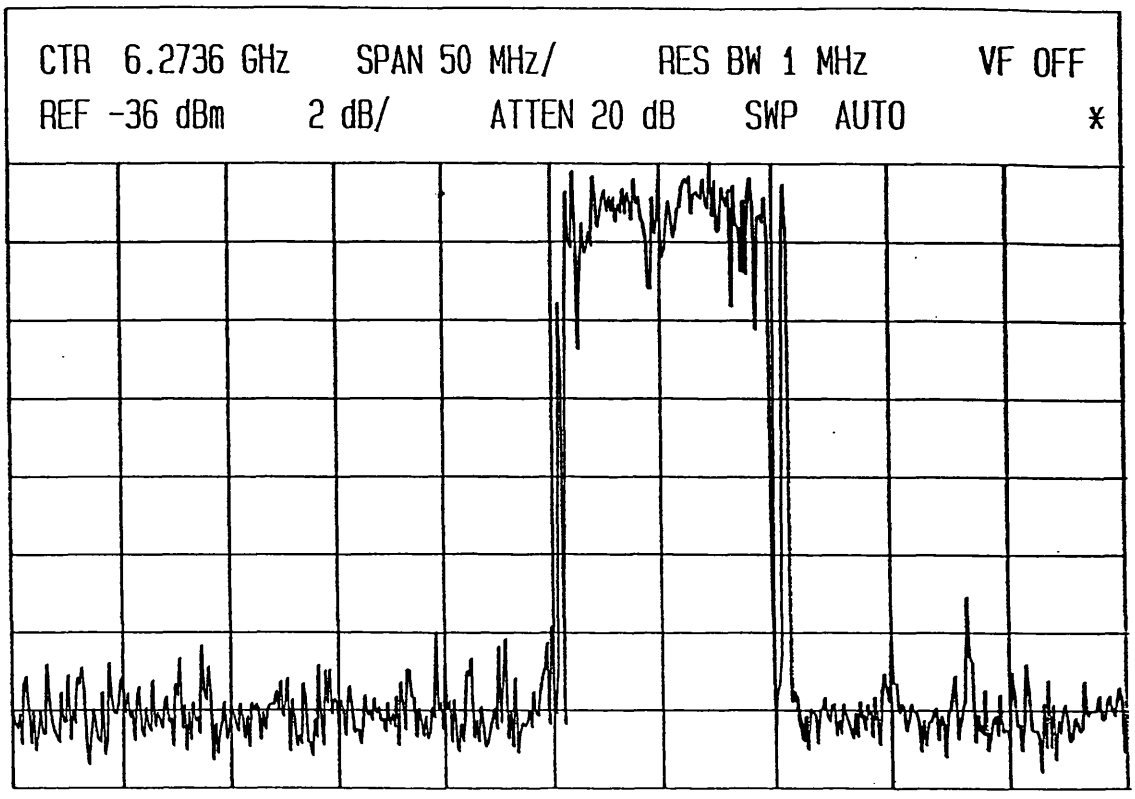

Figure A4.7: Spectrum of the beat signal of two external cavity lasers (hold maximum function used).

Kahn, J. M., "1 Gbit/s PSK Homodyne Transmission System Using Phase-Locked Semiconductor Lasers", IEEE Photonics Technology Letters, 1989, 1(10), pp.340-342.

Kahn, J. M., Burrus, C. A. and Raybon, G., "High-Stability 1.5μm External-Cavity Semiconductor Lasers for Phase-Lock Applications", IEEE Photonics Technology Letters, vol. 1, n. 7, July, 1989, pp. 159-161.

Leep, W.R., Philip, H.K., Scholtz, A.L., Bonek, E.: 'Frequency synchronization and phase locking of CO lasers', Appl. Phys. Lett.,1982, 41(7), pp.592-594.

Macleod, H.A., "Thin film optical filters", second edition, Adam Hilger Ltd.

Mellis, J., Al-Chalabi, S. A., Cameron, K. H., Wyatt, R., Regnault, J. C., Devlin, W. J. and Brain, M. C., "Miniature Packeged External-Cavity Semiconductor Laser with 50GHZ Continuos Tuning Range", Electronics Letters, vol. 24, n. 16, 1988, pp. 988-989.

Norimatsu, S., Iwashita, K., Sato, K., 'PSK optical homodyne transmission detection using external cavity lasers diodes in Costas loop', Photonics Tech. Lett., 1990, 2(5), pp.374-376.

Norimatsu, S., Iwashita, K., Noguchi, K., '10 Gbit/s optical PSK homodyne transmission experiments using external cavity DFB LDs', Elect. Lett., 1990, 26(10), pp.648-649.

Steele, R.C., Creaner, M.J., Walker, G.R., Walker, N.G.: "Optical PSK transmission experiment at 565Mbit/s incorporating an endless polarization control system", Proceedings of SPIE Components for Fiber Optics Applications and Coherent Lightwave Communications, Boston, 1988, vol.988, pp. 302-309.

Appendix 5

Derivation of the photo current from a Mach-Zehnder interferometer and detector, equation (3.5.5). (referred to by section 3.5.3)

Figure A5.1 shows a diagram of an all fibre Mach-Zehnder interferometer. The input optical signal is split into two different paths, with different optical path lengths, and combined at the output.

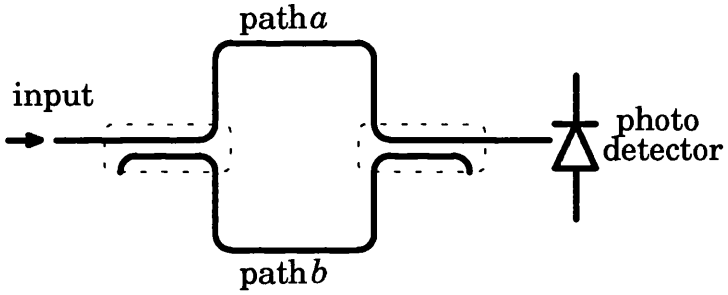

Figure A5.1: Diagram of an all fibre Mach-Zehnder interferometer.

The electrical fields of the signals coming from the a and b paths are given by:

$$e_a = 2\sqrt{\eta\, in_a}\cos(\omega t) \qquad \text{A5.1}$$

$$e_b = 2\sqrt{\eta\, in_b}\cos[\omega (t+\Delta t)] \qquad \text{A5.2}$$

Where in_a and in_b are the intensity of the two signals, ω is the optical frequency of the input signal, η is the characteristic impedance of the medium and Δt is the propagation time difference between the two optical path lengths. Given that the difference between the two path lengths is not longer than the coherence length of the laser, the total electrical field at the output, e_t is the combination of the electrical fields from arms a and b, e_a and e_b:

$$e_t = e_a + e_b \qquad \text{A5.3}$$

The optical intensity at the output is:

$$in_t = \frac{(e_t)^2}{\eta} \qquad \text{A5.4}$$

The photo current at the terminals of the photo detector is given by:

$$i_p = R \cdot \int_A \frac{in_t}{2} \cdot dA \qquad \text{A5.5}$$

Where R is the responsivity and A is the illuminated active area of the photo detector. Assuming the radiation coming from each arm of the interferometer have the same polarisation direction and that there is no misalignment, using (A5.1), (A5.2) and (A5.3) gives:

$$e_t = 2\sqrt{\eta}\left[\sqrt{in_a}\cos(\omega t) + \sqrt{in_b}\cos(\omega (t+\Delta t))\right] \qquad \text{A5.6}$$

Using (A5.4):

$$in_t = 4\left[\sqrt{in_a}\cos(\omega t) + \sqrt{in_b}\cos(\omega (t+\Delta t))\right]^2 \qquad \text{A5.7}$$

Thus,

$$\begin{aligned} in_t &= 2\,(in_a + in_b + 2\sqrt{in_a\, in_b}\cos(\omega\,\Delta t) \\ &+2\sqrt{in_a\, in_b}\cos(\omega\,(2t+\Delta t)) \\ &+in_a\cos(2\omega t) + in_b\cos(2\omega(t+\Delta t)) \end{aligned} \qquad \text{A5.8}$$

From (A5.5):

$$i_p = \frac{R\,A}{2}\,in_t = R\,A\left[in_a + in_b + 2\sqrt{in_a\, in_b}\cos(\omega\,\Delta t)\right] \qquad \text{A5.9}$$

Appendix 6

Temperature controller components

(referred to by Figure 4.5.3 and Figure 4.5.6)

R1 = 7k5Ω	R10 = 10kΩ	R19 = 1Ω
R2 = 25kΩ	R11 = 430kΩ	C1 = 22μF
R3 = 1kΩ	R12 = 1MΩ	C2 = 47pF
R4 = 1kΩ	R13 = 5kΩ	C3 = 0.01μF
R5 = 7k5Ω	R14 = 10kΩ	A1 , A2 = 741
R6 = 1MΩ	R15 = 1kΩ	T1 = BC107
R7 = 430kΩ	R16 = 5kΩ	T2 = TIP121
R8 = 10kΩ	R17 = 10kΩ	T3 = TIP126
R9 = 5kΩ	R18 = 1Ω	

Thermistor: RS.151-237 10KΩ @ 25°C NTC

Peltier Cooler: Marlow Industries 1023T